3-22-2021

Microbiologically Influenced Corrosion of Submerged Steel Bridge Piles in Natural Waters in Presence of Marine-Fouling

Samanbar Permeh
sperm005@fiu.edu

FLORIDA INTERNATIONAL UNIVERSITY

Miami, Florida

MICROBIOLOGICALLY INFLUENCED CORROSION OF SUBMERGED STEEL BRIDGE PILES IN NATURAL WATERS IN PRESENCE OF MARINE-FOULING

A dissertation submitted in partial fulfillment of

the requirements for the degree of

DOCTOR OF PHILOSOPHY

in

CIVIL ENGINEERING

by

Samanbar Permeh

2021

To: Dean John L. Volakis
Collage of Engineering and Computing

This dissertation, written by Samanbar Permeh, and entitled Microbiologically Influenced Corrosion of Submerged Steel Bridge Piles in Natural Waters in Presence of Marine-Fouling, having been approved in respect to style and intellectual content, is referred to you for judgment.

We have read this dissertation and recommend that it be approved.

_____
Shonali Laha

_____
Norman Munroe

_____
Kelli Hunsucker

_____
Kingsley Lau, Co-Major Professor

_____
Berrin Tansel, Co-Major Professor

Date of Defense: March 22, 2021

The dissertation of Samanbar Permeh is approved.

_____
Dean John L. Volakis
Collage of Engineering and Computing

_____
Andrés G. Gil
Vice President for Research and Economic Development
and Dean of the University Graduate School

Florida International University, 2021

DEDICATION

I dedicate this dissertation to my dear mom— Zahra—, whose patience, sacrifice, support, and understanding made the completion of this work possible, and to my beloved sisters— Parima and Parisa—, beautiful niece— Dorsa—, and nephew— Parsa—, for their endless love, support and prayers.

And in memory of my loving father— Abolghasem—, who could not see this accomplishment but who had given me dreams to look forward to…

ACKNOWLEDGMENTS

I would like to give my sincere appreciation and gratitude to my major advisor Dr. Kingsley Lau for his support, presence, insightful guidance, for having confidence in my abilities and expert contribution though the period of research and dissertation development, which without, it would not have been possible to accomplish.

I am very thankful to Dr. Berrin Tansel for her support over the years. I thank Dr. Shonali Laha, Dr. Kelli Hunsucker and Dr. Norman Munroe for their service on the dissertation committee. The suggestions, advice, efforts, and corrections have been helpful during the development and completion of this dissertation. I also want to acknowledge the help of Mathew Duncan during this research and the support from the FDOT State Materials Office.

Last but not the least; I would like to thank my Dear Cousin, Yazdan Sarab for having faith in me and motivating me in pursuing my goal.

ACKNOWLEDGMENTS

Portions of the dissertation were presented in conference proceedings and published in manuscripts, including:

Chapter 4

- S. Permeh, C. Reid, M. Echeverria, K. Lau, B. Tansel, M. Duncan, I. Lasa. In Proceedings of the Corrosion 2017, New Orleans, LA, USA, 26–30 March 2017; NACE International: Houston, TX, USA, 2017.

Chapter 5

- S. Permeh, K. Lau, M. Echeverria, M. Duncan, 2021.ASCE Journal of Materials in Civil Engineering, V.33, Issue 6, June 2021. DOI: 10.1061/(ASCE)MT.1943-5533.0003687
- S. Permeh, M.E. Boan, K. Lau, B. Tansel, M. Duncan, In Proceedings of the Corrosion 2019, Paper No. 13461, Nashville, TN, USA, 24–28 March 2019; NACE International: Houston, TX, USA, 2019.
- S. Permeh, B. Li, M. Echeverría, B.Tansel, K. Lau, M. Duncan,In Proceedings of the Corrosion 2018, Paper No. 11529, Phoenix, AZ, USA, 15–19 April 2018; NACE International: Houston, TX, USA, 2018.

Chapter 6

- S. Permeh, M. Echeverria, K. Lau, M. Duncan, In Digital Proceedings of the Corrosion 2020, Paper No. 14831, NACE International: Houston, TX, USA, 2020.
- S. Permeh, K. Lau, M. Echeverria, B. Tansel, M. Duncan, 2020, ASCE Journal of Materials in Civil Engineering, V.32, Issue 7, July 2020. DOI: 10.1061/(ASCE)MT.1943-5533.0003257
- S. Permeh, K. Lau, B. Tansel, M. Duncan, 2020, Construction and Building Materials Journal, V. 243,118209, May 2020. DOI: 10.1016/j.conbuildmat.2020.118209

Chapter 7

- S. Permeh, K. Lau, M. Echeverria, M. Duncan, 2021, Construction and Building Materials Journal, V. 274,122087, March 2021.DOI: 10.1016/j.conbuildmat.2020.122087
- S. Permeh, K. Lau,, M. Duncan, 2019, Structure and Infrastructure Engineering. V.16, Issue 8, p.1186-1200, Nov 2019. DOI: 10.1080/15732479.2019.1694543
- S. Permeh, K. Lau, M. Duncan, 2019, *Coatings*. V.9. No.8. p.518. August 2019. DOI: 10.3390/coatings9080518

ABSTRACT OF THE DISSERTATION

MICROBIOLOGICALLY INFLUENCED CORROSION OF SUBMERGED STEEL BRIDGE PILES IN NATURAL WATERS IN PRESENCE OF MARINE-FOULING

by

Samanbar Permeh

Florida International University, 2021

Miami, Florida

Professor Kingsley Lau, Co-Major Professor

Professor Berrin Tansel, Co-Major Professor

Recent findings at a Florida bridge showed that submerged steel piles had severe localized corrosion, up to 3" in diameter. Testing indicated strong presence of microbes that can be associated with microbiologically-influenced corrosion (MIC), including sulfate-reducing bacteria (SRB). In addition, the site had heavy marine growth. It was thought that the localized crevice environments created by the macrofoulers support MIC. The objective of the research was to identify (1) if marine fouling can enhance proliferation of bacteria that can support MIC, (2) if macrofouling can affect the efficacy of cathodic protection (CP) to mitigate MIC, and (3) if application of coatings can be used to mitigate the degradation.

Field site visits and review of environmental databases identified common environmental conditions, water chemistry, and micro- and macro-fouling activity. Steel specimens were installed at three estuarial, brackish, and freshwater sites. Microbiological analysis verified that bacteria associated with MIC had developed under the fouling organisms. Testing identified that crevice environments can affect SRB interactions in natural waters. Different modes of nutrient availability allow for SRB activity in supportive environments (including anerobic environments) under foulers. Electrochemical tests showed that MIC can develop under fouling organisms.

Testing was conducted to differentiate the CP currents that develop in the presence of microorganisms under the marine fouling. Results showed that proliferation of the bacteria was not inhibited in the presence of cathodic polarization at -1000 mV_{CSE} and CP alone may not be adequate to mitigate MIC under heavy fouling. It was shown that the cathodic charge was related to the sulfate reduction by SRB, and SRB can be a significant contributor to the electrochemical process for steel corrosion with cathodic polarization. Testing was conducted to identify the mitigation properties of antifouling and polyurea coating in presence of microorganism and marine fouling. Application of electrochemical impedance spectroscopy (EIS) and development of a computational assessment approach identified microbial activity and degradation of an antifouling coating. The results from EIS indicated degradation of the coating due to its self-polishing characteristics and that formation of surface layers associated with SRB can form as biocide components of the coating become depleted.

TABLE OF CONTENTS

CHAPTER PAGE

CHAPTER 1 1
1. INTRODUCTION AND PROBLEM STATEMENT 1

CHAPTER 2 3
2. LITERATURE REVIEW 3
2.1. Microbiologically Influenced Corrosion (MIC) 3
2.1.1. Background 3
2.1.2. Corrosion Mechanisms Related to MIC in Aqueous Environments 5
2.1.3. Characteristics of Bacteria Related to MIC 8
2.1.3.1. Sulfate-reducing bacteria (SRB) 9
2.1.3.2. Metal-reducing bacteria (MRB) 12
2.1.3.3. Slime-producing bacteria (SPB) 13
2.1.3.4. Acid producing bacteria (APB) 14
2.1.4. MIC Diagnosis 14
2.1.4.1. Chemical and Environmental Factors 15
2.1.4.1.a Nutrient Level 16
2.1.4.1.b Temperature and pH 19
2.1.4.1.c Roughness 20
2.1.4.1.d Hydrodynamics 20
2.2. Biofouling and Corrosion 21
2.2.1. Background 21
2.2.2. Macrofouling characteristic 23
2.2.3. Macrofouling and Biofilm 25
2.2.4. Macroorganisms and corrosion 28
2.3. MIC and Fouling Remediation 30
2.3.1. Cathodic Protection 30
2.3.2. Coating application 32

CHAPTER 3 34
3. OBJECTIVE AND APPROACHES 34
3.1. Research Objectives and Approach 34
3.2. Hypothesis 35

CHAPTER 4 36
4. CASE STUDY (SR-312 OVER MANTAZAS RIVER, FL) 36
4.1. Background 36
4.2. Water Quality 38
4.2.1. Field Testing 38
4.2.2. Review of Florida Environmental Database 41
4.2.3. Comparative Florida Natural Waters 45

CHAPTER 5 47
5. BIOTIC CONDITION TO SUSTAIN SRB IN MARINE FOULING CONDITION 47
5.1. Introduction 47
5.2. Methodology 48
5.2.1. Laboratory Testing 48
5.2.1.1. Test Setup 48
5.2.1.2. Microbial Activity 54
5.2.1.3. Electrochemical Testing 55
5.2.1.4. Post Test Analysis 56
5.2.2. Field Testing 56
5.2.2.1. Test Setup 56
5.2.2.2. Microbial Activity 57
5.2.2.3. Electrochemical Testing 59
5.2.2.4. Post Test Analysis 60
5.3. Results and Discussion for Laboratory Testing 60
5.3.1. Microbiological Activity 60
5.3.1.1. Chemical Oxygen Demand 60
5.3.1.2. Sulfide Production 63
5.3.1.3. Microbiological Analysis 68
5.3.2. Corrosion Development 70
5.3.2.1. Open-Surface 70
5.3.2.2. Crevice 74
5.3.3. General Discussion 75
5.3.4. Electrochemical Impedance Spectroscopy 76
5.3.5. Visual Assessment 84
5.4. Results and Discussion for Field Testing 86
5.4.1. Surface Fouling Condition 86
5.4.2. Corrosion Development 89

CHAPTER 6 93
6. MITIGATION OF MIC IN PRESENCE OF MARINE FOULING CONDITION BY CATHODIC PROTECTION 93
6.1. Introduction 93
6.2. Methodology 95
6.2.1. Laboratory Testing 95
6.2.1.1. Test Setup 95
6.2.1.2. Microbial Activity 96
6.2.1.3. Electrochemical Testing 97
6.2.1.4. Post Test Analysis 98
6.2.2. Field Testing 98
6.2.2.1. Test Setup 98
6.2.2.2. Electrochemical Testing 100
6.2.2.3. Post Test Analysis 102
6.2.2.4. Microbial Activity 103
6.3. Results and Discussion for Laboratory Testing 104
6.3.1. Electrochemical cathodic and anodic charge 104
6.3.2. Microbiological activity 109
6.3.2.1. Chemical Oxygen Demand 109
6.3.2.2. Sulfide Production 110

6.3.2.3. Microbiological Analysis 112
6.3.3. Visual Assessment 113
6.3.4. Cathodic reactions 114
6.4. Results and Discussion for Field Testing 117
6.4.1. Field Electrical Potential Measurements 117
6.4.2. Field CP Current Measurements 120
6.4.3. Microbial Growth in Presence of CP 123
6.4.4. Steel Corrosion under CP in Presence of Fouling 124
6.4.4.1. Mass Loss for Field Specimens 124
6.4.4.2. Surface Conditions of Field Specimens 128

CHAPTER 7 130
7. MITIGATION OF MIC IN PRESENCE OF MARINE FOULING CONDITION BY COATING 130
7.1. Introduction 130
7.2. Methodology 131
7.2.1. Laboratory Testing 132
7.2.1.1. Test setup 132
7.2.1.2. Microbial Activity 133
7.2.1.3. Electrochemical Testing 134
7.2.1.4. Post Test Analysis 135
7.2.2. Field Testing 135
7.2.2.1. Test Setup 135
7.2.2.2. Microbial Activity 137
7.2.2.3. Electrochemical Testing 137
7.2.2.4. Post Test Analysis 138
7.3. Results and Discussion for Laboratory Testing 139
7.3.1. Microbiological Activity 139
7.3.2. Electrochemical Measurements 141
7.3.3. EIS (Impedance response) 143
7.3.3.1. High-Frequency Impedance Behavior 149
7.3.3.2. Intermediate Frequency and Biofilm Development 152
7.3.3.3. Low-Frequency Behavior 153
7.3.4. Visual Observation and Surface Analysis 155
7.4. Results and Discussion for Field Testing 158
7.4.1. Surface Fouling Condition 158
7.4.1.1. Site I. Matanzas River 159
7.4.1.2. Site II. Downstream Alafia River 160
7.4.1.3. Site III. Upstream Alafia River 161
7.4.2. Microbiological Analysis 162
7.4.3. Corrosion development 163
7.4.3.1. OCP 163
7.4.3.2. LPR 164
7.4.3.3. EIS 165
7.4.4. Electrochemical impedance response analysis for antifouling coated coupons 166
7.4.5. Surface degradation analysis for Antifouling coated coupons 174

CHAPTER 8 177
8. CONCLUSIONS 177
8.1. Biotic condition to sustain SRB in marine fouling condition 177
8.2. Mitigation of MIC in presence of marine fouling condition by cathodic protection 178
8.3. Mitigation of MIC in presence of marine fouling condition by coating 179

REFERENCES 182

APPENDIX 197

VITA 199

LIST OF TABLES

TABLE PAGE

Table 2.1. Microbial classification base on Temperature 20

Table 2.2. Main hard and soft marine growths (Lehaitre, 2008; Clapp, 1948) 24

Table 4.1. Bridge inspection findings of steel piles 37

Table 4.2. Water sampling location 39

Table 4.3. Microbiological analysis of water samples 40

Table 4.4. Chemical analysis results of water samples 40

Table 4.5. Field dissolved oxygen, pH and water temperature 40

Table 4.6. Water sample conductivity 41

Table 4.7. Water quality data of the case study site from 1996 to 2016. 42

Table 5.1. Laboratory test parameters 49

Table 5.2. Laboratory test conditions 50

Table 5.3. Compositions of modified Postgate B (MPB) medium 50

Table 5.4. Initial Survey of Selected River Water Characteristics. 58

Table 5.5. Experimental Test Condition 59

Table 5.6. Surface SRB levels on open-surface and crevice specimens 69

Table 5.7. Surface bacteria population on field test coupons (replicate test coupons) 88

Table 6.1. Experimental test condition 98

Table 6.2. Field test conditions for CP testing 99

Table 6.3 Estimated values of parameters for power function 106

Table 6.4. Terminal bacteria concentrations (population per mL) for laboratory test samples. 112

Table 6.5. Uncoupled electrochemical potential (mV_{CSE}). 118

Table 6.6. Cathodic protection electrochemical potential (mV_{CSE}) and current (mA) 119

Table 6.7. Cathodic protection E_{IO} and E_{OFF} 119

Table 6.8. Surface bacteria counts (CFU/mL) for field testing. 124

Table 7.1. Experimental Test Conditions. 136

Table 7.2. Bacteria count per mL for laboratory coated specimens. 141

Table A1. Resolved impedance parameters from equivalent circuit fitting for laboratory coating samples. 197

Table A2. Resolved impedance parameters from equivalent circuit fitting for field antifouling coated samples. 198

LIST OF FIGURES

FIGURE		PAGE
Figure 1.1.	Picture of a Florida bridge over Matanzas R. with corrosion of steel piles.	1
Figure 1.2.	Picture of corrosion pits on submerged steel piles and heavy marine biofouling	2
Figure 2.1.	Sequence of Events in Marine Biofouling	23
Figure 3.1.	Test Approach	35
Figure 4.1.	Underwater image of a hole on a steel pile due to corrosion.	36
Figure 4.2.	Cumulative fraction of the steel H-Pile Corrosion.	38
Figure 4.3.	Underwater images of steel piles at SR-312 Bridge over Matanzas River.	38
Figure 4.4.	Chemical analysis of water samples.	43
Figure 4.5.	Salinity, conductivity and dissolve oxygen of water samples.	45
Figure 4.6.	Examples of Florida water bodies that may support MIC.	46
Figure 5.1.	Schematics of working electrodes in test setup A and B.	51
Figure 5.2.	Laboratory test cells.	52
Figure 5.3.	Typical Outdoor Exposure Test Rack at Three Site	57
Figure 5.4.	COD results for laboratory (A) open-surface and (B) laminate and porous crevice specimens.	63
Figure 5.5.	Apparent sulfide production.	65
Figure 5.6.	Assessment of SRB activity by sulfide concentration and COD.	67
Figure 5.7.	Duration of potential ennoblement of (A) open-surface and (B) crevice specimens (>-700mV$_{SCE}$)	71
Figure 5.8.	Calculated corrosion current density for (A) and (B) open-surface and (C) and (D) crevice specimens.	73
Figure 5.9.	Nyquist impedance diagrams for open-surface specimens from (A) and (B) test setup A, and (C) and (D) test setup B	77
Figure 5.10.	Nyquist impedance diagrams for (A), (B), (C) and (D) laminate and (E) and (F) porous crevice specimens.	78
Figure 5.11.	Schematic of equivalent circuit analogs	80

Figure 5.12. Bode impedance diagrams for open-surface specimens in the (A), (B), (C) and (D) de-aerated condition and (E), (F), (G) and (H) naturally-aerated condition..... 81

Figure 5.13. Total impedance values at 100mHz for (A) open-surface and (B) crevice specimens. 84

Figure 5.14. Photos of test specimens after removal from solution and steel surface appearance after cleaning. 85

Figure 5.15. Photo of field test coupons after exposure and after partial cleaning. 86

Figure 5.16. Example of Under Fouling Surface Condition. 88

Figure 5.17. Magnified view of surfaces of specimens from (A) Site I, (B) Site II, and (C) Site III. 90

Figure 5.18. Calculated nominal corrosion rates of steel exposed in the field testing. 91

Figure 6.1. Test Setup B test cells under cathodic polarization. 97

Figure 6.2. Typical marine fouling observed on field exposure test racks at (A) Site I and (B) Site II. 100

Figure 6.3. CP current test configurations for coupled steel and zinc anodes. 101

Figure 6.4. Cumulative cathodic charge measurements for the laboratory samples at polarization levels of -850 mVSCE and -950 mVSCE. 107

Figure 6.5. Cumulative cathodic charge at 1 and 7 days for different geometric conditons. 108

Figure 6.6. Cumulative anodic charge measurement for laboratory samples at polarization level of -500 mVSCE. 109

Figure 6.7. Range of chemical oxygen demand measured in the laboratory test samples at polarization levels -500 mVSCE, -850 mVSCE , -950 mVSCE and OCP condition. 110

Figure 6.8. Apparent sulfide production rate in laboratory inoculated test samples at polarization levels -500 mVSCE, -850 mVSCE , -950 mVSCE. 111

Figure 6.9. Laboratory samples (de-aerated condition) after testing and after sample cleaning. 113

Figure 6.10. Cumulative charge associated with sulfide production and net cathodic reaction rates. 116

Figure 6.11. XRD pattern for field exposed specimens.. 120

Figure. 6.12. CP current (A) and current density (B) distribution for field exposed samples by three configurations. 121

Figure 6.13. Apparent corrosion rate for field exposed specimens by depth (Lower bound apparent CP corrosion rates shown for Site II). 126

Figure 6.14. Comparison of corrosion rates estimated by mass loss and plate thickness at (A) Site I and (B) Site II. 127

Figure 6.15. Surface conditions for test coupons exposed at Site I and Site II before and after cleaning. 128

Figure 6.16. Magnified view of surfaces of field exposed specimens. 129

Figure 7.1. Laboratory test setup. 133

Figure 7.2. Laboratory Test Setup Conditions. 133

Figure 7.3. Example of Marine Growth on the Test Rack Setup in Site I. 137

Figure 7.4. Example of Laboratory Electrochemical Test Setup. 138

Figure 7.5. Chemical oxygen demand for laboratory coated specimens. 139

Figure 7.6. Sulfide production due to sulfate-reducing bacterial (SRB) activity. 140

Figure 7.7. Corrosion potential and corrosion current density for laboratory coated specimens. 143

Figure 7.8. Electrochemical impedance spectroscopy Nyquist diagrams for coated steel samples immersed in inoculated and non-inoculated solutions at day 18. 144

Figure 7.9. Idealized electrochemical characteristics of coated steel specimens. 145

Figure 7.10. Example of decoupled fitted and calculated impedance response for antifouling non-inoculated (1) and inoculated (2) test specimens from impedance at day 4. 146

Figure 7.11. Bode and −Z” plots of measured impedance for antifouling non-inoculated (1) and inoculated (2) test specimens at day 4. 1 MHz > fm > 1 Hz. 147

Figure 7.12. Correlation of τ from equivalent circuit fitting and ωm resolved from decoupled impedance. (A). Antifouling coating. (B). Polyurea coating 147

Figure 7.13. Dispersion of characteristic time constants for isolated impedance components.. 148

Figure 7.14. Total Impedance at 1 Hz and 1 MHz for laboratory coated samples. 149

Figure 7.15 Calculated coating capacitance. 151

Figure 7.16. Resolved nominal coating pore resistance. 151

Figure 7.17. Calculated biofilm capacitance. Arrow indicates that no biofilm developed in the non-inoculated test conditions..... 153

Figure 7.18. Calculated interface capacitance and resolved interface resistance.. 155

Figure 7.19. Surface condition of coated laboratory specimens after testing..... 156

Figure 7.20. Representative metallographic cross-section of antifouling coated samples. 157

Figure 7.21. XRD diffractograms for anti-fouling coated specimens. 158

Figure 7.22. Surface appearance of field exposed antifouling-coated coupons 159

Figure 7.23. Surface appearance of field-exposed polyurea-coated coupons..... 159

Figure 7.24. Surface Bacteria Population ($CFU.mL^{-1}$) after Outdoor Exposure at Three Sites..... 162

Figure 7.25. Corrosion potential of field-exposed coated steel coupons at three sites..... 163

Figure 7.26. Corrosion Current Density of Polyurea-coated Steel Coupons at Three Site 165

Figure 7.27. Total Impedance at 1Hz for Polyurea-coated Steel Coupons at Three Sites..... 166

Figure 7.28. Nyquist diagrams from EIS for antifouling-coated coupons at three sites..... 167

Figure 7.29. Electrochemical impedance equivalent circuit analogs. 168

Figure 7.30. Example of decoupled fitted and calculated impedance response for coated coupon exposed at Site I at 0.9m and 2.5m..... 170

Figure 7.31. Bode and −Z” plots of measured impedance for f coated coupon exposed at Site I at (A) 0.9m and (B) 2.5m 170

Figure 7.32. Resolved time constants for separate impedance components..... 172

Figure 7.33. Resolved coating, biofilm and steel interface impedance parameters..... 173

Figure 7.34. Representative metallographic cross-section of antifouling coated samples. 175

Figure 7.35. Representative metallographic cross-section of antifouling coated samples in presence of the hard foulers. 175

Figure 7.36. XRD diffractograms for anti-fouling coated specimens. 176

CHAPTER 1

1.INTRODUCTION AND PROBLEM STATEMENT

Microbiologically influenced corrosion (MIC) can develop on submerged steel structures that have suitable physical and environmental conditions that support proliferation of certain bacteria (Dexter,1998; Little and Lee, 2009). Civil structures placed in marine environments are also susceptible to physical, chemical, and biological processes that can result in the adverse accumulation of macroorganisms (Hellio et al.,2009).

Recent findings at a Florida bridge (Figure 1.1) showed that submerged steel piles had severe corrosion. Localized corrosion cells/pits were of up to 3" in diameter and penetrated through the steel thickness (Figure 1.2). Sampling and testing of water associated with the anomalous corrosion observations indicated strong presence of microbial growth that can be associated with microbiologically influenced corrosion (MIC). ln particular, anaerobic sulfate reducing bacteria (SRB), acid producing bacteria (APB), and slime producing bacteria (SPB) were recovered in cultures produced from the steel and water samples. The water samples also showed high sulfate and chloride levels. In addition to the microorganisms that can cause corrosion, the affected site also had heavy marine growth (Figure 1.3). Although the role of the macrofoulers on the corrosion of the steel piles was not clear, the macrofoulers may have been associated with the corrosion development. It was thought that the effect of localized crevice environments created by the presence of the macrofoulers may support MIC.

Figure 1.1. Picture of a Florida bridge over Matanzas R. with corrosion of steel piles.

MIC has been identified in many environments associated with vital infrastructure including buried pipelines, marine structures, and waste water facilities. A vast array of various forms of microbial organisms has been reported to be associated with MIC. As such, corrosion and degradation mechanisms can vary significantly depending on biological and chemical characteristics of microbial growth and activity, as well as the interaction with the environment for nutrient supply and sustainable growth.

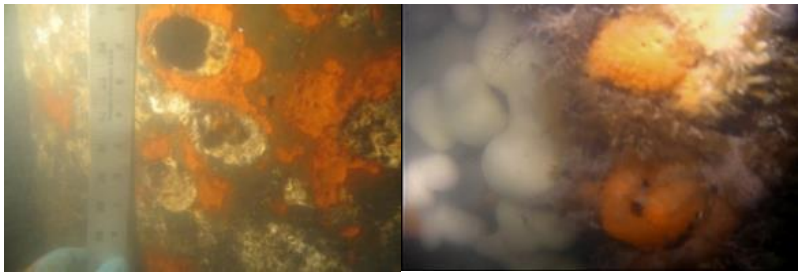

Figure 1.2. Picture of corrosion pits on submerged steel piles and heavy marine biofouling

MIC has not been a major durability concern for Florida coastal and inland bridges, but the recent findings compounded by greater service life performance expectations for transportation infrastructure has made determination of corrosion and material degradation susceptibility of embedded and immersed bridge components to degradation by microbial activity of vital interest. There are several important issues to be addressed to determine the corrosion susceptibility of steel bridge structure in natural water to MIC including to determine if the water environmental chemical condition would support microbial activities that can be associated with MIC and if chemical and environmental conditions and physical sheltering by macrofouler would affect SRB proliferation through different nutrient availability and aeration. Efforts to answer these issues are needed identify appropriate remediation and maintenance decisions to be made including efficacy of cathodic protection and the use of coatings.

CHAPTER 2

2.LITERATURE REVIEW

2.1. Microbiologically Influenced Corrosion (MIC)

2.1.1 Background

MIC is an important degradation mechanism for materials in a wide variety of industries, but limited information has been readily disseminated in the literature on MIC of bridge infrastructure in marine environments. According to Lee et al. (1995) and Videla and Herrera (2009), degradation of marine steel infrastructures such as bridges, wharfs, platforms and pipeline systems associated with MIC accounted for 20% of corrosion costs. Considerable research has been conducted to understand the phenomenon of MIC; however, even though much research has addressed the phenomenon for materials exposed in aqueous environments, the often narrow field of individual studies and the complexities involved with MIC presents difficulties to account for the wide variabilities in microbial biology as well as environmental, physical, and chemical factors (Borenstein, 1994; Mansfeld, 2007; Melchers 2005, 2014).

Microorganisms associated with MIC are microscopic and can include bacteria, microalgae and fungi. Some literature suggest that bacteria and fungi are of particular interest for MIC (Little and Lee, 2014), however, environmental parameters are important to sustain microbiological activities. The main types of bacteria traditionally studied in MIC have been SRB (anaerobic), sulfur/sulfide-oxidizing bacteria (SOB) (aerobic), iron/manganese–reducing bacteria (IRB) (aerobic) and bacteria secreting organic acids and slime (Beech et al., 2000). Microorganisms in natural waters have the ability to adhere to most surfaces. There, they can reproduce, and many can produce exopolymers, also called extracellular polymeric substance (EPS) (Geesey et al., 1986). Some investigations have mentioned that a consortium of microorganisms is involved in the formation of biofilms and consequently different types of microorganisms can live together as a

small unit (at least temporarily) (Kobrin, 1976; Linhardt, 2006; Geesey, 1993). The biofilm is constituted by immobilised cells (Dexter and La Fontaine, 1998) or EPS (Rajasekar and Ting, 2011) developed on the metal interface. EPS also mediate the adhesion to surfaces and can allow formation of a cohesive, three-dimensional polymer network that interconnects immobilizes biofilm cells. Under the biofilm, an occluded space may form where the chemical environment can differ from the bulk solution (Rajasekar and Ting, 2011).

Corrosion of steel can take place under the biofilm at the metal to solution interface (Melchers, 2014). The corrosion involves electrochemical processes where the microorganisms can influence the corrosion kinetics. In general, for MIC to occur, an energy source, a carbon source, an electron donator, an electron acceptor and water, are required (Melchers, 2014). The required energy and nutrients are found from the surrounding environment. At cathodic sites, electrons are accepted from the anodic site (Rajasekar and Ting, 2011). More complicated steps involving charge transfer related to biotic reactions can also occur. For example, MIC due to SRB involves the reduction of inorganic sulfate ion in the presence of hydrogen or organic matter to produce hydrogen sulphide (Javaherdashti, 2008).

MIC does not necessarily occur in the presence of biofilm alone. The wide variety of microorganisms and their interaction with the environment and other organisms can create different electrochemical conditions that can accelerate corrosion and conversely, in some conditions, inhibit corrosion (Videla and Herrera, 2009). In addition, the chemical concentration at the metallic substrate can change significantly due to the extent of biofilm growth as the film can create diffusion conditions for oxygen and nutrients to the metallic surface (Javaherdashti, 2008). Once the biofilm is formed and developed, the outer cells start to consume the nutrients available to them more rapidly than the ones located deeper within the biofilm. Consequently the activity and growth rate of the latter are reduced. Then, while the outer cells increase in number, the biofilm starts acting

as a net, trapping more and more particles (organic and inorganic), thus increasing the biofilm thickness even further (Liu et al., 2000). Factors such as pH, dissolved oxygen, etc. may be drastically different inside and outside the biofilm, thus causing changes in the electrochemistry of the biofilm-metal system. Differential chemistry and bioactivity can lead to a phenomenon known as potential ennoblement (documented for a range of metals and alloys at different salinities) that can result in an increase pitting susceptibility (Geesey, 1993, Dexter and La Fontaine, 1998; Dickinson, 1996; Videla, 1996). This would also coincide with possible changes in the cathodic reaction on the metal due to the microbial activity within the biofilm.

2.1.2. Corrosion Mechanisms Related to MIC in Aqueous Environments

Several damage mechanisms for MIC have been proposed in the literature. Mansfield (2007) pointed out that MIC leads to an increase in corrosion rates owing to the presence of bacteria that accelerate the rates of the anodic and/or cathodic corrosion reaction (Mansfield, 2007). Potekhina et al., 1999 suggested that there are two types of bacteria according to their capacity to induce or inhibit corrosion. The bacteria that causes corrosion are those which create an additional galvanic coupling between themselves and the metal. Under anaerobic conditions, the bacteria is the cathode and the metal is the anode and electrons will flow from metal to bacteria. Consequently, the open circuit potential of the metal increases and moves to more positive values as long as the bacteria are active. Hydrogen consuming bacteria like SRB, certain nitrate-reducing bacteria and phototrophic bacteria are some examples of corrosive bacteria.

SRB has been widely associated with MIC. It is known that SRB easily reduce inorganic sulfates into sulfides in the presence of hydrogen or organic matter and the process is facilitated on iron surface (Mansfeld, 2007), but there has been considerable controversy regarding the mechanism of anaerobic microbial corrosion. In 1934, Kuhr proposed the cathodic depolarization mechanism where it was posited that SRB removes atomic hydrogen from the iron surface (by the

hydrogenase enzyme), providing cathodic reaction to accommodate accelerated corrosion of iron. However, the validity of this mechanism has been questioned as corrosion has been observed on hydrogenase negative strain of SRB. Also, the reaction products (such as hydrogen sulfide and ferrous sulfide) also could act as depolarizing agents, which can account for high rate of corrosion. Costello (1974) also proposed that hydrogen sulfide, rather than the hydrogen ion, was the cathodic reactant. King and Miller (1971) indicated that the addition of chemically prepared ferrous sulfide to the system encourage depolarization. However, the cathodic reaction is considered to be either activation or concentration polarization controlled and hydrogenase may therefore have some role in removing molecular hydrogen and ensuring the supply of hydrogen sulfide for the cathodic reaction. Iverson (1984) suggested a more complex mechanism involving both sulfide and phosphide. Starkey (1985) suggested that several processes concerning the effect of ferrous sulfide, sulfur, ferrous hydrate, phosphide and other product are involved in anerobic corrosion. Other research supported the classical theory (Cord-Ruwisch ,1986; Pankhania et al.,1986; Hardy,1983).

Recent works identified mechanisms involving direct electron transfer from the steel by the SRB (Gu et al., 2019; Xu et al., 2014; Venzlaff et al., 2013). Gu et al., 2009 described the bio-electrochemistry for SRB-MIC with low carbon sources where sulfate-reduction reactions are facilitated by SRB utilizing extracellular electrons from the steel transported to the bacteria cell. As described there ,where local anodes that develop on the steel surface are supported by sulfate-reduction reactions by SRB utilizing extracellular electrons from the steel transferred to the bacteria cell by an extracellular electron transfer, EET, mechanism (Gu et al., 2009; 2019; Xu et al., 2014; Jia et al.,2019a;2019b). The corrosion process generally conforms to the cathodic depolarization theory by Kuhr,1934, by that describes the metabolic activities of the microorganisms to support iron oxidation, where atomic hydrogen on the iron surface is depleted and the electrons from the iron oxidation is used in intracellular biocatalysis required for the cathodic reactions within the biofilm (Jia et al., 2019a;2019b). However Work by Venzlaff et al., 2013 showed results that show

similar outcomes for the corrosion behavior (such as increase in potential and enhanced current densities) but attributed microbial corrosion to a corrosive SRB that mediates direct electron uptake by the cell proteins.

Research by Herrera and Videla (2009) indicated that IRB can induce and enhance corrosion in the absence or presence of other bacteria. The common mechanism to promote corrosion is through reduction of Fe^{3+} corrosion products, which can subsequently exposes the metal surface to the corrosive medium. In addition, these bacteria are able to create anaerobic zones promoting SRB growth within biofilms where both bacteria are present (Herrera and Videla, 2009). Other authors that investigated steel corrosion influenced by anaerobic biofilm in natural sea water detected SRB and IRB bacteria in the anaerobic biofilm under the rust layer on carbon steel. SRB was located in the inner rust layer and IRB in middle and outer layers. Green rust was the main component in the inner rust layer, and both SRB and IRB contributed to the formation of green rust. The isolated SRB bacteria accelerated corrosion. However, the mixed anaerobic bacteria (SRB and IRB) was shown to have inhibited corrosion in part related to the formation of green rust under the biofilm (Duana et al., 2008).

Indeed, other studies have observed that large bacteria populations can inhibit corrosion of different metals and alloys in many corrosive environments (Mansfield, 2007). The other group of bacteria that inhibit corrosion both in aerobic (Pederson and Hermansson, 1991) and anaerobic conditions (Jayaraman et al., 1997) removes oxygen, thus leading to a drop in the cathodic reaction and to a slowdown of metal dissolution. In this case, the protective bacteria act as an anode and the metal as a cathode. Videla and Herrera (2009) indicated that corrosion inhibition can occur at metal surfaces with biofilm, when the extracellular polymeric substances (EPS) of the biofilm impede the dissolution of Fe^{2+} corrosion products. Thus, the EPS behaves as a barrier between the metal and the environment (Videla and Herrera, 2009). The environmental characteristics of the

metal/biofim/medium interface and its surroundings (pH, ionic composition, oxygen levels, EPS distribution) will control the chemical and physical nature of protective layers and may change microbial effects on the metal behavior from corrosive to protective (Herrera and Videla, 2009).

The microbial corrosion inhibition is not usually linked to a single mechanism or to a single species of microorganisms. They can induce corrosion inhibition in accordance with two general mechanisms or their combination: 1) neutralizing the action of corrosive substances present in the environment and 2) forming protective films or stabilizing pre-existing protective films on a metal. However, authors have stressed that in some cases inhibitory action of bacteria can be reversed to a corrosive action in bacterial consortia located within biofilm thickness (Videla and Herrera, 2009).

2.1.3. Characteristics of Bacteria Related to MIC

The presence of microorganisms alone in a system does not necessarily indicate propensity for corrosion development. Some literature suggests that bacteria and fungi are of particular interest for MIC (Little and Lee, 2014). However, environmental parameters are important to sustain the microbiological activities. The type of bacteria can determine specific nutrient and environmental requirements.

There is a wide variability in microbiological organisms involved in MIC. The role of these microorganisms can vary significantly depending on environmental conditions that support their proliferation and therefore, degradation mechanisms can be complex. Also, the type of bacteria can determine specific nutrient and environmental requirements. In 1999, Becch et al., classified the types of organisms (related to corrosion failures of materials) into: sulfate-reducing bacteria (SRB), iron-oxidizing/reducing bacteria (IOB or IRB), manganese oxidizing bacteria, sulfur-oxidizing bacteria (SOB), and bacteria that secret organic acids and extracellular polymeric substances (EPS) or slime. In 2012, Rim-Rukeh reported that steel coupons corroded due to MIC

at a rate of 0.79 mpy after 6920 hours of test periods. Total bacteria population varied from 10^5 CFU/ml to 10^6 CFU/ml in all water samples analyzed, indicating adequate bacterial population for microbiologically influence corrosion activity. It was suggested that SRB levels of 10^4 cell/cm^3 is a clear indication of possible corrosion problems, while a relative population of 10^6 cell/cm^3 of microorganisms indicate potential corrosion problems in an environment (Costello, 1969).

2.1.3.1 Sulfate-reducing bacteria (SRB)

SRB are the organisms mostly identified with MIC (Hu, 2004; Little, 2009). SRB can exist in both marine and fresh water environments. A marine strain of SRB can gradually be converted to fresh water organism if the transition from salt water to a fresh water environment is not too abrupt (Donham, 1976). They are non-fermentative anaerobes that obtain their energy for growth from the oxidation of organic substances and using inorganic sulfur oxy-acids (sulfate) or nitrate as terminal electron acceptors and reducing sulfate to sulfide/hydrogen sulfide (Feio et al., 2000). SRB include all unicellular bacteria that can reduce sulfate to sulfide. The sessile SRB are responsible for localized corrosion of mild steel in industrial and aquatic environments (Hu, 2004; Costerton and Boivin, 1991). Several corrosion mechanisms have been attributed to SRB, including cathodic depolarization by the enzyme dehydrogenase, anodic depolarization, release of exopolymers capable of binding metal ions, stress corrosion cracking, hydrogen induced cracking or blistering, and production of metal sulfides. Recent reviews suggest that SRB can influence a number of corrosion mechanisms simultaneously (Little, 2009).

SRB can grow in conditions within pH 5-10 and temperature 5-50°C. The best temperature ranges from 25°C to 40°C (Javaherdashti, 1999). Also, they can tolerate pressures up to 500 atmospheres (Narayan, 2012). The corrosion process by SRB bacteria is characterized by the formation of black crusts and metal pitting (Donham, 1976). The general energy limitation for the growth of SRB bacteria is the carbon source, but in many systems with mixed population of

organisms, the carbon source is not restrictive and the limitation is sulfate ions. The carbon source for SRB are always low molecular weight compounds such as organic acids (lactate, pyruvate, formate), volatile acids (acetate), and alcohols (ethanol, propanol, methanol, and butanol) (Hao et al., 1996). SRB needs a supply of sulfates for reduction to sulfides for their metabolism.

The counts obtained from water sampling are usually only an approximate indication of the actual bacterial population in the system (Donham, 1976). As SRB can be found in rich sulfate environment (Yuzwa, 1991), the sulfate concentration in a system has a direct influence on the growth and activity of SRB and the amount of sulfide produced (Sanders, 1988). It was found that the initiation of biocorrosion due to SRB only occurred in the presence of sulfate species. As such, the metabolic activity of SRB that causes accumulation of sulfide near metal surfaces can be evidence of potential SRB presence in the system(Little, 2009). Determination of total sulfide as H_2S, HS^-, S^{2-} , in water samples can be used to identify SRB activity (Melchers 2007). Also, Blackburn, 2004 pointed out that the presence of black color and odorous iron sulfide corrosion product (associated with orange bloom) can be a good indicator for MIC by SRB (Blackburn, 2004).

Fonseca et al., 1998 tested the corrosion of mild steel under different media both with and without sulfate ions. The corrosion current density showed an enhancement due to the SRB presence in the lactate/sulfate medium. On the other hand, Castaneda et al., (2008), characterized the electrochemical evolution of the interface formed in carbon steel samples exposed to artificial seawater with nutrients, in the presence and absence of mixed cultures that contained SRB. The anodic dissolution of carbon steel was the dominant process under the abiotic system over time, while the oxygen diffusion limited the corrosion process in the presence of SRB. Phosphorous-based corrosion products were detected in both systems; however, under SRB-biofilm presence the sulfides were also evident. Mohanty et al. (2000) also found that a high sulfate concentration in the

medium could inhibit the sulfate reduction rate of SRB. SRB showed positive growth rate with the increase of biomass and N_2 concentration. In addition, the increase of sulfate and phosphate concentration decreased the bacterial growth.

The relationship between SRB and oxygen is complicated and will influence the corrosion process. The anaerobic bacteria may survive with temporarily exposure to oxygen and become active under anaerobic conditions. However, some genera can still grow at low dissolved oxygen concentrations (Hu, 2004; Hardy and Hamilton, 1981; Abdollahi et al., 1990). Although the oxygen content of seawater is in the range from 5 to 8 ppm, anaerobic microorganisms may survive in anaerobic micro-niches until conditions are suitable for their growth (Little, 2009). If the aerobic respiration rate within a biofilm is greater than the oxygen diffusion rate, the metal-biofilm interface can become anaerobic and provide a niche for sulfide production by SRB (Hamilton, 2003). The critical biofilm thickness required to produce anaerobic conditions depends on availability of oxygen and the respiration rates of organisms in the biofilm. In 2002, Iversen noted that the critical DO concentration for sulfate reduction in wastewater plants was 0.1 to 1 mg/L. It was also mentioned that above a DO concentration of 1 m/L, sulfate reduction might be inhibited because of increase redox potential and inhibition of *Desulfovibrio*. Hamilton (2003), reported on anaerobic corrosion of carbon steel by SRB and concluded that oxygen was required for aggressive SRB-influenced corrosion. In corrosion of mild steel by SRB, oxygen is the ultimate electron acceptor through a series of coupled redox reactions. In the classical cathodic depolarization theory, the corrosion process is related to the depletion of atomic hydrogen on the iron surface by the hydrogenase enzyme produced by the SRB and the cathodic reactions support the corrosion of iron (Kuher,1934).

The interaction of SRB with corrosion process is represented in the following reactions Eq 2.1-2.7 (Borenstein,1994):

$4\ Fe \rightarrow 4\ Fe^{2+} + 8\ e^-$ (anodic reaction) (2.1)

$8\ H^+ + 8\ e^- \rightarrow 8\ H$ (cathodic reaction) (2.2)

$SO_4^{2-} + 8\ H \rightarrow S^{2-} + 4H_2O$ (cathodic depolarization by SRB) (2.3)

$8\ H_2O \rightarrow 8\ OH^- + 8\ H^+$ (dissociation of water) (2.4)

$2\ H^+ + S^{2-} \rightarrow H_2S$ (reversible reaction) (2.5)

$Fe^{2+} + S^{2-} \rightarrow FeS$ (anode corrosion product) (2.6)

$3\ Fe^{2+} + 6\ (OH)^- \rightarrow 3\ Fe(OH)_2$ (anode corrosion product) (2.7)

2.1.3.2. Metal-reducing bacteria (MRB)

As early as 1980, it was shown that corrosion reactions of metals can be affected by a variety of types of bacteria (such as *Pseudomonas* and *Shewanella*, which can facilitate manganese and/or iron oxide reduction (Obuekwe et al., 1981; Myers and Nealson, 1988)). While Mn (manganese) is soluble, all the various manganic (Mn^{2+}) oxidized forms are insoluble. Microbial deposits of manganese oxide on stainless steel samples exposed to freshwater caused an increase in the corrosion potential (Ecorr) and in the cathodic current density (Little, 2009; Dickinson, 1996).

Iron-reducing bacteria (IRB) are another group of microorganisms, which are of interest in MIC. This type of bacteria at near neutral pH, use insoluble ferric iron ion (Fe^{3+}) compounds as an energy source, reducing them into soluble ferrous ion (Fe^{2+}) compounds, exposing the metal beneath a ferric oxide protective layer to the corrosive environment (Javaherdashti, 2008). Oxygen content is very important for their number detection, (Javaherdashti, 2008). In some cases, IRB results in the formation of dense tubercles of filamentous iron oxides.

Some IRB species require ferric iron under anaerobic condition and some use nitrate for anaerobic respiration. Myers and Nealson, 1988 reported that IRB can use oxygen, Fe (III), Mn (IV), NO^{3-}, NO^{2-}, $S_2O_3^{2-}$, SO_3^{2-} and others. In a mixed population of microorganism in a biofilm, the redox potential start to decrease as oxygen is consumed so that reduction of nitrate, then manganic, ferric and sulfate ions can occur (Javaherdashti, 2016). IRB are capable of making the environment suitable for SRB growth. Authors have investigated steel corrosion influenced by anaerobic biofilm in natural seawater where SRB and IRB bacteria have been detected in the anaerobic biofilm under the rust layer on carbon steel. SRB was located in the inner rust layer and IRB in middle and outer layer. Green rust has been the main component in the inner rust layer, and both SRB and IRB have affected the formation of green rust. The isolated SRB have accelerated corrosion and the mixed anaerobic bacteria (SRB and IRB) have inhibited corrosion. The main mechanism of corrosion inhibition is the biofilm-induced formation of green rust (Duan, 2008).

2.1.3.3 Slime-producing bacteria (SPB)

Slime-producing microorganisms are also associated with localized attacks of steels (Hu, 2004). These organisms produce large quantities of extracellular polymeric substances (EPS) during their growth within biofilms and covered the steel surfaces. Most common SPB are including *Clostridium* spp., *Flavobactcrium* spp., *Bacilluls* spp., *Desullfovibrio* spp., *Desullfotomaculum* spp. and *Pseudomonas* spp. (Pope et al., 1984). The sticky polymers they produce referred to as "slime" affect the attachment of the cells to the surface and the permeation of substances through the deposit. Microscopic amounts of EPS ($10ng/cm^2$) can induce or provoke the initiation of microbial corrosion of stainless steels in natural seawater (Hu, 2004). The mechanisms of the EPS in the MIC of stainless steels are still not very clear.

2.1.3.4 Acid producing bacteria (APB)

These bacteria can produce large amounts of inorganic or organic acids as by- products during their metabolism, leading to serious corrosion damages. Heterotrophic organic acid produced is referred to as acid producing bacteria (APB). These bacteria have shown to cause the corrosion of carbon steel in some cases (Hu, 2004; Soracco et al., 1988; Little et al. 1988), also the corrosion of cathodically protected stainless steel was reported with certain acetic-producing bacteria. The mechanism of how acids affects the corrosion of mild steel was well understood in the metallurgical literature (Shreir, 1963). The kinds and amounts of acids produced depend on the type of microorganisms and the available substrate molecules.

Inorganic acid-producing bacteria can oxidize elemental sulfur, thiosulfates, metal sulfides and H_2S to sulfuric acid (corrosive). These microorganisms are generically referred to as thiobacilli or sulfur oxidizing bacteria (SOB). The color of the corrosion products is reported to be yellow (Scott, 2004; Hu, 2004).

2.1.4. MIC Diagnosis

Diagnosing and evaluation of MIC requires a combination of microbiological, metallurgical, and chemical analyses. The first step in the diagnosis is to identify relevant microorganisms in the bulk medium (planktonic cells) or associated with corrosion products (sessile cells), as well as information about pit morphology consistent with an MIC mechanism (Little and Lee, 2009). To identify the microorganisms in each particular environment is very important for the understanding of the MIC mechanism. The microorganisms can be classified based on the corrosion product chemistry. The next step is to identify the chemical/physical characteristics of the environment, which supports the growth and activity of bacteria. The chemical composition of the water must have sufficient specific nutrients and the physical properties of the

site must comply with attachment of these organism. Different conditions supporting MIC will be explained in the following section.

2.1.4.1. Chemical and Environmental Factors

The environment and metal characteristics and features such as the presence of alloying constituents) can encourage the growth/attachment of the bacteria). The chemical aspects related to the bulk water are the water temperature, the water nutrients, anions (sulfate, chloride), cations/metal, pH, the oxygen concentration, the alkalinity, dissolved gases (carbon dioxide, hydrogen sulfide, oxygen), TOC (total organic carbon), the turbidity, the conductivity, the redox potential, as well as TDS (total dissolved solid) and TSS (total suspended solid) content. Redox potential (Eh) of water samples is also another important factor in MIC. Rim-Rukeh, 2012 reported Eh values of studied water samples, which ranged from -450 mV to +850mV. The negative side of the spectrum favors methanogenic bacteria and the positive one correspond to iron bacteria (Newman et al., 1991). Negative Eh values obtained are indicative of corrosive environments.

All these parameters are important factors for the MIC (Javaherdashti, 2008). The chemical oxygen demand (COD) is considered a very useful parameter to assess the concentration of electron donors available for sulfate or metal reduction, Low COD would mean a low risk of availability of SRB or other types of reducers such as IRB (Scott et al., 2004). Beech, 2008 confirmed that Biochemical Oxygen Demand (BOD) and COD values were the highest where high levels of sulfur-oxidizing bacteria (SOB) were detected.

Rim-Rukeh, 2012 studied the physico-chemical and biological characteristics of the Orashi River, in order to identify MIC of the steel exposed to this natural freshwater environment. Reported turbidity values of water samples were high and within the range of 18 NTU to 31 NTU. Also TDS and TOC values in all water samples analyzed ranged from 1908 mg/L to 2571 mg/l, and 11.7 -17.1 mg/L, respectively. The relatively high values of turbidity may be the result of both

suspended and dissolved solids in the water, such as silt, finely divided organic and inorganic matters and soluble colored organic compound or erosion of sediments (Rim-Rukeh, 2012). These materials are potential sources of organic carbon, which constitute the bacteria energy source for production of new cellular material. Carbon is the most abundant cell constituent and is found from organic matter (Videla, 1996). High level of turbidity promotes growth of microorganism within ecosystem (Charaklis, 2009, Rim-Rukeh, 2012). The existence of halophilic SRB in waters with high TDS (240,000 mg/L) has been reported (Alhashem et al., 2004). TDS and TOC results will determine the presence of decaying organic matter (leaves). High levels of TDS and TOC provide an excellent condition for bacteria growth (Rim-Rukeh, 2012). Melchers, 2005 showed the nutrient level and chemical condition of water with pH ~8, conductivity ~47000(μS/cm), Nitrate ~0.01 mg/L, Sulfate ~3000 mg/L was indicative of condition which support the high corrosion activity by microorganism.

2.1.4.1.a Nutrient Level

The availability of nutrients and water are essential for survival of microorganisms. It is also an important factor in determining whether the bacterial population will be planktonic or sessile. This would affect the spatial position of bacteria and its ability to attach to surfaces perhaps in biofilm. When the environment is poor in nutrient level, the bacteria may settle on surfaces. In contrast, in rich nutrient environments, bacteria do not need to necessarily settle, so planktonic growth (floating) takes place (Gandy et al.,1980, Enos and Taylor, 1996).

Microorganism need energy, carbon sources, nitrogen, phosphorus and trace elements to survive and grow (Thierry and Sand, 2011). Gandy et al., 1980 has pointed out that carbon, nitrogen, oxygen and hydrogen constitutes 90% of the dry weight of a cell. From them, hydrogen and oxygen comes from the water used by the cell, while carbon, oxygen and nitrogen are the limiting nutrition requirements of the cell (Gandy et al., 1980).

The water needs to have suitable forms of carbon, hydrogen, oxygen, sulfur, phosphorus, potassium, magnesium, calcium, manganese, nitrogen and traces of zinc, cobalt, etc. (Mansfeld, 2007; Little, 2014). Lin and Madida in 2015 studied the role of gram positive *Bacillus sp* in corrosion of steel by biofilm formation. Three nutrient media were chosen including, carbon source (fructose, galactose, or sucrose), $MgSO_4$ and nitrate source (NH_4NO_3 or $NaNO_3$). The results showed different corrosion loss in each media and corrosion retardation in media without any nutrients. Different nutrients can mediate different metabolic pathways resulting in acceleration or mitigation of the corrosion rates.

Carbon occurs in the biosphere in either the reduced (methane, fatty acid, carbohydrate) or the oxidized (alcohol, aldehyde, carbonic acid, carbon dioxide) form. Microorganisms control the carbon cycle by using CO_2 from the air for their cell carbon generation. Producers of carbon include green plants, algae, cyanobacteria, and photosynthetic bacteria (Thierry and Sand, 2011). The generated carbon cell will be degraded by other organisms with the production of carbon dioxide. Also, the incomplete degradation in sediment can cause high accumulation of organic matter in shallow marine areas (Thierry and Sand, 2011).

Nitrogen can be in the form of inorganic ammonium, nitrate, nitrite, and also originally bound nitrogen such as amino acid and can be found in proteins, nucleic acids, amines, and urea (Thierry and Sand, 2011). Some microorganisms with the nitrogenase enzyme like bacteria and cyanobacteria can use nitrogen from the atmosphere to produce ammonia, which is incorporated in cell constituents. After degradation of the cell constituents, ammonia is liberated and used for the synthesis of other nitrogenous compounds or become involved in nitrification. Nitrifying bacteria (the ammonia oxidizers and the nitrite oxiders) oxidize ammonia via nitrites to nitrate. The ammonia oxidizers are responsible for the oxidation of ammonia to nitrite, and the nitrite oxidizers

are responsible for converting nitrite to nitrate (acidification). Nitrate may act as electron acceptors and be reduced to nitrite, NO, N_2O, and finally N_2 (Thierry and Sand, 2011;Baumgärtne, 1990).

Dissolved inorganic nitrogen (DIN) has been proposed to be important for MIC (Melchers, 2014; Melcher and Jeffrey, 2013). Recent studies by Melchers have evaluated experimental data from several marine sites in the world, in order to quantify the effect of DIN on long-term seawater immersion corrosion loss of structural steels. Results showed that DIN concentrations from 0.01 mg/L to 0.4 mg/L (in sea and brackish waters) influence MIC of steel piling below the water tide for all sea water temperatures studied (Melcher and Jeffrey, 2013). For aerated seawaters, the major component of DIN is nitrate in part due to that nitrites and ammonia oxidize to nitrate (Little, 2007).

Phosphorous is typically available in waters as inorganic phosphates and orthophosphates or as organically bound phosphorylated compounds such as phosphorus-containing sugars and lipids. Phosphate plays an important role as main energy storage in biological life as a backbone of DNA and RNA, and as an important component of Adenosine Triphosphate (ATP) (Thierry and Sand, 2011). Phosphate has been implicated in the steel corrosion exposed to bacterial cultures (Odom, 1993).

Sulfur is present in the biosphere in many compounds and is essential for the formation of the sulfurylated amino acids, methionine and cysteine/cystine. Other compounds include those containing reactive thiol (organosulfur compound that contains a carbon-bonded sulfhydryl or sulphydryl) groups; such as coenzyme A or iron-sulfur redox centers involved in electron transfer reactions (Thierry and Sand, 2011). Sources of sulfur include deposits of metal sulfide and sulfur. Metal sulfides can be degraded by certain bacteriathat oxidize the metal sulfide to a metal sulfate (Schippers et al., 1999) and the production of sulfuric acid. Such microorganisms involved in these processes tolerate high heavy metal concentrations (up to several grams per liter), low pH values below 1.5, and grow at temperatures 4- 90°C. A process similar to denitrification may take place

after the productin of sulfate. If sufficient organic matter is available and anaerobic conditions exist, sulfate will act as an electron acceptor, being reduced to sulfide (Dilling and Cypionka, 1990) by SRB. This is a physiologically diverse group of microorganisms including photosynthetically active bacteria

Trace elements are needed to support vital metabol functions although Iron as Fe^{2+} or Fe^{3+} is necessary for the electron transport system and functions as an oxidizable/reducible central atom in cytochromes or in non-heme iron–sulfur proteins. Magnesium plays a role in the chlorophyll molecule. Cobalt functions in the transfer of methyl groups from/to organic or inorganic molecules. Copper is an integral part of a cytochrome, which at the terminal end of the electron transport system mediates the reduction of oxygen to water (cytochrome oxidase) (Thierry and Sand, 2011).

Oxygen concentration may not always be useful as biofilms are capable of forming anaerobicregions in aerobic bulk solution. For example, tt was reported that biofilm with thickness of 2 micrometer can create anaerobic conditions.

2.1.4.1.b Temperature and pH

Both biological and electrochemical events depend on the pH and temperature at the metal water interface (Dexter,1993). Hydrogen ion concentration is an important factor in microbial growth. Microorganisms may be distinguished by their ability to grow under acidic (acidophiles), neutral (neutrophils), or alkaline conditions (alkaliphiles). (Thierry and Sand, 2011). Bacteria has been detected at negative pH conditions as well as pH values greater than 12. Fungi are able to grow over a large range of pH values, and . penicillium have been found at pH 2-12 (Thierry and Sand, 2011). However, most of the microorganisms live in the neutral pH range from 6 to 8. As Rim-Rukeh (2012), reported, acidic environment with pH<6 and alkaline environment with pH>8 are more corrosive than an environment with pH ranges from 6 to 8 .

Microbial life is possible between −5°C and +114°C and microorganisms can be classified base on the temperature they need, as can be seen in Table 2.1. Most organisms live in the mesophilic range (20°C to 45°C), corresponding to the usual temperature on the surface of the earth. Only a special group of bacteria, called archae bacteria, are able to grow at elevated temperatures (above 70°C). (Thierry and Sand, 201).

Table 2.1 Microbial classification base on Temperature

Temperature	Microbial classification
−5°C to 20°C	Psychrophiles
5°C to 30°C	Psychotrophs
20°C to 45°C	Mesophiles
55°C to 85°C	Moderate thermophiles
Up to 120°C and Above	Extreme thermophiles

2.1.4.1.c Roughness

Surface roughness influence microbial cell attachment and transport rate by increasing connective mass transport near the surface, providing shelter from shear forces for small particles and increase surface area for attachment. (Characklis, 2009; Flemming et al., 2009). The effect of surface roughness on MIC has been studied for carbon steel coupons due to corrosion by SRB culture. The roughness has an important role on the development of pitting corrosion. The pit density on the rough unpolished coupon surface was much higher than that on the polished surface (Chen et al., 2013).

2.1.4.1.d Hydrodynamics

The physical stability of the biofilm is affected by the fluid flow velocity. Generally, lower fluid flow velocity will not disturb the formation of biofilm and MIC will increase, in part due to the absence of mechanical sheer forces (Stoodley et al., 1998; Wen et al., 2006; Wen et al., 2007; Javaherdashti, 2008). Also, flow rate affects the thickness of the biofilm. In turbulent flow system,

wet biofilm thickness rarely exceeds 1.000 mm (Characklis, 2009). Stoodley, 1998 reported that fluid flow can enhance mass transfer but it may also produce a high shear that inhibits cell attachment and causes even detachment of an established biofilm. Wen, 2006 research showed that the fluid flow rate had a considerable impact on MIC corrosion rates of carbon steels. In 2007, his experimental results in the glass cell inoculated with D. desulfuricans indicated, that at 3,000 rpm (roughly equivalent to 3.5 m/s in pipe flow) sessile SRB cells could not adhere on the coupon surface to form an SRB biofilm. The results confirmed that a high linear flow velocity could indeed prevent SRB biofilm formation. Some researchers suggested that stagnant water conditions can provide less severe conditions and do not enhance corrosive attack (Borenstein, 1994).

2.2. Biofouling and Corrosion

2.2.1 Background

Structures placed in natural marine environments are susceptible to physical, chemical and biological events that can result in the accumulation of microorganisms such as bacteria, archea and macroorganism such as barnacles, macroalgae, mussels, bryozoans and tube worms (Hellio and Yebra, 2009).

It is known that a film of microscopic fouling organisms start forming on structural metals within a few hours of their immersion in natural waters (Dexter, 1993). The sequence of events related to the biofouling process is shown in figure 2.1 (Lehaitre, 2008; Dexter, 1993). The numerous fouling organisms may be divided into micro-organisms (or so called biofilm, slime, micro-fouling) and macroorganism (or macro-fouling), according to their size (Lehaitre, 2008). Microfouling is defined as a result of adhesion and growth of microorganism at the metal water interface, and macrofouling is due to the attachment of macroorganism. Macrofouling organisms are found at all depths and in all natural bodies of water (Little, 2008).

Biofouling has a negative economic impact in the industry. For the global shipping industry, biofouling costs billions of dollars per year in prevention, maintenance, and fuel consumption (Alliance for Coastal Technologies, 2004). In 1999, a report by the naval research laboratory indicated that the use of antifouling paints could save up to 10% of the US Navy's annual fuel bill (Jones-Meehan, 1999). A heavy layer of macroorganisms also have a number of undesirable physical effects on marine structures. The fouling layer will increase both weight and hydrodynamic drag on the structure. Interference with moving parts may also occur (Little, 2008).

In addition to the macrofouling of marine steel structures where damage can result in the loss in tensile strength (Subramanian et al.,2013). Surface fouling also can enhance corrosion (Javaherdashti at al.,2013; VR de Messano et al.,2014), but its effects can be diverse, and studies are relatively limited (Neville,1998; LaQue,1982; Eashwar et al.,1990; Palraj et al.,2002,2006; de Rincon et al.,2003; De Brito,2007; VR. de Messano et al.,2009; Sangeetha et al., 2010; Palanichamy et al.,2014). Non-uniform macrofouling of such organisms may initiate localized corrosion by creating crevice conditions and oxygen concentration cells (Little,2007) as well as producing local changes in pH and anaerobic environments (Pipe,1981; Zhang et al.,1995; Newman et al.,1989; Salvago et al.,1987).Barnacles are considered as the dominant biofoulers and are the primary target of anti-fouling industries and technologies (VR de Messano et al.,2014; De Brito,2007; Eashwar et al.,1992). It has been reported that barnacles must reach to critical size to initiate crevice corrosion (Eashwar et al.,1992; Hodgkiess et al.,1998). It was suggested that the extent of the corrosion under the remnants of barnacles can be more severe than under the living ones, suggesting that the acidic chemicals produced during the decay of the barnacles can accelerate the corrosion rate (Hodgkiess et al.,1998;Blackwood et al.,2017).

Therefore, both microfouling and macrofouling influence the corrosion process (Javaherdashti, 2013; VR de Messano, 2014). The effects of marine biofilm on corrosion have been well disseminated in the literature. Biofilm creates oxygen heterogeneities and increases mass transport resistance near a metal surface. Also, metabolic reactions in biofilms generate corrosive substances (such as an acid), and other substances that serve as cathodic reactants (Flemming, 2009). However, limited information is available on the role of macrofouling and corrosion. (LaQue, 1982; Eashwar et al., 1990; Neville and Hodgkiess, 1998; Palraj et al., 2002; Rincon and Morris, 2003; Palraj and Venkatachari, 2006; de Brito et al., 2007; de Messano et al., 2009; Sangeetha et al., 2010; Palanichamy,2014).

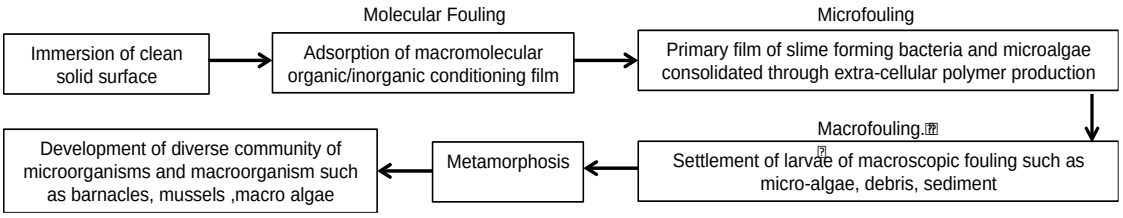

Figure 2.1. Sequence of Events in Marine Biofouling

2.2.2. Macrofouling characteristic

Macrofouling can occur by two groups of macroorganisms such as plants (e.g. seaweed) and animals (e.g. barnacles and mussels) (Javaherdashti, 2013), generally classified into " soft " and " hard " fouling as visualized in table 2.2. The hard species present a solid skeleton such as a shell or a calcareous tube (calcareous algae, barnacles, mussels, tubiculous worms), which protects the body within, whereas the soft species have no such protection (sponges, anemones, bryozoa) (Lehaitre, 2008).

The settlement of fouling organisms can be influenced by the surface water temperature, salinity, water motion, and light (Palraj et al.,2006). The literature suggests different mechanisms for marine fouling settlement where some suggest the prerequisite of biofilms (Javaherdashti et

al.,2013; Neville et al.,1998; Crisp,1974; Walters et al.,1996; Egan et al.,2002; Keough et al.,1995) while others provide other ideas on larval site selection (Lehaitre et al.,2008;Roberts et al.,1991). Surface roughness influence larval cell attachment and transport rate by increasing connective mass transport near the surface, providing shelter from shear forces and increase surface area for attachment (Flemming et al.,2009;Characklis,2009) as the shape and size of different fouling organisms can be very different: ~1µm for bacteria, 3-15µm for diatoms, and 120-500 µm for macrofouling organisms (Hellio et al.,2009).

Table 2.2. Main hard and soft marine growths (Lehaitre, 2008; Clapp, 1948)

Sessile Organisms	
Hard fouling (calcareous or chitinous shells)	Soft fouling
Mollusks: Mussel, oysters Barnacle: which built cone-shaped shells built up of laminated plates Corals Annelids :which form coiled or twisted tubes like tubeworm Encrusting sponge and Bryozo : colonial animals which form flat, spreading, multi-cellular	Seaweed Coulenterates or Hydroid such as “Tubularia” with stalk-like or branching Growths, each branch terminating in an expanded tip; also “Bougainvillia” And “Campanularia” Marine algae : “Ceranium”, “Fucus” “Polysiphonia” ,“Ulva” Soft coral Calcareous and siliceous Sponge Sea Anemone

Larvae exhibit different settlement behaviors in response to flow, pressure, light, surface texture and color (Roberts et al., 1991). The effect of the surface texture was evaluated through laboratory tests in the presence of *Balanus improvisus* cyprids macrofouler. Results concluded that this macrofouler attached in much higher numbers to the control polystyrene than to control glass surfaces (O'Connor, 1996). A hard, smooth surface generally provides a more secure footing for fouling organisms than a soft material. Fouling organisms must become attached to some base which is stable with no motion. Many of the fouling organisms are affected by light whereby some preferentially settle on shaded, or dark surfaces. On the other hand, the heaviest fouling is generally found on the northern side of stationary objects in the northern hemispheres. This is true for

mussels, hydroids, and many of the algae. Corrosion products also have an effect on these organisms settling. When corrosion products form very quickly (on ordinary steel) and the character of the surface is changed; the organisms are fastened not to the metal, but to the surface of the film of corrosion products.

The growth of macroorganism can enlarge the corrosion anodic sites on steel, but if the fouling is equally adherent to a metal over the entire area, the barrier may protect the steel against corrosion. If the surface is uneven, and water penetrates, there will be differential oxygen concentrations at points under the fouling and elsewhere on the surface of the metal. Oxygen concentrations cells may then accelerate corrosion. While these macroorganism grow and expand through the surface, they can cover smaller organism. The covered organism quickly dies and degeneration sets in, followed by the production of hydrogen sulfide, which can promote accelerated corrosion. Table 2.3 provides further information on the macrofoulers relating to life cycle, nutrient, reproduction, metamorphosis and settlement process

2.2.3. Macrofouling and Biofilm

There is uncertainty on how adhesion of settling invertebrates is influenced by microbial films. Generally, biofilm formation is an important factor in macrofouling (Neville and Hodgkiess, 1998). When a biofilm is formed, it becomes a suitable environment to allow the mussels and barnacles (larvae) to attach themselves onto it. These larvae then use this opportunity for growth and transformation into adults (Javaherdashti, 2013). It was shown in the literature that water soluble pigments (serve as positive or negative cues) produced by biofilms provide chemical and physical conditions to support larval settlement and metamorphosis (Walters et al., 1996; Egan et al., 2002). Also, the composition of microbial communities on surfaces strongly influences the rates of larval settlement of some invertebrate species (Keough and Raimondi, 1995). Therefore, biofilm

often have the determining role in initiating macrofouling for some macroorganisms and any factor supporting the biofilm formation can also be related to macrofouling.

Some marine invertebrate larvae can settle on clean surfaces. Settling condition of a wide variety of macroorganism has been investigated by different researchers. According to available data, some macroorganism do not necessarily need the presence of a biofilm on a surface to settle (Roberts et al., 1991; Lehaitre, 2008). However, most of studies have concluded that the settlement of many larval species on hard surfaces is enhanced by the presence of biofilm (of certain individual bacterial isolates) (Crisp, 1974).

Biofilms can also modify physical surface properties such as wettability or texture, which are important to settling larvae. The presence of a thick and slimy organic layer, underlying the relatively small attachment organs of settling larvae, would be expected to inhibit the ability of larvae to adhere tightly to a substratum (Zardus, 2008). Overall, surface-associated bacteria have important influences over the settlement of many invertebrate larvae. Bacteria may stimulate, inhibit or not affect the settlement of invertebrate larvae (Lau, 2002; Brancato & Woollacott, 1982). In 1988, Maki studied the effects of marine bacteria on the attachment of cypris larvae of the barnacle Balanus Amphitrite. The author reported that most bacteria either inhibited or did not influence larval attachment compared to clean surfaces. Hence, larval settlement will depend on the species of invertebrates and bacteria of concern. In summary, bacterial biofilms have been found to be important in the settlement process of representatives of most marine invertebrate groups including sponges, tubeworms, cnidarians, annelids, echinoderms, phoronids, bryozoans, ascidians, and algae (Unabia and Hadfield,1999; O'Connor and Richardson,1998; Lau et al., 2002).

O'Connor ,1996 showed that barnacle settlement was different from bryozoans. Barnacles were settled in control condition and the higher numbers of settlement were observed in presence of bacterial cells. However in the case of bryozoans, negligible number were succeed to settle in

control condition. Zardus, 2008 tested four species of common marine fouling organisms (a polychaete worm, an ascidian, a barnacle, and a bryozoan), which differed according to their responsiveness to biofilms at settlement. Larvae of four species of biofouling invertebrate were allowed to attach to tested surfaces that were either clean or coated with a natural biofilm. Measuring larval removal under precisely controlled flow forces, indicated that biofilms significantly increased adhesion strength in the ascidian *Phallusia nigra*, the polychaete tubeworm *Hydroides elegans*, and the barnacle *Balanus Amphitrite*, at one or more developmental stages. In addition, the attachment strength in the bryozoan *Bugula neritina*, was neither facilitated nor inhibited by the presence of a biofilm. These results suggest that adhesive strength and perhaps composition may vary across different invertebrate taxa at various recruitment stages, and mark a new path of inquiry for biofouling research.

Several authors have suggested that the effect of surface-associated bacterial communities on larval settlement is a function of bacterial species composition (Keough & Raimondi 1995). Lau, 2002 has studied the effect of different bacterial strains (isolated from marine biofilms) on the settlement of the tubeworm *Hydroides elegans*. Results showed 20% settlement for clean surfaces, over 60% settlement for natural biofim condition (bacterial strains of different species) and 0 to 60 % settlement for different bacterial strains isolated from marine biofilms.

Unabia, 1999 studied the role of bacteria in larval settlement and metamorphosis of the polychaete *Hydroides elegans*. His investigation showed that the settlement of Hydroides was prompted by specific bacteria up to 60%. However one bacteria strain showed settlement less than 20%. As high as 80% settlement was achieved on multi-strain water-table biofilm. Hydroides was also succeeded to grow (settlement ~20%) on the clean surface without presence of bacteria.

2.2.4. Macroorganisms and corrosion

The role of macrofoulers on corrosion in marine environment is unclear. There are some studies showing inhibition or acceleration of corrosion, resulting from marine biological activity. A heavy deposit of macrofouling organisms on structural steel immersed in seawater will often decrease the corrosion rate of the steel, as long as the cover of organisms remains complete and relatively uniform (Little, 2008). The heavy fouling layer acts as a barrier, limiting the dissolved oxygen at the metal surface. A layer of hard-shelled organisms (barnacles or mussels) on steel in the splash zone also shields the metal from the damaging effect of wave action. If fouling layers are incomplete, the fouling is more likely to cause initiation of localized corrosion by creating oxygen concentration cells.

A report prepared by the Electric Power Research Institute (EPRI) noted that more than 75% of condenser loss in fossil-fueled power plants (with a capacity of more than 600 MW) is due to biological factors, of which 30% were due to macrofouling. This research indicated that barnacles are capable of inducing localized corrosion (De Brito, 2007).

A scatter of individual barnacles on a stainless steel surface can create oxygen concentration cells. The portion of the metal surface covered by the barnacle shell is shielded from dissolved oxygen in the water and thus becomes the anode. The result is crevice corrosion under the base of the barnacle (Little, 2008).

Most researchers agree that balanoid barnacle growth is a primary cause of biocorrosion, especially on passive alloys (VR de Messano, 2014). VR de Messano (2014), reported on the effect of *amphibalanus amphitrite* barnacle on the corrosion behavior of three stainless steels. Open circuit potential (OCP) measurements indicated corrosion conditions on stainless steel in the presence of these organisms. Crevice corrosion in part due to differential aeration caused by the

lack of oxygen around the base of the barnacles was detected during visual inspections, despite the small size of the barnacles and the short duration of the experiments.

De Brito (2007) conducted field experiment to evaluate the influence of macrofouling on the corrosion of carbon steel panels over a 6-month period. Three treatment conditions were applied, including a ‘Control’ treatment (absence of macrofouling), a ‘Community’ treatment (in presence of macroalgae, barnacles, hydroids and encrusting bryozoans) and a ‘Barnacle’ treatment. In the 'Control’ treatment the corrosion (uniform) rate was higher than other cases, indicating that the presence of macrofoulers provided protection against mass loss. On the other hand, the highest percentages of localized attacks were found in the ‘Community’ and the ‘Barnacle’ treatments, showing that not only barnacles, but also other marine organisms induce localized corrosion.

Eashwar, 1990 investigated the role of marine fouling (algae and barnacles) on the corrosion process of the steel in the coastal water of India. Higher corrosion rates of steel was observed in presence on heavy algae, which was accelerated during certain growing season. In the case of barnacles, lower corrosion rates of steel was observed in comparison with the absence of any microorganism. The findings indicated that the fouling was effective in inhibiting the corrosion of steel. In 1992, Eashwar et al., investigated the mechanism of barnacle induced crevice corrosion in stainless steel. Based on his result, corrosion would occur only under dead barnacles (flesh remained inside the shell). Aerobic microorganism and oxygen must present to initiate crevice corrosion at barnacle sites. At first the decomposition of organic matter (barnacle flesh) start the acid production. A corrosion cell develops between crevice area and exposed surface of stainless steel to the sub stream, followed by crevice corrosion starting from the edges and propagate inward and possibly creating a deep pit at the center in anaerobic condition.

2.3. MIC and Fouling Remediation

Generally coating and cathodic protection have been employed to protect against MIC. In the following, a general review of the application of antifouling and polyurea coating and use of sacrificial zinc anode in MIC and fouling suspected environment is presented.

2.3.1. Cathodic Protection

Cathodic protection can be afforded on steel structures submerged in natural waters, but complications arise in the presence of microbial influenced corrosion (MIC) and marine fouling organisms. The current demand for cathodic protection depends on the chemical changes in the environment (e.g. oxygen concentration, pH and temperature) and physical and chemical characteristic of the metal surface (e.g.corrosion products, calcareous deposits, and biofilms (Little, 1993).

Reported research described the negative role of microorganisms on cathodic protection (Little 1993; Olivares et la.,2003). Cathodic polarization to -850 mV_{CSE} has been reported to be inadequate in presence of MIC and levels more active than -950 mV_{CSE} have been suggested (Horvath et la.,1964; Barlo and Berry ,1984; Fischer,1981; Jack et al.,1996). However there remains uncertainty about the effectiveness of this value in presence of SRB. Olivares, 2003 reported polarization as negative as ~-925 mV_{CSE} led to lower corrosion rates and reduced mass loss, but SRB population was shown to continue to proliferate due to an electrostatic attraction between the bacteria and the electric charges created by cathodic protection as well as a supporting role of calcareous deposits that contained sulfates (Olivares,et al.,2003). Although total mass loss was reduced, the proliferation of SRB may still allow some level of localized corrosion to develop. Later studies by Olivares showed that -950 mV_{CSE} was not enough to control the MIC and localized corrosion developed (Olivares,et al.,2006). Research by de Romero, 2006 and 2008 showed that

polarization up to -950 mV_{CSE} in laboratory and field conditions was not sufficient to prevent corrosion development and sessile bacterial growth remained high in conditions up to -1.3V_{CSE} (de Romero, 2006;2008).

There are different views on how these microorganisms affect the cathodic protection efficiency. Bacteria may have an effect by acting as depolarizing agent and increasing the required current for cathodic protection (de Romero, 2009; Booth et al.,1960). It is also considered that biofilm formation by bacteria electrically insulates the metal from cathodic protection (Booth et al.,1960; Bryant et al.,1990). Also extracellular polymeric substances in biofilm can generate an effect of ohmic drop (de Romero, 2009).

Guezennec,1994 described the relationship between cathodic polarization and development of biofilm on surfaces exposed to both synthetic and natural seawater and showed that cathodically-produced hydrogen can encourage the growth of hydrogenase-containing bacteria such as SRB and the biologically-produced iron sulfide can contribute to an increase in cathodic current demand. Bacteria in the biofilm can act as a depolarizing agent and increase the required current for cathodic protection (De Romero et al., 2009; Booth and Tiller, 1960; Venzlaff et al., 2013).

The presence of macro-marine fouling organisms with encrustation, such as marine sedentary fauna and flora, on steel elements can create aggressive crevice environments and inhibit effective cathodic current distribution on the steel surface. Results from studies by Swain and Maxwell,1990 showed that biofouling on aluminium anodes increase the resistance value and reduces anode current output (Swain et al.,1990). Blackwood, 2010 reported that sacrificial anodes such as zinc and aluminum remained effective even after being completely coated with biofouling in maintaining a galvanic current to reduce and control corrosion (Blackwood.2010).

Eashware, 1995 showed that SRB activity on cathodically protected steel persisted due to shielding provided by of barnacles and development of anaerobic conditions (Eashwar et al.,1995).Eshware also showed that interfacial alkalinity generated by cathodic protection might enhance shell growth in the organism. However, information in the literature on the role of fouling on CP remain inconclusive (Blackwood.2010; Eashwar et al.,1995; Houghton,1978; Edyvean,,1985; Maruthamuthu et al.,1990; Pipe 1981). Littauer and Jennings showed indication of reduced biofouling in seawater using pulsed cathodic polarization of steel (Littauer et la.,1968). Sander and Maxwell,1983 found that cathodic protection doesn't alter the rate of attachment of fouling, but it inhibits the activity of biofilm (Sanders et al.,1983).

2.3.2. Coating application

Coatings have been developed to prevent MIC in biologically active environments (Al-Darbi et al.,2002; Jack et al.,1995; Jones et al.,1992), however the long-term durability of the coatings can be affected by many factors including microbial activity. Certain bacteria are preferentially attracted to iron corrosion products and colonize in scratches and holiday coating defects allowing for localized corrosion (Mansfield et al.,1998). Furthermore, studies have shown that coating blistering and disbondment can occur as a result of microbial attack due to the production of metabolites that degrade coating chemical and physical properties (Muntasser et al.,2002).

Antifouling and antibacterial coatings, that have been commercially developed to manage macrofouling of marine structures, may be applicable to prevent the MIC that possibly cab develop in those same environments. However, long term durability of the coating mitigation technology can be compromised. Antifouling coatings have a long history and has an important impact on managing macrofouling (Wells et la.,2009; Yebra et al.,2004; Brady, 2005; Chambers et la.,2006). Antifouling coatings with biocides have been traditionally employed for fouling control for

organisms such as bacteria, fungi, algae, plants and molluscs. Anti-fouling coatings are categorized as self-polishing copolymers (SPC), controlled depletion polymers (CDP), and foul-release (Wells and Sytsma 2009, Yebra at al. 2004; Chambers et al. 2006). Hydrolysis reactions in SPC and CDP antifouling coatings with the ionic constituents in natural waters can produce a soluble layer that subsequently exposes the antifouling agents. Foul-release coatings provide fouling protection by hydrolysis of polymers that allow ready detachment of fouling organisms with the eroded coating layer (Brady 2005; Wells and Sytsma 2009; Lejars et al. 2012). Antifouling coatings utilizing copper as a biocide have been widely used for the last 200 years; however, due the concerns about their negative environmental impacts, biocides are subject to regulatory restrictions.

CHAPTER 3

3. OBJECTIVE AND APPROACHES

3.1 Research Objectives and Approach

The objectives of the research were to identify 1) if marine fouling that create crevice conditions can enhance proliferation of bacteria that can support MIC in Florida natural waters, 2) if macrofouling can affect the efficacy of cathodic protection to mitigate MIC, and 3) if application of coatings can be used to mitigate marine fouling and bacteria settlement.

To address the research objectives, the following research questions were posed:

1. Can marine macrofouling create adverse crevice conditions that support MIC?
2. How can nutrient and planktonic bacteria source availability affect sustained SRB populations including in occluded crevice environments?
3. Can cathodic protection systems provide sufficient cathodic polarization to mitigate MIC in presence of marine foulers?
4. Can cathodic polarization affect bacteria growth and proliferation?
5. How do physical characteristics of marine foulers affect the efficacy of CP?
6. Can commercially available coatings be used to mitigate macrofouling and MIC?

Testing to address objective 1 included two major subsets of laboratory test setups and a set of field exposed steel coupons as shown in Figure 1.4. Laboratory experiments made under test setup A varied the availability of isolated sulfate reducing bacteria and nutrient levels. Experiments in test setup B followed a modified laboratory test setup and a single inoculation of isolated sulfate reducing bacteria was initially introduced and the level of biotic and electrochemical activity was continuously monitored. Field corrosion testing utilized freshly recovered steel coupons from test

sites in natural waters in Florida to provide a control condition in real life natural conditions. Testing to address objective 2 included field testing utilizing sacrificial bulk anodes and laboratory testing using lab potentiostats. Testing to address objective 3 included field and lab testing of commercially available polyurea coating and an antifouling coating.

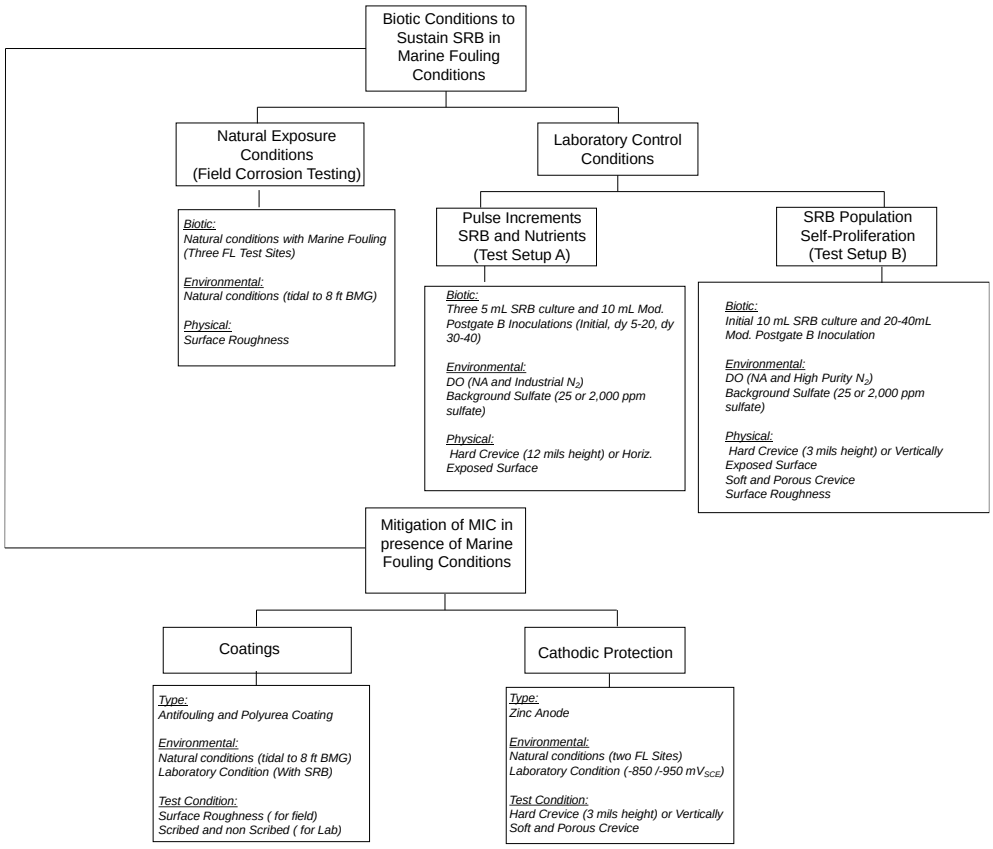

Figure 3.1. Test Approach

3.2. Hypothesis

Marine macrofoulers can create adverse physical and environmental conditions that can support sustained microbial growth that can promote localized MIC. The marine foulers can create conditions physical and chemical conditions that would affect the efficacy of cathodic protection and protective coatings.

CHAPTER 4

4. CASE STUDY (SR-312 OVER MANTAZAS RIVER, FL)

4.1. Background

Sampling of water near the bridge was tested to characterize water pH, chloride and sulfate content, mineral content and microbe content. This information was compared to earlier testing and available environmental databases and used to help identify other locations that may be susceptible to MIC. Florida State Road 312 (SR-312) bridge over Matanzas River (Saint Augustine, Florida) was constructed in 1976 (Figure 4.1). FDOT coordinates routine bridge inspections. In the earliest underwater inspection records reviewed by the researchers (dated on 5/12/2004), significant corrosion of some of the submerged H-piles were detected. This corrosion advanced upon subsequent inspections and was suspected to be MIC. A level III inspection in 2006 and further subsequent inspections in 2008-2016 showed and verified severe metal section loss in increasing number of H-piles. A summary of the FDOT inspection reports from 2004 to 2016 is shown in Table 4.1.

Figure 4.1. Underwater image of a hole on a steel pile due to corrosion. Photo courtesy of FDOT.

The locations with suspected MIC often had heavy marine growth. An example of a corrosion hole in a steel pile suspected to be due to MIC; Figure 4.2 shows the cumulative fraction of reported H-pile corrosion deficiencies for the bridge. The depths of corrosion pitting or holes ranged from ~ 0.3mm -9m (~1 to 30 ft) below the pile cap. The median value of the depths where

corrosion deficiencies were observed was 0.76m (2.5 ft) indicating that a large fraction of the deficiencies occurred close to the water surface. Most of the corrosion pits were 0.32cm (1/8 inch) in diameter but pits up to 1.27cm (1/2 inch)were recorded and corrosion holes were as large as 7.62cm (3 inch) in diameter.

Table 4.1. Bridge inspection findings of steel piles

Inspection Date	Description
2004, 2006	Steel H-pile with metal loss due to corrosion. Higher level of inspection revealed greater number of H-piles with severe corrosion.
2008, 2010	H-pile locations showed random areas of corrosion cells/pits of up to 7.62cm (3") in diameter and varied up to full depth. The corrosion cells/pits were covered with a bright orange plume, which when removed revealed flakey grey, black corrosion product. The localized corrosion in these areas was presumed to be due to MIC.
2011	Steel H-piles typically revealed pitting from 0.32cm (1/8")up to 5.08 cm (2"). Also, 28 steel piles had corrosion.
2014-2016	The H-pile pilings, two per footing for a total of 28, were in poor condition. They depicted random dense patterns of corrosion cells or pits (up to 7.62cm (3")) diameter and vary up to full depth). Corrosion cells/pits were covered with a bright orange plume, which when removed revealed flakey grey, black corrosion product. The next layer is a bright bare metal, several with holes through the web and or flange. Some of these corrosion cells/pits were located at the flange web interface. This condition appears to be MIC.

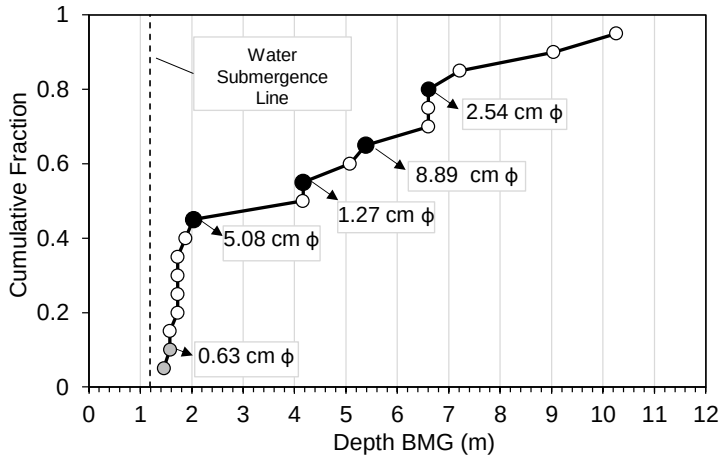

Figure 4.2. Cumulative fraction of the steel H-Pile Corrosion.

Figure 4.3 depicts a selection of some underwater images of the piers. Heavy marine grow and macrofoulers covering the steel surface was evident and it was difficult to see the corrosion problems (pitting corrosion) already mentioned in previous FDOT reports. From the underwater video monitor, only small areas of the H-piles appeared without marine growth.

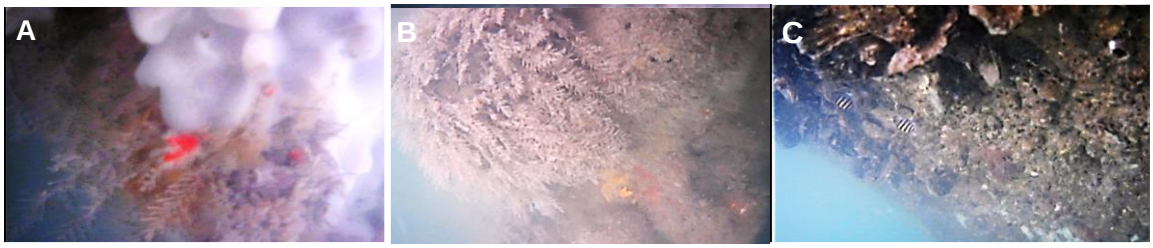

Figure 4.3. Underwater images of steel piles at SR-312 Bridge over Matanzas River. A-C. View of steel piles covered by heavy marine grow.

4.2. Water Quality

4.2.1. Field Testing

FDOT preliminary assessments of steel coupons and water samples in 2013 have revealed the presence of bacteria often associated with MIC (FDOT, 2013, 2016). Laboratory results of steel coupons using swabs have revealed aerobic organisms (>1,000 per swab). Anaerobic SRB were present >100,000 colony forming units CFU/mL. Acid producing bacteria (Bacillus sp.) were

present >100 CFU/mL. Slime producing bacteria including Pseudomonas luteola, Sphingomonsa paucimobilis and Brevundimonas vesicularis were also recovered. Analysis of water samples revealed the existence of anaerobic SRB ranging from ~100 to 10,000 CFU/mL, acid producing bacteria (Bacillus sp.) >100 CFU/mL and recovery of slime producing bacteria including Brevundimonas diminutia and Pseudomonas oryzihabitans.

Additional testing was conducted by the researchers in June 2016 to verify microorganism presence as well as to characterize the water environmental conditions (including dissolved oxygen, pH, conductivity, sulfate, chloride, phosphorus, nitrate, total organic nitrogen, total nitrogen, ammonia, and iron content) that may support the microorganisms related to MIC. Water samples were collected from two locations at the bridge site as well as at two depths reported in feet below high tide (BHT) (Table 4.2).

Table 4.2. Water sampling location

Bridge Location		Depth (ft BHT[a])	Depth (m BHT[1])
A	A1	~10	~3
	A2	~20	~6
B	B1	~10	~3

[a.] Below High Tide

Microbiological analysis of the water samples are presented in Table 4.3. Similar to earlier testing, slime-forming bacteria, SRB and acid producing bacteria were identified in all the water samples. Iron-reducing bacteria were also identified. It is uncertain if iron-reducing bacteria were considered in the earlier analysis. It is noted that there was high accumulation of SRB (~27,000 CFU/ml) in both assessments. Although it is understood that the quantity of bacteria in the analysis of water samples cannot directly correlate to MIC risk, the high resolved concentrations are indicators that there is greater possibility for the bacteria to proliferate and contribute to MIC. Furthermore, analysis of the water samples showed the presence of important nutrients (such as

sulfate, phosphorous, nitrogen and iron) that can support microorganism activity (Table 4). Data presented in Tables 4.3 -4.6 show results of pH, DO, temperature, and conductivity for water samples.

Table 4.3. Microbiological analysis of water samples

Sample ID	Iron-Reducing Bacteria (IRB) CFU.mL^{-1}	Slime-Forming Bacteria (SFB) CFU.mL^{-1}	Sulfate Reducing Bacteria (SRB) CFU.mL^{-1}	Acid Producing Bacteria (APB) CFU.mL^{-1}
A1	150	13,000	27,000	450
A2	500	13,000	27,000	450
B1	500	13,000	27,000	450

Table 4.4. Chemical analysis results of water samples

Parameters	Sample ID		
	A1	A2	B1
Sulfate/mg.L^{-1}	2,700	2,700	2,700
Chloride/mg.L^{-1}	20,000	19,000	20,000
Phosphorous/mg.L^{-1}	0.11	0.12	0.1
Ammonia/mg.L^{-1}	0.03	0.03	0.05
Iron/mg.L^{-1}	0.58	0.08	0.08
Nitrate/mg.L^{-1}	0.5	0.5	0.5
Total Organic Nitrogen/mg.L^{-1}	0.29	0.41	0.51
Total Nitrogen/mg.L^{-1}	0.81	0.93	1.06

Table 4.5. Field dissolved oxygen, pH and water temperature

Location	Depth / ft (m)	pH	Temp. / ^{o}C	DO / mg.L^{-1}	DO / %	pH	Temp. / ^{o}C	DO / mg.L^{-1}	DO / %
			Time 11:00				Time 13:00		
A	10 (3)	8.3	30.7	4.13	67	8.1	30	3.75	60
	20 (6)	8.3	29.9	4.29	69	8.1	30	3.63	60
	30 (9)	8.1	29.9	4.27	68.4	8.1	30	3.25	54
	40 (12)	8.1	29.9	4.18	67	NA	NA	NA	NA
	50 (15)	8.1	29.9	4.13	65.3	NA	NA	NA	NA
			Time 12:00				Time 13:00		
B	10 (3)	7.96	31.7	4.13	67	7.96	30	3.7	61.5

Table 4.6. Water sample conductivity

Sample ID	Conductivity / $\mu s.cm^{-1}$
A1	33.9 T=16.9 °C
A2	38.2 T=12.8 °C
B1	38.7 T=13.8 °C

It is noted that the bacteria concentration of the water samples collected at 10 feet BHT and 20 feet BHT were generally similar. At the same depths, the sulfate, chloride, phosphorus, ammonia, iron, nitrate, total organic nitrogen, total nitrogen, DO, temperature, pH, and conductivity were similar. DO, temperature, and pH measurements at depths down to 50 feet BHT were also comparable. It is remarked that water movement can be fast during tides. Table 5 shows results of field water environmental conditions during an incoming high tide. Although the convection of the water during the tide event seemed significant from the surface, DO measurements did not increase as expected and indeed diminished after 2 hours. Further evaluations on the influence on microorganism activity especially anaerobic SRB will need to be considered.

4.2.2. Review of Florida Environmental Database

The possible contribution of water nutrient concentrations to bacterial proliferation was considered as a first approach to identify locations with similar environments and that may also support microbial activity. The water chemistry data from the case study was reviewed and compared with available databases from water management districts in Florida. Florida has five water management districts: Northwest Florida, St. Johns River, Suwannee River, Southwest Florida and South Florida. Water quality data of the Florida bridge case study for the last 20 years (1996-2016) is presented in Table 4.7. It can be seen from the table that this site has high concentration of sulfate, chloride, calcium, sodium, potassium and magnesium. Also, the amount

of total nitrogen and phosphorus is low to medium and the pH and dissolved oxygen (DO) are in the intermediate level. Chemical analysis data (sulfate, chloride, iron, phosphorous, Nitrate, Nitrite, pH, temperature, alkalinity, etc.), as well as salinity, conductivity and dissolved oxygen are depicted in Figure 4.4 and 4.5, respectively. For comparison, the recent field data were also plotted and are highlighted in red.

Table 4.7. Water quality data of the case study site from 1996 to 2016.

Analytes	N Data	Min	Median	Max	Range
Water temperature/°C	151	10.90	22.62	30.80	Mid
Specific conductance/ µmhos.cm^{-1} @ 25 °C	152	28640.00	49770.00	55937.00	High
Sample collection depth/ meters	155	0.50	0.50	2.93	Mid-High
Dissolved oxygen analysis /mg.L^{-1}	154	4.28	6.42	9.89	Mid
pH/standard units	153	6.77	7.85	9.78	Mid
Total alkalinity/mg.L^{-1} as $CaCO_3$	86	69.58	115.91	125.70	High
Total nitrogen/mg.L^{-1} as N	150	0.01	0.43	1.01	Low
Total phosphorus/mg.L^{-1} as P)	152	0.02	0.08	0.61	Mid
Total organic carbon/mg.L^{-1} as C	87	1.25	3.05	27.40	Low
Total calcium/mg.L^{-1} as Ca	87	140.36	373.80	811.00	High
Total magnesium/mg.L^{-1} as Mg	87	1.14	1227.00	6490.00	High
Total sodium/mg.L^{-1} as Na	86	2820.00	10265.00	17500.00	High
Total potassium/mg.L^{-1} as K	86	152.77	416.50	3640.00	High
Total chloride/mg.L^{-1}	87	5973.67	19300.00	44352.60	High
Total sulfate/mg.L^{-1} as SO_4	86	164.00	2642.34	6170.64	High
Hardness/mg.L^{-1} Ca+Mg	85	1790.00	5957.62	7380.00	High
Lab turbidity/NTU	156	1.09	5.63	23.60	Mid-High
Sample site depth/meters	155	1.50	6.20	14.10	High

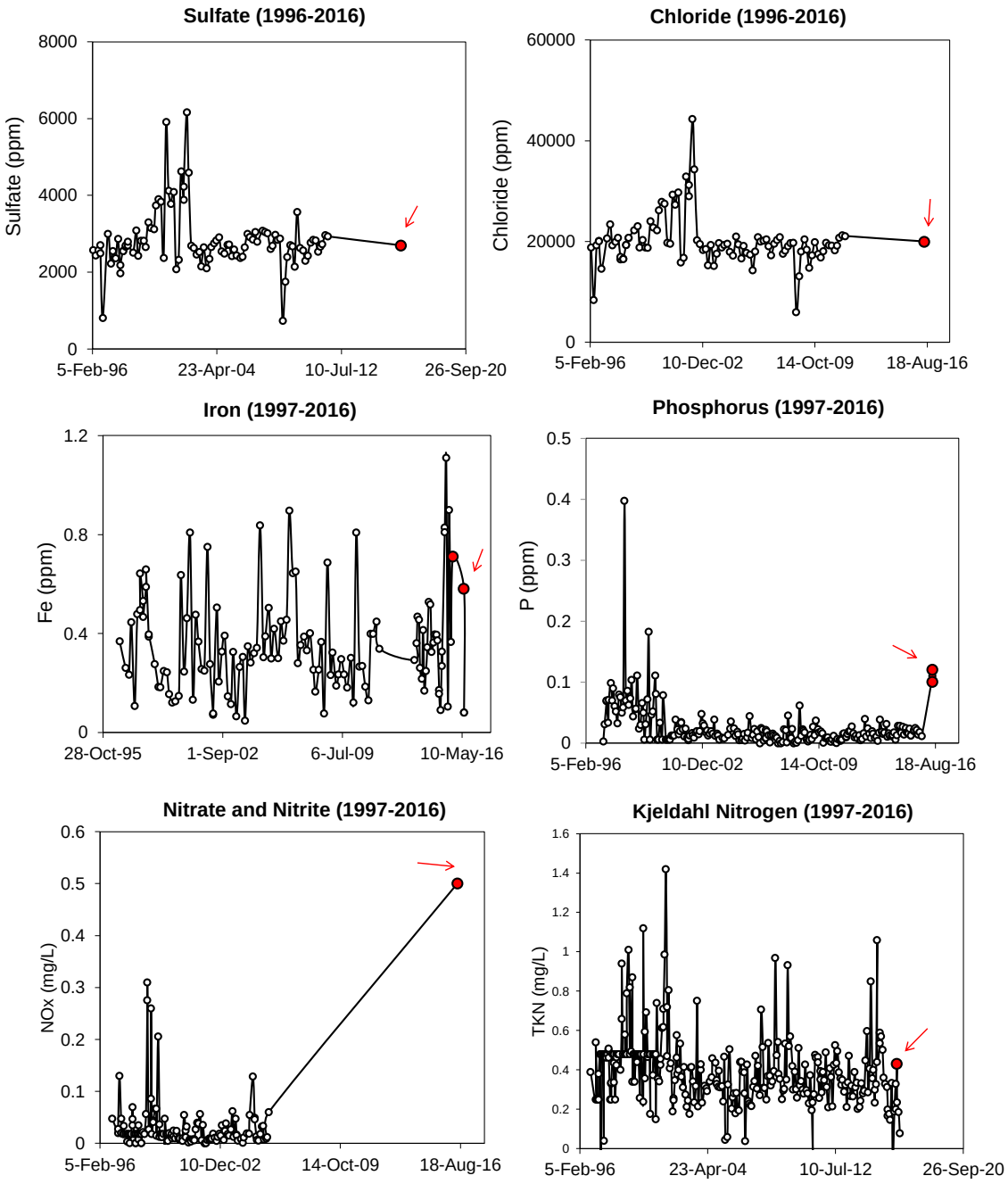

Figure 4.4. Chemical analysis of water samples.
Red full point: recent measurements during site visit [continued].

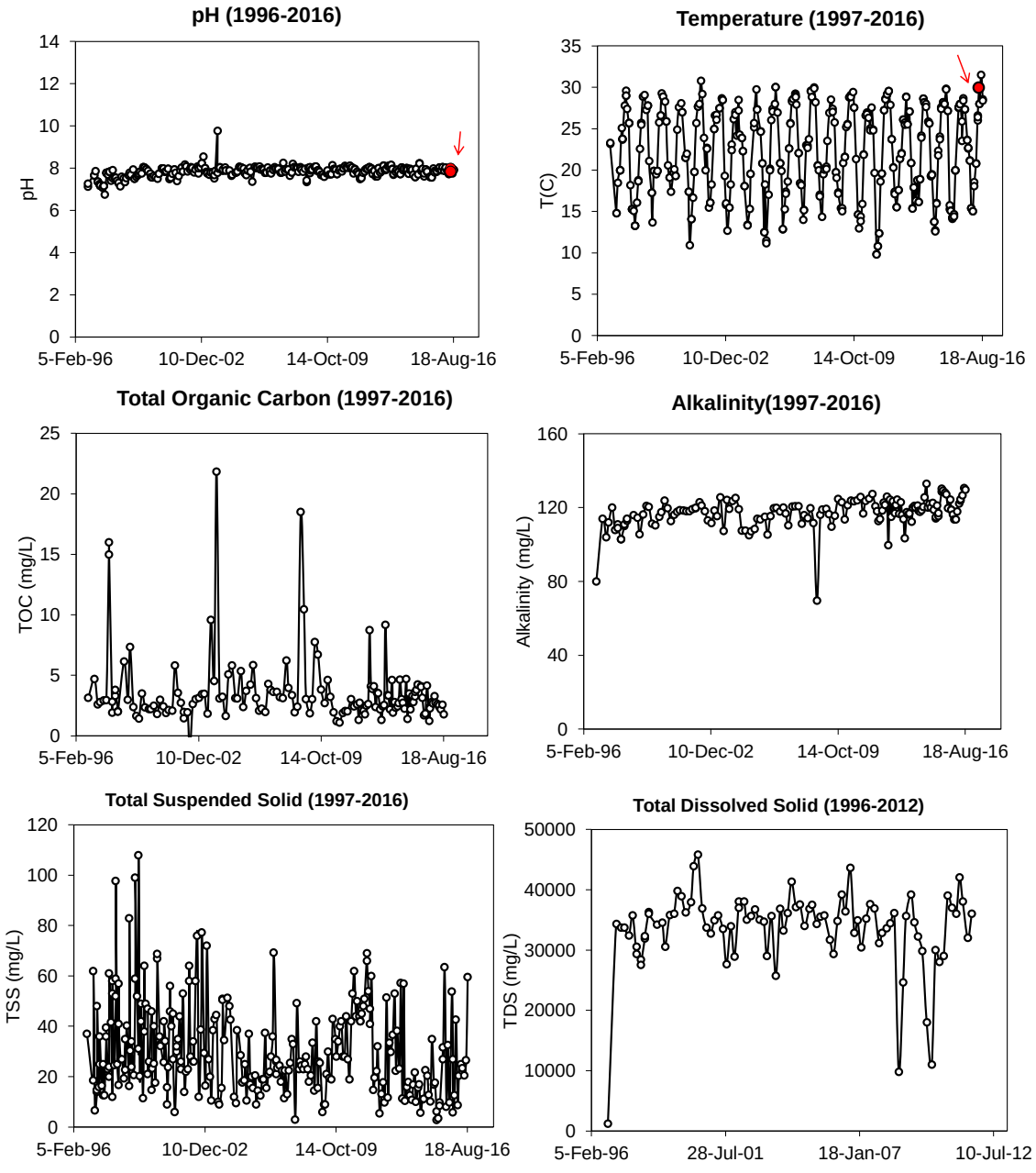

[continued] Figure 4.4. Chemical analysis of water samples.
Red full point: recent measurements during site visit.

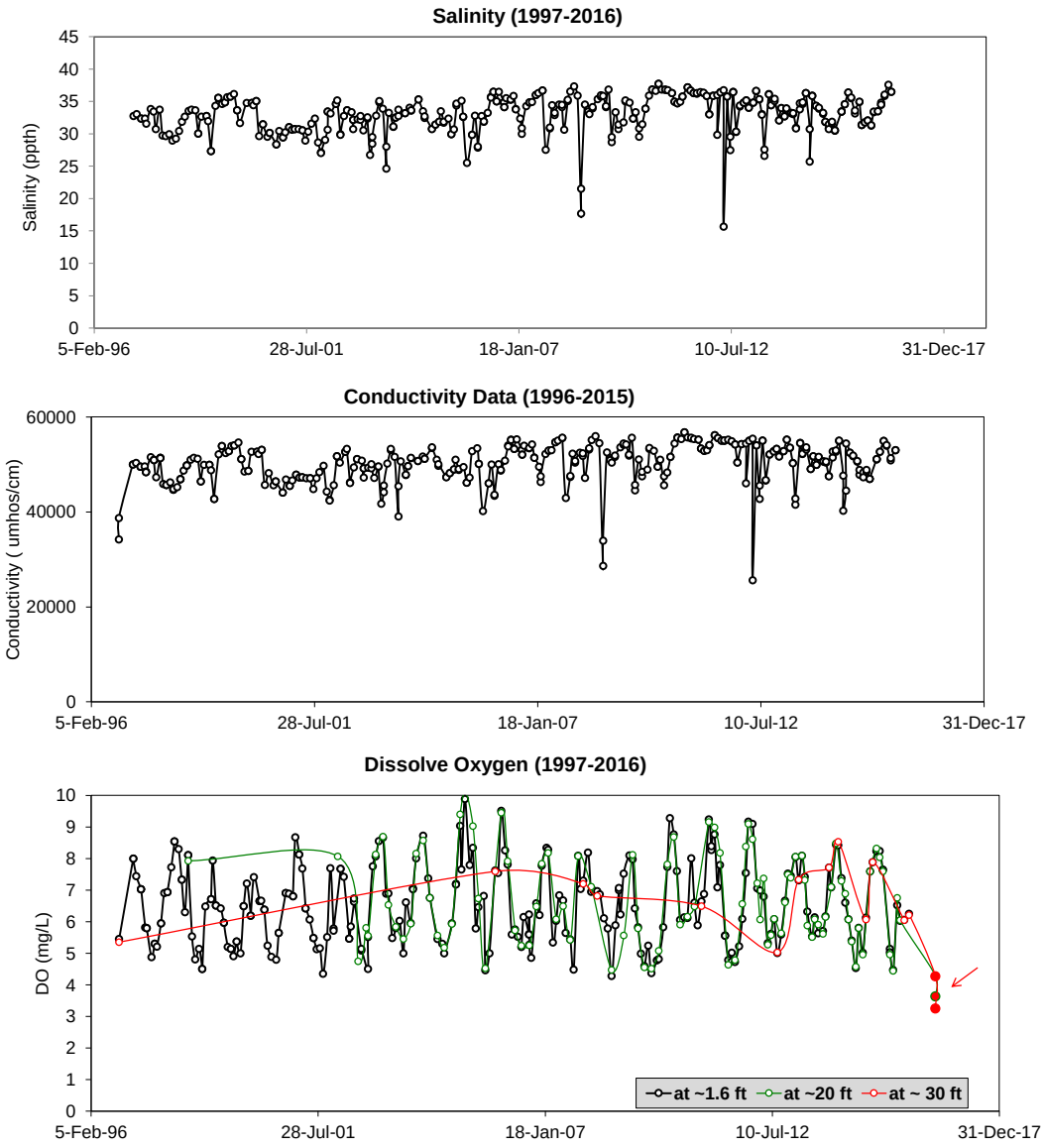

Figure 4.5. Salinity, conductivity and dissolve oxygen of water samples.
Red full point: recent measurements during site visit.

4.2.3. Comparative Florida Natural Waters

As shown in Figures 3.4 and 3.5, most of the recent measurements are in agreement with previous historical data. From the recent and historical environmental field data, concentrations of carbon (1.25<C<27.40 mg/L), sulfate (>2500 mg/L), nitrogen (0.01<N<1.01 mg/L), phosphorus (0.02<P<0.6 mg/L), as well as high concentration of Ca, K, Na, Mg in water samples were

coincident with the MIC development. This is consistent with previous studies that have reported that carbon, oxygen and nitrogen are considered as important nutrients for sustained microbial activity related to MIC (Gaudy et al.,1980). Environmental parameters such as high alkalinity, high chloride concentration (>20,000 mg/L), water temperature (around 30°C) and pH (from 6 to 9.5) could also contribute to the biocorrosion of steel piles. The available databases from the water management district of Florida were reviewed to identify marine environments that were similar to the case study. It was apparent that there are many sites that have similar conditions as the case study. Select sites with similar environmental conditions are shown in Figure 4.6.

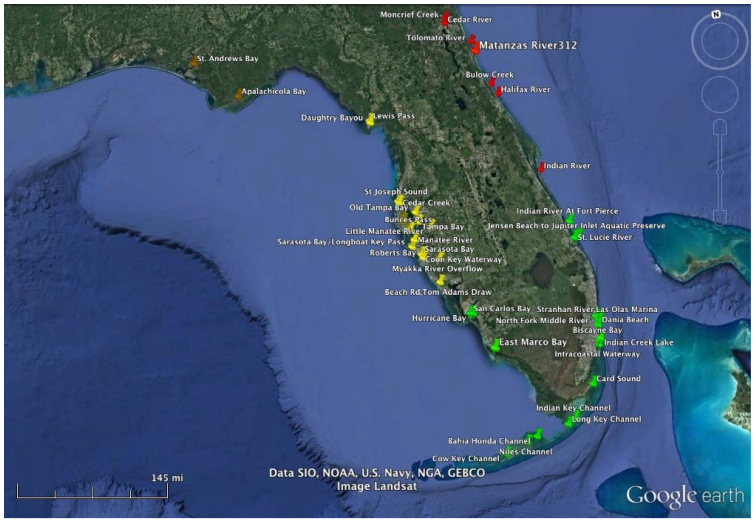

Figure 4.6. Examples of Florida water bodies that may support MIC.
Red: St. Johns River Water Management District, Yellow: Southwest Florida Water Management District, Green: South Florida Water Management District, Brown: Northwest Florida Water Management District. Image captured from Google Earth.

In light of the findings from the case study, review of the technical literature and available environmental databases; there may be locations in Florida that meet environmental conditions and nutrients requirements for microorganism colonization and sustained activity. Verifying microbial activity at other sites and importantly identifying possible MIC is of interest and further laboratory and field testing is ongoing.

CHAPTER 5

5. BIOTIC CONDITION TO SUSTAIN SRB IN MARINE FOULING CONDITION

5.1. Introduction

Microbiologically influenced corrosion (MIC) can develop on submerged steel structures that have suitable physical and environmental conditions that support proliferation of certain bacteria. The macrofouling can occur by marine macroorganisms such as marine flora (e.g. seaweed) and sedentary fauna (e.g. barnacles and mussels), generally classified into soft and hard fouling categories (Javaherdashti et al., 2013). Settling conditions of a wide variety of macroorganisms have been investigated and it was suggested that settlement of many larval species on hard surfaces is enhanced by the presence of biofilm ((Lehaitre et al., 2008; Javaherdashti et al, 2013; Crisp,1974; Zobell and Allen,1935; Roberts et al., 1991; Neville et al., 1998; Walters et al., 1996; Egan et a.,2002; Keough and Raimondi, 1995). However, some researchers have reported that biofilm presence may not necessarily be important for the settlement of marine macroorganisms, but the crevice environments may promote enhanced growth to accelerate MIC. The crevices have physical and environmental conditions that may promote microbial growth associated with MIC such as sheltering from extreme tidal action and creating anaerobic conditions.

The dense coverage of marine organisms on the steel substrate may reduce access of oxygen. Also, strong barrier conditions may diminish access to microbes and nutrient availability, thereby disrupting conditions that would otherwise enhance corrosion. On the other hand, loose attachment and non-uniform macrofouling of organisms may initiate localized corrosion by creating oxygen concentration cells resulting in crevice corrosion under the occluded spaces (De Brito, 2007; De Messano, 2009). Porous macrofouling organisms such as sponges also allow sustained microbe and nutrient flow through the marine flora mass. Marine fouling organisms can create de-aerated environments and provide shelter to support microorganisms in running natural

waters with convective tidal flow, where MIC can develop. In particular, in such anaerobic environments, sulfate reducing bacteria (SRB) which are widely associated with MIC and has received much attention in the literature, can proliferate. Sustained MIC of steel require continued sessile SRB activity at the steel interface.

As part of research efforts to identify biotic condition to sustain SRB in marine fouling condition , the objective of the work presented here was to identify the influence of microbe availability to promote SRB proliferation under occluded and porous fouling spaces and development of MIC there. This chapter include testing to monitor SRB proliferation during successive pulse inoculations (Test Setup A) and new testing to monitor SRB self-proliferation after early inoculation (Test Setup B) and also testing in field exposures that supported high SRB populations and heavy marine fouling (Test Setup C).

5.2. Methodology

5.2.1. Laboratory Testing

Laboratory experiments made under test setup A varied the availability of isolated sulfate reducing bacteria and nutrient levels. Experiments in test setup B followed a modified laboratory test setup and a single inoculation of isolated sulfate reducing bacteria was initially introduced and the level of biotic and electrochemical activity was continuously monitored.

5.2.1.1. Test Setup

The two phases of laboratory tests (Setup A and B) were primarily differentiated by SRB inoculation modality although other test parameters and conditions as shown in Tables 5.1 and 5.2, differed. In test setup A, the SRB was added in three inoculation events on days 0, 15, and 35. In test setup B, the SRB was only added in the initial inoculation event on day 0. The SRB was introduced in its Modified Postgate B (MPB) culture medium (Table 4.3) (Postgate,1979; TM0194,2014). For the control non-inoculated specimens, injection of blank MPB solution was

added concomitantly. The time of these solution augmentations for test setup A and B are referred to as injections. Due to the sequential inoculation (injection) events in test setup A on (16 test cells), the experiments were tested for a longer duration (for up to 70 days) to identify the effects of the successive introduction of nutrients and SRB on SRB growth and steel corrosion with time for the laminate crevice conditions. In the testing here, the test solution was not replenished or circulated so that periodic in-situ environmental and electrochemical measurements could be made. The effect on the sessile SRB activity was not expected to be severe in the given test volume as aeration levels, nutrient levels, and solution pH were either controlled or did not significantly vary during testing.

In test setup B, short-term experiments (on 30 test cells) for up to 15 days were made to compare the effects of laminate crevices to porous crevices. Inoculation of SRB or blank MPB injection for test setup B was only made at the onset of the experiments.

Table 5.1. Laboratory test parameters

	Test Setup A	Test Setup B
Duration (days)	70	15
Inoculation Time (day)	0, 15-20, 30-40 (in 5 mL MPB)	0 (in 10 mL MPB)
Nutrient Replenishment (day) 10 mL MPB	3, 15-20, 30-40	0
Initial Sulfate Concentrations (ppm)	<100, (2,000[a])	100, (2,000[a])
Bulk Solution De-aeration	95-97% N_2	99.98% N_2
Solution Volume	600 mL DI 10 mL MPB	300 mL DI 20mL MPB
Surface Roughness	20 micron	~20, ~200 micron
Crevice	Open	Open
	Laminate h= 0.3mm	Laminate h=0.1mm
	-	Porous

[a] from data in reference (Permeh et al.,2019a) shown for comparison

Table 5.2. Laboratory test conditions.

Test Setup	Test Solution	Inoculation	Working Electrode Condition	No. of Specimens	
				De-Aerated	Naturally Aerated
A	Postgate	Inoculated	Open (Control)	2	2
			Laminate Crevice	2	2
		Non-Inoculated	Open (Control)	2	2
			Laminate Crevice	2	2
B	Postgate	Inoculated	Open (Control)	3	3
			Laminate Crevice	3	3
			Porous Crevice	2	2
		Non-Inoculated	Open (Control)	3	3
			Laminate Crevice	2	2
			Porous Crevice	2	2

Table 5.3. Composition of modified Postgate B (MPB) medium.

Constituents	Composition (%)
Potassium Phosphate (KH_2PO_4)	0.05
Ammonium Chloride (NH_4Cl)	0.1
Sodium Sulfate (Na_2SO_4)	0.1
Sodium Chloride (NaCl)	2.5
Iron Sulfate ($FeSO_4.7H_2O$)	0.05
Sodium Lactate	0.5
Yeast extract	0.1

For all laboratory testing, test specimens were made from 1.27 cm (0.5-inch) diameter low-carbon steel (A36) rods cut into 1.9 cm (0.75-inch) long sections. An insulated copper wire was soldered to the back-transverse steel surface to provide an electrical connection to the steel section. The steel section was then encapsulated in an epoxy resin to expose the front transverse surface that was subsequently prepared by wet-grinding on diamond abrasive disks to various roughnesses. The surface roughness generally can influence larval cell attachment as the shape and size of different fouling organisms can be very different: ~1 μm for bacteria, 3-15 μm for diatoms, and 120-500 μm for macrofouling organisms (Characklis et al., 2009; Hellio et al., 2009; Flemming et

al., 2009). In test setup A, replicate testing was made on specimens with 20-micron finishes. For test setup B, testing of specimens made with 20-micron and 200-micron surface finishes did not show major differentiation in the lab test findings with the absence of marine fouling organisms and were thus considered here to be replicate specimens. Test setup A and B incorporated steel open-surface specimens open to the bulk solution as well as test-crevice conditions. The open-surface test specimens provided comparative results of SRB growth and steel corrosion in the various solution environments that can be representative of in-crevice solutions and ideally would elucidate the effect of the SRB and nutrient injection modality (such as those through marine fouling encrustations). The open-surface specimens also served as a control test condition for the specimens with the idealized physical crevice geometries. Occluded laminate crevice regions idealizing hard fouling were made by the placement of plastic shims and an annular cover sheet over the steel surface. Porous crevices idealizing soft fouling were made by the placement of a synthetic sponge over the steel surface. The setup and geometry of crevice environments for test setup A and B are shown in Figure 5.1 and 5.2.

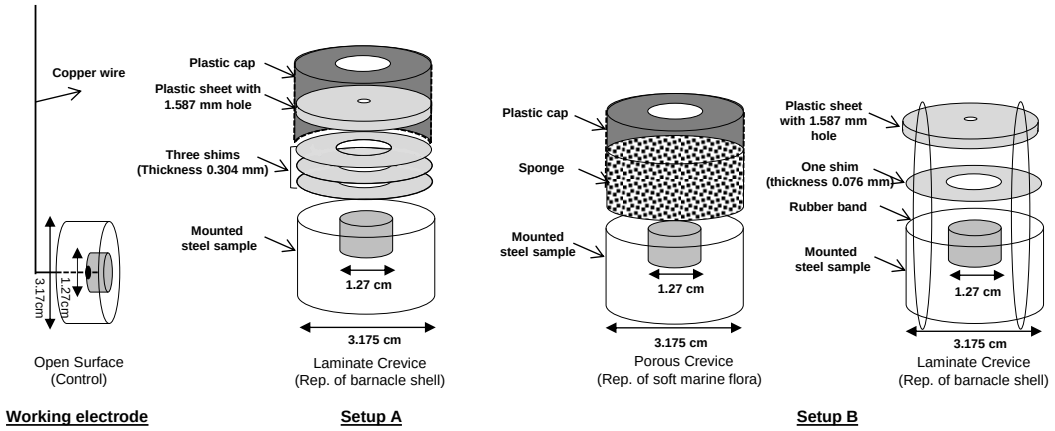

Figure. 5.1. Schematics of working electrodes in test setup A and B.

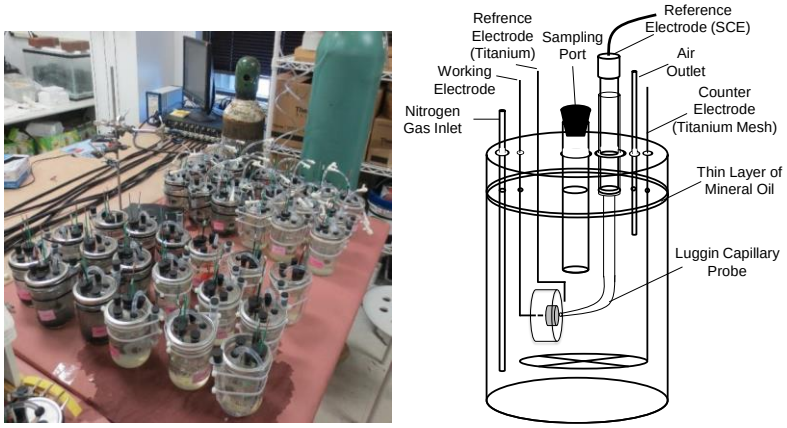

Figure 5.2. Laboratory test cells.

The test cells were made from 946-mL or 473-mL sealed glass containers for test setup A and B, respectively. The test cells were initially filled with 600 mL of deionized (DI) water and 10 mL of MPB solution for test setup A and 300 mL of DI water with 20 mL of MPB solution for test setup B prior to subsequent injections by SRB inoculations and additions of MPB. The initial nutrient concentrations were lower in test setup A than test setup B at the onset of testing in consideration of the subsequent successive additions of SRB and MPB made in the former. As the laboratory experiments sought to identify the effects of nutrient availability (i.e. access to the crevice environments from the bulk solution), test setup A provided sequential injections of cultured bacteria inoculum in 5 mL aliquots and additional 10 mL provisions of MPB after the second and fourth week of testing. In test setup B, only the single injection of cultured inoculum in a 10 mL aliquot and a 20 mL provision of MPB was made on day 0.

In the testing, the SRB inoculation levels and nutrient availability were assumed to be similar for test setup A and B and only the distribution of the external SRB and nutrients differed. Even though there will inevitably be variability in the in-situ SRB population and nutrient levels in time due to the changes in SRB growth kinetics, the related environmental factors would be similar to in-service conditions, and the in-situ population was posited to be largely influenced by injection

modality. The initial additions and sequential pulse injections of MPB with and without cultivated SRB (up to 55 mL of MPB and SRB in three 5 mL aliquots in the 600 mL solution) in test setup A allow for the assessment of crevice and fouling conditions that have intermittent interaction with the bulk solution (such as in porous crevices). The initial 30 mL of MPB with and without cultivated SRB (in one 10 mL aliquot) in the 300 mL solution in test setup B characterized occluded crevice regions with poor bulk solution interaction (such as in laminate crevices).These additions provided the test solutions that contained up to 100 ppm of sulfates (corresponding to some natural water sites in Florida (Permeh et al., 2019a) although the actual sulfate concentrations with time would be lower due to the microbiological reactions associated with SRB. For reference, results in complementary testing reported in reference (Permeh et al., 2019a) with higher sulfate concentrations (up to 2,000 ppm sulfate) were compared.

The pH of the test solutions for test setup A and B was 6.5-8.0 throughout the experiments and was within the range suitable for sustained SRB growth (Barton and Tomei, 1995). The SRB inoculations were made from the bacteria cultured in MPB solution from river water samples by serial dilutions and incubated in the laboratory at 30^{o}C following NACE standard TM0194-2014. In the serial dilutions, the SRB growth was detected by the production of hydrogen sulfide and iron sulfide that was evident by the pungent smell and visual blackening of the broth.

The experiments in both test setups were made with the bulk solution in naturally aerated or de-aerated conditions. Nitrogen gas was periodically introduced into the bulk solution. Lower-grade nitrogen that would provide some level of oxygen in the bulk solution was used in test setup A, and differential aeration conditions were expected within the occluded space of the crevice test specimens. This type of differential aeration closer represents natural conditions. High purity nitrogen gas was later adopted for the short-term testing in setup B. For both test setups, a thin layer of mineral oil was added to containers for the de-aerated cases to minimize oxygen ingress. All

electrodes and test cell components were made from sterile elements or cleaned with ethanol prior to introduction of inoculated mediums.

5.2.1.2 Microbial Activity

Environmental conditions to support bacterial activity in the test cell were in part assessed by measuring the chemical oxygen demand (COD), hydrogen sulfide production (Scott, 2004) and bacteria population. Although COD levels in itself do not directly indicate SRB populations, COD levels are considered as a metric of environmental conditions to support SRB activity (Gubner and Beech ,1999). The COD is associated in part with the concentration of electron donors available for sulfate or metal reduction used by SRB in its metabolic activities associated with oxidation of organic compounds (such as in wastewater systems) or cathodic depolarization of steel (such as in MIC). The COD of each specimen in 2 mL aliquots was measured by a colorimetric COD method (O'Dell, 1993). For specimens with crevices, sampling of solution within the crevice was not feasible. Instead, the solution was extracted with a micro-pipette with the tip placed as at the crevice orifice.

The COD measurements were made during regimes corresponding to the injection events that included the SRB inoculations and the blank MPB additions. Three COD measurement regimes after the SRB inoculations for test setup A and one COD measurement regime after the SRB inoculation for test setup B were considered. The initial COD measurement was made within 1 hour after the first inoculation for the inoculated specimens and concomitantly for non-inoculated specimens. Additional measurements were periodically made within the measurement regimes, and the maximum, minimum, and average COD from each regime were reported. A hydrogen sulfide color disc test kit was used to periodically measure the sulfide content in the test solution for all specimens in test setup A and B.

Early phases of research incorporated laboratory test setup A and the field testing (setup C). Testing for setup C is later introduced. During these phases, Biological Activity Reaction Test (BART) kits were adopted to assess microbe activity for field practicality and reporting consistency with evaluations made in contracted work by a commercial vendor for the original case study and in these experiment. For test Setup A, BART tests were made to verify the population and the activity of the four common MIC related bacteria (SRB, IRB, SFB, and APB). In the later research phase for test Setup B, Biotechnology Solutions sessile test kits were used for the detection of sulfate-reducing bacteria by serial dilution in MPB following NACE standard TM0194-2014. Serial dilution of the 1 ml phosphate buffer solution (PBS) ranged from 4-8 times. For all test methods, sterile cotton swabs were used to gently scrape the surface of the steel specimen (1 cm^2 area) and the slime (solid) was placed into the test vial for reaction.

The SRB presence on the surface of the test specimens was determined by the reaction of the surface film residue (sampled by swabbing a uniform surface area) with the test reagents in the commercial test kits. The BART and BTS tests allowed for general relative comparisons of the SRB levels for the various test conditions. The SRB content was described in units of SRB colony-forming units (CFU) and population count, each per mL of test reagent for the BART and BTS tests, respectively; but generally, the results were considered to account for the sessile SRB activity on the test specimen surfaces from the surface swabs.

5.2.1.3. Electrochemical Testing

The corrosion testing consisted of periodic measurements of the open-circuit potential (OCP), the linear-polarization resistance (LPR), and electrochemical impedance spectroscopy (EIS). The scanned potentials for the LPR testing were made from the OCP and cathodically polarized 25 mV at a scan rate of 0.05 mV/s. The corrosion current density was calculated from the resolved polarization resistance corrected for solution resistance, Rp, following the equation

i_{corr}=B/(RpxA) where B was assumed to be 26 mV and A was the surface area of the working electrode. EIS testing was made at the OCP condition with 10 mV AC perturbation voltage from frequencies 100 kHz > f >100 mHz.

The testing was made using a three-electrode configuration. The reference electrode used for OCP testing was a saturated-calomel electrode (SCE) introduced through a Luggin probe. For the multiplexed LPR and EIS polarization tests, an activated titanium wire (calibrated with an SCE) was used as the reference electrode. An activated-titanium mesh was used as a counter electrode.

5.2.1.4. Post Test Analysis

After testing, the steel working electrodes and the coverings on the crevice specimens were removed from the test solution. All specimens were rinsed with ethanol and dried. Photo-documentation for corrosion development and remnant physical effects of microbial activity was made.

5.2.2. Field Testing

5.2.2.1. Test Setup

Steel coupon specimens were installed at three Florida sites (Table 5.4). Site I was at the SR- 312 Bridge over the Matanzas River. Site II was at the US-41 bridge, downstream over the Alafia River. Site III was at the US-301 bridge upstream over the Alafia River. The selected sites comprised of different types of water bodies (estuarial/brackish and freshwater) with different environmental conditions. Table 5.4 shows the environmental, chemical, and planktonic microbial characteristics of the test sites.

One hundred and twenty-six 5x3x1/8" steel coupons (composition of 0.02 %C, 0.16 %Mn, 0.006 %S, 0.03 %Si, balance Fe) were installed for testing, 42 at each test site and were comprised of subsets of 14 specimens that were prepared in the as-received condition as well as abraded to a uniform 268-micron and 22-micron (60-grit and 400-grit) finish with an orbital sander (Table 5.5).

The specimens were installed on a polypropylene sheet secured to the test rack on the bridge pier. The position of the test racks at each site relative to the water surface varied due to the different geometry of the bridge substructure where the test racks were installed as well as due to variation in tidal levels. The specimens were all placed below the marine growth line. Some specimens were subjected to spray and tidal action although most of the specimens were permanently submerged in water up to 2.44 m (8 ft) BMG. At Site I, acorn barnacles were predominant in the tidal region. Hydroids and marine flora amassed below low tide levels. At the sites II and III, bay barnacles were the predominant macrofouler but the barnacles were more prolific at the Site II. Fig. 5 shows an example of test rack installation and marine growth.

5.2.2.2 Microbial Activity

As previously indicated, BART kits were adopted as a user-friendly test that could be conducted in the field. The testing allowed for a general assessment of the sessile SRB, IRB, APB, and SFB population below the marine growth layers. Interim verification checks on marine fouling and SRB growth are described in reference (Permeh et al., 2019a). Final visual photo-documentation of the steel coupon surface condition and analysis of the surface bacteria population was conducted at the end of the field testing when the test racks were decommissioned after ~280 days for Site I, ~248 days for Site II, and ~168 days for Site III.

Figure 5.3. Typical Outdoor Exposure Test Rack at Three Site

Table 5.4. Initial Survey of Selected River Water Characteristics.

	Parameters	Site I. Matanzas R.	Site II. Alafia R. (Downstream)	Site III. Alafia R. (Upstream)
General	Water Type	Estuarial/Brackish	Estuarial/Brackish	~Fresh
	Max. Water Depth/ft (meter)	~30 (9)	~5 (1.5)	~5 (1.5)
	Dissolved Oxygen(mg/L)	4.20	7.90	6.53
	Avg. Salinity (ppth)	30-35	15-20	10-15
	Conductivity (mS/cm)	38.2	36.55	10.73
	Macrofouler[1]	Tunicates, Hydroids, Barnacles, Sponge	Barnacles	Barnacles
Water Chemistry (mg/L)	Sulfate	2,700 (2,800)	620 (1,900)	2,200 (58)
	Chloride	19,000 (21,000)	3,800 (14,000)	71
	Phosphorous	0.12 (0.081)	0.28 (0.096)	0.71 (0.95)
	Ammonia	0.03 (0.1)	0.08 (0.029)	0.04 (0.12)
	Iron	0.08 (0.049)	3.5 (1)	0.15 (0.64)
	Nitrate	0.50	0.65 (8.8)	0.5 (0.76)
	Total Organic Nitrogen	0.41 (0.25)	0.48 (0.80)	0.52 (0.80)
	Total Nitrogen	0.93	1.1 (9.72)	0.56 (0.76)
Microorganisms[a] (CFU/mL)	Sulfate Reducing Bacteria (SRB)	27,000 (A)	325.00 (M)	500,000 (A)
	Iron-Reducing Bacteria (IRB)	500 (M)	9,000 (A)	9,000 (A)
	Acid Producing Bacteria (APB)	450 (M)	82,000 (A)	82,000 (A)
	Slime-Forming Bacteria (SFB)	13,000 (M)	1,750,000 (A)	1,750,000 (A)

Data in parenthesis was at time of sample installation.

[a] Aggressivity. (NA) Not Aggressive, (M) Moderately Aggressive, (A) Aggressive, (General guidelines for BART test for corrosion)

Table 5.5. Experimental Test Condition

Test Sites	Steel Condition	No. of Coupons	Distance BMG (m)
Matanzas R. (Site I)	As-received	14	0.6 to 2.44 (~2 to 8 ft)
	400 Grit surface roughness	14	0.6 to 2.44 (~2 to 8 ft)
	60 Grit surface roughness	14	0.6 to 2.44 (~2 to 8 ft)
Alafia R. (Downstream) (Site II)	As-received	14	-0.15[a] to 1.8 (~ -0.5[a] to 6 ft)
	400 Grit surface roughness	14	-0.15[a] to 1.8 (~ -0.5[a] to 6 ft)
	60 Grit surface roughness	14	-0.15[a] to 1.8 (~ -0.5[a] to 6 ft)
Alafia R. (Upstream) (Site III)	As-received	14	0 to 1.8 (~0 to 6 ft)
	400 Grit surface roughness	14	0 to 1.8 (~0 to 6 ft)
	60 Grit surface roughness	14	0 to 1.8 (~0 to 6 ft)

[a] Minus sign denotes distance above the marine growth line.

5.2.2.3. Electrochemical Testing

The corrosion potentials of the steel specimens during the field exposure were measured using a copper/copper-sulfate reference electrode (CSE) placed in the water. Disparities arose for those specimens placed in the tidal regions that were not immersed in the water during the field visits (timed to the slack low tide cycle to facilitate the fieldwork by boat access). Therefore, supplemental electrochemical tests were made in the laboratory within 24 hours of specimen extraction. The specimens were removed from the test rack and stored in sealed containers containing river water for transport back to the laboratory. In the laboratory, individual coupons were immersed in the collected river water, only immersing ~52 in^2 of the coupon in solution. Lab testing of the field specimens included OCP and LPR measurements, following similar methodologies described earlier.

5.2.2.4. Post Test Analysis

Retrieved specimens were cleaned to remove surface fouling and photo documentation of surface corrosion was made under magnification with a stereomicroscope. Corrosion pit diameter and pit depths were documented for 24 coupons per test site. Select specimens from various immersion

depths were further cleaned following ASTM G1-03 but immersed in the cleaning solution for up to 2 hours . Control testing of clean steel coupons was made and used to calibrate final mass measurement. The corrosion rate, reported in mg/dm^2/day (mdd), was determined by Eq 8.

$$CR_{mass\ loss} = \frac{m_f - m_o}{t \times A} \quad (5.1)$$

where m_f and m_o were the coupon mass after cleaning and the initial coupon mass (mg), respectively, t is the time of exposure (day) and A is the total coupon surface area (dm^2).

5.3. Results and Discussion for Laboratory Testing

5.3.1. Microbiological Activity

5.3.1.1. Chemical Oxygen Demand

Figure 5.4 shows the results of COD measurements conducted for all test conditions. COD levels are often used to describe environmental conditions and corrosion risk associated with SRB (Gubner and Beech ,1999). For example, initial low COD levels would be associated with a low risk of SRB-MIC (Scott, 2004). In the test solution, the additions of the MPB with its organic material, iron, and other electron donor contents that support SRB activity would result in higher COD. In addition, it was posited that changes in COD with time may reflect a series of possible reactions in solution associated with the SRB activity. In the following, the observations of the changes in COD are presented as a series of possible sequences later corroborated with other test findings.

In test setup A, the initial COD levels were expectedly lower (<200 mg/L) upon the first injection in both naturally aerated and de-aerated inoculated solutions as well as the non-inoculated cases (Figure 5.4). The COD levels significantly increased (max values >1,200 mg/L) in the de-aerated solution during the first measurement regime. In comparison to related test results detailed in reference (Permeh et al., 2019a) , the initial and terminal COD upon SRB inoculation in the MPB solution with the higher initial sulfate concentrations (~2,000 ppm sulfates) did not show major differentiation in the COD values measured here. The sulfate levels were not apparent limiting factors for SRB growth and it would be evident that other environmental factors are relevant. Upon subsequent inoculations up to 70 days, the COD remained high in the de-aerated condition indicating support for sustained SRB activity. Unlike the de-aerated inoculated solution conditions, the COD remained low (<200 mg/L) in the naturally-aerated inoculated solution conditions. No changes in COD was measured in the second and third measurement regimes. Low COD values were measured for all solutions extracted from the non-inoculated test specimens. Similar trends in COD were observed for the test specimens with the laminate crevice (Figure 5.4). It was anticipated that local oxygen depletion within the crevice environment could develop to support SRB development in the naturally-aerated solutions. However, the results did not show any significant changes in COD, indicating no broadening of SRB growth in the localized occluded environments after any of the inoculation events. The relatively low COD values, in this case, were likely in part due to the sampling limitations with the solution not directly extracted within the crevice itself where the SRB population can be concentrated.

In test setup B, the overall COD levels were higher than in test setup A in part due to the greater levels (~4 times higher concentration) of MPB solution initially added to the solution at the onset of testing in the former. Within the setup B specimen population, the COD levels for non-inoculated specimens were generally lower than the inoculated specimens. In the de-aerated inoculated solution, COD levels were elevated throughout the test where the average initial and

terminal COD values were greater than 400 mg/L. Conversely in the de-aerated non-inoculated solution, the average COD levels showed a substantial drop from >400 mg/L to 200 mg/L. A similar drop in COD was observed in the inoculated and non-inoculated naturally aerated solutions. The drop in COD in the inoculated solutions captured the effects of the early SRB growth that corresponded in part with the oxidation of organic compounds and the subsequent precipitation of iron sulfides in the control test volume. In congruity with the observation of prolonged periods of high COD after the initial inoculation in the open non-crevice conditions, the average COD levels for the de-aerated inoculated solutions from the specimens with laminate and porous crevices were greater than 400 mg/L. The relatively high values despite the drop from initial values were indicative of conditions to support SRB. In contrast, the terminal COD values for the test solutions sampled from the crevice specimens in the naturally-aerated inoculated solutions and all non-inoculated solutions showed a significant drop relative to the initial condition.

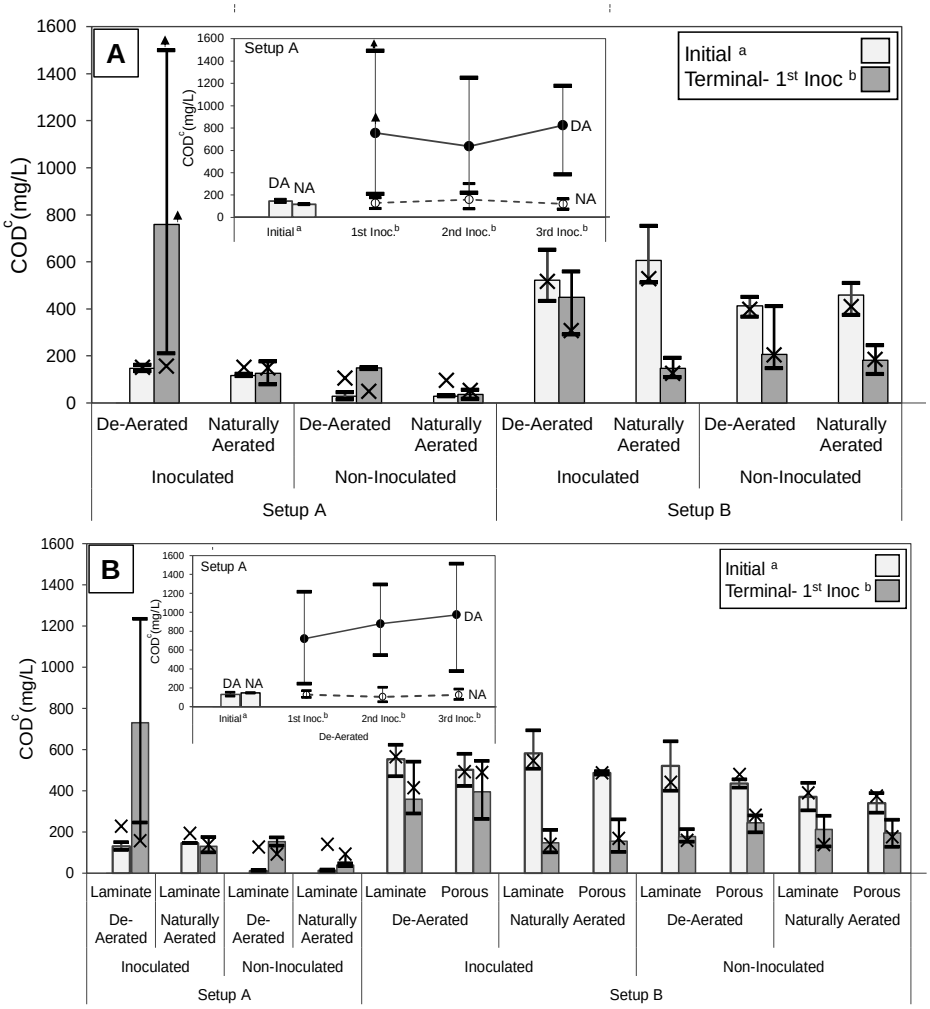

Figure 5.4. COD results for laboratory (A) open-surface and (B) laminate and porous crevice specimens. a. Initial COD at start of 1st measurement regime (<1 hr after 1st inoculation). [b.] COD at the end of measurement regime (prior to subsequent inoculation or termination). [c.] For test setup A, the COD values were from days 5 and 10 in the 1st measurement regime; days 15, 20 and 30 in the 2nd measurement regime, and days 35 and 50 in the 3rd measurement regime. For test setup B, the COD values were from days 10 and 15. (Cross shows the average COD level from testing with 2,000 ppm sulfate from (Permeh et al., 2019a))

5.3.1.2. Sulfide Production

SRB proliferation in the inoculated test solutions was visually evident by the precipitation of black iron sulfide in the test solution. The distinct black coloration was observed for the test setup A open-surface and crevice specimens after the second inoculation event and remained throughout testing as well as for test setup B open-surface and crevice specimens immediately after

the inoculation at the onset of testing. As expected, no coloration was observed in any of the non-inoculated solutions in either test setup A or B. For discussion, the apparent rate of sulfide production was calculated for each time interval between sulfide testing. The apparent sulfide production rate, k_S, described as sulfide mass per time was calculated per Eq 5.2,

$$k_s(t_n) = \frac{\Delta C_n \times V}{\Delta t_n} \tag{5.2}$$

where ΔC is the difference in sulfide concentration (mg/L) and Δt is the difference in time (day) in the interval n between test measurements, and V is the test solution volume (L). The k_S values are shown in Figure 5.5, for test setup A and B for the open-surface and crevice test specimens.

In test setup A, there were distinct spikes in the apparent sulfide production rate corresponding to each inoculation event. The spikes in the sulfide production rates captured the renascent sulfate reduction reactions that occurred upon the injection of external SRB populations at each inoculation event. The elevated k_S values corresponded well with the visual observations of the sulfide precipitation. After the first inoculation, only a slight visual indication of sulfide precipitation was observed and accordingly, the sulfide production rate was relatively lower (<0.1 mg/day). However, after the second inoculation, the darkening of the test solution corresponded to the spike in k_S to levels greater than 0.4 mg/day. However, the time duration of the spikes was not prolonged and the increase in k_S typically lasted only for a few days.

Larger sulfide production rates (>1 mg/day) were observed for specimens in the de-aerated SRB inoculated test solutions in comparison to the naturally-aerated SRB inoculated test solutions (<0.5 mg/day) attesting to the supporting environmental conditions in the former and the apparent detriment of aerated conditions for SRB. In either case, the short duration of the sulfide production indicated that even though prolonged aggressive SRB activity was not promoted with the subsequent injections of external SRB populations, the injections apparently could allow for overall

sustained SRB activity. The inoculations of SRB introduced in the aliquots of the MPB solution allowed for the nutrient concentrations in the test solution to be augmented. This allowed for greater subsequent SRB growth as was evident by the significantly larger sulfide production rates after the subsequent inoculations.

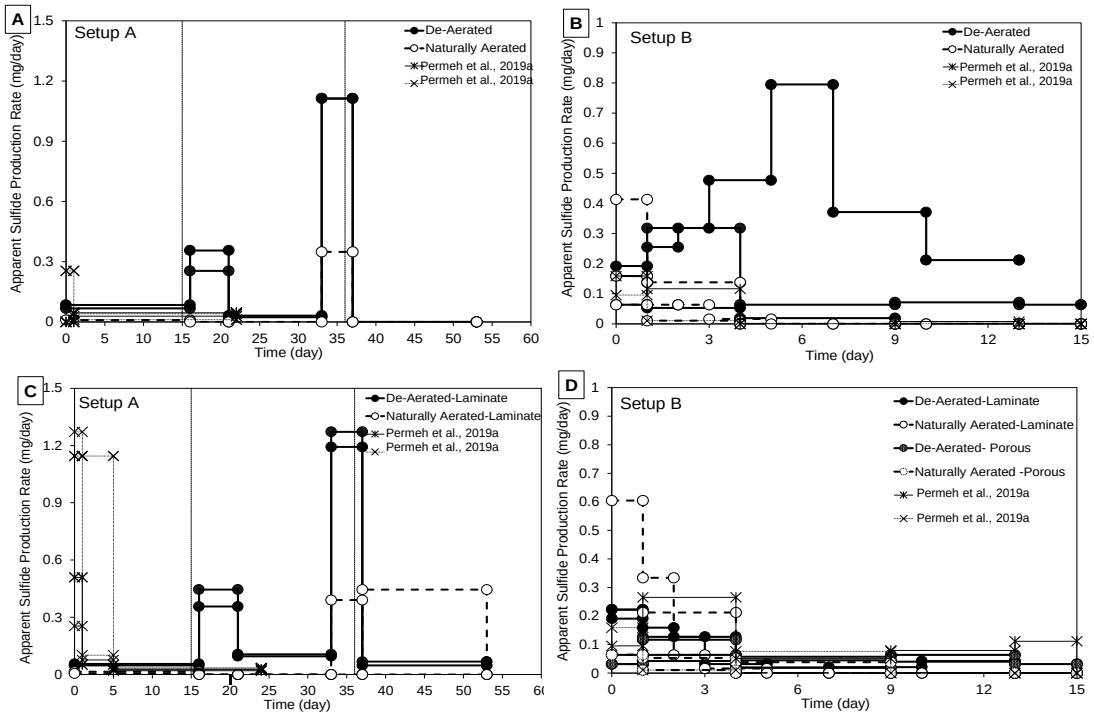

Figure 5.5. Apparent sulfide production.
(A) and (B) open-surface specimens. (C) and (D) laminate and porous crevice specimens.
Data from (Permeh et al., 2019a) : ˣ -Naturally-Aerated ˣ -De-Aerated

Similar spikes in k_S were observed for the crevice specimens. However, there was an indication that the laminate crevices can allow for changes in the crevice solution that can support SRB growth. After the third inoculation after day 35, one of the test specimens had a sustained k_S value (>0.4 mg/day) above the unaffected sulfide production rates (<0.1 mg/day) for more than two weeks. This observation implicated that deaeration conditions or accumulation of nutrient levels within the crevice can develop to facilitate SRB growth. These localized environments would provide better sheltering conditions than the de-aerated bulk solution testing. The trends in sulfide measurements for open-surface and crevice specimens were generally consistent with the COD

characterizing SRB development. For the specimens with the de-aerated solutions inoculated with SRB, the increase in COD that remained high after subsequent inoculations characterized the environment to support growth in SRB from the inoculations. In contrast, the low COD that remained low in the naturally aerated solutions was consistent for an environment with limited SRB activity.

In test setup B, the early SRB activity due to the inoculation at the beginning of testing was evident by the early higher sulfide production rates, consistent with the early coloration of the sulfide precipitation. All inoculated specimens showed a blackening of the solution, but the de-aerated solutions showed higher levels of sulfide precipitates. The sulfide production rates generally dissipated for all test specimens except for the inoculated open-surface specimens in de-aerated test solutions. These results were consistent with the sustained high COD for the latter case and the drop in COD for the former. As expected, the de-aerated solution conditions allowed prolonged SRB growth there during the test period as was evident by the increase in k_S after the initial inoculation and sustained values (as high as 0.8 mg/day) higher than the initial k_S values. As in test setup A, the naturally aerated conditions for the open-surface test specimens did not allow for the greater SRB activity observed for the de-aerated test conditions.

For the crevice specimens, the general trend in the apparent sulfide production rate was similar to the open-surface specimens where the early high sulfide production rates dissipated with time. The sustained sulfide production rates as observed for the complementary open-surface de-aerated test specimens was not reproduced in the crevice specimens, even though similar COD trends were observed. However, the apparent sulfide production rate was elevated (0.6 mg/day) for the laminate crevice test specimens where the bulk solution was in the naturally-aerated condition. It was evident that the local laminate crevice environment allowed for conducive conditions for early SRB proliferation.

Test data for both COD and sulfide levels from test setup A and B were correlated as shown in Figure 5.6. As expected, the apparent sulfide production rates were higher in the test solutions with higher COD and there is an indication of higher rates in the de-aerated conditions compared to the naturally-aerated conditions. In general, sulfide levels larger than 0.1 mg/L were present when COD exceeded a lower minimum bound of 250 mg/L for the inoculated specimens. Non-inoculated specimens as expected did not show sulfide production. In test setup A, it was evident that the high COD levels associated with the consecutive pulse injections of nutrients corresponded to high k_S values. Indeed, the highest k_S values (>1mg/day) were observed after the final pulse injection. The k_S values in test setup B (k_S<1 mg/day) generally did not show as large variability during the times of activity as in test setup A, and the maximum k_S values in test setup B were lower than in test setup A. The pulse distributions of external SRB and nutrients appeared to have a positive effect to enhance SRB growth (whether associated with MIC or not) compared to the closed condition. However, as discussed earlier, the enhanced growth rates did not appear to be sustained and other environmental conditions such as aeration levels are critical.

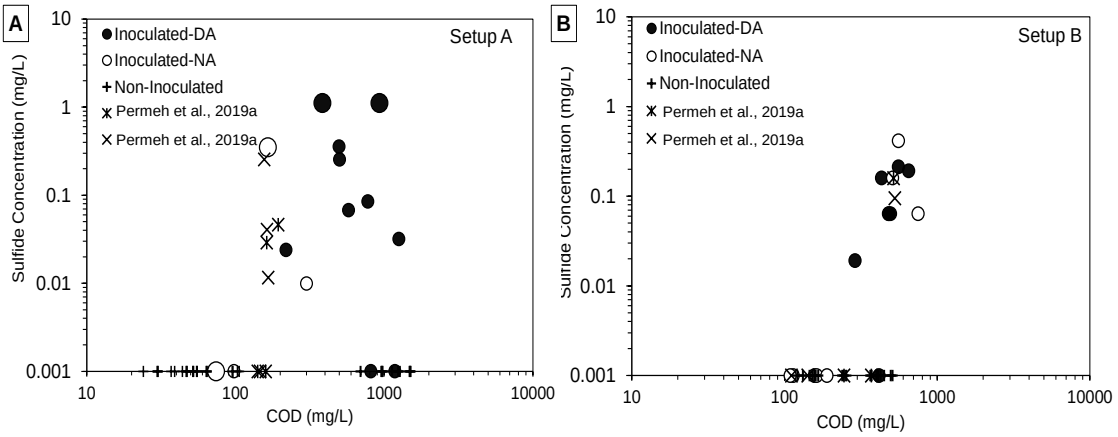

Figure 5.6. Assessment of SRB activity by sulfide concentration and COD.
(A) Test Setup A. (B) Test Setup B. Data from (Permeh et al., 2019a), × -Naturally-Aerated ✱ -De-Aerated. 0.001 mg was arbitrarily selected for the tests where no sulfide was measured.

5.3.1.3. Microbiological Analysis

Table 5.6 shows the surface SRB levels on the open-surface and crevice specimens. As expected, the SRB levels were zero or negligible for the non-inoculated test specimens for both test setups. At the end of testing in setup A, the SRB content was 500,000 CFU in the de-aerated condition and 27,000 CFU in the naturally aerated condition. Also, higher SRB levels ($>10^8$) were measured in the deaerated conditions than naturally-aerated conditions (10^6) on the open-surface specimens from test setup B. Comparisons of data from reference [9] showed similar SRB populations in similar testing at higher sulfate concentrations.

Differentiation of the SRB populations was not well manifested in the comparative testing of the laminate and porous crevice geometries test setup B. Commensurate SRB levels were observed for both crevice geometries within their respective subgroups of bulk solution aeration levels. The SRB levels were higher on the steel surfaces within the crevices on the specimens subjected to de-aeration than natural-aeration conditions for the inoculated specimens for test setup A and B. It was evident that the external aeration levels in part influenced the crevice environmental conditions during the testing, and anoxic conditions may not necessarily have developed within the crevices for the specimens where the bulk solution was naturally-aerated. The results were consistent with the higher sulfide production levels associated with larger SRB populations in the de-aerated solutions than the naturally-aerated solutions. In field service conditions, it was expected that the crevice environments will promote differential aeration conditions.

The SRB populations did not show differentiation by the mode of external SRB and nutrient injections. The relatively high SRB levels at the end of testing for both test setup A and B and in both naturally aerated and de-aerated conditions indicated that SRB can be present regardless of the modality of external population and nutrient injection. The detected bacteria populations would not solely be involved in the metabolic paths associated with MIC as the test solution also contained organic matter that can be used by the SRB. Gu et al., 2019 described mechanisms where

SRB metabolism to promote MIC occurs in regions with low carbon content. If environmental conditions are optimal, SRB can continue to proliferate to levels that can facilitate MIC.

Table 5.6. Surface SRB levels on open-surface and crevice specimens

Test Condition		Inoculated		Non-Inoculated		Inoculated		Non-Inoculated	
						Laminate	Porous	Laminate	Porous
Setup A[a]	De-Aerated	500,000 (A), 500,000 (A)	-	-	-	500,000 (A), 115,000 (A)	-	<1 (NA), <1 (NA)	-
	Naturally Aerated	27,000 (A), -	-	<1 (NA), -	-	27,000 (A), 6,000 (A)	-	<1 (NA), <1 (NA)	-
Setup B[b]	De-Aerated	$\geq 10^8$, $\geq 10^8$	$\geq 10^8$ [c]	0, 10^2	10^3 [c]	$\geq 10^8$, $\geq 10^8$ 10^7 [c]	10^6, 10^7 10^7 [c]	10^3, 0 0 [c]	0,0 0 [c]
	Naturally Aerated	10^6, 10^6	10^6 [c]	10^1, 10^3	0 [c]	10^6, 10^6 10^6 [c]	10^6, 10^6 10^6 [c]	10^1, 10^3 10^4 [c]	0,0 0 [c]

[a] BART (CFU/ml), [b] BTS (counts/mL), [c] from (Permeh et al., 2019a), for solutions with 2,000 ppm sulfate

The results from the COD, sulfide production and SRB populations provided verification that adequate nutrient levels initially present in the crevice environment can support SRB activity for some time although the initial sulfate concentrations did not have a major influence in the laboratory setting. Sequential injections of nutrients and viable SRB alone did not necessarily broaden SRB growth but the injections allowed for SRB populations to be sustained. The effect of the idealized laminate and porous crevice environments on SRB activity was not well differentiated here and it was apparent that other environmental conditions especially oxygen levels appear to be dominant factors. It was evident that SRB populations can be sustained. In the following, their role in corrosion is discussed.

5.3.2. Corrosion Development

5.3.2.1. Open-Surface

The OCP of the open-surface specimens in the absence of SRB was approximately -750 mV_{SCE} and -650 to -750 mV_{SCE} in the de-aerated and naturally-aerated solutions, respectively, consistent with the expected values for steel in open neutral pH solutions (Roy et al., 1996). The corrosion potentials developed from the polarization of the iron oxidation half-cell reaction and the reduction reactions from hydrogen reduction and oxygen reduction through the developed oxide layer on the steel surface. For the laboratory tests, concentration polarization of the oxygen reduction reaction was expected as the solutions had generally low oxygen levels (relative to field conditions) with the introduction of nitrogen gas for the de-aerated solutions and the limited solution convection to promote oxygen diffusion for the naturally aerated conditions.

As shown in Figure 5.7, more electropositive potentials developed and were sustained for longer times for the inoculated test specimens, generally consistent with the potential ennoblement often associated with the cathodic reactions in SRB-MIC such as in equations 2 and 3. Subsequent drops in potentials to more electronegative values during the inoculation period were thought to be due to loss of SRB activity associated with MIC where adsorbed hydrogen on the steel surface could redevelop. For test setup A, the apparent ennobled potential for the steel in the de-aerated solutions was as electropositive as -581 mV_{SCE} and the time duration of the potential ennoblement was 7 days in the 1^{st} inoculation period and 1 day in the 2^{nd} inoculation period. The potential remained electronegative after the 3^{rd} inoculation event. Potential ennoblement was not well manifested in test setup A for the specimens in naturally aerated solutions. For test setup B, the ennobled potential was as positive as -574 and -568 mV_{SCE} for the deaerated and naturally aerated inoculated specimens, respectively; and the time duration of the potential ennoblement was the entire 15 day period of the test and 10 days for the deaerated and naturally aerated conditions, respectively. As expected, potential ennoblement was not observed for the control non-inoculated

test specimens except for one outlying result in the 1st inoculation period in test setup A. In a similar way, potential ennoblement was observed in the testing of inoculated solutions with higher sulfate concentrations as detailed in reference (Permeh et al., 2019a).

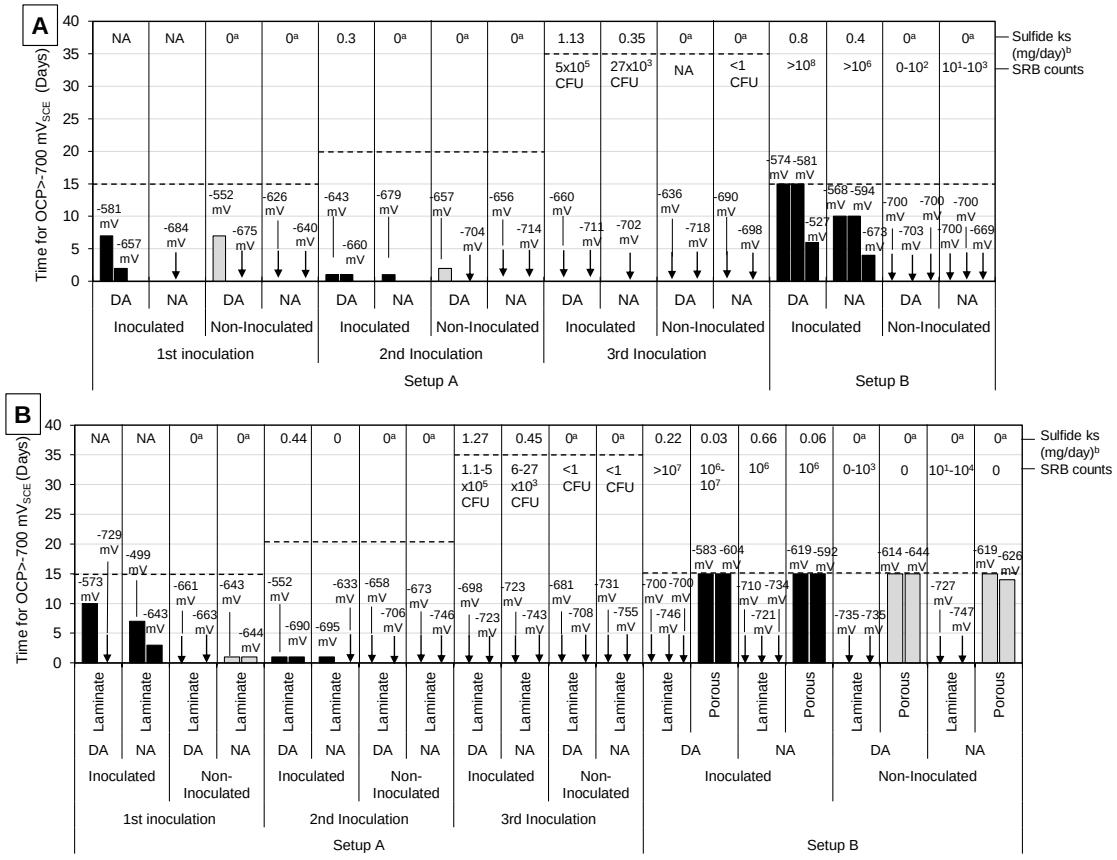

Figure 5.7. Duration of potential ennoblement of (A) open-surface and (B) crevice specimens (> -700mVSCE),Potential values indicate the most electropositive recorded value for each inoculation period. Horizontal lines represent the time duration of each inoculation period. [a]. No sulfide precipitation observed. [b.] Maximum calculated ks.

The results of the LPR tests generally conformed with the OCP results and provided a general indication of the steel corrosion rates that developed in the test solutions, although errors associated with the non-uniform corrosion below the biofilm exists as well as with the crevice specimens. The corrosion of the steel specimens in the non-inoculated solutions was moderated by

oxygen-reduction (albeit under concentration polarization conditions) and to some degree hydrogen-reduction reactions.

As shown in Figure 5.8, the corrosion rates in the chloride-containing solutions in the absence of the SRB was dependent on the oxygen levels. The terminal corrosion current density for the testing was 5-10 $\mu A/cm^2$ and 0.5-1 $\mu A/cm^2$ in the naturally aerated and de-aerated open-surface solutions, respectively. On the other hand, the SRB activity in the inoculated solutions allowed for surface films to develop on the steel surface. All specimens in inoculated solutions developed a layer of the black metal sulfide deposits, but the layer was overall thicker in test setup A than test setup B, in part relating to the longer test period in the former. Corrosion products also accumulated. This layer can reduce the effective steel surface area. Indeed, the overall apparent corrosion current densities (calculated using the nominal surface area) in the inoculated naturally-aerated solutions were lower than the non-inoculated naturally-aerated solutions in test setup A. The SRB activity and environmental conditions below the biofilm have a major effect on the corrosion, and the level of aeration outside of the biofilm in the bulk solution would not be a dominant factor. De-aerated conditions to facilitate SRB growth would be expected to develop naturally under the biofilm for the de-aerated bulk solutions. De-aeration conditions may develop under the biofilm in the naturally-aerated bulk solutions as well, but that can be affected by factors such as the film thickness, film homogeneity, SRB activity, solution convection, etc (Little et al., 1992).

The similar trends in the corrosion current densities with time measured in test setup A and the relatively high corrosion current densities during the test period in test setup B for the specimens in the inoculated naturally aerated and de-aerated solutions would indicate that the environmental conditions below the biofilm were similar regardless of the bulk solution aeration. As such the duration of more electropositive potentials observed in the inoculated test solutions (such as that

better manifested in the de-aerated test conditions) was attributed to the cathodic depolarization associated with SRB-MIC.

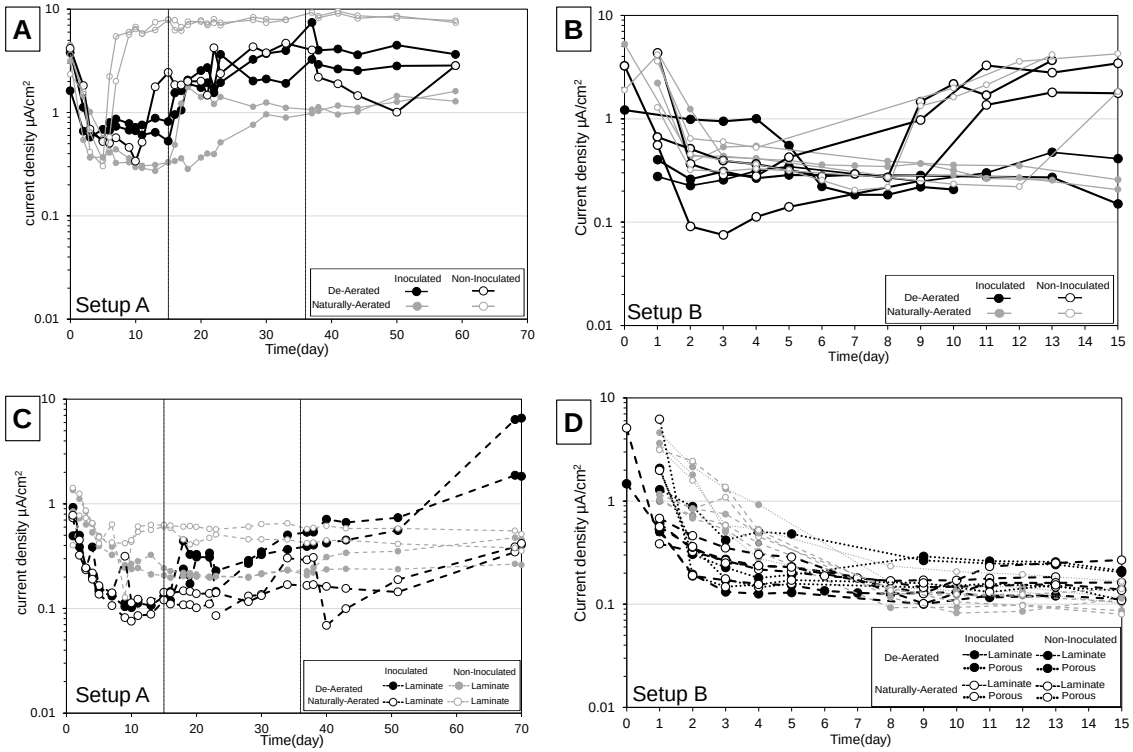

Figure 5.8. Calculated corrosion current density for (A) and (B) open-surface and (C) and (D) crevice specimens.

The high corrosion rates (>1 µA/cm^2) measured at the onset of the 1st and 2nd inoculation in test setup A and during the inoculation period in test setup B coincided with the observed apparent potential ennoblement. In the first inoculation period in test setup A, the terminal current density for the inoculated specimens dropped to the order of 0.5-1 µA/cm^2 indicating a decrease in activities associated with charge-transfer processes involving the steel substrate. After the 2nd inoculation event, the corrosion current density increased (>1 µA/cm^2), also coinciding with the recurring potential ennoblement. No further increases in corrosion current density were observed during the 2nd inoculation event and associated with the 3rd inoculation event. In test setup B, the

corrosion current density was >1 μA/cm^2 for the de-aerated inoculated specimens and was as high as 4 uA/cm^2 for the naturally-aerated inoculated specimens.

The apparent positive shift in the measured potentials and the generally high corrosion current densities after inoculation was generally consistent with the observed increase in COD and sulfide production after the inoculation events. For example, in test setup A, the potential ennoblement and increase in i_{corr} to values greater than 2 μA/cm^2 at the time of the second inoculation coincided with the measured spike in sulfide production. In test setup B, the longer time duration of the potential ennoblement coincided with the prolonged times of i_{corr} greater than 1 μA/cm^2 as well as the measured extended sulfide production time. The results from testing of the open-surface specimens verified that the environmental parameters of the solution under the biofilm are important. However as discussed above, there were consistent trends in the SRB activity, electrical potential, and corrosion current that relate to MIC due to the modality of SRB and nutrient access, that may develop in service by the type of macrofouling.

5.3.2.2. Crevice

There were indicators of the SRB activity within the crevices by the OCP measurements that corroborated with the SRB activity detected by the sulfide production levels and SRB surface populations. Electronegative potentials in the range of -500 to -700 mV_{SCE} were measured for all cases with the laminate and porous crevices including both the inoculated and the non-inoculated cases in test setup A and B (Figure 5.7). In the inoculated solutions in test setup A crevice specimens, there were instances in the first two inoculation periods where relatively more noble potentials (as electropositive as -499 mV_{SCE}) developed. The potential ennoblement here was similar to that observed for the specimens with the open surface conditions in test setup A and B. As discussed earlier, the elevated sulfide levels and SRB surface counts on the steel surface at the end of the experiment confirmed that SRB can be supported in the laminate crevices in test setup A. In contrast, the electronegative potentials (<-700 mV_{SCE}) measured for all the laminate crevice

specimens in test setup B with the tighter crevice environment in part related to the limitations on the ionic connectivity between the crevice environment and the bulk solution as well as the placement of the reference electrode in the bulk solution. Even though the potential ennoblement was not well manifested in test setup B, the high sulfide levels and SRB surface populations showed that the SRB can develop in these tight laminate crevices as well. In a similar manner, the measured potentials for the steel coupons with the porous crevices in test setup B exhibited similar potentials regardless of aeration level, sulfate level, and inoculation; albeit at noble potentials (>-650mV_{SCE}) compared to the complementary laminate-crevice specimens.

As shown in Figure 5.8, the calculated corrosion current densities for the crevice specimens in test setup A and B had overall lower values in comparison to the open-surface specimens due to the non-uniform polarization of the steel surface below the crevice. The overall trends for test setup A and B described earlier for the open-surface specimens were similar here. Like that of the open-surface specimens, it was apparent that the environmental condition at the biofilm-to-steel interface had conditions that allowed for SRB-MIC to develop. In test setup B, the inoculated specimens trended to higher terminal i_{corr} values than the non-inoculated specimens. These enhanced corrosion currents coincided with the prolonged potential ennoblement during the short term inoculation period corroborating that the SRB at the steel interface initiated MIC. The successive injections of external SRB and nutrients in test setup A were shown to promote SRB activity and there was an indication that MIC can recur.

5.3.3. General Discussion

From the trends in OCP, potential ennoblement, and corrosion current density described above, certain corrosion conditions and mechanisms may be surmised. For the non-inoculated open-surface specimens, general corrosion of steel in the chloride neutral-pH solution is expected albeit corrosion rates may be moderated by aeration levels. For comparative specimens inoculated

with SRB, the formation of biofilm on the steel surface could create interfaces to develop MIC that would also be regulated in part by aeration and nutrient levels.

The electrochemical testing for the laminate and porous crevice specimens did not elucidate major differences by the modes of nutrient injection into the bulk solution. As such, the effect of the physical nature of the crevice (such as the laminate and porous crevice as well as its tightness) to facilitate the biologically-influenced charge-transfer process in SRB-MIC was not evident in the testing. In field service, the type of marine organisms, adhesion, and growth can affect the level of shelter and nutrient availability from the natural water.

It was shown that environments such as these with occluded regions that have high initial nutrient levels can sustain SRB-MIC for some period of time. Furthermore, the subsequent introduction of SRB and nutrients into these environments that allow sustained SRB activity can prolong MIC. These results indicate that the hard and soft marine foulers that provide sheltered anaerobic regions for the biofilm that allow periodic nutrient injection can create aggressive conditions to prolong MIC. The developed biofilm with active SRB can develop localized regions at the steel interface where the bio-electrical mechanisms for SRB-MIC as described by Gu et al, 2019can develop .

5.3.4. Electrochemical Impedance Spectroscopy

EIS was measured for all laboratory specimens. For the open-surface specimens, the EIS results would ideally elucidate the steel interface characteristics as SRB develops and differentiate the behavior per the injection modes in test setup A and B. EIS would also differentiate the characteristics of the idealized physical geometries of the macrofouling. Examples of the impedance spectrum in the Nyquist form are shown in Figure 5.9 and 5.10.

Figure 5.11 presents schematics of possible equivalent circuit analogs that may be applicable for the measured impedance response. For the open-surface specimens without SRB inoculations, the impedance response would relate to the solution resistance, steel interfacial

capacitance and charge transfer resistance, characterized by the Randles circuit with a low frequency (*lf*) impedance loop as shown in Figure 5.11A. However, for the inoculated specimens, the effects of the SRB growth on the steel surface can be evident by changes in the impedance response (Permeh et al., 2019b). With the inoculation of SRB, an additional high frequency (*hf*) loop on first approximation can be related to the capacitive and resistive characteristics of the biofilm.

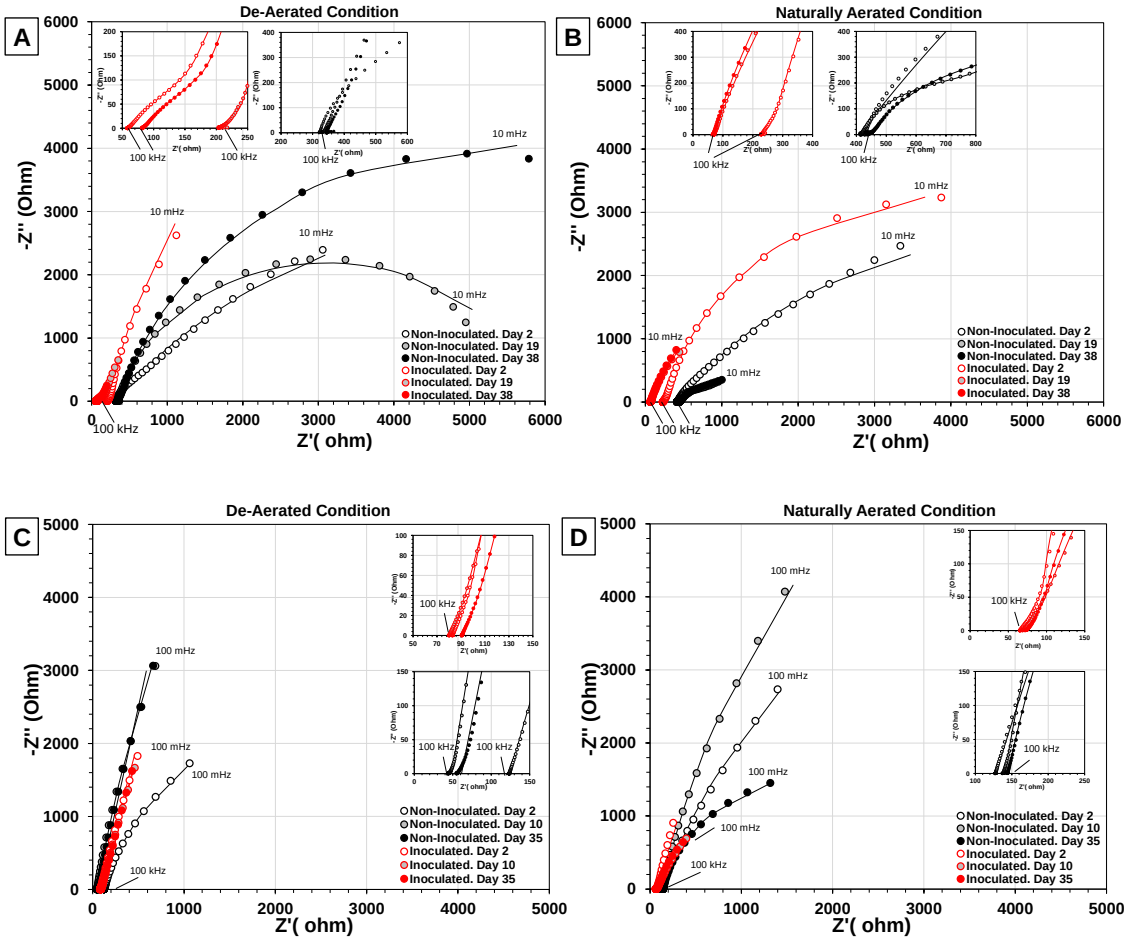

Figure 5.9. Nyquist impedance diagrams for open-surface specimens from (A) and (B) test setup A, and (C) and (D) test setup B. Markers represent measured data and lines show the results of equivalent circuit fitting.

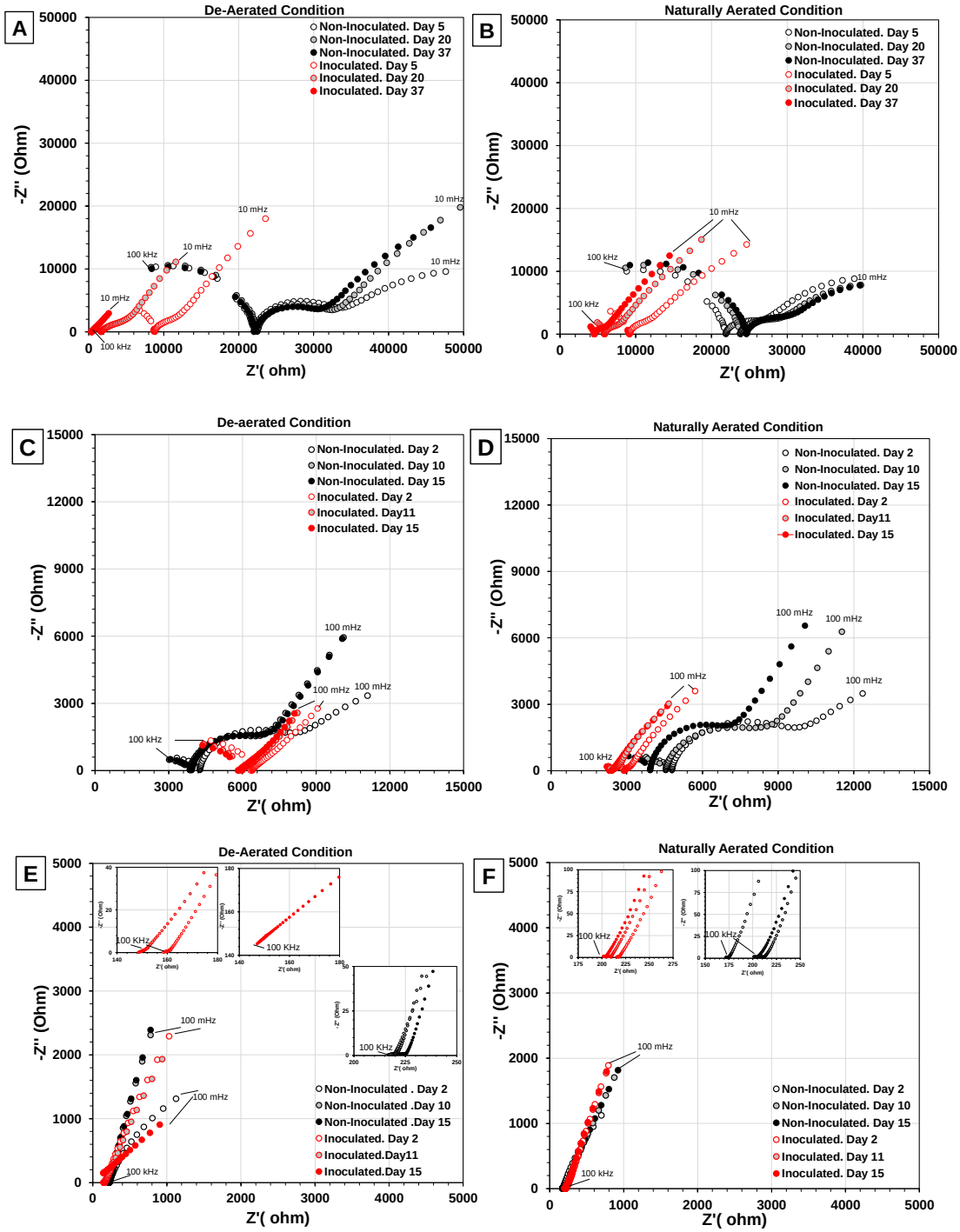

Figure 5.10. Nyquist impedance diagrams for (A), (B), (C) and (D) laminate and (E) and (F) porous crevice specimens. Markers represent measured data.

Figure 5.11B shows the impedance corresponding to the dielectric behavior of the biofilm on the steel. In crevice environments, a more complicated behavior arises due to uneven current distribution and heterogeneous impedance within the crevice. The impedance behavior for the porous and laminate crevices can be characterized by multiple time constants associated with the crevice outer material, steel interface, and the current distribution effects in the crevice that can be considered by treatments such as a transmission line (De Levie, 1963; Diaz et al., 1993; Lau and Sagues, 2011). Figure 5.11C shows an equivalent circuit analog for an idealized case for a porous medium on steel, but impedance dispersion may arise as well. Figure 5.11D shows a case for distributed impedance within a laminate crevice.

As expected, the open-surface non-inoculated specimens in test setup A and B in both aeration conditions typically showed the single *lf* impedance loop in the Nyquist diagrams. The equivalent circuit analog in Figure 5.11A (with the use of an impedance constant phase element, CPE, for the capacitive terms) characterized well its impedance response as shown by the fitted impedance data shown in Figure 5.11A-D. The inoculated de-aerated and naturally aerated specimens likewise showed a similar *lf* impedance loop in the Nyquist diagrams for test setup A and B but with some frequency dispersion (that was visually acute for the de-aerated test setup A specimens). The *lf* impedance loop was graphically smaller for the inoculated specimens than the non-inoculated specimens. The smaller impedance loop corresponds to an increase in the interface capacitance and a lower polarization resistance that in part relates to the conditions below the biofilm that accommodate MIC (for example enhanced ionic concentrations, removal of the surface oxide film and enhanced iron oxidation rates (Ter Heijine et al., 2018; Grden, 2017).

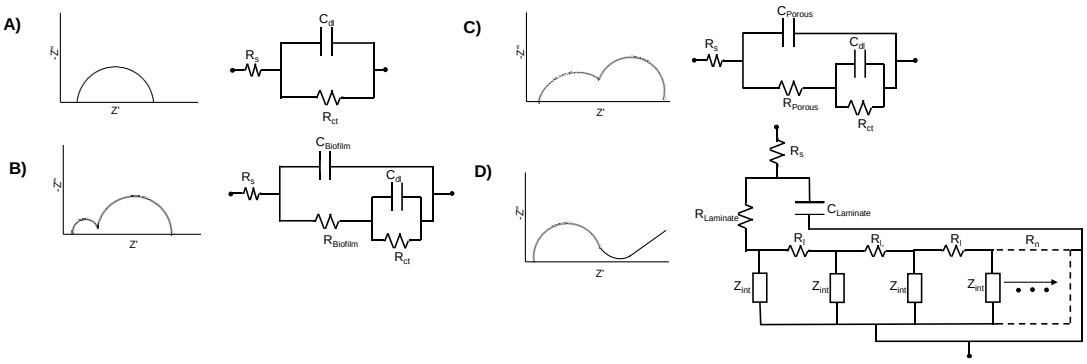

Figure 5.11. Schematic of equivalent circuit analogs
A). steel interface. B). biofilm on steel interface. C). porous layer (crevice) on steel Interface. D). steel interface under a crevice.

At the higher frequencies, the nascent impedance dispersion was not manifested as a defined *hf* impedance loop but did show more distinctive features for the inoculated specimens especially for the test setup A de-aerated condition. Even though the developed biofilm in those test conditions (as corroborated in the previous sections) had electrochemical characteristics such that its impedance was not visually discrete, all of the impedance spectra for the inoculated specimens could be fit to the equivalent circuit analog in Figure 5.11B but replacing the capacitance elements with a CPE. The impedance associated with these features was also discriminated in the Bode phase angle diagram shown in Figure 5.12. The fit data for the inoculated specimens are shown in Figs. 5.9A-D and Figs. 5.12A-D.

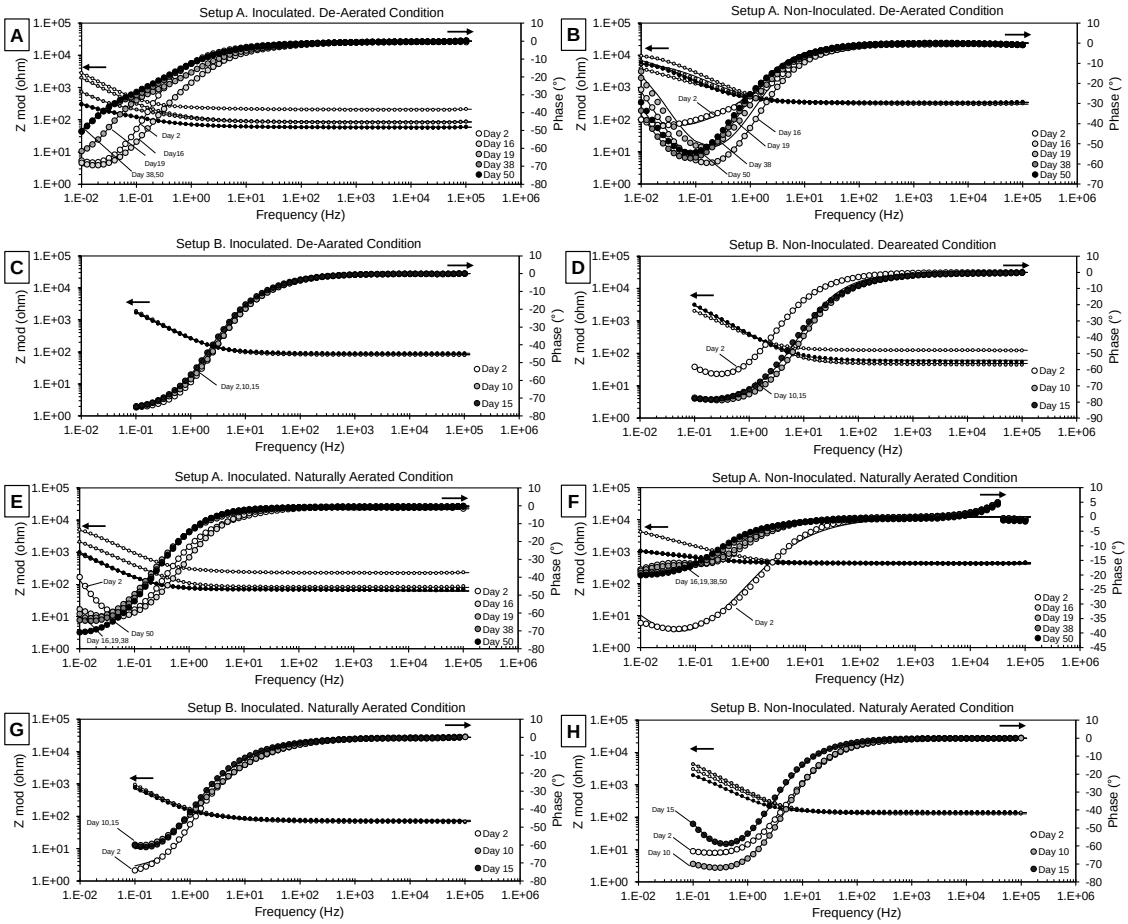

Figure 5.12. Bode impedance diagrams for open-surface specimens in the (A), (B), (C) and (D) de-aerated Condition and (E), (F), (G) and (H) naturally-aerated condition. Markers represent measured data and lines show the results of equivalent circuit fitting.

In the test setup A de-aerated test conditions, the development and gradual buildup of the thick layer of the biofilm and slime on the steel surface were apparent by the change in the shape of the Bode plot with time. At early times after the initial inoculation, the Bode phase angle plot showed a more uniform valley with a distinct trough between 10 and 100 mHz. With time, two unique troughs developed at frequencies below 1 Hz. This effect was not as well manifested in the inoculated naturally-aerated conditions or within the shorter time period for the specimens in test setup B. This is in part due to the lesser accumulation of biofilm in those conditions relative to the longer de-aerated tests in setup A.

The *hf* impedance loops for the inoculated specimens had a pre-exponential CPE admittance term in the order of $1x10^{-4}$ to $8x10^{-3}$ Ss^{n}. The CPE n term ranges from 0.3 to 0.9. Following the approach developed by Hsu and Mansfeld, 2001, the capacitance associated with the *hf* loop was $6.5x10^{-7}$ to $1.5x10^{-2}$ F for test setup A and B, similar to the values resolved for biofilms by Permeh et al., 2019b and discussed in chapter 7. The film resistance was in the range of 5-600 ohm in test setup A and 150-400 ohm in test setup B. The film resistance and capacitance terms typically increased with time for test setup A and B consistent with the biofilm growth (Ter Heijine et al., 2018).

As discussed for the idealized impedance described in Figs. 13C and 13D, the impedance spectra for the laminate and porous crevice specimens in test setup A and B (Figs. 12A-F) showed multiple time constants and frequency dispersion that resulted in spectra characterized by a zero imaginary impedance such as that described by Lau and Sagües, 2011 for crevice environments. The non-uniform polarization of the steel surfaces below the plastic shim and the sponge produced such complicated impedance responses that require consideration of treatments such as an electrical transmission line. Work by Urquidi and MacDonald introduced a radial transmission line model that may be representative of the crevice environments under marine fouling (Diaz et al., 1993), Like the impedance response for the open-surface specimens described earlier, the size of the impedance loops for the inoculated specimens was graphically smaller than the non-inoculated specimens relatively for each test condition, relating to the conditions developed by the SRB and biofilm in the inoculated cases. Otherwise, the other impedance processes that exhibited separate time constants were similar in nature with apparent changes in their resistive components with time. Until the complicated impedance associated with the frequency dispersion is defined, the differentiation of SRB growth and activity due to the injection modes and the physical crevice environments were not deduced.

In part to provide a quantitative comparison of the overall impedance of the systems (despite the complicating factors for the crevice specimens), on first approach, the total impedance at 100 mHz ($|Z_{100mHz}|$) was compared (Figure 5.13). The differences in the total impedance for the various test conditions would reflect the resistive and capacitive electrical behavior of the electrolyte, biofilm, and the steel interface that in turn are directly or indirectly related to SRB activity. As described earlier, the increase in biofilm capacitance that was reflected in the smaller impedance loops would also be manifested in smaller total impedance at the 100 mHz metric. The SRB activity referred to here also includes the effects of the SRB growth that may include changes in the net electrical resistance between the steel surface and the reference electrode as well as changes in charge-transfer resistance associated with MIC.

Z_{100mHz} for the inoculated cases was lower than the non-inoculated cases for all test conditions in test setup A and B except for some terminal values in the setup B naturally aerated (open-surface and crevice) specimens. Z_{100mHz} was typically lower for the steel in the de-aerated inoculated solutions relative to the naturally aerated inoculated solutions. In test setup A, the impedance showed a distinct drop after the second inoculation (more so for the de-aerated than the naturally aerated condition). Comparisons of these findings show that SRB activity is associated with low total impedance and confirms the benefit of low oxygen environments and the availability of nutrients to support SRB activity. In the physical crevice environment, there was a similar drop in impedance as the open-surface specimens after the inoculation events in test setup A indicating that the sequential injections promoted SRB activity in the crevices. In test setup B, Z_{100mHz} was lower for the porous crevice specimens than the laminate crevice specimens regardless of aeration and inoculation, thus differentiation between the crevice geometry was not identified.

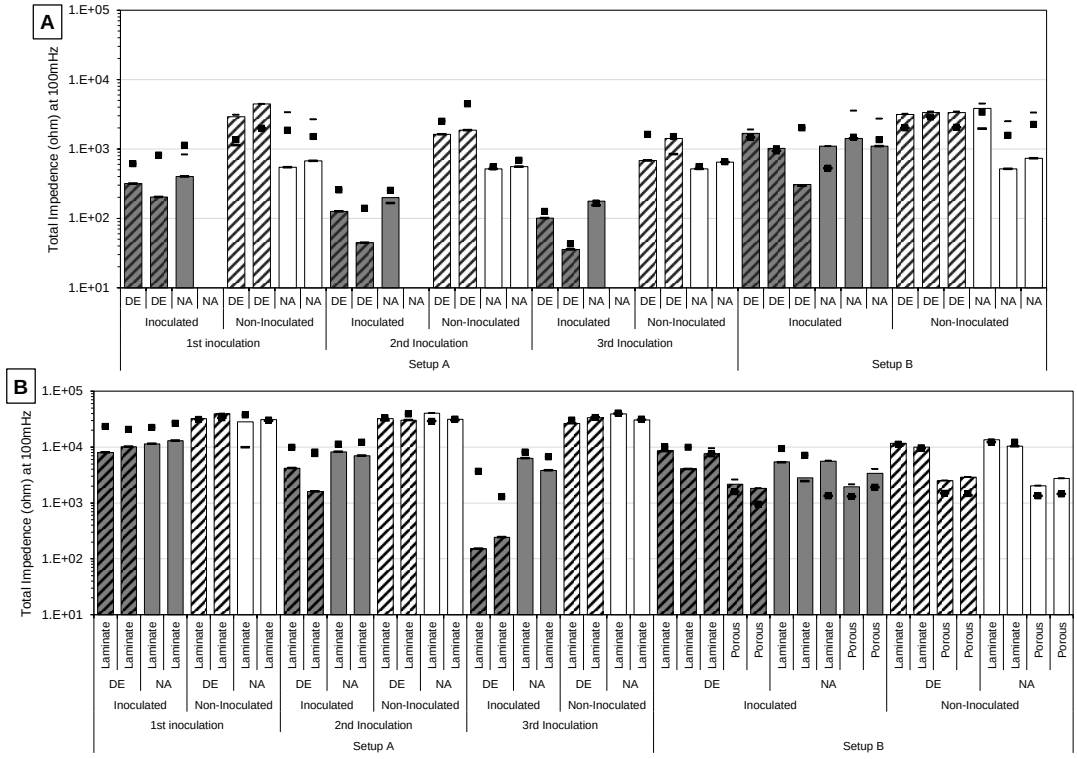

Figure 5.13. Total impedance values at 100mHz for (A) open-surface and (B) crevice specimens. (Square marker shows the initial value and dshline shows the minimum and maximum values)

5.3.5. Visual Assessment

Figure 5.14 shows the test specimens after removal from the solution and the steel surface after cleaning for each test condition. Consistent with the COD and sulfide measurements described earlier, the biofilm and the layer of sulfide deposits formed from the SRB activity developed on the surface of the specimens exposed in the inoculated solutions. As expected per the extended time of testing and captured by EIS testing, this layer was much thicker for the test setup A specimens in the de-aerated condition than its complementary naturally aerated test specimens and the inoculated test setup B specimens. For test setup A and B, the film was less prominent in the naturally-aerated condition.

Surface corrosion was apparent for all specimens due to the chloride ion presence in the neutral pH solution. Consistent with the LPR testing, the aeration level moderated the level of

corrosion for the non-inoculated specimens. After cleaning the open-surface specimens, localized surface tarnishing and small pits were significant in the inoculated specimens (more so in the de-aerated condition) in part attributed to the biofilm and SRB, whereas a more uniform surface appearance was evident below the surface rust for the non-inoculated specimens.

All crevice specimens showed an indication of discoloration of the steel surface underneath their plastic covers and holders. The center orifice of the laminate crevice specimens, as well as the regions radially extended from the center (consistent with the impedance frequency dispersion), showed corrosion in all of those specimens, but a greater extent of non-uniform corrosion further extended within the crevice was evident for the inoculated specimens in test setup A. All of the porous crevice specimens showed a mottled surface appearance but the discoloration was visually more distinct for the inoculated specimens for each of the test bulk solution aeration cases.

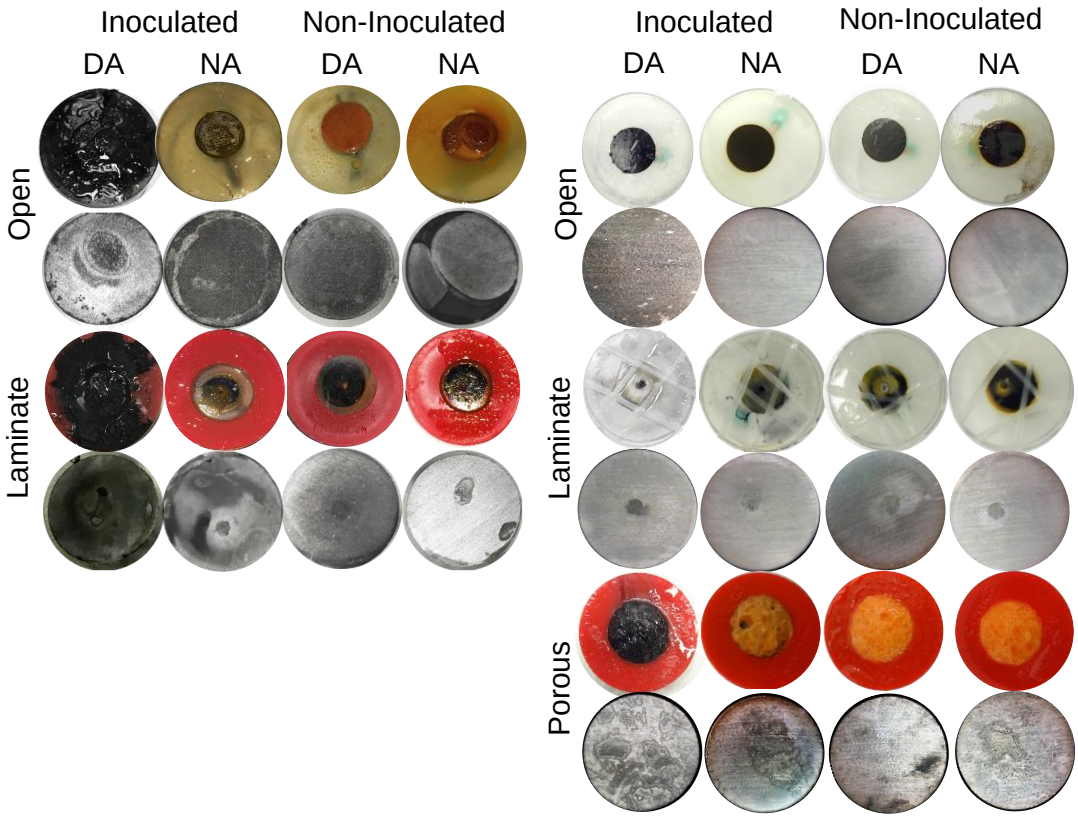

Figure 5.14. Photos of test specimens after removal from solution and steel surface appearance after cleaning

5.4. Results and Discussion for Field Testing

5.4.1. Surface Fouling Condition

Figure 5.15 shows the exposed specimens from the three test sites before and after cleaning at various depths up to 2.44 m (8ft) BMG. Growth and spread of the various marine fouling organisms can create sheltered environments with conditions that affect SRB growth as well as corrosion development. For example, the dense coverage of the substrates reduces the access of dissolved oxygen. Loose attachment and non-uniform macrofouling of organisms may create oxygen concentration cells resulting in crevice corrosion under the base of the barnacle. Furthermore, the attachment an encrustation of the foulers can modulate the availability of nutrient access from the bulk solution to the bacteria colonies at the steel substrate.

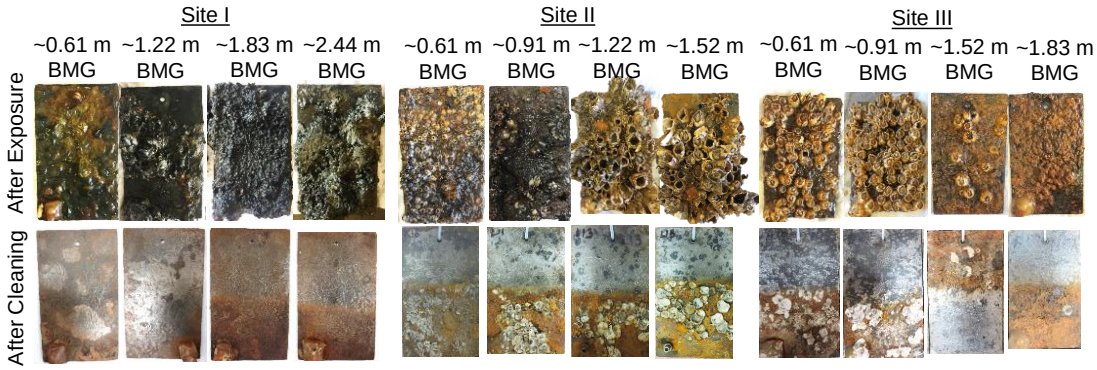

Figure 5.15. Photo of field test coupons after exposure and after partial cleaning.

Site I. Marine fouling by hydroids, bryozoans, barnacles, and oysters developed. Clustered acorn barnacles and soft marine masses (hydroids) were predominant at 0.92-1.22 cm (3-4 ft) BMG and 1.22-2.44 m (4-8 ft) BMG, respectively. Some of the acorn barnacles were visually identified as established species in Florida coastal waters such as *Amphibalanus amphitrite* (diameters less <10 mm) at the intertidal zone and *Megabalanus coccopoma* (diameters > 10 mm diameter) in the submersion zone due to their characteristic coloration and size (Carlton and Ruckelshaus,1997); McPherson et al., 1984).

Site II. The steel coupons in the brackish water at the mouth of the Alafia River emptying into the Gulf of Mexico developed a dense coverage of fouling organisms including acorn barnacles. The barnacles had visual characteristics of barnacle species, such as *Balunus eburneus* and *Amphibalanus improvises*, that have been established in the Gulf of Mexico (Kaplan, 1988; Felder and Camp, 2009).

Clustered and interlayered populations of the barnacles with diameters from 5-16 mm were observed from 0.61-1.68 m (2-5.5 ft). BMG. Specimens placed at 0.15-0.30 m (0.5 to 1 ft) BMG developed a thick iron oxide layer even after hand cleaning. The fouling and oxide layers could be easily hand cleaned off of the specimens placed from 0.61-1.68 m (2-5.5 ft) BMG, revealing a non-uniform sinuous texture.

Site III. Similar fouling organisms as Site II were observed at Site III, but the barnacle population was significantly lower due to the lower salinity and nutrient levels upstream. The barnacles were clustered at 0.61-1.37 m (2-4.5 ft) BMG but in less-dense communities as compared to Site II. Barnacle diameters were from 5 to 15 mm. Coupons at 0.15 -0.61 m (0.5 to 2ft) BMG (intertidal zone) had thick outer oxide film with a rough surface after cleaning.

Anaerobic environments can develop beneath the fouling organisms which can host sulfate-reducing bacteria. Figure 5.16 shows an example of the conditions below the marine foulers where a sulfide deposit, slime film, and corrosion products were black in color. In addition to SRB, three other types of corrosion-related bacteria (IRB, APB, and SFB) were measured under the fouling surfaces using BART test kits (Table 5.7). All three sites had high surface populations of IRB, APB, and SFB, indicative of the aggressive conditions that can form underneath the marine fouling.

Figure. 5.16. Example of Under Fouling Surface Condition.

Table 5.7. Surface bacteria population on field test coupons (replicate test coupons)

Bacterial	Site I				Site II	Site III
Population (CFU/mL)	~1.22m BMG	~1.52m BMG	~2.32m BMG	~2.44m BMG	~1.68m BMG	~1.83m BMG
SRB	6,000(A), 6,000(A), 6,000(A)	75(M), 1,400(M), 6,000(A), 500,000(A)	1,400(M), 6,000(A), 27,000(A)	75(M), 115,000(A)	5(NA), 20(NA), 1,400(M), 27,000(A)	20(NA), 1,400(M)
IRB	2,200(M). 2,200(M). 2,200(M)	150(M), 2,200(M), 2,200(M), 9,000(A)	9,000(A), 35,000(A), 35,000(A)	35,000(A), 2,200(M)	150(M), 150(M), 9,000(A), 9,000(A)	35,000(A), 140,000(A)
APB	82,000(A), 82,000(A), 82,000(A)	14,000(A), 82,000(A), 82,000(A), 82,000(A)	82,000(A), 82,000(A), 82,000(A)	82,000(A), 475,000(A)	82,000(A), 82,000(A), 82,000(A), 475,000(A)	475,000(A), 475,000(A)
SFB	1,750,000(A), 1,750,000(A), 1,750,000(A)	1,750,000(A), 1,750,000(A), 1,750,000(A), 1,750,000(A)	1,750,000(A), 1,750,000(A), 1,750,000(A)	1,750,000(A), 440,000(A)	440,000(A), 440,000(A), 1,750,000(A), 1,750,000(A)	1,750,000(A), 1,750,000(A)

Aggressivity. (NA) Not Aggressive, (M) Moderately Aggressive, (A) Aggressive (General guidelines for BART test for corrosion)

5.4.2. Corrosion Development

The lab-measured potentials of the freely corroding specimens were not dissimilar to in-situ field measurements indicating that the effects of the changes to the steel electrode during the extraction and lab test setup were minimal. The potentials for the steel specimens were $-731 < E < -535$ mV_{CSE} for Site I, $-693 < E < -385$ mV_{CSE} for Site II, and $-690 < E < -196$ mV_{CSE} for Site III for the specimens from the various exposure depths. The lab and field in-situ measured potentials showed more negative values for the freely-corroded specimens originally placed at depths with continuous immersion (>1.52 m BMG for Site I, >0.92 m BMG for site II and III). This can be in part reflective of the thick corrosion oxide layer that developed on the specimens that have cyclic immersion as well as the greater coverage of marine fouling on the steel substrate from the depths with continuous immersion. Marine flora amassed at depths greater than 1.52 m (5ft) BMG at Site I and interlayers of clustered barnacles formed at depths greater than 0.92 m (3ft) BMG for Site II and III. The presence of the marine fouling could reduce the surface area for oxygen reduction, possibly create local anodes below the occluded regions, and support localized development of MIC. Laboratory LPR measurements for the coupons from depths with continuous immersion showed greater instantaneous corrosion rates at Site I than Site II and III ($[i_{corr}(\text{Site } I_{>1.5m\ BMG}) \sim 50\ \mu A/cm^2] > [i_{corr}(\text{Site } II_{>0.9m\ BMG}) \sim 30\ \mu A/cm^2] > [i_{corr}(\text{Site } III_{>0.9m\ BMG}) \sim 5\ \mu A/cm^2]$). The instantaneous corrosion rates for specimens collected from the tidal regions (measured in a static lab test solution) were lower than that measured for the specimens with continuous immersion and did not capture the aggressive conditions (such as the cyclic wetting) at the field site.

Figure 5.17 shows representative magnified images of the steel substrate after cleaning depicting the corroded surface and corrosion pits. For Site I, the observed pit diameter and depth ranged from 2 mm to 9 mm and 0.1 mm to 1.3 mm, respectively. Specimens from Site II had pit diameters in the range of 3.5 mm-12 mm and depths of 0.14 mm-0.74 mm. Specimens from Site III had pits diameters in the range of 2 mm-5 mm and depths of 0.12 mm -0.9 mm. In many cases,

corrosion pits were observed under the remnant barnacle base plates that were adhered to the steel. Results of the nominal corrosion rates calculated by Eq 5.1 are shown in Figure 5.18.

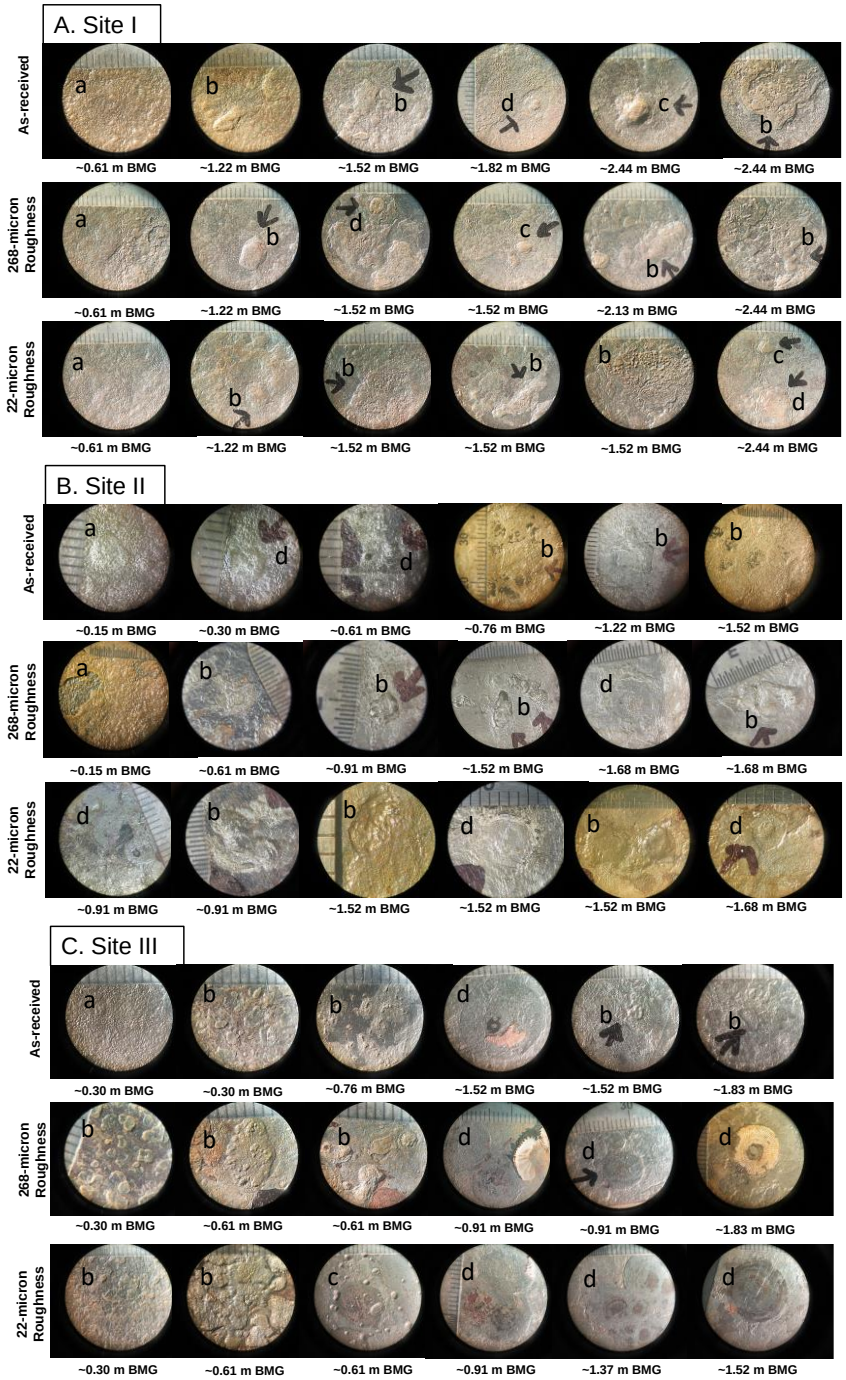

Figure 5.17. Magnified view of surfaces of specimens from (A) Site I, (B) Site II, and (C) Site III. Arrows highlight notable features such as rough surface (a), irregular pitting (b), circular pitting (c), and remnant barnacle (c) location. Rule at 1 mm intervals

Tomilson,2014 made an extensive survey of the corrosion on steel piling in marine structures from various sites (with both seawater and freshwater) and reported a probable maximum corrosion loss rate for the various pile exposure regions including the splash, intertidal, low water and immersion zones. As shown in Figure 5.18, the corrosion loss of the specimens from Site I was greater than those reported values. Maximum corrosion rates reported in Japan were also high (~37 mpy) (Gubner and Beech, 1999). For Site II and III, the mass loss at the immersion zone was consistent with the reported values from Tomilson and less than that calculated for Site I. The trends in the corrosion mass loss for the three test sites were similar to that measured by the LPR measurements described above.

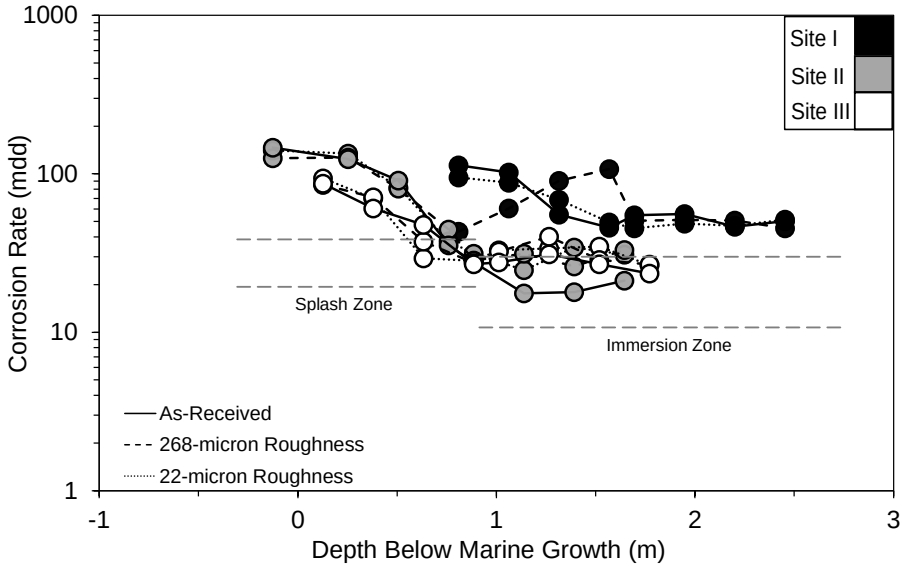

Figure 5.18. Calculated nominal corrosion rates of steel exposed in the field testing. Horizontal lines represent average corrosion rates at intertidal and immersion zones reported by Tomilson, 2014.

Results from the field testing confirmed a strong microbe presence (including SRB) under the marine fouling encrustations and localized corrosion was shown to develop under the foulers. The particularly high corrosion rates and localized corrosion at Site I was associated with the heavy accumulation of both hard and soft foulers. The high flow rate of the Mantanzas River (0.28-8.49 m^3/s or 10-300 ft^3/s (Braun, 2005)) and 1.25 m/s or 4.12 fps maximum average ebb velocity (Mehta

and Jones, 1977)) with high nutrient concentrations (Permeh et al., 2017) would allow continuous availability of nutrients to feed the sedentary fauna and flora. Likewise, the flowrate would allow greater availability of the SRB and nutrients from the bulk water to the sheltered biofilm below the marine foulers. A similar effect would develop at Sites II and III that had the loose barnacle encrustations and can account for the observed local pitting. As described by Salgar-Chaparro, 2020, continuous access to nutrients allowed for more active biofilm and supported greater localized corrosion.

The findings in the field were consistent with the trends observed in the lab. The lab testing indicated that the SRB colonies developed in conditions with limited interaction with the bulk solution if sufficient nutrient levels were present. But SRB growth can be sustained by the incremental injections of SRB and nutrients. Importantly, it was shown that aeration levels had a large effect. The different crevice-like conditions that affect its interactions with the bulk solution including SRB, nutrient, and oxygen levels can develop in the natural water environments due to the chemical and physical characteristics of the water body as well as the micro- and marine-organism populations. SRB proliferation occurred and was facilitated when the marine organisms provided supporting environments. Crevice environments associated with the well-adhered barnacles would have less interaction with the bulk solution that that of the poorly-adhered and interlayered barnacles or the porous nature of marine flora. Aeration levels would be similarly affected. Different mitigation strategies can be implemented to address the localized corrosion under the marine foulers. Based on the findings of this work, the complications of cathodic protection due to the marine fouling has been assessed in chapter 6 and possible benefits of anti-fouling and protective coatings in have been addressed in chapter 7.

CHAPTER 6

6. MITIGATION OF MIC IN PRESENCE OF MARINE FOULING CONDITION BY CATHODIC PROTECTION

6.1. Introduction

The corrosion of steel in marine environments is often characterized as uniform corrosion, and design of steel elements in part accounts for the expected mass loss during the design life of the structure.[1]However, other natural interactions (surface fouling) of steel in the marine environment can intersect, creating complex systems exacerbating material degradation. This unexpected form of corrosion in the Florida bridge was interrelated to macro- and micro-fouling. In terms of macrofouling, the surface of the piles had heavy coverage of sedentary marine fouling. The coincident presence of sessile bacteria (SRB) under the macrofouling encrustations provided indication that the severe localized corrosion was mediated by the combined effects of chemical and biological processes. Non-uniform macrofouling can create crevice conditions and oxygen concentration cells as well as producing local changes in pH and anaerobic environments which can further support microbial activity.

Cathodic protection (CP) can be applied to steel infrastructure submerged in marine environments, However, complications arise due to the various physical, chemical, and biological interactions of the steel and the marine environment. In addition to the environmental characteristics that influence the relevant electrochemical reactions (e.g., oxygen concentrations, pH, temperature, etc.) (Little and Wagner, 1993), the effect of steel surface modifications developed by biological and chemical interactions also affect the efficacy of cathodic protection.

Shielding of current provided by CP systems by separation of the steel surface from the bulk solution (such as that used in pipeline systems by the application of coatings and electrolyte media with high electrical resistance (Nunez et al., 1989; Fessler et al., 1983; Kuang and Cheng,

2015) can also develop in marine structures with the presence of uniform fouling encrustations. The incomplete and porous layering of fouling organisms, too, can create crevice conditions that support differential aeration corrosion cells. These nonuniform ionic paths would likewise prevent uniform polarization of the substrate steel and allow for regions where the efficacy of cathodic protection would be reduced.

Systems susceptible to microbially influenced corrosion (MIC) require greater cathodic polarization levels (<-950 mV_{SCE}) than in systems unaffected by MIC (Horvath and Novak, 1964; Barlo and Berry, 1984; Fischer,1981; Jack et al., 1996) and yet further complications exist as bacteria such as SRB continue to proliferate on cathodically polarized surfaces (Olivares et al., 2006; De Romero et al., 2006;2008;2009) and are even supported in symbiosis with macrofoulers. For example, research by Eashwar et al., 1995 and Permeh et al., 2018,2019, indicated that SRB growth was maintained under fouling encrustation (Eashwar et al., 1995; Permeh et al., 2019a;2019b). However, the synergistic role of fouling on CP remains unclear (Little and Wanger,1993;Littauer and Jennings, 1968; Sanders and Maxwell, 1983; Swain and Maxwell, 1990).

The microorganisms change surface conditions where the occurrence of reduction reactions affect the required CP currents. For example, some bacteria can act as depolarizing agents while some bacteria electrically insulate the metal from cathodic protection (Booth and Tiller 1960; de Romero et al. 2009; de Brito et al. 2007). Olivares et al, 2003 described proliferation of SRB with CP polarization as negative as -925mV_{CSE} due to an electrostatic attraction between the bacteria and the electric charges created by cathodic protection. Large cathodic polarization can also change surface conditions by chemical reactions (e.g. by allowing deposition of calcareous compounds). Although it is well documented that calcareous deposits can influence surface cathodic reactions by providing a protective barrier, research studies have indicated that biofilm

ecology can affect deposit properties and diminish the protective characteristics (Hartt et al. 1984; Dexter 1991; Eashwar et al. 2009).

The objectives of this chapter were to verify mitigation of MIC in presence of marine fouling condition by cathodic protection . Also to identify if marine fouling can reduce the effective steel surface area for CP, how bacteria proliferation is affected under the fouling layer in presence of CP, and identify the level of reduced efficacy of CP to mitigate steel corrosion. Laboratory testing consisted of potentiostatic cathodic polarization of steel specimens with laminate and porous crevices that are representative of different marine fouling morphology in solutions inoculated with SRB. Field testing incorporated submerged steel coupons subjected to CP, provided by submerged bulk zinc anodes, in two Florida natural water bodies that could sustain microbiological activity associated with MIC as well as heavy marine fouling.

6.2. Methodology

6.2.1. Laboratory Testing

Laboratory experiments followed test setup B, as previously discussed in 5.2.1.1 section. Experiments in test setup B followed a modified laboratory test setup and a single inoculation of isolated sulfate reducing bacteria was initially introduced. Cathodic potentiostatic polarization tests (at -850 and -950 mV_{SCE}) were applied for up to 7 days.

6.2.1.1.Test Setup

The test setup followed test B in section 5.2.1.1 and a schematic of test cell is shown in Figure 5.1 and 5.2. The working electrode consisted of the transverse cross section of a steel bar with 1.27 cm in diameter and 10-micron grit surface roughness that either had an open or crevice surface condition. Crevice environments were considered as representations of the physical laminate and porous crevice conditions characteristic of hard shell barnacles and soft marine flora and fauna deposits. A saturated calomel electrode (SCE) was used as a reference electrode. An

activated titanium mesh was used as the counter electrode. Test cells were filled with 300 mL deionized water and 20 mL modified Postgate B medium solution (Postgate, 1979). The pH of all test solutions was between 6.5-8.0. All test cells were assembled with sterile components and test specimens were rinsed in deionized water and sterilized with ethanol solution prior to testing.

6.2.1.2 Microbial Activity

Chemical oxygen demand (COD), sulfide production, and sessile SRB population levels were monitored to determine the extent of microbiological activity. The COD values provide indication of environments that can support microbial development and thus is a marker for microbial activity in the test solution. COD of each sample was measured by a colorimetric COD method on the first and final day of testing (O'Dell, 1993).

The sulfide concentrations relate to the level of sulfate reduction that is in part due to the metabolic activity of the SRB in the bulk solution and on the metal surface. The changes in the concentrations of sulfide products and sulfate reactant during exposure can be used as a measure of SRB activity in (Scott, 2004). As a first approach to identify the role of SRB in corrosion development, the total sulfide production levels during the course of the testing were considered to be proportionate to the sulfate reduction reactions on the metal surface. Thus, the changes in sulfide levels are considered here qualitatively. A hydrogen sulfide color disc test kit was used for monitoring sulfide concentration. After ~7 days, the steel working electrodes were removed from the test solution, and coverings were removed from crevice specimens. Sessile test kits by Biotechnology Solutions (Houston, Texas, US) were used for detection of sulfate reducing bacteria by serial dilutions in Modified Postgate B (MPB) following the NACE standard TM0194-2014 . Sterile cotton swabs were used to gently scrape the surface of the sample (~1 cm^2 area) and the soft deposit (formed by microbial activity) collected on the swab was placed into a sterile phosphate buffer solution (PBS). Serial dilutions of the 1 mL PBS ranged from 4 to 8 times.

6.2.1.3. Electrochemical Testing

The experimental parameters for the laboratory tests are shown in Table 6.1. Figure 6.1 shows the test experiment connected to the power supply. Cathodic potentiostatic polarization levels in the range associated with cathodic protection of steel (-850 and -950 mV_{SCE} (-927 and -1,027mV_{CSE})), were conducted for up to 7 days. Supplemental testing at -500 mV_{SCE} was also conducted for comparative testing with anodic polarization. The net cathodic or net anodic currents were periodically measured (more frequently for the first 2 days and then daily until day 7). The cumulative charge, Q, at each measurement period, n, was calculated by equation 8 for the duration of the tests, where I (A) is the measured current and t (s) is the measurement period.

$$Q(t_{n+1}) = \sum_{n=0} I_{n+1} \cdot (t_{n+1} - t_n) \quad (6.1)$$

Figure 6.1. Test Setup B test cells under cathodic polarization

Table 6.1. Experimental test condition

Polarization level[a]		Inoculation	Working electrode condition	No. of samples	
				Naturally aerated	De-aerated[b]
Cathodic	-850 mV_{SCE}	Inoculated[c]	Open (Control)	2	2
			Laminate crevice	2	2
			Porous crevice	2	2
		Non-inoculated	Open (Control)	2	2
			Laminate crevice	2	2
			Porous crevice	2	2
	-950 mV_{SCE}	Inoculated[b]	Open (Control)	2	2
			Laminate crevice	2	2
			Porous crevice	2	2
		Non-inoculated	Open (Control)	2	2
			Laminate crevice	2	2
			Porous crevice	2	2
Anodic	-500 mV_{SCE}	Inoculated[b]	Open (Control)	2	2
			Laminate crevice	2	2
			Porous crevice	2	2
		Non-inoculated	Open (Control)	2	2
			Laminate crevice	2	2
			Porous crevice	2	2

[a] Open circuit potential (OCP) -650 to -750 mV_{SCE}.
[b] High purity nitrogen gas introduced for 10 minutes on days 1 and 3. Mineral oil added.
[c] Inoculated with 10 mL SRB in Postgate medium.

6.2.1.4. Post Test Analysis

Images of the corrosion development and remnant physical effects of microbial activity were captured by a digital camera under microscope.

6.2.2. Field Testing

6.2.2.1. Test Setup

The field test setup samples and installation were previously discussed in section 5.2.2. A total of fifty-six steel coupons subjected to natural corrosion or CP conditions were tested at two field installations as listed in Table 6.2. The steel coupons, 3 inch x 5 inch x 1/8 inch (12.7 cm x 7.6 cm x 0.32 cm), (composition of 0.02% C, 0.16% Mn, 0.006% S, 0.03% Si, balance Fe) were installed to bridge piers in two Florida natural waters that supported proliferation of bacteria often associated with MIC as well as heavy marine fouling. The characteristics of the test sites was shown

in Table 5.4. At Site I (Matanzas River), hydroids and marine flora amassed with sporadic growth of barnacles at test depths. At Site II (Alafia River), barnacles were the predominant macrofoulers at test depths. Figure 6.2 shows the marine growth developed on the test arrays as well as the placement of a subset of 14 steel coupons and the zinc anode.

Table 6.2. Field test conditions for CP testing

Test Sites	Steel condition	Test duration (days)	No. of coupons	Depth below marine growth (m)	Corrosion Test Methods
Site I Matanzas River	Cathodic protection (Group A)	191	14	~1.7 to 2.5	CP on-potential, CP current configurations 1-3, Visual, Mass loss.
	Control-OCP (Group B)	279	14	~ 0.8 to 2.5	OCP, Visual, Mass loss.
Site II Alafia River	Cathodic protection (Group A)	245[a] (169[b])	14	~ 0.9 to 1.6	CP on-potential, CP current configurations 1-3, Visual, Mass loss.
	Control-OCP (Group B)	245	14	~ 0.1 to 1.6	OCP, Visual, Mass loss.

[a] Coupling to zinc anode upon steel immersion.
[b] Connection to auxiliary zinc anode.

At both test sites, the array of 14 steel coupons for the Group A subset were electrically coupled to the commercially-available bulk zinc anode (composition: 0.1-0.5% Al, 0.02-0.07% Cd, 0.005% Fe, 0.006% Pb, 0.005% Cu, and balance Zn) for the duration of the exposure (from ~190 to~250 days, Table 1). A complementary subset of 14 steel coupons (Group B) were maintained at the open-circuit potential (OCP) throughout the exposure test period (~250 days). A second zinc anode was installed to monitor the free zinc anode corrosion potential. All electrical connections to individual steel coupons were encapsulated in an epoxy resin to prevent corrosion of the contact points. Connections were terminated at a control box and the Group A array was inter-connected with electrical switches to accommodate current measurements between the steel coupons and the zinc anode.

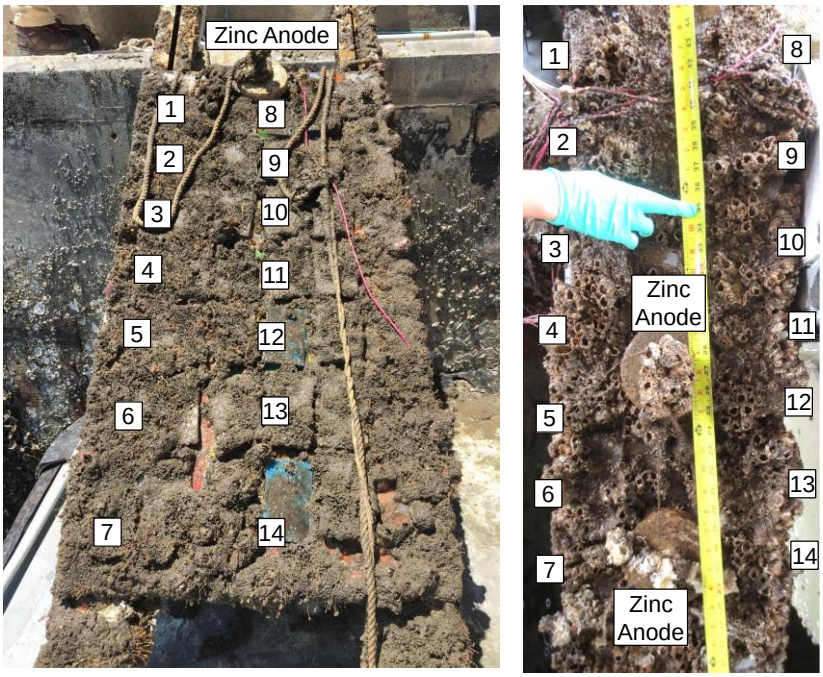

(a) (b)

Figure 6.2. Typical marine fouling observed on field exposure test racks at (a) Site I and (b) Site II. Arrangement of steel coupons (1-14) and zinc anode on the test racks are indicated.

6.2.2.2. Electrochemical Testing

All test coupons were placed below the marine growth (BMG) line (up to 2.5 m BMG) as shown in Table 1. All Group A specimens (with applied CP) remained submerged during tidal events. For Site I, the Group A specimens were initially corroded at the OCP condition for 88 days prior to coupling to the zinc anode. At Site II, Group A specimens were installed together with the zinc anode; however, due to a possible bad electrical contact to the initial zinc anode, reconnection to an auxiliary zinc anode was made at day 77.The initial free corrosion potential of the uncoupled steel coupons (E_{OCP}) and zinc anodes (E_{Zinc}) as well as the subsequent mixed potential (E_{ON}) after coupling of the coupons and zinc anodes were measured. Short term depolarization tests including instant-off potentials, within 1-sec, (E_{IO}) and de-coupled steel array potentials (E_{OFF}) were made at both test sites. The corrosion potentials of all Group B specimens at both test sites were periodically measured. A CSE was used for all potential measurements.

Heterogeneities on the steel surface as well as specimen-to-specimen variability formed due to the natural site selection of the macro- and micro-foulers. The localized fouling and related corrosion cells that develop at discrete locations in the coupled steel array can affect the efficacy of CP provided by the zinc anode. Coupling of all the individual steel coupons within the array would allow for the development of a galvanic-coupled system potential relating to the natural distribution of the organisms and the surface conditions that they produce. The natural polarization of localized regions of the steel array due to the coupling of the entire array would better represent the behavior of the distributed interfaces of extended surfaces and was considered an important test condition to identify how the extended surface heterogeneities affect the efficacy of CP.

For Group A specimens at both test sites, the electrical current measurements were conducted in three configurations of coupled steel coupons and zinc anode with an ammeter immediately (within 5 seconds) after decoupling (from the normally coupled on-condition) via the electrical switch (Figure 6.3). The measured currents were largely due to the driving force of the galvanic-coupled potential of the extended steel array and the zinc anode, and depolarization during the quick current measurements would be nominal because the steel interfaces would require long time periods to depolarize to its isolated steady-state condition. The system was reset to the on-condition immediately after each individual measurement.

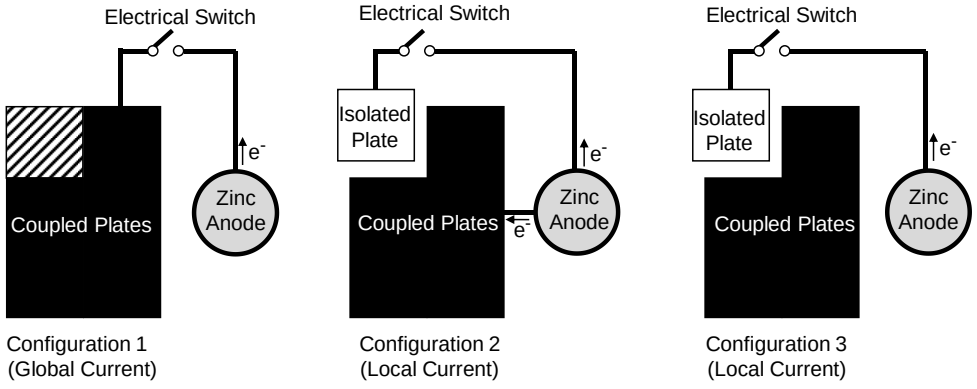

Figure 6.3. CP current test configurations for coupled steel and zinc anodes.

The current provided by the anode to the steel coupons in the three configurations allows for the identification of differences in anodic behavior of individual steel coupons in the array as well as the global current between the zinc anode and the entire steel array. For the first test configuration, the global CP current from the zinc anode to the entire coupled array of test coupons was measured. These values provided indication of anode behavior and allowed general comparison between the two test sites with different levels and types of marine fouling. For the second test configuration, the local CP current from the steel-anode system to a single isolated test coupon was measured. This relates to the extent to which CP is afforded at local steel sites with respect to the galvanic-coupled potential of the entire steel array when the CP current from the zinc anode is afforded to the entire array. For the third test configuration, the local CP current from the anode to a single isolated test coupon was also measured with respect to the galvanic-coupled potential of the entire steel array, although the instantaneous decoupling of the extended steel array may allow for a greater extent of depolarization than configuration 2. However, the quick current measurements would minimize that effect and the measured currents provided by the anode to the isolated test coupon would not be restricted by the demand from the entire array. The measurement would ideally provide a direct indicator if the surface heterogeneities of each specimen affect CP current. Results were reported in current, (I in mA) as well as a nominal current density (i in $\mu A/cm^2$) where $i=(I\text{x}1000)/A$ and A is the total steel coupon surface area in cm^2.

6.2.2.3. Post Test Analysis

The test racks were decommissioned after about 279 days at Site I and about 245 days at Site II. All retrieved samples were hand cleaned to remove the surface fouling and were examined with a stereo microscope. Remnant traces of barnacle attachment as well as steel corrosion including corrosion pit morphology were documented. Images of corrosion development and physical conditions of surfaces were captured. Eight Group A specimens from Site I and 4 Group A specimens from Site II as well as 8 Group B specimens each from test site (from various

immersion depths) were further cleaned following ASTM G1-03 (ASTM 2017) and immersed in cleaning solution for up to 2 hours. Mass loss of control steel coupons was measured and used to calibrate final mass measurements. The apparent corrosion rate (*CR*) given in mg/dm^2/day (mdd) was determined from the difference in mass before and after field exposure following Equation 1 where m_f and m_o are the final (after cleaning) and initial (pre-exposure) coupon mass, respectively in grams, t is the time of exposure in days, and A is the total surface area of the coupon in dm^2.

$$CR_{\text{mass loss}} = \frac{(m_f - m_o) \times 1000}{t \times A} \tag{6.2}$$

For comparative purposes, the apparent corrosion rate given in mdd determined from the difference in specimen thickness before and after field exposure (after cleaning) following Equation 2 where t_f and t_o are the average final coupon thickness and initial coupon thickness (pre-exposure), respectively in cm, l is the coupon length in cm, w is the coupon width in cm, ρ is 7.85 g/cm^3, t is the time of exposure in days, and A is the total surface area of the coupon in dm^2. The t_0 value was taken from the average thickness of six spot measurement on ten control steel coupons from the same steel production, and the final apparent sample thickness, t_f, was determined as the average of six measurements for each specimen. The thickness measurement used a micrometer with 0.001-inch (0.00254 cm) precision.

$$CR_{\text{thickness reduction}} = \frac{\frac{(t_f - t_o) \times l \times w}{\rho} \times 1000}{t \times A} \tag{6.3}$$

X-ray diffraction analyses were conducted on representative specimens from each test site at a range of 2θ from 20 to 80 degrees with a scan rate of 0.02 degree/min.

6.2.2.4 Microbial Activity

Verification tests to identify the marine fouling and surface bacterial growth were conducted at the end of the testing. Tests included visual examination and photo-documentation of

the steel coupon surface conditions and analysis of the surface bacteria population. Small sections of marine growth (~1 in^2 (6.45 cm^2)) were removed where swabs of the steel substrate were collected for the microbiological analyses. The swabs were used for the Biological Activity Reaction Test (BART) to assess the population and the activity of four common MIC related bacteria (SRB, IRB, SLYM, and APB). Aggressivity was defined based on the general guidelines for BART (Droycon Bioconcepts Inc).

6.3. Results and Discussion for Laboratory Testing

6.3.1. Electrochemical cathodic and anodic charge

The open circuit potential for the specimens in the laboratory test solution was between -650 and -750 mV_{SCE}, including conditions with apparent cathodic ennoblement. Polarization at -850 and -950 mV_{SCE} can provide net cathodic currents. The total net cathodic reactions in the presence of the cathodic polarization include oxygen reduction (diffusion controlled), hydrogen formation by activation polarization, and the sulfate reduction associated with SRB. In the non-inoculated solutions, the reduction reactions include oxygen reduction and hydrogen reduction. The limiting current density for the oxygen reduction reaction should be lower due to concentration polarization in the de-aerated condition.

Figure 6.4 presents the cumulative charge associated with the measured cathodic reactions for all test cases. Figure 6.5 shows the comparative cumulative cathodic charge on day 1 and day 7. Testing at the -850 and -950 mV_{SCE} polarization levels showed increasing trend of cumulative cathodic charge. Potentiodynamic polarization testing of non-inoculated control samples confirmed that concentration polarization of oxygen reduction reaction was dominant at -850 mV_{SCE} and hydrogen reduction reaction become significant at -950 mV_{SCE} for the tested aeration conditions. The trend of the potentiostatic data with time was evaluated by regression analysis using a power model as follows:

$$C = a \cdot t^b \tag{6.4}$$

where a is the scaling factor, and b is the power factor. The regression analyses showed that some decay in cathodic rates was apparent but was not significant in any of the test cases. Table 6.3 presents the values of the estimated model parameters (a and b) for all test cases. The power coefficient estimated by regression was typically about 1 in both aeration conditions at -850 and -950 mV_{SCE}. At -850 mV_{SCE}, the power factor was typically greater in the naturally aerated conditions than the de-aerated conditions as expected due to the larger oxygen concentration in the bulk solution. At -950 mV_{SCE}, the scaling factor was similar in both aeration conditions as hydrogen reduction would be dominant. The transient rate limitations in oxygen and hydrogen reduction as well as possible limitations in available surface atomic hydrogen were not significant with time during the testing (Scott, 2004; Lee et al., 2010).

The larger cumulative cathodic charge developed for the more electronegative test condition and the scaling coefficient was higher for the -950 mV_{SCE} polarization level than for the -850 mV_{SCE} polarization level. The scaling coefficient estimated was generally smaller for the cases with crevice environments and had lower cumulative cathodic charge in comparison to the specimens with open no-crevice condition. This is consistent with the hypothesis that there is smaller metal surface area available to support the reduction reactions especially for the laminate-crevice conditions. The laminate crevice environments can also reduce the interaction of the inoculated SRB (within occluded crevice regions) with bulk solution; therefore reduce the level of cathodic reactions associated with SRB.

For the open surface condition, the magnitude of the cumulative cathodic charge was not dissimilar for the polarized specimens in the inoculated and non-inoculated solutions. The large steel surface area can accommodate oxygen and hydrogen reduction reactions and any contribution of sulfate reduction reactions by SRB was not discernable. The test results did indicate that relatively high cathodic reaction rates developed in the porous crevice environments and more so

with the presence of SRB. The porous crevice environments provided sheltered and localized low oxygen regions with sufficient supply of nutrients to support SRB growth. The role of different crevice geometries on cathodic polarization behavior studied by other researchers (Xu et al., 2014; Jia et al.,2019a) show that large SRB populations can develop in the crevices regardless of cathodic polarization levels as electronegative as -1,000 mV_{CSE}. Conditions which allow sustained growth of SRB within the crevices suggest that cathodic reaction related to sulfate reduction can be an important mechanism.

Table 6.3. Estimated values of parameter for the power function[a].

		Test condition	De-aerated		Naturally aerated	
			a	b	a	b
At -850mV_{SCE}	Open (Control)	Inoculated	0.62	0.98	1.00	1.00
			0.95	0.86	1.14	0.96
		Non-inoculated	0.75	0.89	1.40	0.90
			1.47	0.82	1.78	0.91
	Porous crevice	Inoculated	0.45	0.72	0.64	0.81
			0.56	1.14	1.93	1.09
		Non-inoculated	0.40	0.82	0.92	0.70
			0.55	0.69	0.45	0.82
	Laminate crevice	Inoculated	0.33	1.07	0.46	1.01
			0.24	0.87	0.37	0.90
		Non-inoculated	0.21	0.92	0.61	0.93
			0.39	0.94	-	-
At -950mV_{SCE}	Open (Control)	Inoculated	2.21	0.88	2.75	0.85
			2.66	0.96	2.99	0.93
		Non-inoculated	1.78	0.91	0.75	0.90
			3.37	0.97	2.83	0.97
	Porous crevice	Inoculated	2.26	0.94	2.75	0.93
			3.75	1.08	3.08	1.04
		Non-inoculated	1.59	0.68	1.07	0.65
			2.38	0.75	1.14	0.72
	Laminate crevice	Inoculated	0.62	0.91	0.80	0.98
			0.64	0.92	0.49	1.01
		Non-inoculated	0.80	0.85	0.89	0.89
			-	-	0.63	0.90

[a] $C = a \cdot t^b$ fitted to the cumulative cathodic charge data (a: scaling factor, b: power factor).

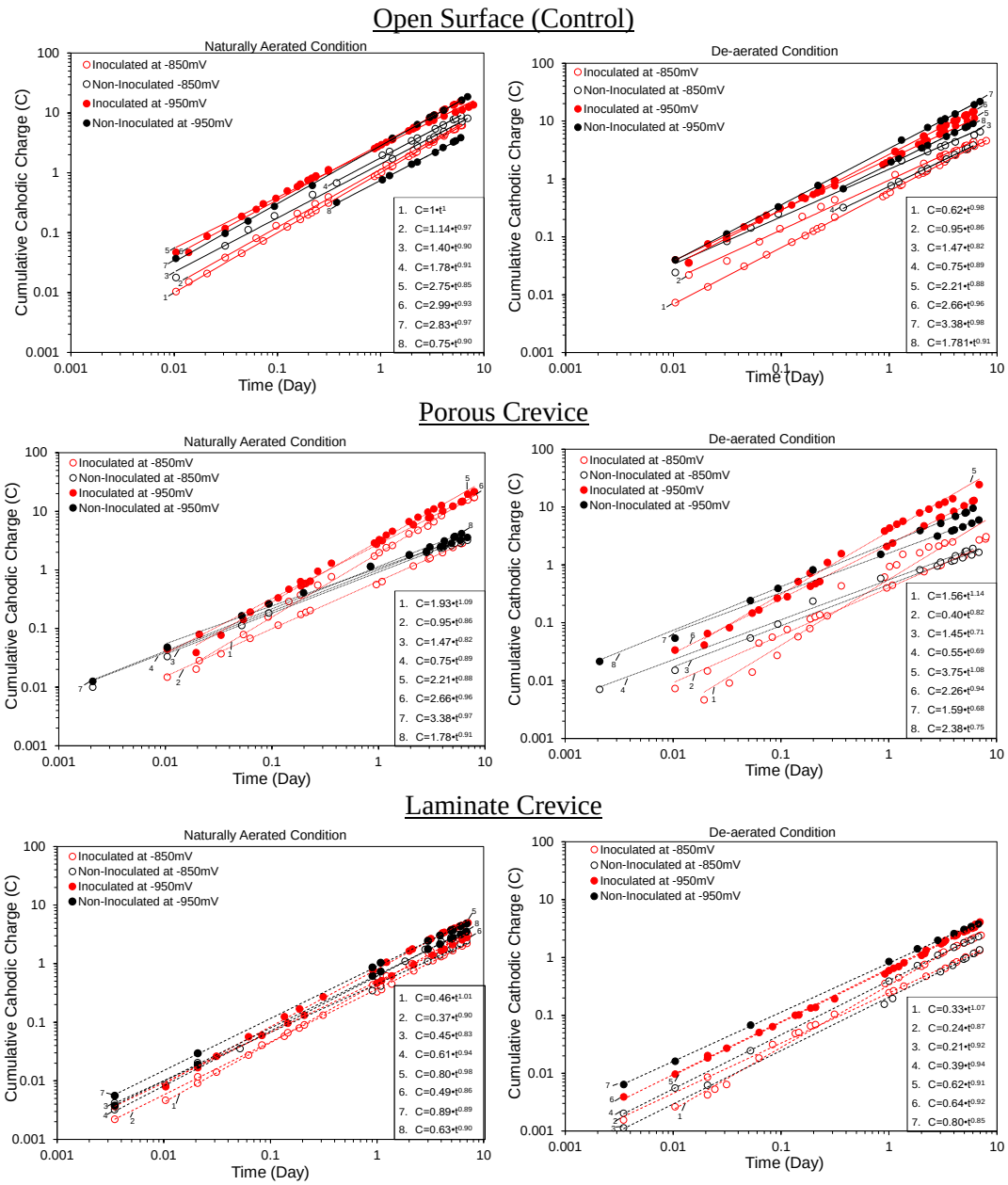

Figure 6.4. Cumulative cathodic charge measurements for the laboratory samples at polarization levels of -850 mVSCE and -950 mVSCE. The lines show the fitted power function.

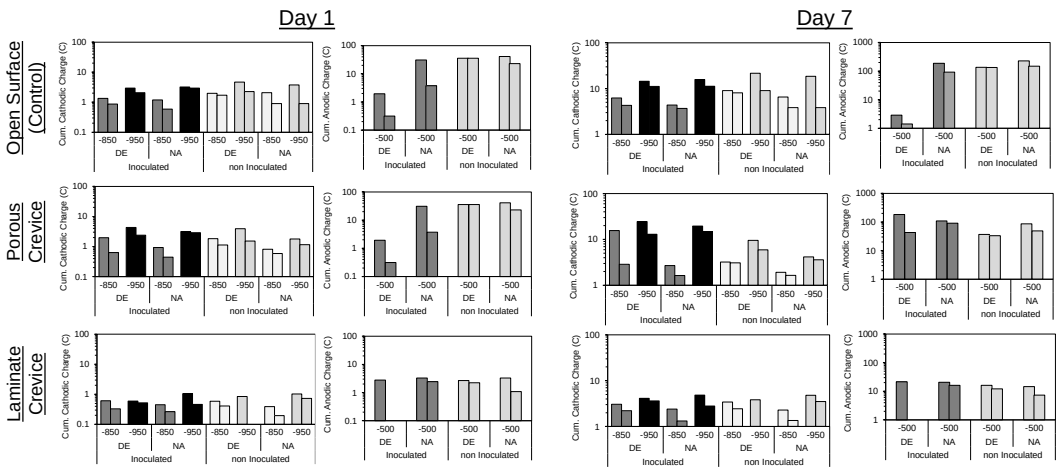

Figure 6.5. Cumulative cathodic charge at 1 and 7 days for different geometric conditons. DE: de-aerated, and NA: naturally aerated.

The specimens with the applied -500 mV_{SCE} polarization consistently showed net anodic currents as shown in Figure 6.6. Anodic polarization behavior of the steel was not expected to be significantly different in the presence of SRB inoculum as the test solution itself allowed for corrosion initiation. The oxygen and more so hydrogen reduction reaction rates at this level of anodic polarization would be minimal as these electrochemical half-cell reactions would follow Tafel behavior. However, there were changes in the anodic currents during the testing period. This can in part be accounted for by the physical effects of rust accumulation or biofilm film formation on the surface of the specimen. However, conceptually, any increases in reduction reaction rates that occur due to the growth of SRB would correspondingly have an inverse effect on the measured net anodic reaction rate. To the latter two points, as shown in Figure 6.6, there was indication of lower net anodic rates for test specimens in the inoculated solutions (i.e., with SRB activity) particularly for the de-aerated open and soft crevice conditions.

There are complex mechanisms which sustain the SRB metabolic activities involving charge transfer associated with cathodic reactions (e.g., reaction 2 shown in equation 2) when those reactions are suppressed. The ubiquitous nature of SRB suggests that the microorganisms can

continue to develop; however, limitations on available surface hydrogen required for sulfate reduction as described by the classical depolarization theory may regulate the SRB growth. Work by Moreno et al., 1993 and Kloeke et al., 1995 on the roles of cytochromes and hydrogenase in transfer of electrons from charged surfaces elucidate the mechanisms of bioelectrochemical reductions occurring in engineering systems.

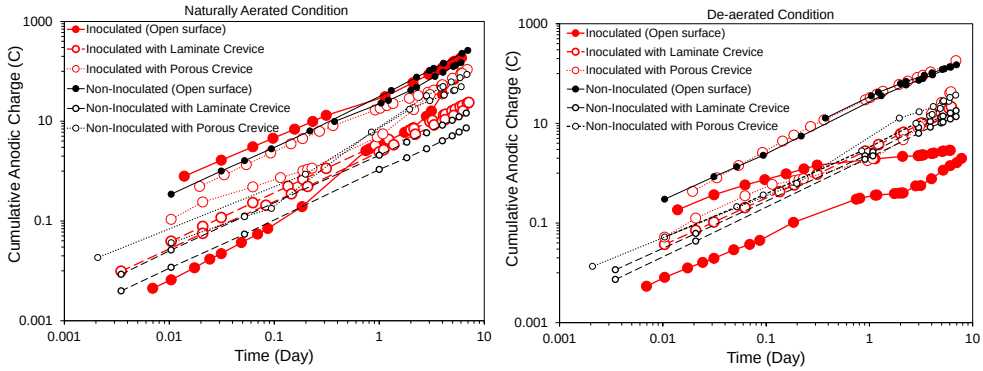

Figure 6.6. Cumulative anodic charge measurement for laboratory samples at polarization level of -500 mVSCE.

6.3.2. Microbiological activity

6.3.2.1. Chemical Oxygen Demand

Chemical and microbiological analysis were conducted for the solutions of the cathodic and anodic polarization test samples to identify the levels of SRB activity. Although COD levels do not directly give indication of SRB populations, COD levels are considered as a metric of environmental conditions to support SRB activity. As shown in Figure 6.7, COD measurements of the test solutions at the onset of the test showed high COD levels indicating environments that can support SRB growth. The COD levels typically dropped overall by the end of the testing; however, the final COD levels were consistently higher in the inoculated solution than the control non-inoculated solutions indicating that the environments in the former allowed more suitable conditions for the SRB growth as observed by increase in organic content that can develop with SRB proliferation. Correspondingly, the low final COD levels in the non-inoculated solutions are

indicative of low SRB activity. Generally similar COD levels were measured for the de-aerated and naturally aerated inoculated solutions for the samples with open and crevice environments and any differences in SRB development in the occluded spaces were not distinctly captured.

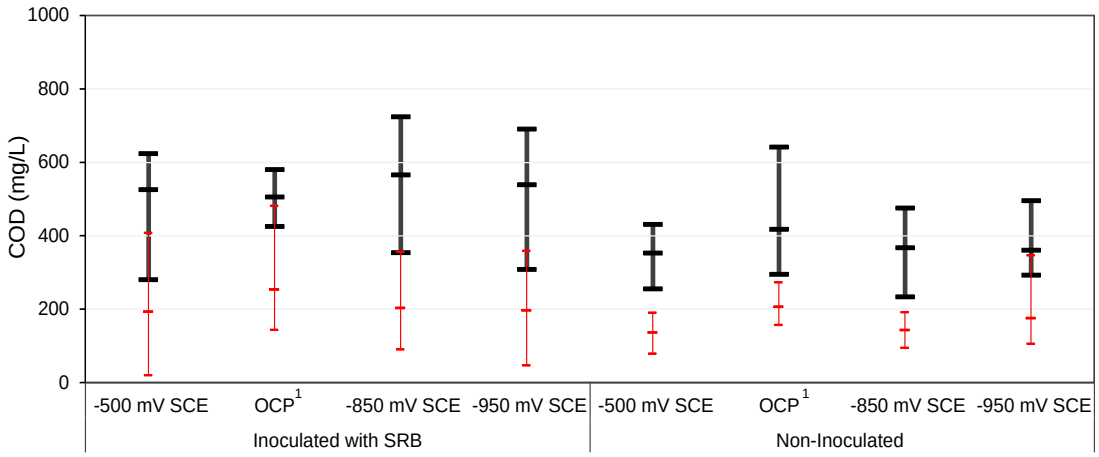

Figure 6.7. Range of chemical oxygen demand measured in the laboratory test samples at polarization levels -500 mVSCE, -850 mVSCE , -950 mVSCE and OCP condition. (Black lines: measurement on Day 1, Red lines: measurement on Day 7), 1: data from (Permeh et al., 2019a).

6.3.2.2. Sulfide Production

Sulfide concentrations in the form of hydrogen sulfide and metal sulfide from the extracted aliquots of solution were measured with a color disc test kit during the course of the lab tests. Figure 6.8 presents the apparent sulfide production rates estimated for the different test conditions including polarization levels, aeration levels and crevice geometries. The test results showed that sulfide production occurred at different levels depending on the surface conditions throughout the duration of the test regardless of the level of cathodic polarization. The different forms of hydrogen sulfide detected by the test kit derived from sulfide, S^{2-}, produced by the sulfate reduction reaction as part of SRB metabolic activities were considered in part associated with charge transfer reactions. The sulfide levels measured at discrete times during the exposure were used to calculate the apparent rate of sulfide production within the fixed solution volume. The apparent rate of sulfide

production was assumed to be constant during the time intervals between sulfide measurements and on first approach was assumed to be primarily related to SRB presence.

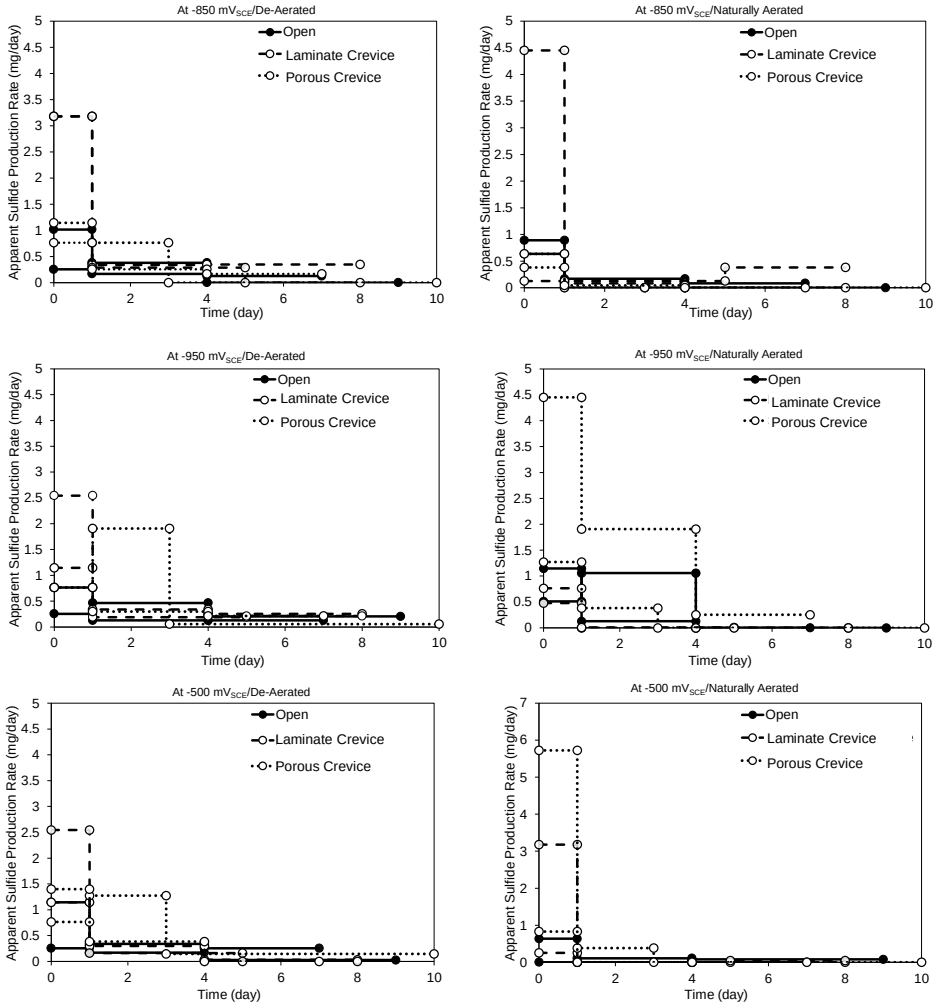

Figure 6.8. Apparent sulfide production rate in laboratory inoculated test samples at polarization levels -500 mVSCE, -850 mVSCE , -950 mVSCE.

It was apparent that overall, the level of sulfide production was greater with the larger cathodic polarization and smaller in presence of the anodic polarization. In all cases, the level of sulfide production decreased over time indicating decrease in SRB activity during testing. However, it was also apparent that SRB continued to grow to some extent as sulfide production continued in many cases throughout the test exposure. In congruity with the high total bacteria population (sampled from the surface of the specimens) in the crevices (Table 6.4), the apparent

sulfide production rate for the samples with crevices was higher and prolonged relative to the open geometry. The effects of oxygen and iron levels and ionic strength were assumed to be not significant in the oxidation of sulfide (Millero, 1986).

6.3.2.3. Microbiological Analysis

Table 6.4 presents the terminal surface SRB populations for all test cases on day 7. The results show that for the cathodically-polarized specimens in the inoculated solutions, the crevice environments can facilitate the SRB growth in similar manner to that occurring in anaerobic environments by providing shelter within the occluded space. In this case, crevice spaces could adequately protect SRB even with strong cathodic polarization. Indeed, steel under porous crevices with SRB showed high cathodic currents reflecting favorable electrical properties (low resistance) through the sponge that allowed relatively high cathodic currents but did not produce a change in environment that could reduce SRB growth. On the specimens subjected to anodic polarization, the SRB populations were relatively depressed.

Table 6.4. Terminal bacteria concentrations (population per mL) for laboratory test samples.

Aeration	Polarization mV_{SCE}	SRB inoculation			No SRB inoculation		
		Open	Crevice		Open	Crevice	
			Laminate	Porous		Laminate	Porous
Naturally aerated	-950	10^2-10^4	10^3-10^6	0-10^6	0	0-10^2	0
	-850	10^2-10^4	10^3-10^8	0-10^6	0	10^2-10^3	0
	OCP[a]	$\geq 10^8$	10^7	10^7	10^3	0	0
	-500	10^3-10^8	10^2-10^4	0	10	0-10^4	0
De-aerated	-950	10^2-10^6	10^3-10^8	0-10^6	10^4	0-10^2	0
	-850	10^1-10^3	10^1-10^8	0-10^8	10^1	0-10^2	0
	OCP*	$\geq 10^8$	$\geq 10^8$	10^7	0	10^3	0
	-500	10^2-10^4	10^1-10^6	0-10^3	0	0-10^2	0

[a] OCP: from -650 to -750 mV_{SCE} (Data reported from (Permeh et al.,2019a))

6.3.3. Visual Assessment

Figure 6.9 show the visual surface appearance of the test specimens for the de-aerated conditions immediately upon removal from the test solution and after cleaning. The visual appearance of the specimens in the naturally aerated conditions were similar. The test specimens (with all tested surface conditions) placed in inoculated solutions showed thick accumulation of iron sulfide precipitates consistent with the chemical and microbiological analyses discussed previously.

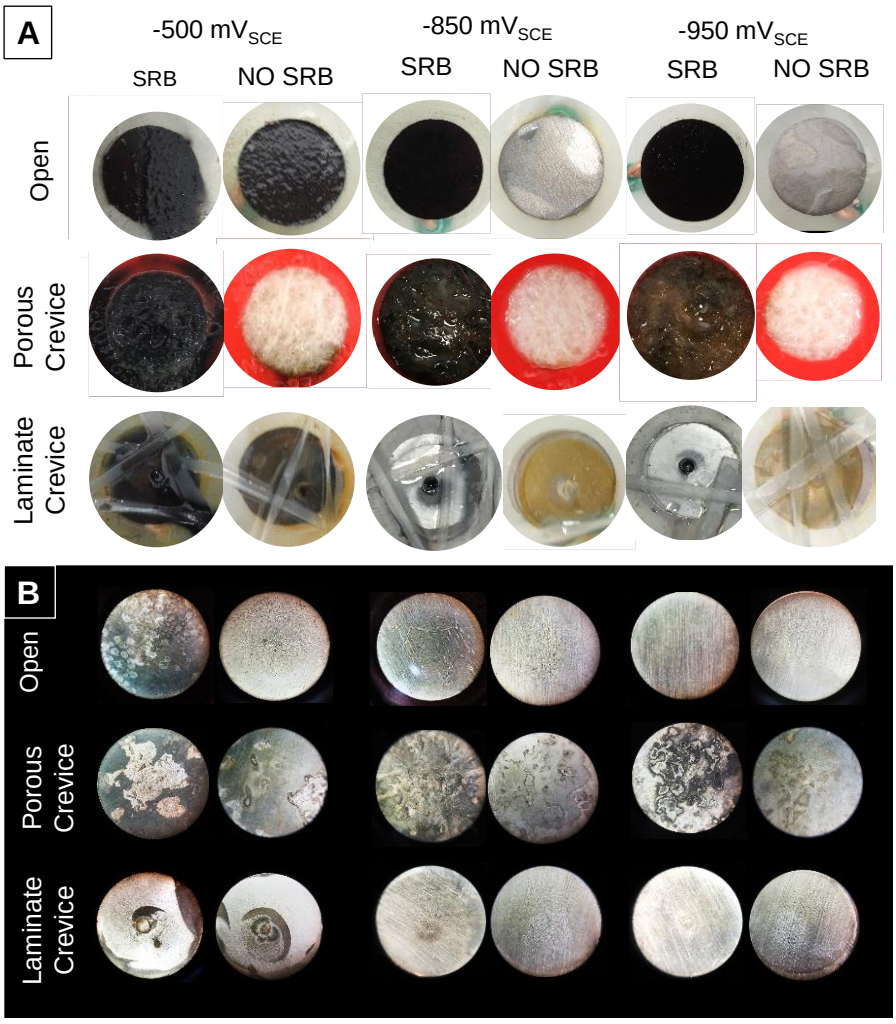

Figure 6.9. Laboratory samples (de-aerated condition) after testing and after sample cleaning.

The surface of the steel specimens with open non-crevice geometry and inoculated with SRB had irregular and localized surface tarnishing for both cathodic polarization levels (-850mV_{SCE} and -950mV_{SCE}) whereas the surface was observed to be smooth and clean in the non-inoculated solutions. Surface pitting that formed due to the anodic polarization on all specimens polarized to -500 mV_{SCE} appeared to be larger in the inoculated case. These observations indicate that the surface layer (due to microbial growth) created adverse underfilm conditions even with cathodic polarization. The surface of the steel specimens with laminate and porous crevices showed indication of corrosion regardless of the level of cathodic polarization as well as in the anodic polarization case.

Corrosion was also apparent in the non-inoculated test cases; although, the surface oxidation was different if not more severe with the presence of SRB. The steel samples with laminate crevices showed concentric surface tarnish from the center defect opening. The surface oxidation was black in color in the presence of SRB and was red-orange in the non-inoculated case. The steel surface of the specimens with the soft crevice showed mottled surface oxidation that was more severe with the presence of SRB. The development of surface oxidation indicated that there was non-uniform cathodic polarization under the crevice environments.

6.3.4. Cathodic reactions

Trends of the measured cathodic current and the apparent sulfide production rate shown in Figure 6.10 were consistent with the observed surface corrosion characteristics for the specimens in solutions with SRB. For the open surface geometry, local cells under sulfide precipitates and biofilm created irregular and local tarnishing even though overall large cathodic reduction reactions including oxygen and hydrogen reduction can develop with the polarization provided by CP. For the porous crevice environments, the large cathodic currents and the corresponding high level of sulfate reduction coincided with the SRB development. Localized surface heterogeneities developed under the porous crevices caused sinuous irregular surface corrosion as shown in Figure

6.9B. Similar corrosion conditions can occur under the hard crevice, especially as non-uniform protection of the steel is exacerbated by the higher electrical resistances under the crevice. This is consistent with the observed concentric geometry of the surface corrosion in the test specimens. The localized crevice environment created favorable conditions for SRB proliferation which allowed non-uniform cathodic polarization and development of localized corrosion.

The cumulative molar sulfide content was estimated from the test data and assumptions based on the relevant charge transfer theory and methodologies. As a first approach, based on the stoichiometry of the sulfate reduction reaction ($SO_4^{2-} + 8H \rightarrow 4H_2O + S^{2-}$) and associated reaction with surface adsorbed hydrogen ($H^+ + e^- \rightarrow H$) by the hydrogenase enzyme in SRB, a charge associated to the sulfate reduction reaction was derived from the sulfide levels ascribed by Faradaic conversion. A comparison of cumulative charge associated with the sulfide production and the measured net cathodic reaction rates is shown in Figure 6.10. On first inspection, it was evident that the rate of sulfide production corresponded to an apparent cathodic charge larger than the total measured net cathodic reactions. As such, it was apparent that the measured sulfide levels developed in part by the reactions that do not exhibit charge transfer characteristics corresponding to the idealized simple stoichiometry for the classical depolarization theory. Nevertheless, the results can be gleaned to provide qualitative generalizations on the cathodic reactions that can occur.

For the open surface and porous crevice geometries, a positive trend relating the net cathodic charge to charge related to sulfate reduction was generally observed. Larger cumulative charge relating to the apparent sulfate reduction corresponded to the greater levels of cathodic polarization. This observation indicates that sulfate reduction reactions due to SRB can be a significant part of the electrochemical process for steel with cathodic polarization (and reduce the effect of CP).

In presence of SRB, the high cathodic rates for the steel in the cathodically polarized condition would not necessarily mean enhanced steel corrosion if the electron donor is ascribed to the CP source. The high cathodic currents typically indicate cathodic polarization of the steel and corresponding reduced anodic corrosion currents. Heterogeneities on the steel surface can occur by other reasons including biofilm and microbial metabolites (e.g., marine fouling in field exposure) which can create local steel anodic sites, as exemplified by the irregular surface corrosion observed in the laboratory samples as well as field samples (detailed in (Permeh et al., 2019a)).

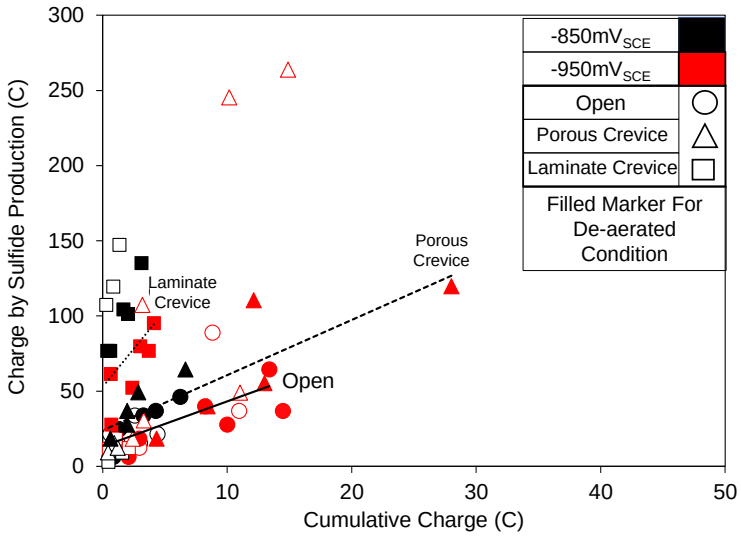

Figure 6.10. Cumulative charge associated with sulfide production and net cathodic reaction rates (lines correspond to the fitted curve).

The observation of generally lower measured cathodic current relative to the charge associated with sulfide production indicate that sulfide production by metabolic activities that are not associated with charge transfer of electrons on the steel surface is significant. However, the results (especially for the crevice conditions) show that surface heterogeneities including occluded spaces can have non-uniform polarization and linear resistances along the length of the specimen from the polarization source that can reduce the overall rate of the cathodic reaction. Presence of biofilm can also contribute to this effect. Non-uniform cathodic polarization for CP systems could allow localized corrosion to occur. This behavior was well manifested for the cases with the hard

crevice and less so for the porous crevice reflecting the better ionic connectivity through the pores in the latter. Nevertheless, some portions of the steel in contact with the sponge (in porous crevice) can exhibit similar non-uniform cathodic polarization.

6.4. Results and Discussion for Field Testing

6.4.1. Field Electrical Potential Measurements

Tables 6.5 and 6.6 provide the periodically measured electrical potentials for the test systems at Site I and Site II. The open-circuit potential of the uncoupled bulk zinc anodes, E_{Zinc}, at the beginning and end of the test was electronegative (<-1,000 mV_{CSE}) indicating sustained zinc corrosion activity throughout the ~200-day exposure period in the brackish waters at both test sites. The test specimens prior to coupling to the zinc anode had E_{OCP} values ranging from -691 to -722 mV_{CSE} for Site I and from -657 to -674 mV_{CSE} for Site II. The submergence depths of the test samples at Site I were relatively deeper than those at Site II, and the type of marine fouling developed on the test samples at the two sites exhibited visually different characteristics. Different oxygen levels, due to test depths and crevice environments, at the steel interface can account for the variations in potentials; however, relatively more negative potentials measured at Site I may indicate larger apparent anodic current exchange density and thus higher corrosion activity.

As reference, the Group B control steel coupons (from a wider range of test depth) had E_{OCP} from -612 to -798 mV_{CSE} for Site I and from -637 to -772 for Site II during the immersion period. Potentials measured after coupling of the zinc anode, E_{ON}, gave indication of some level of cathodic polarization of the steel array assuming small ohmic drop (Table 6.6 and 6.7). At Site I, the E_{ON} was in the range of -938 to -1,142 mV_{CSE} during the exposure. Indeed, E_{IO} at day 279 was -1,022 mV_{CSE}, indicating at least 300 mV of cathodic polarization from the initial OCP conditions at day 88. At Site II, the E_{ON} was not distinctly different from the initially measured steel E_{OCP} even though the zinc anode itself was about -1,018 to -1,104 mV_{CSE}. However, steel off-potentials (partial depolarization after 5 min.), E_{OFF}, on day 77 showed distinct shift to more noble

potentials as listed in Table 6, indicating that some effect of the cathodic polarization was present. Nevertheless, due to possible apparent electrical connection problems of the steel array to the initial zinc anode, coupling of the steel array was switched to an auxiliary bulk zinc anode. Subsequently, the system E_{ON} was measured as about -1,004 to -1,011 mV_{CSE}. The median E_{ON} and E_{IO} values were -1,007 and -1,003 mV_{CSE}, respectively. With regard to the initial E_{OCP} at day 0, the zinc anode provided at least 150 mV cathodic polarization. Some anomalous results were evident in the potential measurements. Notably, some test coupons had E_{IO} values less than industry accepted criteria of -850 mV_{CSE} (NACE-SP0408 (2014). Also, 4 of the 14 test coupons at Site II showed E_{IO} values more electronegative than its E_{ON}, relating to random field errors associated with electrical potential measurements with placement of the reference electrode in the water during strong tidal period.

Table 6.5. Uncoupled electrochemical potential (mV_{CSE}).

Parameter	Site I		Site II	
	Exposure Time (Coupled Time), days	Potential Min, (Median), Max mV_{CSE}	Exposure Time (Coupled Time), days	Potential Min, (Median), Max mV_{CSE}
E_{Zinc}	88, (0)	-1,148[a], -1,037Aux	0, (0)	-1,104[a], -1090Aux
	279, (191)	-1,135[b], -1,370Aux	245, (245)	-1,018[b], -1,074Aux
E_{OCP}[a]	88, (0)	-691, (-700), -722	0, (0)	-657, (-662), -674
E_{OCP}[c]	0, (-)	-750, (-762), -774	-	-
	107, (-)	-694, (-709), -798	0, (-)	-637, (-686), -710
	195, (-)	-684, (-701), -712	77, (-)	-727, (-764), -772
	279, (-)	-612, (-713) -723	245, (-)	-688, (-706), -725

E_{zinc}: Zinc anode potential. E_{OCP}: Steel coupon OCP.

[a.] Potential prior to coupling. [b.] Potential after disconnection. [c.] Control (Group B) specimens (Permeh et al., 2019b).

Table 6.6. Cathodic protection electrochemical potential (mV_{CSE}) and current (mA).

Site I					Site II				
Exposure Time (Coupled Time) (days)	Potential, E_{ON} (mV_{CSE})	*I*, Current (mA)/ *i*, Current Density ($\mu A/cm^2$)			Exposure Time (Coupled Time) (days)	Potential, E_{ON} (mV_{CSE})	*I*, Current (mA)/ *i*, Current Density ($\mu A/cm^2$)		
		Config 1	Config 2[a]	Config 3[a]			Config1	Config 2[a]	Config 3[a]
88, (0)	-938 to -1,142	-	-	-	0, (0)	-	-	-	-
191, (107)	-1,008 to -1,086	-	-	0.02 / 0.1 (1.9) / (9.0) 4.5 / 21.7	77, (77)[b]	-620 to -708[c]	-	-	0.2 / 1.1 (0.5) / (2.5) 0.8 / 3.8
279, (191)	-1,052 to -1,065	14.0 / 5.2	0.2 / 0.8 (0.6) / (3.1) 1.0 / 4.9	0.4 / 1.9 (0.7) / (3.6) 1.1 / 5.6	245, (245)	-1,004 to -1,011	10.75 / 3.7	0.9 / 4.6 (1.4) / (6.5) 2.2 / 10.4	7.2 / 34.7 (8.3) / (40.5) 9.9 / 47.9

E_{ON}: CP on-potential. [a] Current value: Minimum, (Median), Maximum. [b] Initial and Aux. zinc anode switched at Day 77. [c] E_{ON} potentials prior to switching zinc anode.

Table 6.7. Cathodic Protection E_{IO} and E_{OFF}

Site I			Site II		
Exposure Time (Coupled Time), days	Potential Min, (Median), Max mV_{CSE}		Exposure Time (Coupled Time), days	Potential Min, (Median), Max mV_{CSE}	
88, (0)	E_{ON}	-938, (-975), -1,142	77, (77)[a]	E_{ON}	-620, (-640), -708[b]
	-	-		E_{OFF} (5 min)	-485, (-520), -580[b]
279, (191)	E_{ON}	-1,052, (-1,057), -1,065	245, (245)	E_{ON}	-1,004, (-1,007), -1,011
	E_{IO}	-1,022[c]		E_{IO}	-832, (-1,003), -1,026[d]
	E_{OFF} (10 min)	-990[c]		E_{OFF} (4 hrs)	-704, (-788), -887[d]

E_{ON}: CP on-potential, E_{IO}: Steel instant-off potential, and E_{OFF}: Steel off-potential (partial depolarization). [a] Initial and Aux. zinc anode switched at Day 77. [b] Potentials prior to switching zinc anode. [c] E_{IO} and E_{OFF} for steel array. [d] E_{IO} and E_{OFF} for individual coupons.

As anticipated, due to the more electronegative corrosion potential of the steel array at Site I, possibly relating to the development of calcareous deposits on specimen as indicated by the X-ray diffraction (XRD) pattern (Figure 6.11), the E_{ON} was more electronegative. For both test sites, no differentiation in corrosion potentials was observed by immersion depth.

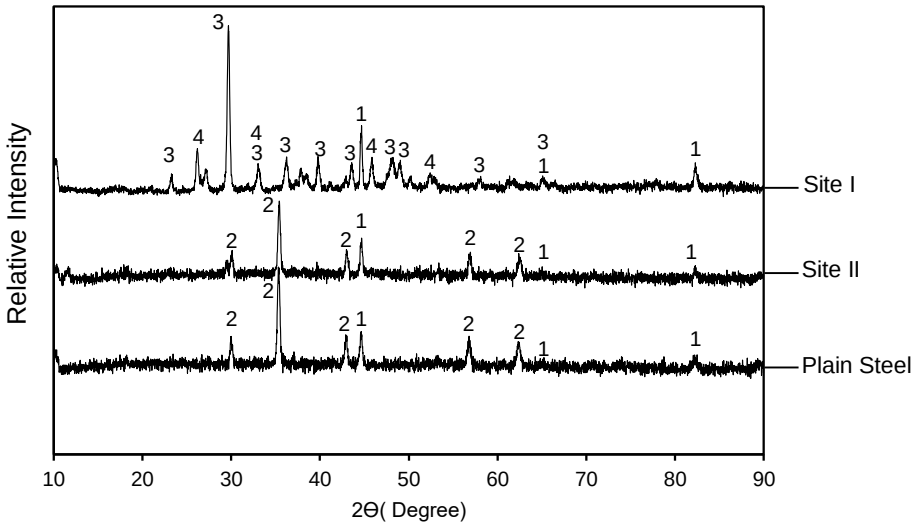

Figure 6.11. XRD pattern for field exposed specimens.1. Iron (Fe), 2. Iron and manganese (Fe.Mn), 3. Calcium carbonate $CaCO_3$, 4. Calcium phosphate $Ca_3(PO_4)_2$.

6.4.2. Field CP Current Measurements

Table 6.6 shows the range of afforded CP current for the 14 coupons at Site I and II, each. CP currents were measured after 279 days of exposure (191 days of CP) and after 245 days of exposure at Sites I and II, respectively. For reference, the CP current measured at Site I after 191 days of exposure (107 days of CP) and after switching the anodes at Site II after 77 days of exposure were shown as well. The CP currents at Site I after 191 days was larger than by the end of the experiment at day 279. This was thought to be related to the accumulation of marine growth that was postulated to reduce the effective steel surface area. The currents at Site II at day 77 were measured shortly after reconnection to the auxiliary anode and the relatively low currents reflected the initial polarization. CP current data at the end of the testing with the mature development of

micro- and macro-fouling better represent the long-term polarization behavior in natural coastal marine environments.

Figure 6.12 shows the cumulative fraction of CP current measured by the three measurement configurations for each site. For comparison, the nominal current density was calculated by steel area (13 and 14 plates for test configuration 1 at Site I and II, respectively; and 1 plate for the local test configurations 2 and 3 for both test sites). For test configuration 1, at Site I, one sample was decoupled from the array due to failure of an electrical switch.

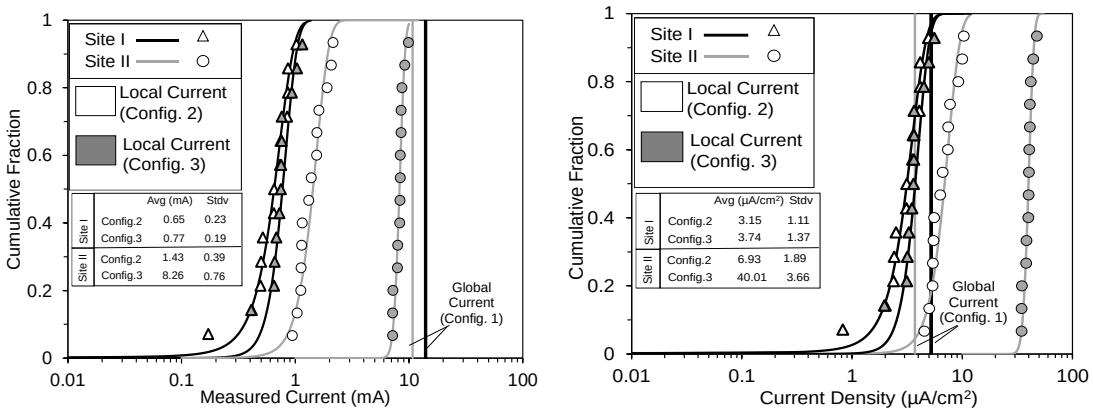

(a) (b)

Figure. 6.12. CP current (a) and current density (b) distribution for field exposed samples by three configurations. (Fitted curves show normal distribution of the data)

Consistent with the cathodic polarization level provided by the zinc anode (>150 mV from the initial OCP) at both sites up to end of testing, configuration 1 global CP currents to the steel array exceeded 10 mA. Global nominal current density was 5.2 and 3.7 μA/cm^2 for Site I and Site II, respectively and exceeded levels associated with sufficient protection (>3μA/cm^2) (Chess and Broomfield 2005). Also, E_{IO} and short term E_{OFF} at the end of the test showed (Table 6.7) at least 60 mV depolarization after 10 minutes at Site I and greater than 100 mV after 4 hours at Site II. These observations indicated that the zinc anode can generally provide significant polarization and currents to the steel array even with the presence of surface fouling. For the polarization of the

commensurate surface areas in test configurations 2 and 3, the local CP currents at individual steel plates were smaller than the global current provided to the entire array (configuration 1). The local currents ranged from 0.1 to 1.0 mA for Site I and were relatively higher for Site II (1 to 10 mA). The local nominal corrosion current densities were between 0.8 and 5.6 $\mu A/cm^2$ for test configurations 2 and 3 at Site I. At Site II, they ranged from 4.6 to 10.4 $\mu A/cm^2$ and from 34.8 to 47.9 $\mu A/cm^2$ for test configurations 2 and 3, respectively. The decoupling of extended reactive surfaces from the large steel array in test configuration 3 allowed the system potential to become more electronegative due to the reduced overall rate of cathodic reaction when compared to configuration 2. Due to the larger developed cathodic polarization from the OCP condition in the test configuration, larger cathodic current per specimen can be provided by the zinc anode in configuration 3 in comparison to configuration 2. Current measurements between the isolated steel coupons and the steel array coupled to the zinc anode in configuration 2 conversely were lower due to the relatively higher noble system potentials. The results indicated that local CP current densities may not be sufficient at some regions, particularly at site I.

The measurements of similar global currents but discrepant local currents at Site II in comparison to Site I indicated that changes to the steel surface (due to development of deposits and marine fouling) at the test sites affect the CP current levels. For test configurations 2 and 3, no major differentiation in currents was observed in relation to sample immersion depth or marine growth at each test site, and the data did not show significant effects due to solution resistance by distance (up to 1 m) from the zinc anode. Also, localized steel regions (i.e. individual steel coupons) did not appear to have strong indication of differential polarization. A combined effect of the preceding would contribute to the resulting distribution of CP currents. More distinctly, development of differential surface features including deposits and marine fouling with different morphologies at the two test sites appeared to be a contributing factor for the observed differences in the levels of CP currents developed.

Presence of calcareous deposits (Figure 6.11) at Site I in part contributed to the lower local currents measured at this location; however, the cathodic area effect can also satisfy the trends in the current afforded by the anode at Site I and Site II for the test configurations. Compilation of data from both sites showed that smaller local currents were afforded by the zinc anode at Site I in comparison to Site II. The mat-like soft coverage of marine flora and well-adhered barnacles on steel coupons at Site I created a compact crevice environment compared to the loose, porous and protruding layering of barnacles at Site II. This observation indicated that there were smaller cathode surfaces available at Site I and the dense and tightly bound marine fouling significantly reduced the availability of cathode surface areas. The laboratory testing described next provided supporting information to relate the effect of crevice morphology.

6.4.3. Microbial Growth in Presence of CP

As shown in Table 6.8, Group A and B steel test specimens from test Sites I and II had high populations of SRB, IRB, APB, and SFB. In general, steel coupons subjected to CP did not show consistent differentiation in bacteria populations in comparison to the control samples, and it was apparent that proliferation of the bacteria was not inhibited in the presence of the cathodic polarization up to -1,142 mV_{CSE} at Site I and -1,011 mV_{SCE} at Site II provided by the zinc anode. As shown in Table 8, viable SRB populations on the surface of laboratory test specimens (at the different polarization and crevice conditions), were measured by serial dilutions. SRB counts were not consistently or significantly lower when subjected to cathodic polarization.

The morphology of the crevice environments from the fouling layer on steel allowed SRB to be protected even with strong cathodic polarization. Higher pH levels (developed in occluded regions by the enhanced oxygen reduction rates) that could diminish bacteria activity was not a significant factor.

Table 6.8. Surface bacteria counts (CFU/mL) for field testing.

Bacteria	Site I		Site II	
	Control (Group A)	CP (Group B)	Control (Group A)	CP (Group B)
Sulfate reducing (SRB)	6,000 [A]	1,400 [M]	27,000 [A]	27,000 [A]
Iron reducing (IRB)	35,000 [A]	2,200 [M]	9,000 [A]	35,000 [A]
Acid producing (APB)	82,000 [A]	475,000 [A]	475,000 [A]	475,000 [A]
Slime forming (SFB)	1,750,000 [A]	1,750,000 [A]	1,750,000 [A]	1,750,000 [A]

Aggressivity: [M] Moderately Aggressive, [A)] Aggressive, based on the general guidelines for BART test provided by Droycon Bioconcepts Inc. (Regina, Canada).

6.4.4. Steel Corrosion under CP in Presence of Fouling

6.4.4.1. Mass Loss for Field Specimens

The corrosion rates calculated from the mass loss data from the Group A field specimens and comparable Group B field specimens (installed at commensurate depths as Group A specimens) are shown in Table 6.9. The average free corrosion rates (Group B specimens) at Site I and Site II were 52 mdd and 21 mdd, respectively. Due to the initial free corrosion at Site I for the first 88 days and the corrosion due to partial CP coupling at Site II for the first 77 days, the apparent corrosion rates for the different test intervals were calculated, including an upper and lower bound for Site II. It was assumed that the free corrosion rates of the steel samples prior to coupling to the zinc anode was equal to the rates determined by the mass loss of control (Group B) steel coupons at concomitant submerged depths. The steel mass loss that occurred during the time of zinc coupling was calculated by calibrating the final mass by the mass loss associated with the free corrosion rate prior to electrode coupling. Equation 1 would accordingly be modified with

$m_o = m_{f,B} - m_{o,B}$ where $m_{f,B}$ and $m_{o,B}$ are the final (after cleaning) and initial (pre-exposure) mass for the respective Group B coupon in grams. The average corrosion rate for the steel specimens with CP at Site I was 12 mdd.

Table 6.9. Apparent corrosion rate for field exposed samples.

Condition	Site I		Site II	
	Range (mdd)	Average (mdd)	Range (mdd)	Average (mdd)
Free corrosion	46-56	52	17-27	21
CP	4-19	12	6-13 13-15	9[a] 14[b]

[a]Lower bound assuming free corrosion for the first 77 days and CP for ~170 days.
[b]Upper bound assuming effective CP for entire 245-day exposure period.

For Site II, the upper and lower bounds were calculated by assuming either the entire 245 days had CP or that the first 77 days had free corrosion and CP was only provided in the last ~170 days. Corrosion rate calculations with the assumption that CP was provided for the entire 245 days would then provide an overestimation of the expected corrosion rate if the system was fully coupled. On the other hand, it should be noted that the assumption of free corrosion for the first 77 days would not reflect any partial corrosion mitigation afforded by the partial CP connection during that time. Corrosion mitigation would not be significant as the corresponding on-potential was the same as the initial steel OCP (~-600 mV_{CSE}) when coupled to the initial zinc anode. Calculations were made as described for Site I with consideration for free corrosion prior to the application of CP. The average calculated corrosion rate was 9 and 14 mdd for the lower and upper bounds, respectively. The actual corrosion rate would be between these values.

Figure 6.13 compares the apparent corrosion rates for Group B steel specimens at OCP and Group A specimens coupled to the zinc anode at Site I and II. It was evident by comparison of the apparent corrosion rates to reported average and maximum corrosion rates (Tomlinson and Woodward, 2014) that the submerged region of Site I was relatively more aggressive where the apparent corrosion rate (100 $mg/dm^2/day$ (mdd)) was as much as 2 times greater than the maximum values reported for marine environments (38 mdd). Nevertheless, coupling of the steel to the zinc anodes reduced the apparent corrosion rates (4-19 mdd).

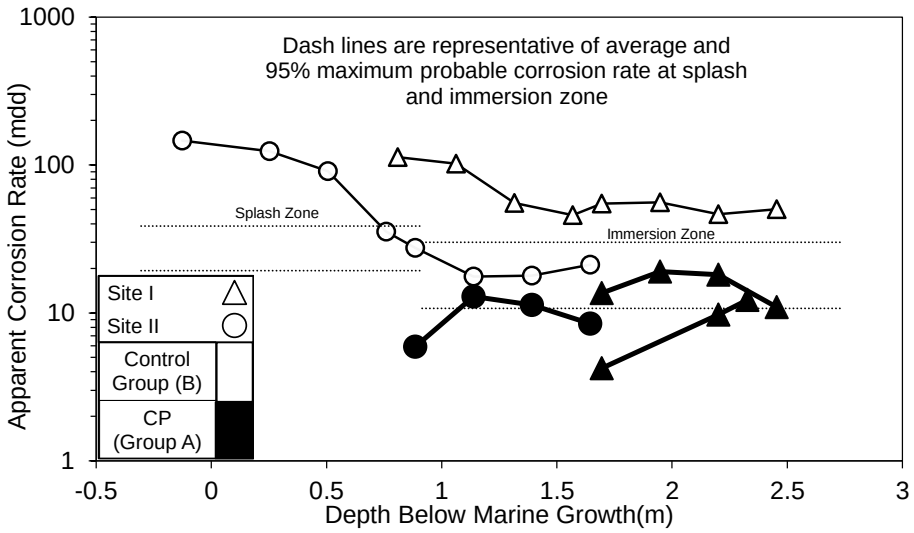

Figure 6.13. Apparent corrosion rate for field exposed specimens by depth (Lower bound apparent CP corrosion rates shown for Site II).

Figure 6.14 presents a compilation of apparent corrosion rates calculated in terms of mass loss and apparent specimen thickness per Equations 1 and 2, respectively. The apparent corrosion rates calculated by mass provided indication that the control specimens at both test sites had significant mass loss, and the corrosion rate calculated by mass was consistently larger than the apparent corrosion rates calculated by thickness. This would provide characterization of the corrosion modality of the control specimens as having significant localized corrosion and indeed the surfaces of these specimens had a sinuous surface texture and localized regions with cross-section loss. It was evident that the free corrosion at both test sites will cause significant heavy localized corrosion. Specimens with irregular cross section loss or localized corrosion would not be well qualified by the corrosion rates calculated from thickness measurements, and pitting could not be elucidated by either approaches to calculate apparent corrosion rates.

The application of CP at both sites substantially reduced the overall rate of steel corrosion. The calculated corrosion rates by mass and thickness were generally well correlated, indicating that much of the loss was due to general corrosion. However, small pits such as that developed at Site

I would not be well captured by the calculation. Application of CP at Site II did mitigate the development of localized corrosion and no pitting was observed on the steel coupons coupled to the zinc anodes, whereas comparatively heavier localized steel loss was observed on the control samples. It was uncertain if coupling of the zinc anodes to the steel array at Site I had similar effect, as free corrosion was allowed for the first 88 days there; however, localized corrosion (irregular surface corrosion) was reduced when coupled to the zinc anode in comparison to the free-corrosion (Group B) test specimen.

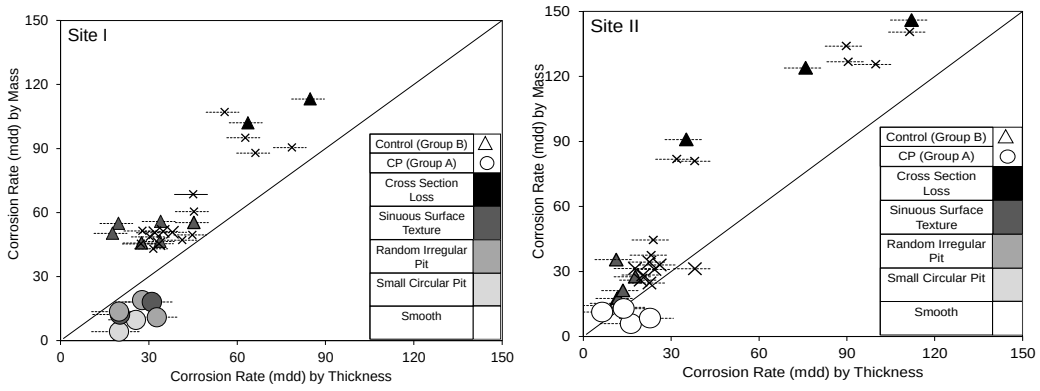

(a) (b)

Figure 6.14. Comparison of corrosion rates estimated by mass loss and plate thickness at (a) Site I and (b) Site II. Crosses represent data reproduced from (Permeh et al. 2019b).

The higher apparent corrosion rates and lower CP currents at Site I indicated that there remained localized regions on the steel array where CP was not effective, indicating the detrimental effects of marine fouling or MIC under biofilm. These findings showed that localized corrosion can continue when marine fouling create localized corrosion cells and where MIC can develop in regions unprotected by CP.

6.4.4.2. Surface Conditions of Field Specimens

Heavy fouling occurred during the time of exposure at both sites. Figure 6.15 shows the representative visual appearance on the steel coupons at the end of the field exposure period for both sites (after 245-279 days of exposure) before and after hand cleaning. The general fouling organisms at Site I included well adhered large diameter acorn barnacles as well as broad but compact coverage of marine flora, hydroids, and bryozoans. Site II had predominantly loose multilayer encrustation of small diameter bay barnacles.

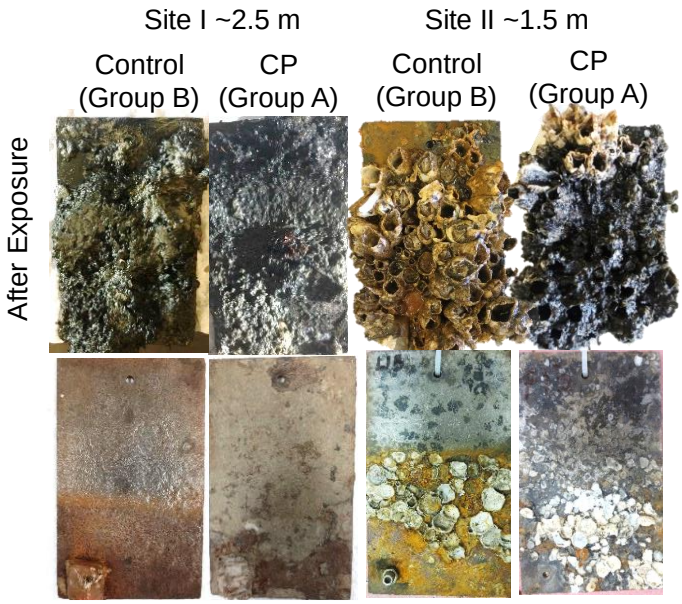

Figure 6.15. Surface conditions for test coupons exposed at Site I and Site II before and after cleaning.

Figure 6.14 parses the steel substrate condition by the apparent corrosion rates. In the figure, the samples were categorized according to the most severe level of surface corrosion. The levels of surface corrosion in order of severity were categorized as smooth, small circular pits, irregular pits, sinuous surface texture, and heavy cross-section loss. However, specimens often had multiple steel surface corrosion modalities. In particular, specimens with a sinuous surface texture typically coincided with pit development. As described before, severe corrosion developed on the

freely corroded test samples at both Site I and II. The submerged specimens typically developed localized corrosion in the category of sinuous surface texture and lower. This type of localized corrosion is highlighted in Figure 6.16.The irregularity of the sinuous surface texture and pitting were posited to be related to surface irregularities due to the marine fouling and possibly MIC. Fig. 11 also identifies a location where differential mass loss occurred under the base of a barnacle.

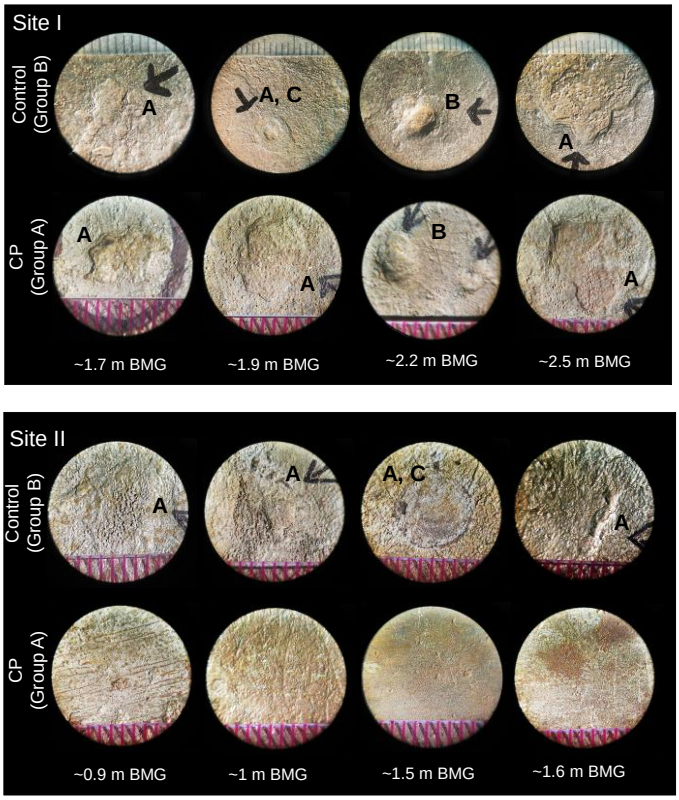

Figure 6.16. Magnified view of surfaces of field exposed specimens. Arrows highlight notable features such as surface corrosion (A), pitting (B), remnant barnacle (C) location. Ruler at 1 mm intervals

At Site I, the irregular steel surface corrosion often coincided with placement of barnacle base plates on both control and CP specimens which would indicate shielding of current and correspond to electrochemical data (and smaller cathodic surface areas) discussed earlier. The corrosion of steel with CP at Site II had generally smooth surface textures (general corrosion) indicating better current distribution provided by the anode.

CHAPTER 7

7. MITIGATION OF MIC IN PRESENCE OF MARINE FOULING CONDITION BY COATING

7.1. Introduction

Coatings are applied to steel elements exposed in natural waters to mitigate the deleterious effects of naturally occurring physical-, chemical-, and biodegradation processes. Among these degradation processes, steel structures submerged in natural waters are susceptible to corrosion and degradation by marine biofouling and also microbiologically influenced corrosion (MIC) (LaQue,1975; Dexter,1993;Dexter and LaFontain, 1998; Permeh et al.,2019a). Recent findings (chapter 5) indicated that there are synergistic effects of surface fouling to facilitate biocorrosion. Steel bridge piles in a Florida bridge showed severe localized corrosion that was associated with microbial activity under the marine fouling organisms.

Biofouling formation starts with development of a conditioning film (by adsorption of the available organic molecules and ions in the water) leading to microfouling and then macrofouling (Wells and Sytsma, 2009; Whitehead and Verran,2009; Fleming and Ridgway, 2009), conditioning film allows settlement of the fouling organism to the substrate surface. Microorganisms such as bacteria can further colonize on the conditioning film and form a biofilm that facilitate the attachment of microorganism (Fleming and Ridgway, 2009; Murthy, and R. Venkatesan,2009). Some have suggested that the biofilm is required for attachment of fouling organisms (Crisp, 1974; Keough and Raimondi,1995; Neville and Hodgkiess,1998; Yebra et al., 2004).

Mitigation technologies include protective coatings and antifouling coatings. Antifouling coatings have a long history and have an important impact on managing macrofouling (Wells et al.,2009; Yebra et al., 2004; Brady,2005; Chambers et al., 2006). These coatings are categorized by its self-polishing and foul-release characteristics (Lejars et al., 2012; Mungar,1985). Much research has been conducted regarding the performance of different coatings exposed to

biologically active environments (Jones et al., 1992; Muntasser et al., 2002; Al-Darbi et al., 2002; Telegdi et al., 2010; Skaja, 2015; Galicia et al., 2017) and antifouling coatings with biocides have been shown to be effective to reduce growth of marine fouling organisms such as bacteria, fungi, algae, plants and molluscs . Anti-fouling coatings with metal-free biocides were developed and are commercially available.

Polyurea coatings have garnered interest in industry due to some of their advantageous properties. Polyurea a has short curing time, excellent adhesion strength, chemical resistance (to mild hydrogen sulfide concentrations, carbon dioxide and sulfuric acid) and corrosion resistance which makes it a favorable candidate for wet environments (Broekaert et la., ,2002) Polyurea coatings have been used for corrosion mitigation for steel and concrete in wastewater infrastructure, water pipelines, marine structures, fuel storage tanks and fuel pipelines**.**

Due to the development of severe localized steel corrosion with high population of bacteria associated with MIC under the marine fouling observed in a Florida bridge, it was of interest to identify mitigation of MIC in presence of marine fouling condition by coating. Laboratory testing was made to identify SRB development on the surfaces of antifouling coatings and possibly any coating degradation and corrosion that may occur with the proliferation of SRB. Field testing was made to verify microbe activity on coated steel samples in presence of natural fouling as well as verifying coating degradation and natural corrosion development.

7.2. Methodology

As described in section 5.2.2.1, steel plates (12.7cm x 7.6cm x 0.32cm) with composition of 0.02%C, 0.16 % Mn, 0.006% S and 0.03% Si) were used also for coating testing. The surface of the steel plates was ground to a uniform 60 grit size (265 μ) finish using a power orbital sander and cleaned with acetone prior to application of a commercially available water-based copper-free self-polishing antifouling coating. The coating consisted of a metal primer, two coats of a tie coat and

one coat of the anti-fouling coating (chemical constituents included organic metal-free biocide, ZnO, TiO_2, and zinc pyrithione) following the manufacturer's recommendations. In part to verify the antimicrobial performance of the biocides, comparative testing of steel coupons with a polyurea barrier coating without active antibacterial components (as part of a larger test matrix (Permeh et al.2019a)) was made. The average coating thicknesses for antifouling and polyurea were 0.1-0.3 mm and 0.63-1.37 mm, respectively.

7.2.1. Laboratory Testing

7.2.1.1. Test setup

Testing was made on 6 antifouling-coated and 6 polyurea-coated steel coupons for 25 days. Each coated steel coupon accommodated two test cells by placement of two separate cylindrical acrylic test vessels (diameter 5 cm) on the steel plate surface as shown in Figure 7.1. Experimental conditions for testing included SRB inoculation, de-aeration, and coating defects (Figure 7.2). Scribed samples with coating defects were made by drilling a 0.16 cm diameter hole in the middle of the specimen.

Test cells were filled with 80 mL of deionized water (DI) and 10 mL of modified Postgate B solution (Table 5.3) [23] and the pH of all test solutions was ~6.5–8 for the duration of testing. For the inoculated test conditions, 10 mL of inoculated Postgate B broth containing SRB cultures (previously isolated from water samples collected from the field) were used. For de-aerated test conditions, high purity nitrogen gas was bubbled through the solution for 10 minutes on the first day and a thin layer of mineral oil was added. For naturally aerated-conditions, the head space above the test solution was open to the atmosphere. All test cells were fabricated with sterile components and test specimens were rinsed in deionized (DI) water and sterilized with ethanol solution prior to testing.

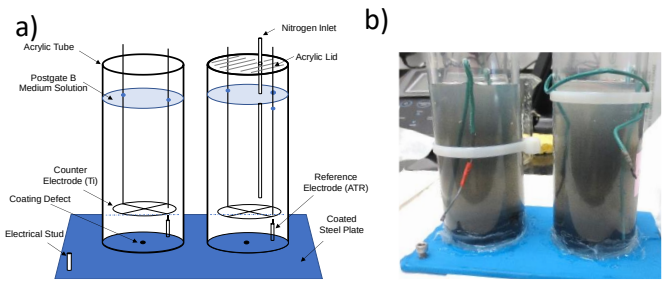

Figure 7.1. Laboratory test setup. (a) Schematic of test cell. (b) Examples picture of antifouling coated coupon in inoculated test solution

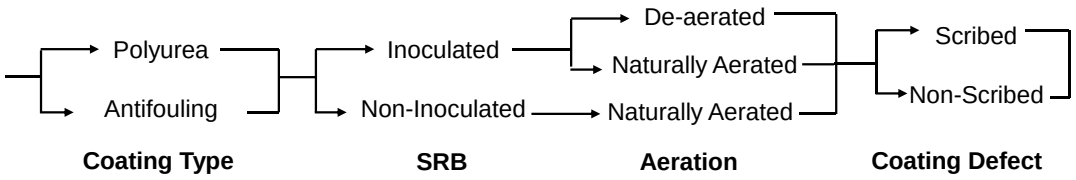

Figure 7.2. Laboratory Test Setup Conditions.

7.2.1.2. Microbial Activity

Microbial activity was assessed by the chemical oxygen demand (COD) and sulfide production during testing as well as final sessile bacteria population at the end of the test. COD and sulfide measurements only provide an indirect assessment of sessile SRB activity on the surface of the coated steel specimen but nevertheless provide information on the environmental conditions of the test cells to support microbial activity on the specimen surface with time. The sessile test kits provide better assessment of surface microbial activity at the end of the testing.

COD was measured at the beginning and end for all test cells. Each sampled test solution was measured by a colorimetric COD method (O'Dell,1993). As it was mentioned before COD levels are considered as a metric of environmental conditions to support SRB activity (Scott,2004). Sulfide levels were periodically measured for all inoculated test cells. A hydrogen sulfide color disc test kit was used for the sulfide measurements. Sessile test kits were used at the end of testing for detection of sessile sulfate reducing bacteria on each test cell. Per test protocol, the sampled

sessile bacteria were collected by swabbing a 1 cm^2 sample area of coated steel in each test cell with a sterile cotton swab. The solid sample was converted into a planktonic sample (in phosphate buffer solution, PBS) and then tested by serial dilutions in Modified Postgate B (MPB) following the NACE standard TM0194-2014.

7.2.1.3. Electrochemical Testing

Electrical connection to the steel coupon was made with a bolt stud mechanically tapped into the steel coupon. Activated titanium wire and saturated calomel (SCE) electrodes were used as reference electrodes. An activated titanium mesh was used as a counter electrode. Electrochemical measurements included open circuit potential (OCP), linear polarization resistance (LPR) and electrochemical impedance spectroscopy (EIS). Electrochemical measurements were conducted for each test cell upon placement of the test solution and made periodically for up to 25 days of testing. OCP and LPR testing was made to identify corrosion development (that would differentiate coating degradation and SRB proliferation). LPR testing was made from the initial OCP to -25mV vs OCP at a scan rate of 0.05 mV/s. The apparent corrosion current, i_{corr}, was calculated from the polarization resistance, Rp, following the equation $i_{corr}=B/Rp$ where B was assumed to be 26 mV for the active corrosion conditions (Jones, 1996).

EIS measurements was conducted at the open-circuit potential (OCP) condition with a 10 mV AC perturbation voltage from 1 MHz > f > 1 Hz to identify dielectric characteristics of the coating and interfacial characteristics of the steel. The impedance response would ideally elucidate coating degradation, steel corrosion rates, and the development of surface layers that may include biofilm and surface oxides.

7.2.1.4. Post Test Analysis

Representative test specimens for the antifouling coating were prepared for microscopic evaluation as well as x-ray diffraction (XRD) to identify coating degradation. Four specimens from the inoculated de-aerated, inoculated naturally aerated, non-inoculated naturally aerated, and a control as-received conditions were prepared following conventional metallographic preparation procedures. Small sections were mounted in epoxy resin and cross-sections were made following typical metallographic procedures (20µm, 3µm, 0.05µm grinding and polishing steps) using oil-based lubricants and extenders. Five representative specimens (from the field and the lab testing as well as control as-received condition) were evaluated by XRD. Testing was made at a range of 2θ from 20 to 80 degrees with a 0.02 degree/min scan rate.

7.2.2. Field Testing

7.2.2.1. Test Setup

In the field testing, antifouling coated steel specimens, polyurea-coated steel specimens along with plain steel specimens (section 5.2.2.1) were installed at the three Florida bridge site location (Table 5.4). The coated samples aligned vertically by depth in a single column. Specimen placement was measured relative to the marine growth line, identified as distance below the marine growth line (BMG). Even though the position of the test racks of each test site relative to the water surface varied due to the variation of the bridge substructural elements as well as due to variation in tidal levels at each test site, general exposure depths were similar and the test specimens were considered replicate for material subjected to tidal as well as submerged exposure depths. Table 7.1 shows the test condition and range of depths that the steel specimens were placed (for both tidal and submerged regions) for each test site. The exposure time was around ~250 days for Site I and II, and ~170 days for Site III. Figure 7.3 shows the field test setup

Table 7.1. Experimental Test Conditions.

Test Site	Coating Material	Exposure Condition	No. of Test Coupons	Distance BMG[1] (m)	Coating Thickness Front/Back (mm)
Site I Matanzas R.	Polyurea	Tidal	3	~0.8-1.4	0.99/0.45, 0.88/0.46, 0.63/0.68
		Submerged	3	~1.5-2.5	1.3/0.4 ,0.83/0.46,0.61/0.43
	Antifouling	Tidal	4	~0.8-1.4	0.15/0.18, 0.18/0.23, 0.15/0.15,
		Submerged	4	~1.5-2.5	0.20/0.20, 0.15/0.18, 0.13/0.10, 0.18/0.20, 0.18/0.13
Site II Alafia R.	Polyurea	Tidal	1	~0.1-0.6	0.91/-,0.91/-,0.71/-
		Submerged	2	~0.7-1.6	
	Antifouling	Tidal	3	~0.1-0.6	0.15/-, 0.18/-, 0.18/-, 0.15/-,
		Submerged	4	~0.7-1.6	0.20/-, 0.15/-, 0.10/-
Site III Alafia R.	Polyurea	Tidal	3	~0.1-0.6	1.0/-,0.86/-,0.83/-,0.74/-,1.24/-
		Submerged	3	~0.8-1.8	,0.89/-
	Antifouling	Tidal	4	~0.1-0.6	0.30/-, 0.33/-, 0.13/-, 0.18/-,
		Submerged	4	~0.8-1.8	0.23/-, 0.15/-, 0.15/-, 0.15/-

1.BMG: Below marine growth

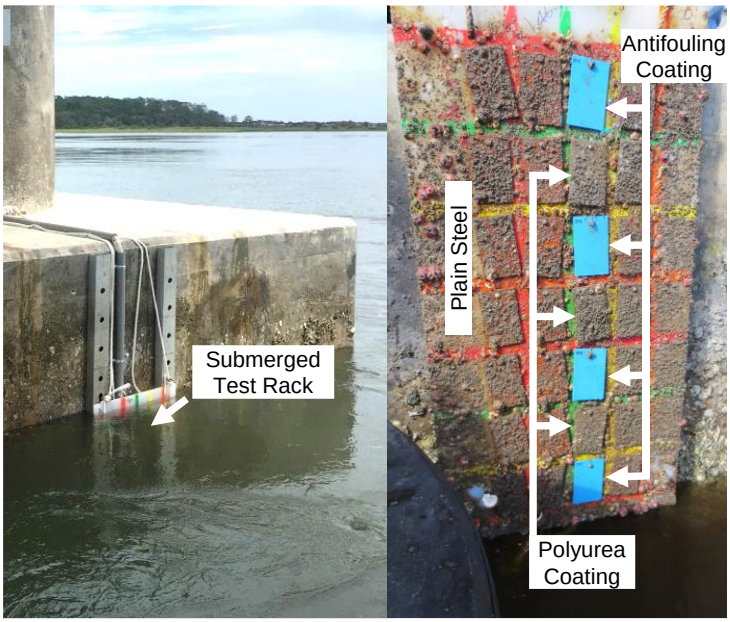

Figure 7.3. Example of Marine Growth on the Test Rack Setup in Site I.

7.2.2.2 Microbial Activity

Analysis of the developed surface bacteria population was conducted in the lab after sample retrieval. The surface fouling was left intact for the photo-documentation, but marine growth was removed from a small portion ~ 6.4 cm^2 (~1 in^2) of the coupons where swabs were collected for the microbiological analyses. Microbiological tests were conducted with Biological Activity Reaction Test (BART) kits to estimate the population of the four common MIC related bacteria (SRB, IRB, SLYM and APB) on the steel coupon surface below the layers of marine growth.

7.2.2.3. Electrochemical Testing

The retrieved test samples were immersed in sealed containers containing river water for transport back to the laboratory. In the laboratory ,the coupon working electrodes were placed 8.9 cm deep, immersing a nominal ~335.5 cm^2 steel surface area, in the collected river water solution. Figure 7.4 presents pictures of the test setup used in the laboratory. Corrosion evaluation consisted of measurements of the open circuit potential (OCP), linear polarization resistance (LPR), and electrochemical impedance spectroscopy (EIS) using a three-electrode configuration. A saturated

calomel electrode (SCE) was used as the reference electrode for all tests. An activated titanium mesh was used as the counter electrode. The scanned potentials for the LPR testing were made from the open-circuit potential and cathodically polarized 25 mV at a scan rate of 0.05 mV/s. The corrosion current was calculated from the polarization resistance, Rp, following the equation icorr=B/(Rp) where B was assumed to be 26 mV and A was the nominal surface area of steel coupon immersed in the solution. EIS testing was conducted at the OCP condition with 10 mV AC perturbation voltage from frequencies 1MHz > f >1Hz. EIS fitting parameters were applied only antifouling coated coupons, as the polyurea coated coupons showed severe disbondment condition.

Figure 7.4. Example of Laboratory Electrochemical Test Setup.

7.2.2.4. Post Test Analysis

Visual photo-documentation of the coated steel coupon surface conditions was made immediately after removal from solution and after surface cleaning. The outer-shell of the hard foulers and marine flora were removed, and the specimens were rinsed with tapwater and surface dried. Metallographic cross-sections from representative antifouling coated specimens from the three sites were prepared to verify the extent of the coating degradation under the fouling. Sections were mounted in epoxy resin and were ground and polished following typical metallographic procedures (3 and 0.05 µm polishing steps using polycrystalline diamond and colloidal alumina with oil-based lubricants and extenders). X-Ray diffraction of the antifouling coated specimens

were made to identify degradation of the biocide constituents in the coating. Testing was made at a range of 2θ from 20 to 80 degrees with a 0.02 degree/min scan rate.

7.3. Results and Discussion for Laboratory Testing

7.3.1. Microbiological Activity

As shown in Figure 7, the initial COD results ~1 day after inoculation for all solutions were generally high (>1,000 mg/L for the inoculated solutions and >500 mg/L for non-inoculated solutions) reflective of the admixed sulfate and other oxidizing chemical constituents in the diluted Postgate B base solution. Within that data set, the relatively higher initial COD values for the inoculated solutions would in part relate to early SRB activity and resulting sulfide production. However, by the end of the 25-day test exposure, the overall COD decreased as iron sulfide reaction products precipitated and the test conditions became less favorable for sustained SRB activity in the closed laboratory test cells. The COD levels observed in the test cells with the polyurea coated specimens at the end of the testing were consistently lower than that of the antifouling coating indicating that the higher SRB growth in the former allowed for greater consumption of sulfate and organic compounds in the Postgate B solution in the closed test cell.

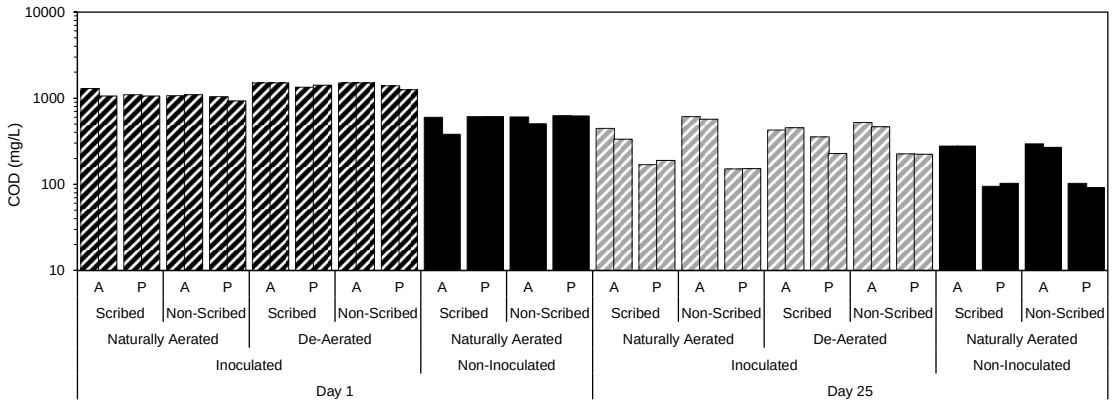

Figure 7.5. Chemical oxygen demand for laboratory coated specimens.
A: Antifouling, P: Polyurea

Indication of initial SRB activity for all inoculated test cases (consistent with the high initial COD levels) was corroborated by early sulfide production within the first week of testing. The sulfide levels were measured on days 1, 5, 8, 14, and 27. As shown in Figure 7.6, cumulative sulfide production (assumed to be constant for the time intervals between sulfide measurements) within the test volume was calculated. Consistent with the high initial COD levels, early sulfide production (as the major metabolic activity of SRB) was identified during the first week of laboratory testing. Relatively higher sulfide concentrations were measured for one of the inoculated antifouling coated specimens (as well as for all polyurea coated specimens) at the initial day. Contrasting the results from the anti-fouling and the polyurea coating, there was indication that the antimicrobial components of the anti-fouling coating allowed for reduced proliferation of SRB as shown by the overall lower rates of sulfide production (both the initial rates and duration of sulfide production).

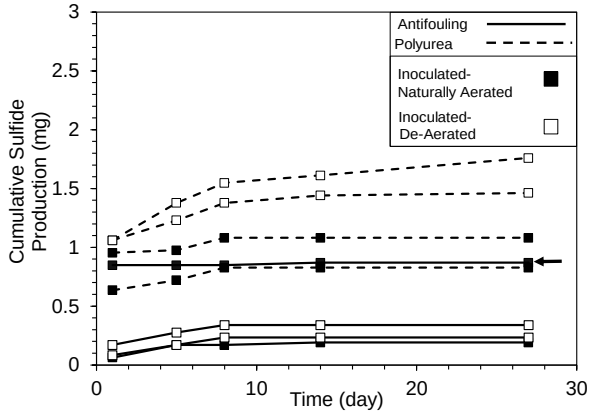

Figure 7.6. Sulfide production due to sulfate-reducing bacterial (SRB) activity. Arrow indicates antifouling coating specimen with greater SRB activity.

The total sessile SRB population for each test condition is shown in Table 7.2. In agreement with the higher sulfide levels, larger SRB populations developed on the surface

of the polyurea-coated samples. The SRB population was as high as $1x10^6$ bacteria per mL for scribed samples in de-aerated condition and ranged from $1x10^2$-$1x10^4$ bacteria per mL in the other test conditions. In contrast, the sessile SRB populations on the surface of the coupons with the antifouling coating were lower and generally showed zero population of SRB (except one sample in naturally aerated condition where the SRB population was $1x10^4$ bacteria per mL). Overall, the lab results were consistent with the COD and sulfide measurements and showed that there were beneficial effects of the anti-microbial constituents to mitigate SRB growth within the time duration of the testing.

Table 7.2. Bacteria count per mL for laboratory coated specimens.

		Scribed Inoculated	Non-Scribed Inoculated	Scribed Non-Inoculated	Non-Scribed Non-Inoculated
De-Aerated	Antifouling	0, 10^1	0, 0	-	-
	Polyurea	10^6, 10^6	10^4, 10^4	-	-
Naturally Aerated	Antifouling	0, 10^4	0, 0	0, 0	0, 0
	Polyurea	10^2, 10^4	10^2, 10^3	0, 0	0, 0

7.3.2. Electrochemical Measurements

Corrosion potential and corrosion current density for test specimens are shown in Figure 7.7. Steel with the antifouling coating without coating defects generally showed noble electrochemical potentials upon exposure to solution, representative of the poor interaction of the steel surface with the bulk solution as may be expected for polymeric coatings. With longer exposure times, the potentials dropped to more electronegative values in the order of -400 to -500 mV_{SCE} due to wetting of the coating and possibly coinciding with coating degradation. Concurrently, the corrosion currents increased with

time. The test coupons with intentional defects immersed in non-inoculated solution generally developed a potential of ~-700 mV_{SCE} representative of electrochemical interaction of the steel interface with the solution. Specimens in SRB inoculated solution generally showed similar results, but a scribed sample in naturally-aerated solution showed possible indication of MIC including potential ennoblement related to cathodic depolarization (Borenstein,1994) and coincident higher SRB activity (high sulfide concentration and SRB sessile population) during the test exposure. The corrosion current density for the specimens in non-inoculated solutions was lower than for the specimens in inoculated solution where SRB activity was evident.

Polyurea-coated steel specimens without surface defects showed noble potentials indicative of good barrier coating characteristics. LPR testing of these specimens yielded poor results reflective of its large coating electrical resistance. For specimens with the intentional coating defects, the developed OCP was characteristic of a steel interface in aqueous solution, but there was distinct differentiation between the inoculated and non-inoculated cases (Figure 8). Non-inoculated samples had OCP ~-800 mV_{SCE} indicative of active corrosion conditions (Matsukawa et al., 2011). The inoculated samples however showed a positive shift (~100 mV) of OCP from -700 mV_{SCE} to -600 mV_{SCE} within 5 days. The potential ennoblement coincided with the early high SRB activity where large sulfide concentrations were measured. The corrosion current density for the coated specimens with exposed steel defects placed in non-inoculated solution showed relatively lower corrosion currents than the comparative specimens placed in inoculated solutions. The higher corrosion activity and potential ennoblement were indicative of MIC relating to SRB in the polyurea coated samples.

The corrosion associated with SRB on coated steel would be localized at defect sites, and formation of SRB biofilm on the steel defect would be in the vicinity of electron donors from the steel and available nutrients from the solution. This would occur as well for the antifouling coatings if local concentrations of biocides are reduced near the steel interface. If the localized corrosion were to continue, extended coating defects such as disbondment may occur. The polyurea coating may reduce degradation of the steel substrate if coating disbondment is minimized.

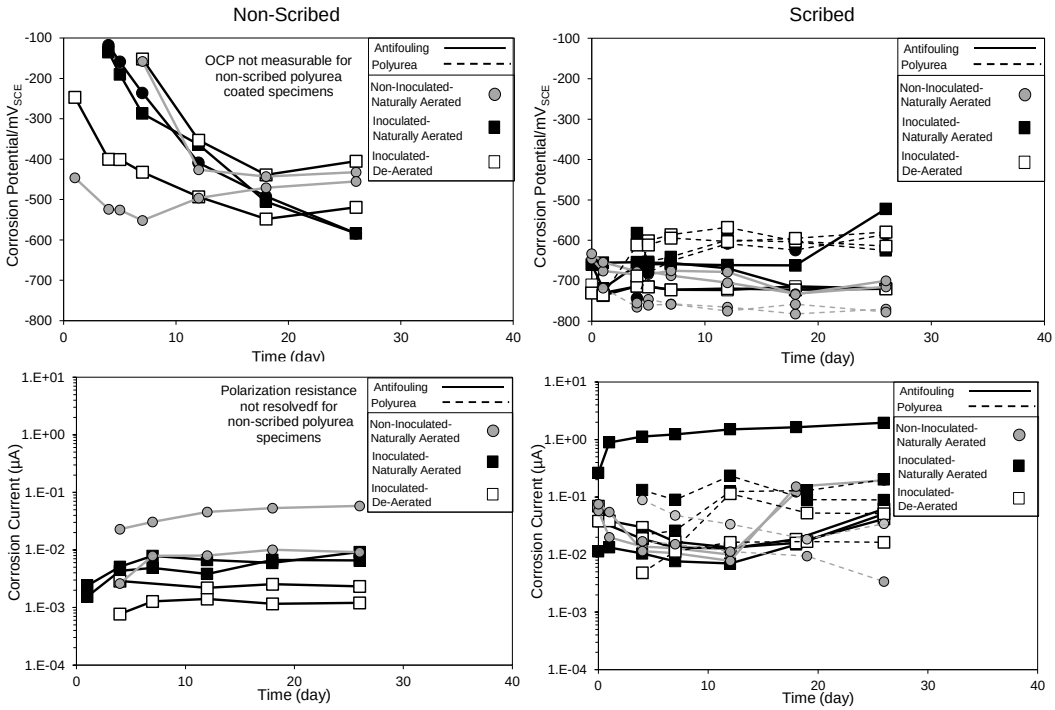

Figure 7.7. Corrosion potential and corrosion current density for laboratory coated specimens.

7.3.3. EIS (Impedance response)

The impedance data presented in Nyquist diagrams (Figure 7.8) generally showed varied responses that reflected the different surface and interfacial characteristics. One or more impedance loops characteristic of coated steel with varying levels of coating defects (possibly associated with coating degradation in presence of SRB growth and MIC) was evident, although was sometimes convoluted with the presence of multiple time constants.

Based on the results of EIS testing for the coated steel specimens exposed in solution, idealized coating conditions and equivalent circuit analogs were posited as shown in Figure 7.9. Defects in surface layers can be characterized by a resolved resistance term where the defects are typically idealized as a population of cylindrical pores. The electrical resistance of the defects, R, can be described by ohm's Law in the form $R = \rho L/A_{po}$ where ρ is the resistivity of the medium within the defect, L is the length of the pore, and A_{po} is the pore area. This treatment has been commonly used to describe defects such as holidays in polymeric coatings and defines a pore resistance R_{po} where $L = d$ (coating thickness). Similar treatments can be used to describe other layers including porous biofilm ($R = R_{bf}$) and oxide layers ($R = R_{ox}$) where $L = t$ (thickness of the layer). All equivalent circuit analogs incorporated constant phase elements (CPE) with impedance $Z = 1/Y_o(j\omega)^n$ where Y_o is the pre-exponential admittance term and $0 < n < 1$.

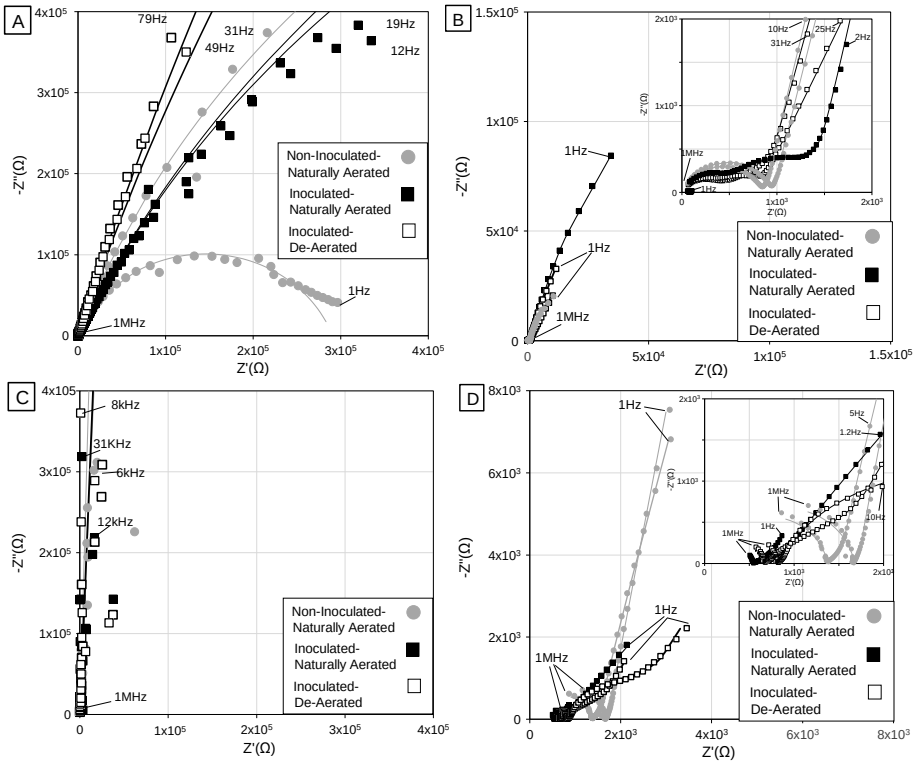

Figure 7.8. Electrochemical impedance spectroscopy Nyquist diagrams for coated steel samples immersed in inoculated and non-inoculated solutions at day 18, (A) Antifouling (Non-Scribed); (B) Antifouling (Scribed); (C) Polyurea (Non-Scribed); (D) Polyurea (Scribed). Line shows the fitted curve.

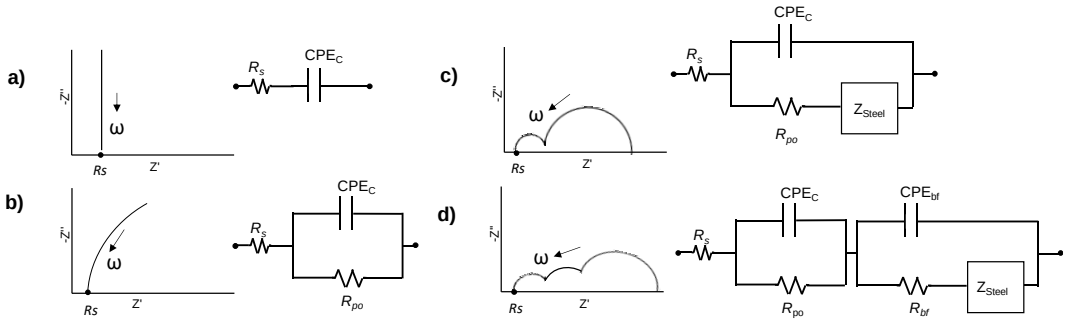

Figure 7.9. Idealized electrochemical characteristics of coated steel specimens. (a,b) Non-Scribed, (c,d) Scribed.

As shown in Figure 7.8, the equivalent circuit analogs were shown to adequately fit the experimental data during the test exposure in the research. In order to provide quantitative comparison of the impedance response, an approach following Hsu and Mansfield,2001, to estimate capacitive behavior was followed. As shown in Figure 7.8, the complicated impedance response prohibited easy differentiation of time constants, τ, especially impedance behavior at intermediate frequencies. Due to the conflation of combined impedance responses of the various surface layers (and as proposed in Figure 7.9), the nested impedance time constants were computationally decoupled (Mansfeld,1981) by plotting the impedance of a parallel combination of separate capacitive and resistive components previously fitted as part of the proposed analog circuits. By doing so, the characteristic frequency where the imaginary impedance component associated with capacitance could be identified. The frequency associated with the maximum imaginary component of impedance, f_m, could be isolated and capacitance was estimated by Equation (7.1).

$$C = Y_o \times (2\pi f_m)^{n-1} \tag{7.1}$$

An example of the decoupled impedance response for specimens showing three separate time constants is shown in Figure 7.10. Table A1 in the appendix, shows the resolved impedance parameters from equivalent circuit fitting, resolved f_m, and calculated nominal capacitances for all test specimens at time 0 and 18 days for the antifouling-coated specimens and at time 4 and 26 days

for the polyurea-coated specimens. The decoupled impedance resolved with the calculated capacitance showed that the associated phase angle was 45° at f_m indicating that f_m is the breakpoint frequency where $C = 1/(2\pi f_m R)$ and $\tau = 1/(2\pi f_m)$.

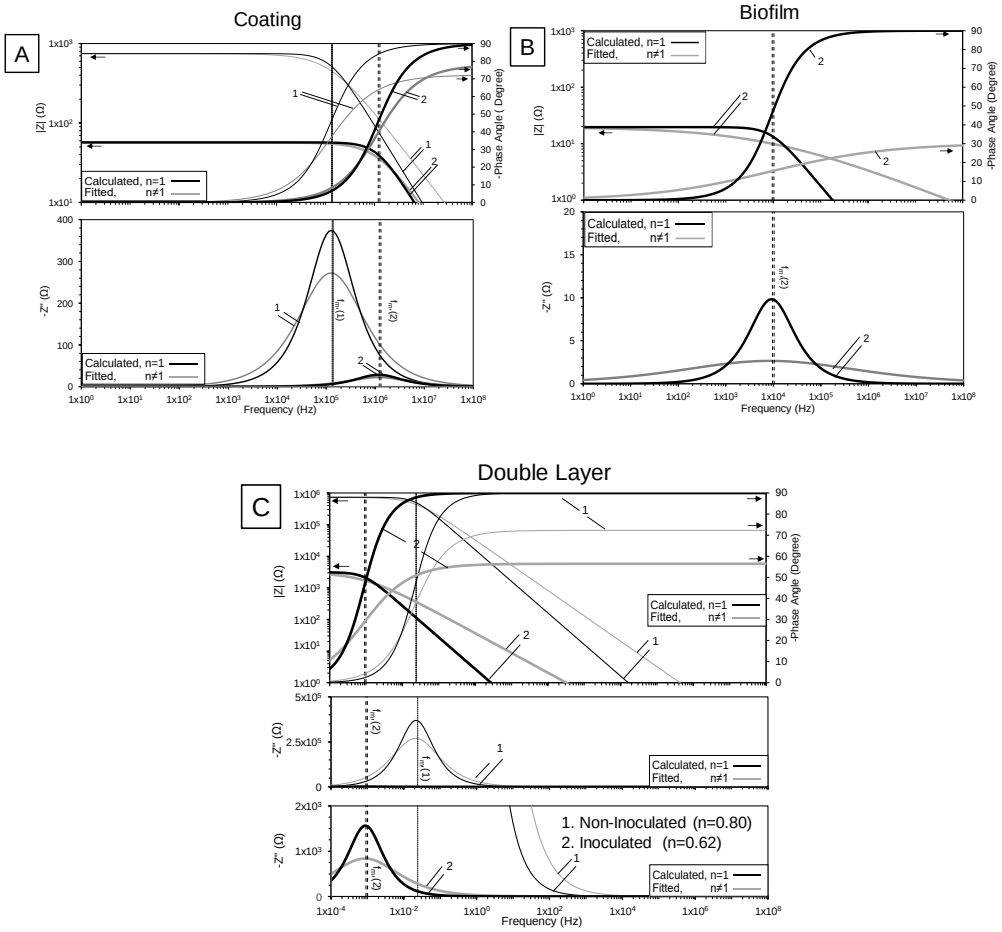

Figure 7.10. Example of decoupled fitted and calculated impedance response for antifouling non-inoculated (1) and inoculated (2) test specimens from impedance at day 4.

As shown in Figure 7.11, f_m for each time constant was shown to visually coincide with the breakpoint of capacitive and resistive behavior in the Bode plots as well as local maxima of $-Z''$, even for complicated impedance spectra with convoluted time constants. The calculation approach for capacitance and equivalent circuit fitting identified different and unique time constants (shown to be consistently proportional to $1/(2\pi f_m)$ as shown in Figure 7.12) apparently relating to the

various surface components described earlier. The calculation approach provided a useful means to compare admittances for the various time constants even when CPE n terms indicated non-ideal capacitive behavior (*n* as low as 0.3) such as for some cases of surface film development and the steel interface. Also, the effect of non-ideal current distribution due to coating degradation may be compared as well, especially to defects that may be induced by microbial activity as described later.

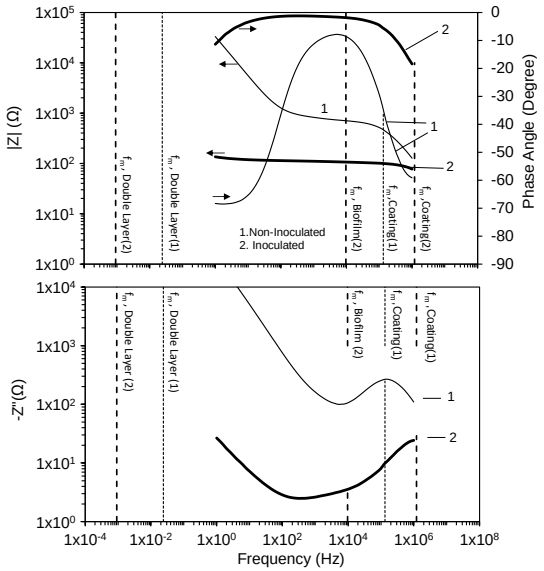

Figure 7.11. Bode and −Z" plots of measured impedance for antifouling non-inoculated (1) and inoculated (2) test specimens at day 4. 1 MHz > fm > 1 Hz.

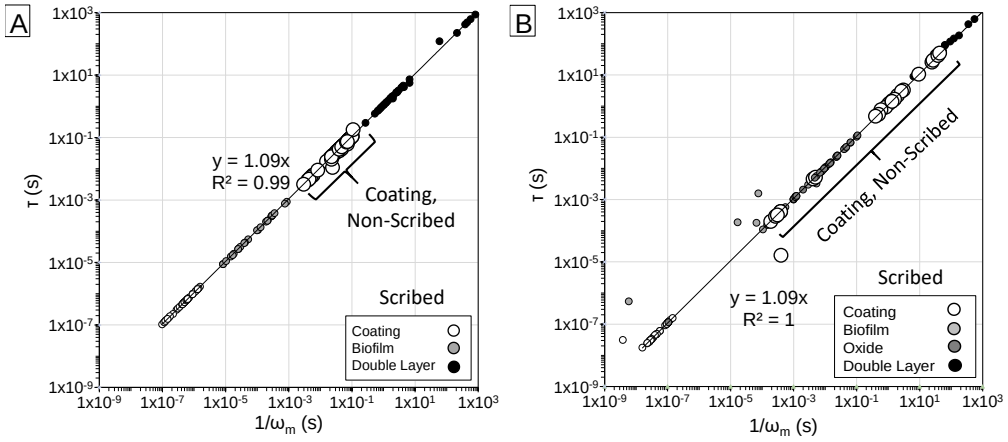

Figure 7.12. Correlation of τ from equivalent circuit fitting and ωm resolved from decoupled impedance. (A). Antifouling coating. (B). Polyurea coating

Figure 7.13 relates the impedance dispersion for antifouling- and polyurea-coated specimens with and without coating defects. τ values representative of the polymer coating was observed for the specimens without the intentional defect as expected, as impedance of the coating would dominate. On the other hand, distinct separation of time constants with characteristic behavior of polymeric coatings (at high frequencies) and the steel interface (low frequencies) as well as intermediate frequency dispersion was apparent for the specimens with coating defects. A separate time constant at an intermediate range (10^{-3} to 10^{-4} s^{-1}) only developed in test conditions inoculated with SRB indicating the effect of microbial activity such as biofilm development or possible non-uniform polarization due to the presence and activity of the microbes.

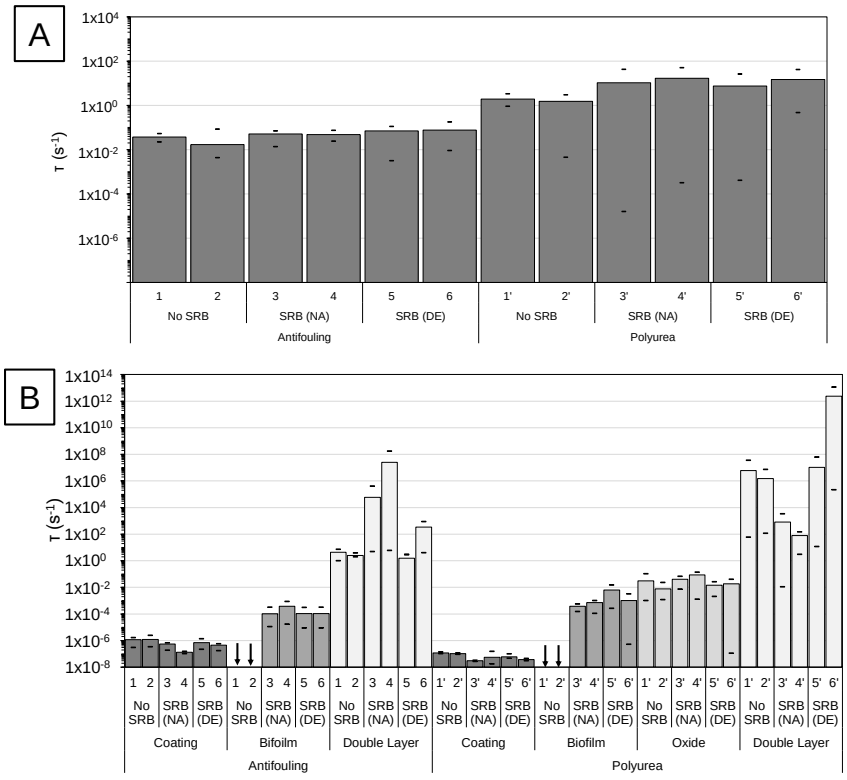

Figure 7.13. Dispersion of characteristic time constants for isolated impedance components. (A) Non-Scribed; (B) Scribed. Arrows indicate that no impedance response was associated with biofilm.

7.3.3.1. High-Frequency Impedance Behavior

As expected, the impedance of the polymeric coatings showed near ideal capacitive behavior. Coating capacitance can be described in terms of the material dielectric parameter (ε) as $C = \varepsilon\varepsilon_o A_s/d$, where ε_o is the permittivity of free space, A_s is the coating surface area, and d is the coating thickness. In the absence of coating defects, the impedance would show ideal capacitive behavior as shown in Figure 7.9A. A high-frequency impedance loop develops with the presence of small coating defects (with a lower high-frequency limit at $R_s + R_{po}$) as shown in Figure 2B–D. The impedance of antifouling and polyurea coating would in part ideally identify behavior characteristic of polymer dielectric capacitance and resistance.

As a first approach, the total impedance at 1 Hz was compared to identify general coating characteristics. As shown in Figure 7.14, the specimens coated with the antifouling coating with no exposed steel showed initially large impedance (~1 GΩ) that dropped after a few days (~1 MΩ). The polyurea coated specimens with no exposed steel also showed large impedances characteristic of a capacitor (exceeding 1 TΩ) throughout the testing regardless of SRB activity. Large impedance is indicative of barrier coating characteristics, and the decrease in impedance of the antifouling coating could be related to water absorption or possibly some form of coating degradation during the time of testing. In this vein, the total impedance for the antifouling and polyurea coating with intentional coating defects, as expected, showed lower values.

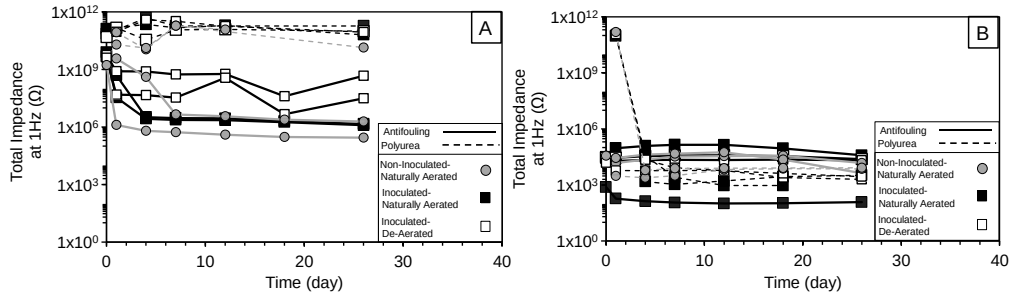

Figure 7.14. Total Impedance at 1 Hz and 1 MHz for laboratory coated samples. (A) Non-Scribed; (B) Scribed.

The impedance response was further assessed by consideration of the equivalent circuit analogs described earlier and the coating impedance components are shown in Figures 7.15 and 7.16. As was presented before, coating capacitive behavior was initially fit with a CPE even though the capacitive behavior was typically near ideal with resolved n terms consistently greater than 0.8. The calculated coating capacitance was in the order of 10^{-8} to10^{-10} Farad for both antifouling and polyurea coatings. The calculated coating dielectric constant for the antifouling ($d \approx 0.02$ cm) and polyurea ($d \approx 0.1$ cm) coating was in the order of 10–100 and <10, respectively, consistent for polymeric materials and polymeric coatings in saturated moisture conditions (Mansfeld1995).

Due to the dissimilarity in initial coating thickness between the antifouling and polyurea coating, R_{po} was normalized by the average d for each coating. The resolved nominal coating pore resistance for the antifouling and polyurea coating specimens without coating defects (10^7 to 10^{12} $\Omega \cdot cm^{-1}$) as expected were significantly higher than comparative samples with the coating scribe (10^3–10^5 $\Omega \cdot cm^{-1}$). The high nominal resistance (~10^8 $\Omega \cdot cm^{-1}$) resolved for the non-scribed antifouling-coated specimens related to initial coating imperfections, and the higher nominal resistance (~10^{12} $\Omega \cdot cm^{-1}$) for the polyurea coating indicated better surface conditions there. Fluctuations of the resolved R_{po} values for the polyurea specimens were due to noise in measurements at the large impedance values. SRB presence in testing of non-scribed specimens had not a major contribution on R_{po}, indicating generally good overall coating adhesion and barrier characteristics for both coating types.

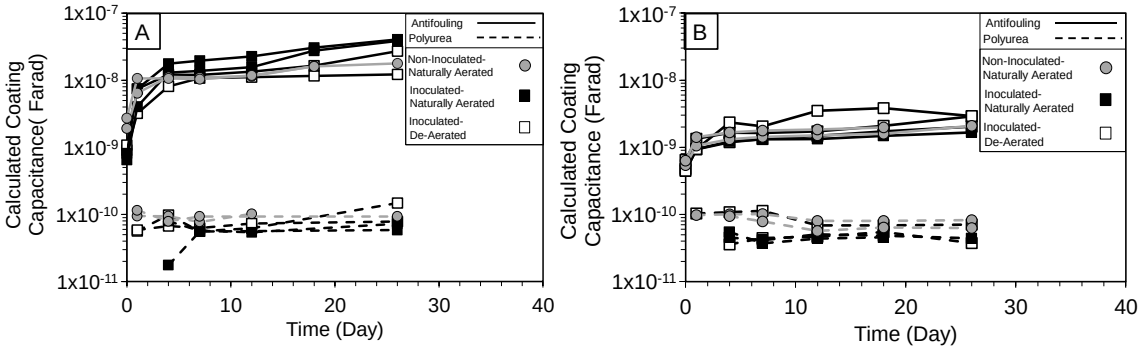

Figure 7.15. Calculated coating capacitance. (A) Non-scribed; (B) Scribed.

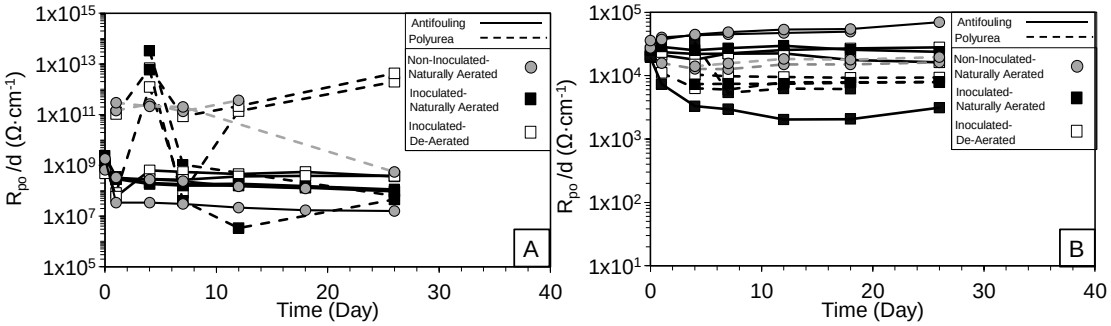

Figure 7.16. Resolved nominal coating pore resistance. (A) Non-scribed; (B) Scribed.

In contrast, for the scribed specimens, the nominal R_{po} for specimens immersed in inoculated solutions were lower than those in non-inoculated solutions. An antifouling-coated specimen inoculated with SRB that had greater sulfide production levels throughout the test period (Figure 7.6) and surface rusting, showed a significant drop in the nominal R_{po}, likely reflecting topcoat degradation due to biocide depletion and subsequent corrosion.

Nominal R_{po} for polyurea specimens (that showed tendency to disbond) also showed a decrease early in the exposure, especially in inoculated solutions. The drop was ascribed enhanced coating disbondment around the coating defect site that was exacerbated by microbial activity. The results indicated that microbial activity could create conditions that would promote coating degradation.

The general increase in coating capacitance for the antifouling coating and general trends in pore resistance was related to phenomena relating to the self-polishing characteristic of the coating. The increase in coating capacitance would relate to greater water presence in the coating after

immersion and to some extent reduction of the topcoat thickness especially in solutions with active SRB. As it will be detailed in section 7.3.5, there was a resulting 3%–20% decrease of the total coating thickness due to the topcoat self-polishing characteristics but that alone would not account for the 3–6 times increase in capacitance calculated by EIS. Water absorption during early exposure would account for the increase due to its higher dielectric constant. The drop in R_{po} would also in part relate to an increase in the effective pore solution conductivity as macropores in the coating become wetted.

Polyurea is a hard coating that does not exhibit characteristics of the antifouling coating. Near uniform coating capacitance and pore resistance was resolved throughout testing due to the good barrier characteristics of the bulk material in the non-scribed condition. Disbondment developed and moisture accessibility from the coating defect allowed larger steel exposure resulting in early decreases in R_{po}/d.

7.3.3.2. Intermediate Frequency and Biofilm Development

As described earlier, an intermediate frequency impedance loop ($10^{-4} < \tau < 10^{-3}$ s^{-1}) only developed for scribed specimens for both coating types immersed in inoculated solutions even at early times. This intermediate frequency impedance loop was associated with SRB activity whether it be bulk biofilm characteristics or the effects on current distribution through coating defects due to the bacteria. It was posited that the impedance loop characterized the electrical characteristics of biofilm that form within the coating defect sites. Resolved nominal biofilm capacitance is shown in Figure 7.17. With the assumption that the dielectric constant for biofilm is $\varepsilon \approx 70$ (Hoog et al., 2015) , the resolved capacitance for the antifouling and comparative polyurea coating (in the order 10^{-4} to 10^{-8} F) would result in a calculated film thickness $t < 10^{-4}$ mm (Liu et al., 2007).

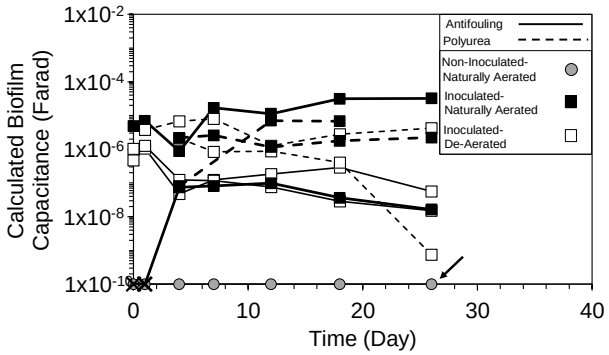

Figure 7.17. Calculated biofilm capacitance. Arrow indicates that no biofilm developed in the non-inoculated test conditions.

The biofilm-associated impedance was typically resolved at day 0 for the polyurea coating and after some days for the commercially available antifouling coating. The polyurea coating would not mitigate biofilm development within the coating defects but the antifouling coating should provide some mitigation due to the presence of biocides. The results did show indication of benefit provided by the biocides at early times. The initial bacteria activity in the laboratory testing was due to the localized inoculation. The calculated film capacitance generally decreased until day 12 for the polyurea coating and day 4 for the antifouling coating, consistent with initial film growth. The times coincided with prolonged SRB activity in the polyurea specimens and the early SRB activity in the antifouling specimens as indicated by the sulfide production levels as described earlier (Figure 11). Another intermediate frequency loop ($1 \times 10^{-2} < \tau < 1 \times 10^{-1}$) developed for polyurea coated samples regardless of inoculation and is discussed in the next section. Due to the self-polishing characteristics of the antifouling coating, it was evident that the biocide concentration in the topcoat can decrease and later reduce its efficacy to control microbe activity.

7.3.3.3. Low-Frequency Behavior

The impedance of other surface reaction components including surface and steel interfacial layers typically have non-ideal capacitive behavior. Steel interfacial impedance, Z_{Steel}, relating to the double layer capacitance and charge transfer resistance (represented by parallel combinations

as in the Randles circuit) would develop with electrolytic contact. Z_{Steel} may also incorporate extended reactive surfaces related to porous surface oxides or surfaces under crevices. Resolved impedance parameters are shown in Figure 7.18. In general, the resolved steel interfacial capacitance was in the order of 10^{-3} to 10^{-7} F (10^{-1} to 10^{-5} F/cm^2). The antifouling-coated specimen in naturally aerated inoculated solution with discrepant impedance results described earlier, likewise showed diverging trends and higher nominal interfacial capacitance (~1 F). Consistent with earlier discussion, greater coating degradation in the specimen would allow larger exposed steel area and account the trend to higher capacitance. The polarization resistance resolved by EIS resulted in corrosion currents in the order of ~0.026 and ~0.0026 μA/cm^2 for antifouling and polyurea, respectively, given $i_{corr} = B/R_p$ where B was assumed to be 26 mV. The resolved polarization resistance was generally consistent with values obtained by linear polarization resistance measurements described in previous works (Permeh et al., 2019a).

The impedance associated with the oxide layer observed for scribed polyurea samples was attributed to undercoating corrosion that developed due to the disbondment of the polyurea coating and electrolytic interaction from the coating defect opening. Visual observations of a black surface layer that reddened after sample autopsy indicated corrosion oxide products that remained under the coating during testing.

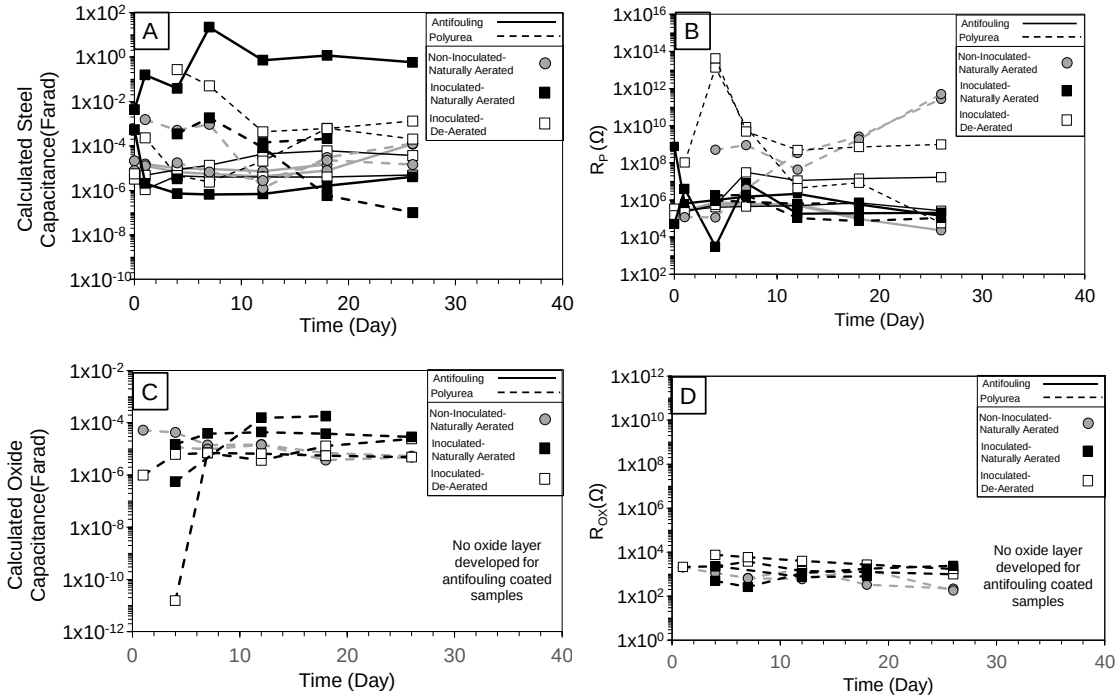

Figure 7.18. Calculated interface capacitance and resolved interface resistance. (A) Double layer capacitance. (B) Polarization resistance. (C) Oxide layer capacitance. (D) Oxide layer resistance.

7.3.4. Visual Observation and Surface Analysis

Figure 7.19 shows the surface appearance of the test specimens immediately after testing. The steel coupons coated with the antifouling coating placed in non-inoculated solutions did not exhibit strong visual indicators of coating degradation (even though coating material could be easily rubbed off by hand) regardless of the presence of the initial coating defect. The surface retained color and no differentiation in surface texture was readily apparent. In contrast, samples exposed to inoculated solutions where SRB activity was high, showed distinct discoloration and some flaking of the topcoat similar to the topcoat degradation observed in the field. The visual observations would be consistent with the indicators that the concentration of antifouling agents within the topcoat may be reduced and would subsequently allow for the higher levels of SRB development. The concentration of antifouling agents on the surface of the topcoat may not be effective for long-term mitigation in aggressive environments where there are strong SRB

concentrations. It was evident that degradation of the topcoat and loss of antifouling performance would allow subsequent enhanced SRB development.

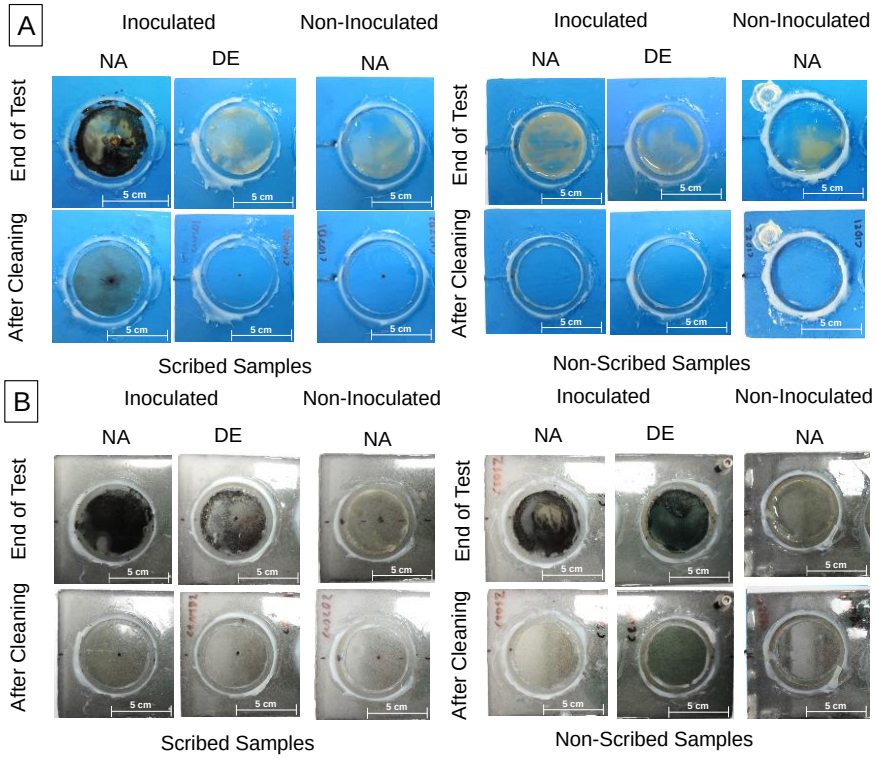

Figure 7.19. Surface condition of coated laboratory specimens after testing.
A. Antifouling Coated samples, B. Polyurea Coated Samples
NA: Naturally Aerated Condition, DE: De-aerated Condition.

There were no strong visual indicators of surface degradation of the bulk polyurea coating during the test exposure. For the defect-free samples, the coating retained its smooth surface texture even under deposited precipitates of iron sulfide for the specimens in inoculated solutions. For the samples with the coating defect, the surface finish was likewise not affected and there was not strong visual indication of bulk coating degradation. However, some level of coating disbondment could be seen circumferentially around the defect site as discussed earlier.

Cross-sections of the steel specimens coated with the anti-fouling coating showed the various layers including the primer, tie-coat, and the topcoat (Figure 7.20). The cross-section of specimens

exposed in solution revealed that significant reduction in topcoat thickness can occur; but for each test case, the thicker tie-coat bulk material remained mostly intact during testing. As such, the degradation of the thinner topcoat (that contained the anti-bacteria and anti-fouling compounds) was not well differentiated by measurements of the total coating thickness. The total coating thickness after topcoat degradation decreased at least 3-20% and the decrease in total coating thickness would correspond to ~1-1.25 increase in coating capacitance. However, the values were not commensurate with the >3 times increase in resolved coating capacitance measured by EIS. Instead, the increase in capacitance was in part be attributed to water absorption as earlier discussed (Mansfeld, 1995), especially since the increase occurred within 2 days of expos6re to solution. Similar considerations for Rpo would be consistent with the trends described earlier if water penetration can account for a decrease in pore resistivity.

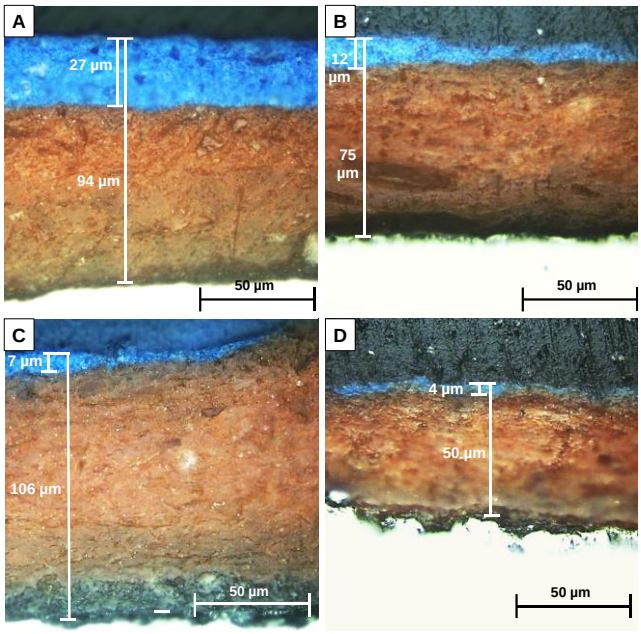

Figure 7.20. Representative metallographic cross-section of antifouling coated samples. As-cured, B. Non-inoculated- Naturally aerated, C. Inoculated- Naturally aerated, D. Inoculated-De-aerated.

X-ray diffraction made on the surface of the as-received and tested steel coupon specimens identified zinc oxide, titanium oxide, and barium sulfate in all specimens regardless of exposure (Figure 7.21). The results could not elucidate the extent of pigment loss during exposure as surface degradation occurred. Other antimicrobial and antifouling compounds that have amorphous structures could not be identified by XRD and deviations in its content may be possible. In the end, the topcoat that contained the anti-bacteria and anti-fouling compounds can degrade in time due to the self-polishing characteristic of the coating system. Consequently, bacteria such as SRB can proliferate. Biofilm can develop and can accommodate subsequent settlement of marine fouling organisms if the anti-fouling agents too are reduced.

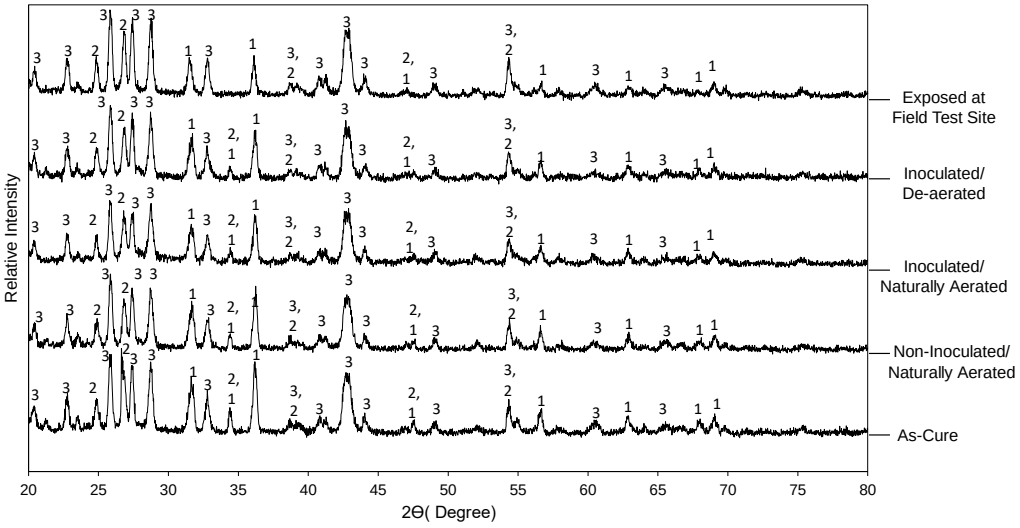

Figure 7.21. XRD diffractograms for anti-fouling coated specimens.
1.Zinc Oxide, 2. Titanium Oxide ,3. Barium Sulfate.

7.4. Results and Discussion for Field Testing

7.4.1. Surface Fouling Condition

Examination of the plain steel samples used (Figure 5.15), showed heavy accumulation of marine fauna for sites I, II, and III indicating that all three test sites are in aggressive environments in terms of barnacle growth. Barnacle growth varied in size and accumulation by immersion depth.

The results of visual observations from the polyurea and anti-fouling coated samples and general comparison to fouling on steel samples are described below (Figure 7.22 and Figure 7.23).

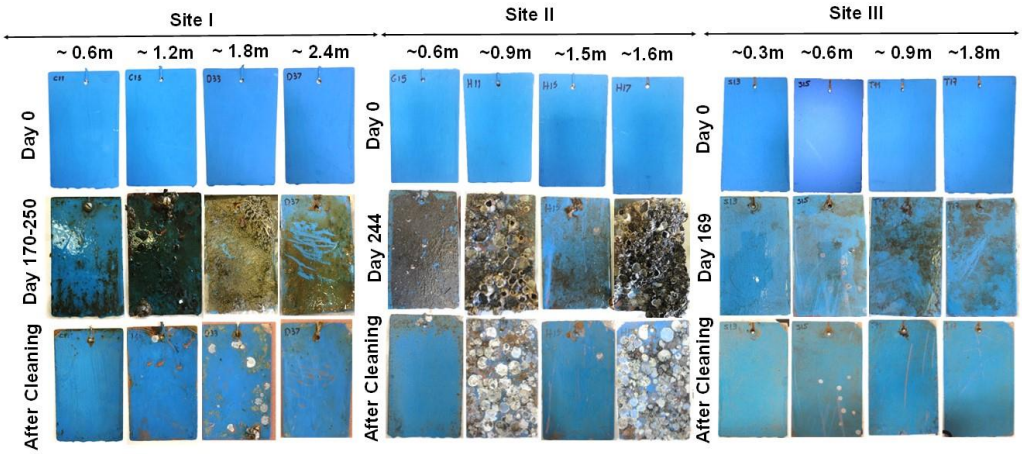

Figure 7.22. Surface appearance of field-exposed antifouling-coated coupons

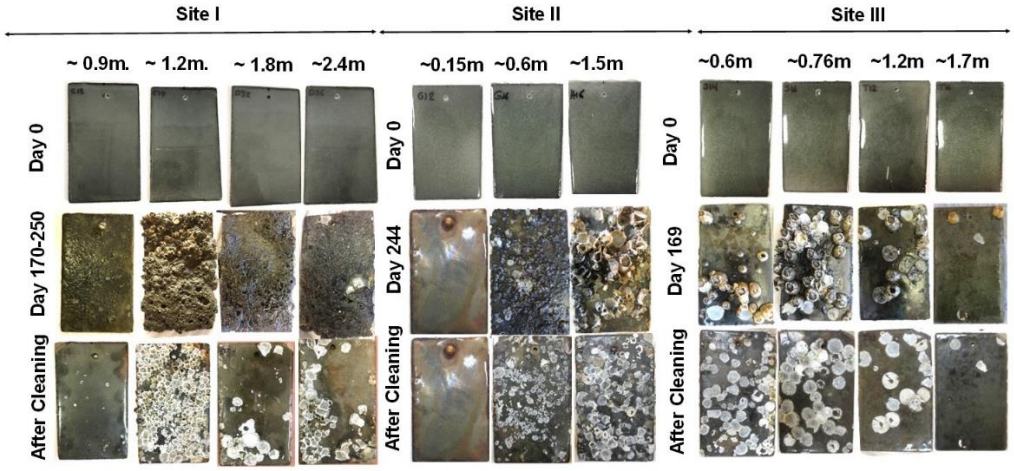

Figure 7.23. Surface appearance of field-exposed polyurea-coated coupons

7.4.1.1. Site I. Matanzas River

Anti-Fouling Coating: Figure 7.22 presents the surface appearance of the water-based copper-free antifouling coating in the initial condition, after field exposure, and after removal of marine growth for comparison. Also, early results after day 60 are provided as reference. As described in (Permeh et al., 2019a), by day 60, coating components (presumed to be topcoat)

degraded, but the anti-fouling coating continued to suppress settlement of fouling organisms. The observation of early coating degradation and surface marine fauna development would indicate that the anti-fouling characteristics of the coating became less effective. The disparity of barnacle growth between the time of retrieval of samples at day 170 and 250, respectively, was thought to be due to the further degradation of the anti-fouling coating and not the difference in depths between the two test sets. In any case, there was less barnacle growth on the anti-fouling coated steel samples than the comparative plain steel and polyurea coated steel samples.

Polyurea Coating: For samples with as-received surface condition, a variety of marine flora and fauna developed on the surface of all samples 0.6m-2.4m below marine growth (BMG) within a month of field exposure and the surface was covered with marine foulers by day 60. As shown in Figure 7.23, clustered formation of barnacles developed in the tidal region (0m-1.5m. BMG) but soft marine masses populated with sedentary fauna developed at >1.2m. BMG. There was differentiation of remnant barnacle plates sizes and population on the sample surface by depth. These observations were consistent with fouling on the plain steel samples. The difference in barnacle size and accumulation for both steel and polyurea coated samples were thought to be related to nutrient availability from the river flow and tidal levels.

7.4.1.2. Site II. Downstream Alafia River

Anti-Fouling Coating: Figure 7.22 shows the surface appearance of steel coupons with the anti-fouling coating in the as-coated condition, after 244 days in marine exposure, and after hand cleaning. It was apparent that the marine fouling could develop on the coating. The level of barnacle formation was heavier at Site II than Site I even though barnacles greatly proliferate at both sites. Coating application on the steel plates for all sites were made from the same batch of steel plates and coating materials and coating application was done together. The difference in fouling may be related to fouling organism types. Whereas Site I generally could accommodate growth of tunicates, hydroids, acorn barnacles, sponges, mussels, and other marine fauna, Site II had predominantly bay

barnacles. It was evident that the antifouling agents in the coating were not effective on the rate of proliferation of the barnacle specie in the saline environments at Site II.

Polyurea Coating: Figure 7.23 shows the surface appearance of coated steel coupons from Site II in the as-coated condition, after 244 days of exposure, and after hand cleaning. Clustered interlayers of bay barnacles formed at depth > 0.6m BMG and had with larger basal plate diameter at larger depths, similar to that observed on plain steel samples from parallel testing (chapter 5).

7.4.1.3. Site III. Upstream Alafia River

Anti-Fouling Coating: As mentioned above, the general activity of bay barnacles in upstream river locations was lower than downstream locations; but as described before, the barnacles can still accumulate to heavy levels. The application of the anti-fouling coating did appear to substantially reduce barnacle settlement as observed in Figure 7.22, where only a few spots with the initial growth of the barnacle shell was observed. In the upstream location, lower barnacle populations could be expected in the fresh water where less nutrients are available. This would provide lower fouling tendency where anti-fouling agent concentrations (such as Zn and Ti oxides) would remain at effective levels for longer service times. In such conditions, the anti-fouling coating may be effective for prolonged periods.

Polyurea Coating: Figure 7.23 shows the surface appearance of coated steel coupons in the as-coated condition, after 169 days of exposure, and after hand cleaning. Bay barnacles could develop on steel surfaces in upstream river locations where the salinity was lower than the downstream test site, even though the extent of barnacle growth was not as aggressive as in the latter. These trends were similar with the presence of the polyurea coating, indicating that the coating could not mitigate the settlement of barnacle larvae. The visual appearance showed somewhat lower level of barnacle settlement for the coatings with roughened surfaces, but this may be due to the generally lower levels of barnacle proliferation in the fresh water, at depths below 1.5m.

7.4.2. Microbiological Analysis

The results of BART tests on the coated steel samples from all three sites are shown in Figure 6.13. The largest measured population of SRB, IRB, APB, and SFB under marine growth layers are shown. The SRB population measured on the polyurea coated test plates showed variability but the testing indicated that large SRB populations at levels indicative of aggressive environments can develop at site I and II. Lower levels (non-aggressive) was observed at site III. For the antifouling coating, SRB populations were categorized as non-aggressive to moderately aggressive at all three test sites. At site III, the lower SRB populations that were measured regardless of coating application, can in part reflect the lower density of marine foulers there in comparison to the more nutrient rich waters at sites I and II. At all three test sites, IRB, APB and SFB maintained high populations for both the polyurea-coated and the antifouling-coated steel (generally categorized as aggressive). Generally, for surfaces without the effect of biocides such as plain steel and polyurea coated steel, presence of large surface bacteria populations coincided with the settlement of fouling organisms and subsequent heavy surface fouling. It was also observed that the anti-fouling coating had differential effects on various bacteria species (incidentally, negligible population of SRB).

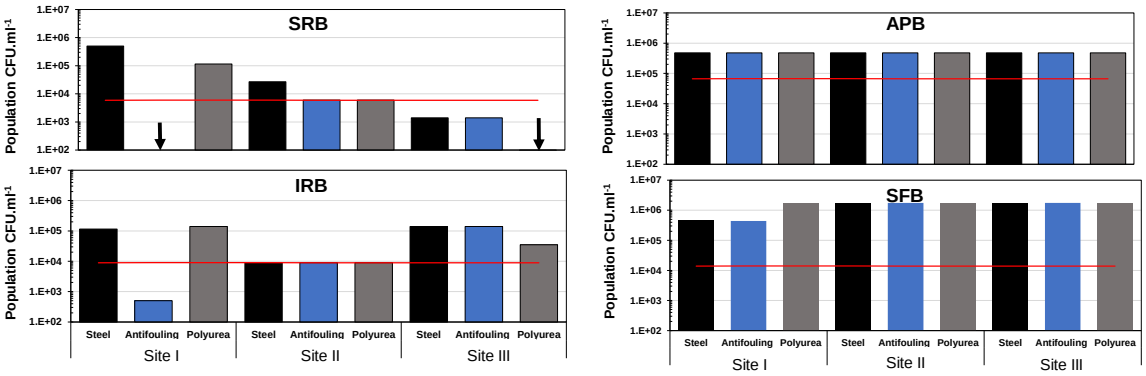

Figure 7.24. Surface Bacteria Population (CFU.mL-1) after Outdoor Exposure at Three Sites. (Red Line shows aggressivity limit for each bacteria)

7.4.3. Corrosion development

7.4.3.1. OCP

The combined results of OCP for the polyurea- and antifouling-coated samples for the three test sites are shown in Figure 7.25. In general, the corrosion potential at all three sites were in the range of -700 <E < -600 mV_{SCE}. There were some samples at site III with more noble potentials, but those values were associated with samples that were in the tidal region where a thick oxide developed. Complementary control as-received polyurea and anti-fouling coating samples that were conditioned in river water for 30 days showed more noble potentials and was likely reflective of the barrier characteristics of the coating. Even though environmental conditions of the field collected test solution (e.g., aeration levels) are likely to be different, the measured potentials of the field extracted coated samples showed electronegative potentials within the range of potentials for plain steel samples measured in the field. This may reflect sufficient coating degradation on the field exposed samples where the electrochemical reactions at the steel surface may become important.

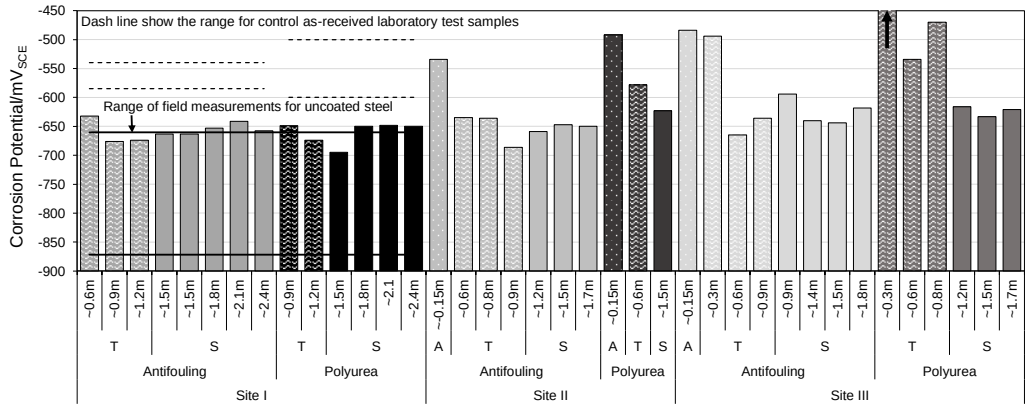

Figure 7.25. Corrosion potential of field-exposed coated steel coupons at three sites, A: Atmospheric, T: Tidal, S: Submerged

7.4.3.2. LPR

Generally high corrosion currents were measured for the polyurea coated steel samples, in the order of 100 µA in sites I and II and 10 µA in site III (Figure 7.26). Although high, these values were lower than that of comparative plain steel samples (section 5.3.2) (Permeh et al., 2019a). Nevertheless, the results (consistent with the measured OCP) indicated that there was significant degradation of the polyurea coating. This was likely due to degradation of the polyurea coating where the multiple and thick applied layers of polyurea may in part account for non-representative and non-ideal conditions that can lead to premature coating failure.

The corrosion currents for these coated samples throughout the test exposure (up to 250 days) were much smaller than the plain steel samples and lower than that of the polyurea coated samples, indicating beneficial effect of the coating. As indicated above, the level of fouling was small at site III and sometimes significant at sites I and II. The corrosion currents coincidently were significantly smaller at site II (and much reduced in comparison to control plain steel samples) which gave indication that marine foulers can have effect on coating degradation. Indeed, at site III, the corrosion current was somewhat higher where some minor fouling did occur. At sites I and II, the largest corrosion currents were measured for those samples where barnacles were present. It was posed that the topcoat of the antifouling coating system can degrade with time especially in environments that heavily promote proliferation of marine fouling organisms. The degradation and reduced concentration of antifouling agents would then allow settlement of the biofoulers.

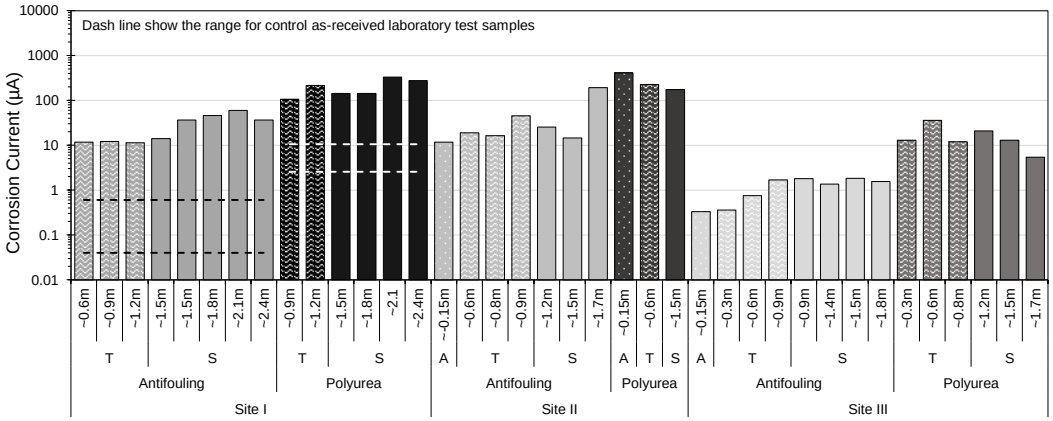

Figure 7.26. Corrosion Current Density of Polyurea-coated Steel Coupons at Three Sites. A: Atmospheric, T: Tidal, S: Submerged

7.4.3.3 EIS

To verify coating degradation, EIS measurements were made for the coated samples. The results from EIS in Nyquist plots generally showed double loops, which can be associated not only with dielectric characteristics of the coating but also metal/solution interfacial behavior. As a first approach to assess coating quality, the total impedance magnitudes taken at 1 Hz were compared (Figure 7.27). The reference control as-cured coating samples had high impedance values (1 to 3 orders of magnitude larger than the exposed samples). Total Z at 1Hz were low (<500 ohm) for polyurea and anti-fouling coatings indicated coating degradation and poor barrier coating characteristics but were significantly lower for the polyurea-coated samples. There, the polyurea samples had values as low as ~10 ohms, consistent with the high corrosion currents. The antifouling coating had low total impedance consistent with the relatively high corrosion current and observations of physical topcoat degradation and development of surface fouling.

Site III samples showed high frequency larger loops in the Nyquist representation of impedance. On first principles, the impedance could be in part idealized as a coating pore resistance for a degraded coating. The impedance at all three sites for both coatings exhibit this characteristic, further implicating coating degradation. The lower conductivity of the river water at site III than

sites I and II would then in part result in higher pore resistance and exhibit the larger high frequency loop. For the antifouling coating, differentiation in electrical characteristics of the coating resulting from biofouling may be identified. Indeed, locations in sites II and III where significant biofouling developed, the high frequency impedance loop was smaller than comparative exposed and control samples without development of biofouling (Permeh et al., 2019a). Further analysis in next section was applied for antifouling coating to identify extent of biofouling degradation.

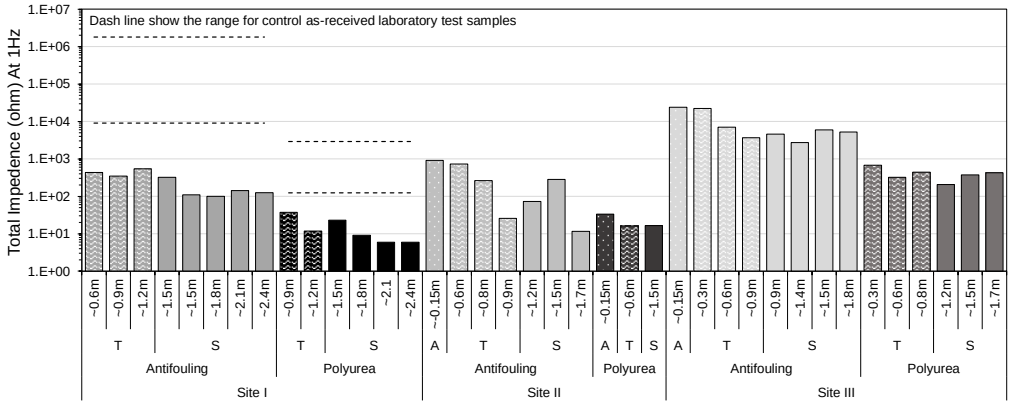

Figure 7.27. Total Impedance at 1Hz for Polyurea-coated Steel Coupons at Three Sites.

7.4.4. Electrochemical impedance response analysis for antifouling coated coupons

Representative results of EIS testing of the antifouling coated specimens (presented in Nyquist diagrams) from the general test depths (tidal and submerged regions) for the three test sites are shown in Figure 7.28. The results generally showed multiple impedance loops associated with the various time constants for the different system components. The presence of the multiple time constants indicated that the coatings, after field exposure, did not have strong barrier characteristics, in contrast to the large impedance (characteristic of a capacitor) of the control undamaged coating freshly immersed in solution. The impedance at the intermediate frequencies showed varying extents of impedance dispersion by a distribution of time constants due to surface heterogeneities (that can be associated with the dielectric behavior of the surface layers). As described by Permeh

et al., 2019b, that dispersion was observed in lab testing in the presence of the sessile bacteria and not in control non-inoculated tests. It was posited that the presence of biofilm (likely heterogenous in coverage and makeup) create conditions for the impedance dispersion there. In the field specimens, that surface heterogeneity can be attributed to a variety of additional reasons including the sporadic macrofouling and the coating degradation that occurred during the exposure period.

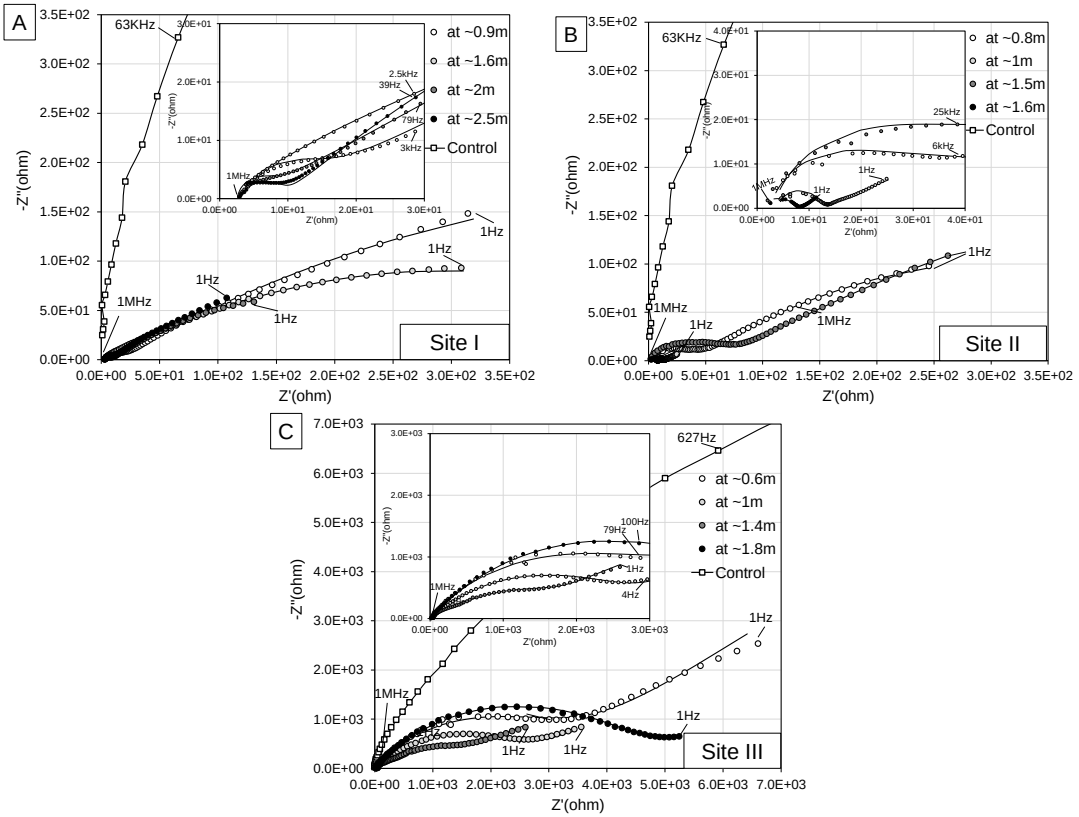

Figure 7.28. Nyquist diagrams from EIS for antifouling-coated coupons at three sites. 1MHz<f<1Hz, 10 points/decade. Lines show fitted curves. (A) Site I, (B) Site II, (C) Site III.

Variants of the circuit analog, including that proposed by Abdoli et al., 2016, for biofilm on an aluminum coated steel metal surface (Figure 7.29a.), did not consistently yield good data fitting for the measured impedance spectrum of the field-exposed coated steel specimens. Treatment of the intermediate frequency dispersion by a parallel R and C elements (Figure 7.29b), such as that presented by Chen et al., 2017 was considered here but with the resolved terms nominally ascribed to an apparent heterogeneous surface film for discourse. As such, the

impedance of the antifouling coating that have coating surface heterogeneity (degradation and formation of surface deposits) was posited to be characterized by the equivalent circuit analog shown in Figure 7.29c and described by Equation 7.2 as a function of angular frequency ω. The circuit analog characterizes an idealized degraded coating with a coating pore resistance, the dispersion relating to the surface heterogeneities, and the impedance of the double-layer capacitance and polarization resistance for the exposed steel interfaces.

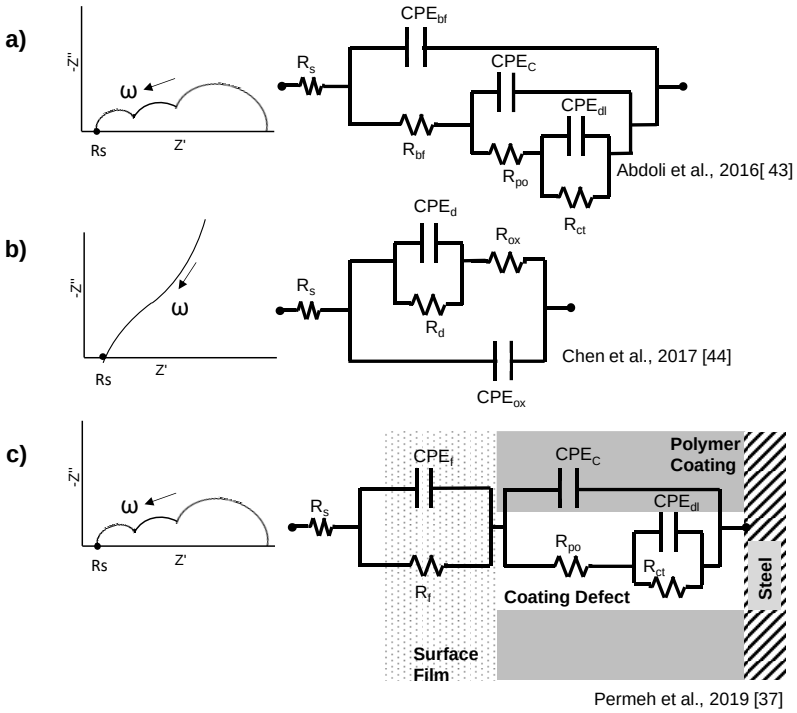

Figure 7.29. Electrochemical impedance equivalent circuit analogs. a)Circuit analog proposed by Abdoli et al., 2016 for biofilm on an aluminum coated steel metal surface , b) Circuit analog proposed by Chen et al., 2017 for an apparent heterogeneous surface film, c) Circuit analog proposed by Permeh et al., 2019a for biofilm on antifouling coated steel metal surface

Constant phase elements, CPE, with pre-exponential admittance *Yo* and *n* terms were used to provide a mathematical expression for impedance that exhibit capacitive-like behavior including the dielectric behavior of the coating (subscript *C*), the surface film (subscript *f*), as well as the double-layer capacitance (subscript *dl*) at the steel interface. The impedance of a CPE is given as $Z_{CPE}=1/Y_o(j\omega)^n$. Resistance terms *R* relate to the bulk solution resistance (R_s), coating pore

resistance (R_{po}), surface film resistance (R_f) and the polarization resistance (R_p) of the steel interface.

$$Z(\omega) = R_s + \left(\frac{1}{Y_{o_f}(j\omega)^{n_f} + \frac{1}{R_f}} \right) + \left(\frac{1}{Y_{o_C}(j\omega)^{n_C} + \left(\frac{1}{R_{po} + \left(\frac{1}{Y_{o_{dl}}(j\omega)^{n_{dl}} + \frac{1}{R_p}} \right)} \right)} \right) \tag{7.2}$$

$$C = Y_o \cdot (2\pi f_m)^{n-1} \tag{7.3}$$

Generally, good curve fitting of the EIS data to the impedance described by the equivalent circuit analog was made. Table A2 in the appendix, shows the resolved impedance parameters from equivalent circuit fitting, resolved f_m, and calculated nominal capacitances for all test specimens at different depth at three sites. Following the approach by Permeh et al., 2019b, the impedance for each fitted *R-CPE* pair was decoupled with analysis of each parallel *R-CPE* circuit independently. The treatment of the EIS data was used to parse the general behavior and other complicating factors relating to non-uniform current distribution on degraded coatings and non-homogeneous surface films. An example of this approach for coated coupons from Site I is shown in Figure 7.30. The capacitance for each CPE term was estimated following approaches developed by Hsu and Mansfeld, 2001 using Equation 7.3, where f_m is the frequency of the maximum imaginary component of impedance. As shown in Figure 7.31, the resolved f_m for each time constant was shown to visually coincide with the breakpoint of capacitive and resistive behavior in the Bode plots as well as local maxima of $-Z''$, even for the complicated total impedance spectra with convoluted time constants.

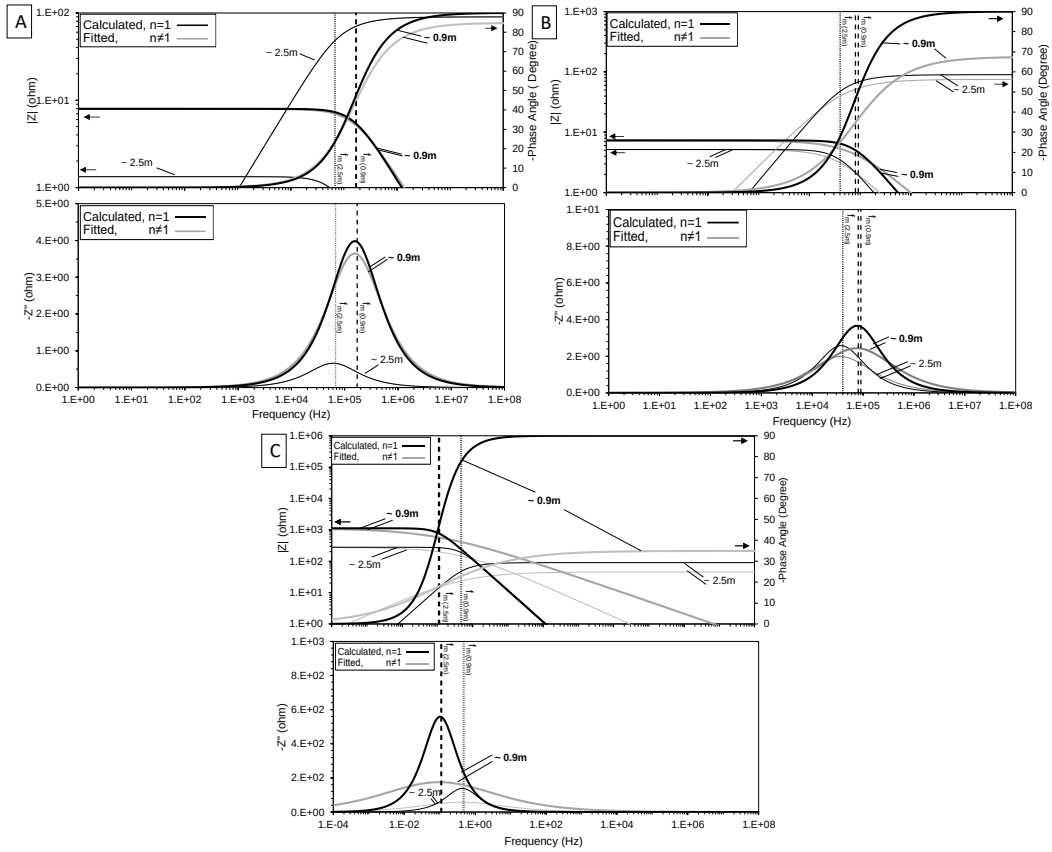

Figure 7.30. Example of decoupled fitted and calculated impedance response for coated coupon exposed at Site I at 0.9m and 2.5m. (A) Coatings; (B) Surface Film; (C) Double Layer.

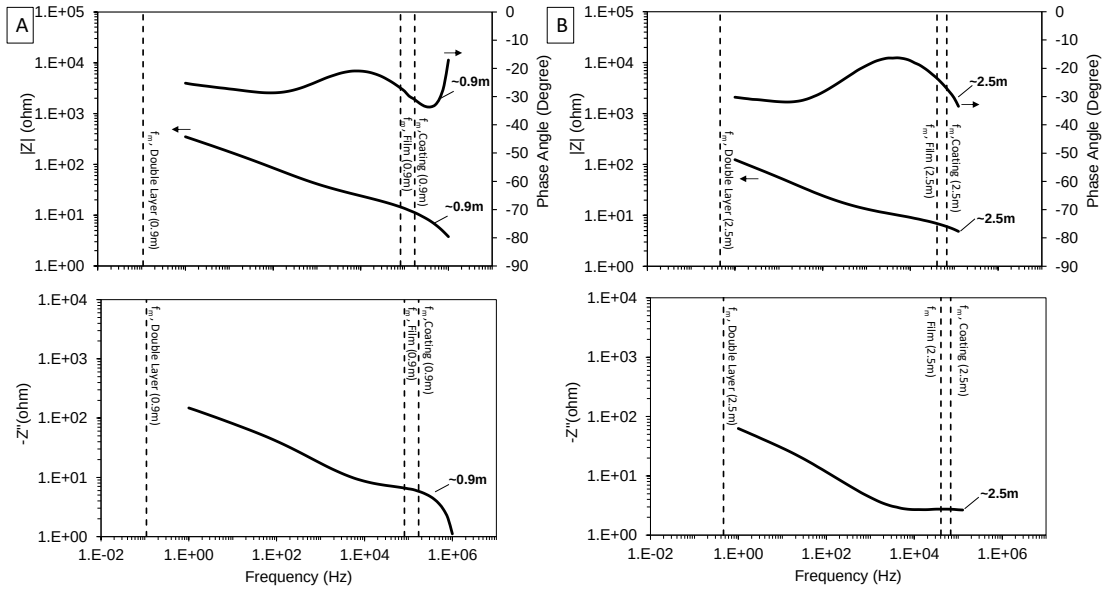

Figure 7.31. Bode and −Z" plots of measured impedance for f coated coupon exposed at Site I at (A) 0.9m and (B) 2.5m .

Based on the resolved impedance terms from the equivalent circuit fitting and the numerical treatment described above and detailed before, separation of impedance time constants ($\tau = 1/RC$) representative of the various system processes was evident as shown in Figure 7.32. Similar to the resolved τ values described for the coating, the steel interface, and the surface films that developed in bacteria inoculated solutions in laboratory testing in reference (Permeh et al, 2019b) , low τ values for the coating, high values for the steel interface, and intermediate values for the apparent surface film were resolved for the test specimens exposed in the three field test sites. Similar τ values were also resolved for the control as-received coated specimen. The results showed impedance that would relate to heterogeneous surface film formation at Sites I and II. The impedance results on only one of the specimens from Site III showed a similar indication.

Comparisons of the resolved impedance components, fit using Equation 7.2. and 7.3, are shown in Figure 7.33. The calculated coating capacitance for all three test sites was similar and in the range of $1x10^{-8}$ and $1x10^{-7}$ F (Figure 7.33A). The capacitance of the coating is characterized by $C_C=\varepsilon\varepsilon_o A/d$. Assuming the submerged steel area, A, the average original coating thickness, d, and the dielectric of free space $\varepsilon_o=8.8x10^{-12}$ F/m, the apparent coating dielectric ε would be in the order of 10-100, consistent to that of wet polymeric coatings (Mansfeld, 1995). The resolved ε, assuming the initial d, sometimes exceeded 100 for some of the permanently submerged specimens. This was in part due to the fact that those specimens had greater coating degradation and reduction of the coating thickness. The calculated coating capacitance for the coatings after field exposure (particularly for the continuously submerged specimens) was consistently larger than that resolved for the control lab specimens attesting to that coating degradation and the increased moisture presence after prolonged immersion in the river water.

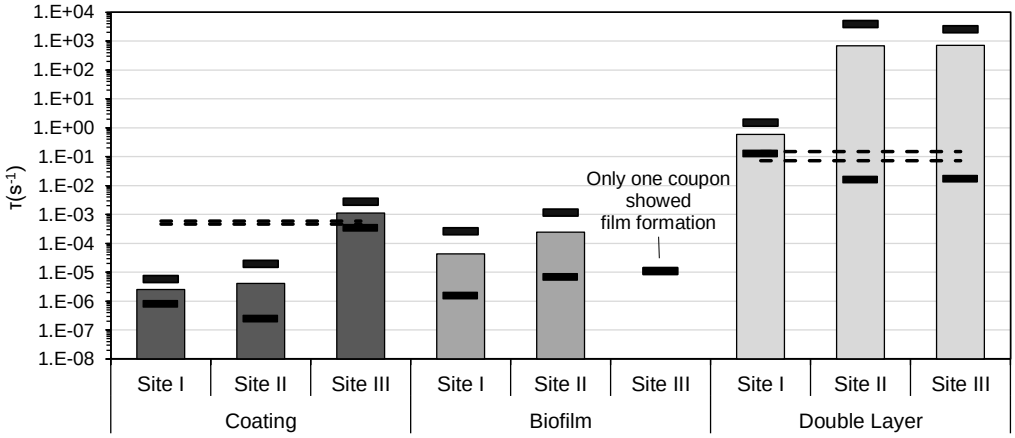

Figure 7.32. Resolved time constants for separate impedance components. (Dash lines show the range for control as-received laboratory samples).

The resolved coating pore resistance (in the order of 1 to 10^2 ohm) for the specimens at Sites I and II (Figure 7.33B) was lower than that of the control lab specimens (~10^4 ohm) consistent to wetting of the coating pore spaces and general coating degradation. The resolved pore resistance for the specimens at Site III was higher, in the order of 10^3 ohm, corroborating with earlier observations of more benign fouling environments there and better coating conditions (ie less depletion of the biocides and topcoat degradation). The resolved pore resistance of test specimens in the submerged region was consistently lower than that for the intermittently immersed specimen at all three test sites for similar reasons of prolonged wetting and more aggressive fouling in the former.

The capacitive and resistive impedance parameters for the apparent surface film were resolved for the test specimens in the submerged regions at the test sites (Figure 7.33C and 7.33D). As previously introduced, the impedance dispersion that manifests as these characteristic capacitive and resistive parameters (Chen et al., 2017) are due to surface heterogeneities that can form due to a multitude of reasons. The sporadic placement of hard shelled foulers and the coating degradation (especially at Sites I and II) would have an effect as well. The lower resolved capacitance for the specimens at Site I than Site II could be indicative of a thicker surface layer within the range as

reported elsewhere (Liu et al., 2007). If that surface layer can be attributed to uniform coverage of biofilm and assuming a dielectric coefficient of 70 (Hoog et al., 2015), the film thickness would be in the order less than 10^{-4} mm, comparable to biofilm thickness reported elsewhere (Liu et al., 2007). The impedance associated with a surface film was not consistently resolved for all specimens at Site III, attributing to the better coating condition in the more benign exposure environment there to mitigate both micro- and macrofouling.

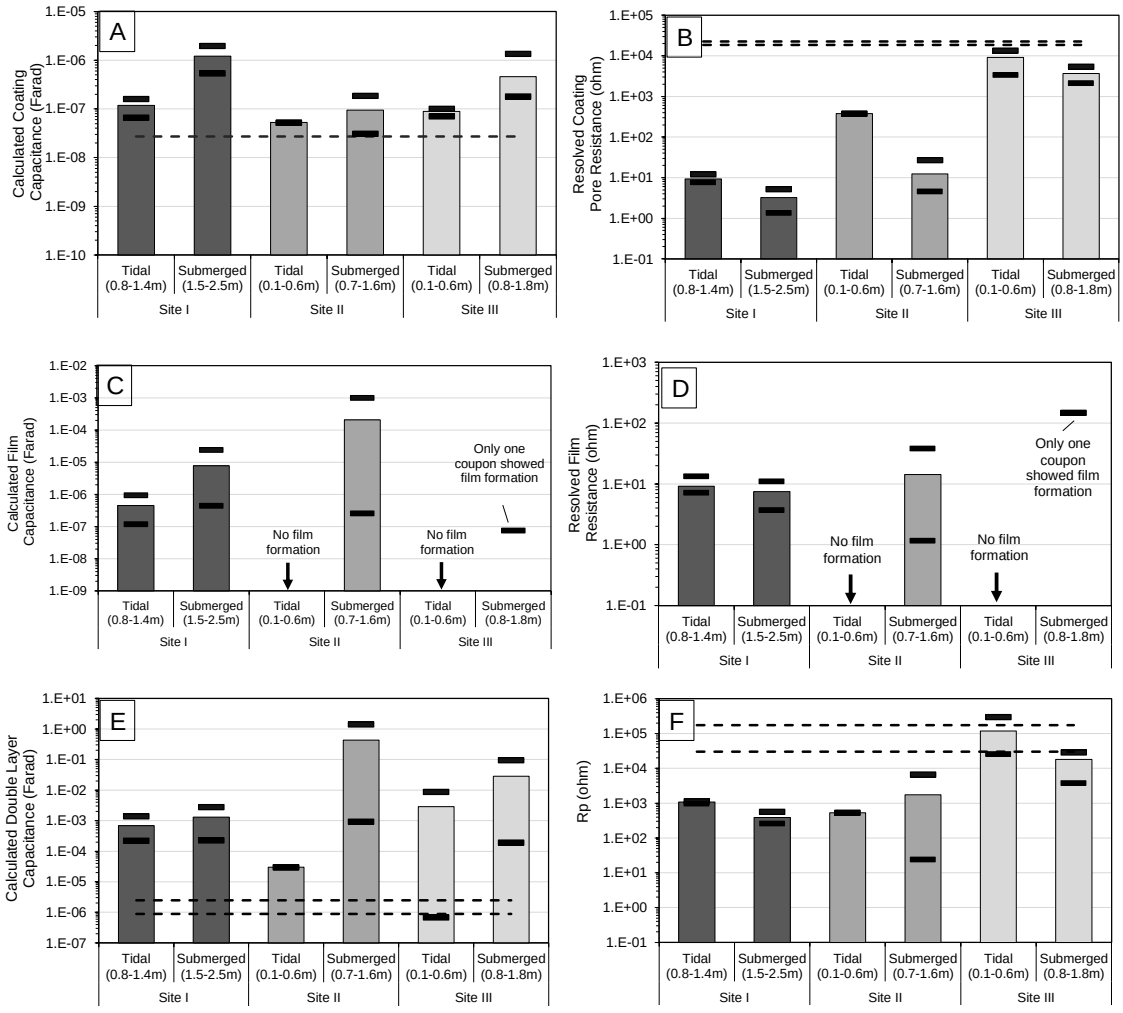

Figure 7.33. Resolved coating, biofilm and steel interface impedance parameters. A: Calculated coating capacitance, B: Resolved coating pore resistance, C: Calculated surface film capacitance, D: Resolved surface film resistance, E: Calculated double-layer capacitance, F: Resolved polarization resistance. (Dash lines show the range for control as-received laboratory samples).

The resolved polarization resistance for the specimens at Site III was generally two magnitudes of order larger than specimens at Sites I and II (and similar to the control lab specimens), in general agreement with earlier observations of less coating damage in the former and thus better barrier characteristics during the time of testing (Fig. 6F). The polarization resistance of the coatings in Site I and II were in the order of 10^2 to 10^3 ohm corresponding to a corrosion current, I_{corr}, in the order of 10-10^2 µA, following the relationship $I_{corr}=B/R_p$ where the Stern-Geary coefficient, *B*, was assumed to be 26-54 mV/decade . In comparison, the polarization resistance was in the order of 10^4-10^5 ohm for the Site III and control lab specimens, corresponding to a corrosion current in the order of 10^{-1}-1 µA. Uniform corrosion is not expected to develop with the presence of the polymer coating, but the steel corrosion would develop in localized regions with respect to coating defects and degradation.

7.4.5. Surface degradation analysis for Antifouling coated coupons

Figure 7.34 shows the cross-sections of the field exposed steel specimens coated with the antifouling coating for Site I, II and III compared with the control lab specimen. Different layers including the tie-coat, the topcoat and calcareous layer of barnacle can be identified. The thicker tie-coat bulk material remained mostly intact during exposure. In agreement with the EIS assessment of coating degradation and the visual observation of the onset of marine fouling, reduction in topcoat thickness was observed on coated specimens after exposure in all three sites (with significant top coat loss in Sites I and II). Figure 7.34B and 7.34C also showed the degraded coating below the base of localized attached barnacles on specimens from Site I and II. Figure 7.35 shows details on the placement of the barnacle base plate on the coated steel surface. The loss of topcoat material would correspond to a decrease in total coating thickness, corresponding to the larger coating capacitance and smaller pore resistance resolved by EIS. The tie coat remained intact

for all cases, and no indication of steel corrosion was evident regardless of the level of coating degradation and onset of marine fouling.

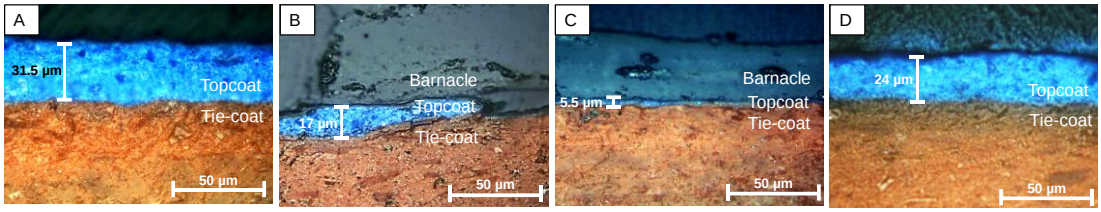

Figure 7.34. Representative metallographic cross-section of antifouling coated samples. (A) As-Cure, (B) Site I, (C) Site II, (D) Site III.

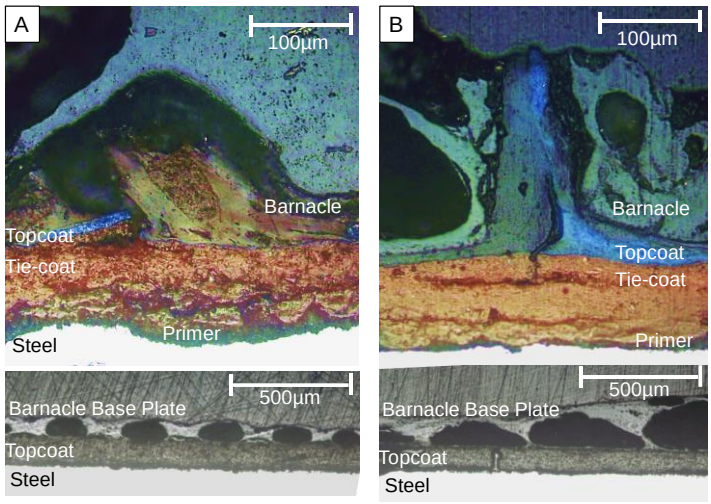

Figure 7.35. Representative metallographic cross-section of antifouling coated samples in presence of the hard foulers. (A) Site I and (B) Site II.

X-ray diffraction measurements (Fig. 10) on the surface of the exposed antifouling coated test specimens showed that the inorganic biocidal components such as zinc oxide, titanium oxide, and barium sulfate were retained despite the topcoat degradation, although the extent of biocide loss was not ascertained. XRD also does not provide indication of the concentrations of other biocide components that have amorphous structures. It was apparent that marine foulers could be inhibited early in the exposure time but prolonged exposures could diminish the level of mitigation. The loss of topcoat material with the biocide pigments and the intrinsic self-polishing characteristic of the coating would anecdotally suggest the progressive loss of performance.

The residual antifouling coating was shown to retain some presence of biocide as shown by XRD but depletion due to the topcoat degradation (in part related to the self-polishing of the topcoat, macro-fouling settlement, and microfouling metabolic activity) can allow for less effective protection. EIS showed that the coating degradation and biofilm development can occur in the aggressive environments (such as at Site I and II) and that the coating has greater longevity in less aggressive environments (such as at Site III). The coating degradation and biofilm formation on specimens in Site I and II were coincident with the onset of marine fouling on the coated steel specimen. Effective coating primers and midcoats are needed to enhance coating durability, but continued exposure without coating maintenance would allow for greater levels of marine fouling and subsequent damage to the steel piles.

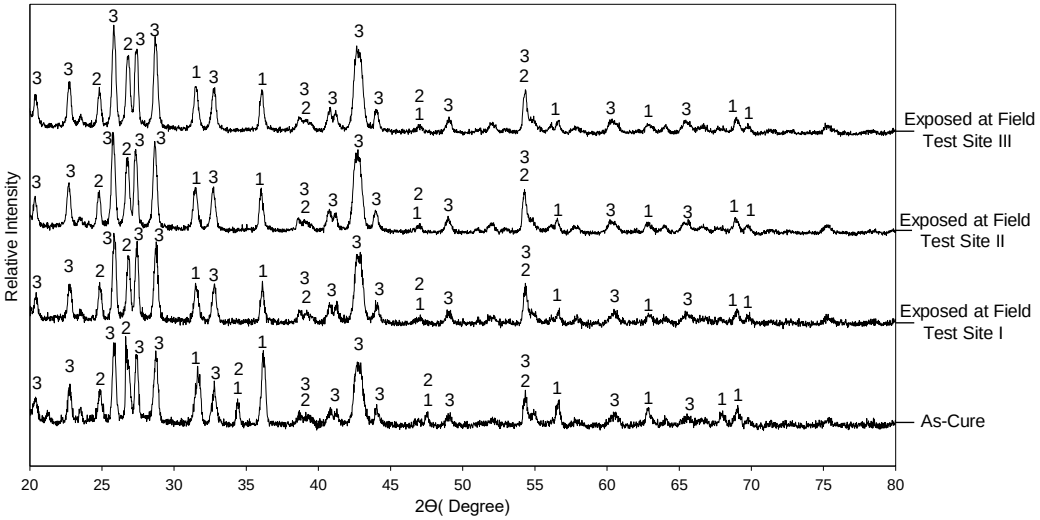

Figure 7.36. XRD diffractograms for anti-fouling coated specimens.
1.Zinc Oxide, 2. Titanium Oxide ,3. Barium Sulfate.

CHAPTER 8

8.CONCLUSIONS

8.1. Biotic condition to sustain SRB in marine fouling condition

- The results from the lab chemical and environmental testing (including COD, sulfide production, and SRB populations) provided verification that adequate nutrient levels initially present in a sheltered environment can support SRB activity for some time. The initial sulfate concentrations did not have a major influence on SRB growth. Sequential injections of nutrients and viable SRB alone did not necessarily accelerate SRB growth but the injections allowed for SRB populations to be sustained.
- As expected, SRB activity was higher in de-aerated solutions. SRB activity was shown to be better supported under porous crevices presumably due to greater nutrient availability and development of local low level oxygen, even in naturally aerated bulk solutions. In de-aerated solutions, crevices also appeared to have positive effects to support SRB.
- There were consistent trends in the SRB activity, the ennoblement of the electrical potential, and increases in corrosion current that indicated that MIC developed in the conditions that may develop in service by the type of macrofouling such as the aforementioned conditions with sequential SRB and nutrient injections. However, the results from laboratory testing verified that the environmental parameters such as aeration levels under the biofilm are important.
- EIS was useful to identify the development of surface films. The development of the surface films showed an increase in its capacitive behavior that resulted in lower relative total impedance at a given low frequency (such as the 100 mHz reference frequency).
- The field sites had heavy marine fouling of different marine organisms and different deposition form. Site I had fouling by well-adhered barnacles and matting of marine flora. Sites II and III had fouling by interlayers of loosely attached barnacles. The different crevice-like conditions

that affect its interactions with the bulk solution (including SRB, nutrient, and oxygen levels) can develop in the natural water environments due to the chemical and physical characteristics of the water body as well as the micro- and marine-organism populations. High SRB populations were measured under the hard and soft fouling. Under the fouling encrustations, black deposits of iron corrosion products developed. Notable features such as deep pits and localized corrosion under the remnant barnacle base plate were observed. Site I had greater corrosion than Site II and III and was related to the heavy accumulation of both hard and soft foulers as well as a fast water flowrate that allowed greater availability of SRB and nutrients from the bulk water to the sheltered biofilm below the marine fouling.

8.2. Mitigation of MIC in presence of marine fouling condition by cathodic protection

- Laboratory testing indicated non-uniform cathodic polarization of steel developed in the specimens with crevice geometries. Cathodic reactions related to SRB activity (sulfate reduction) was significant in the presence of cathodic polarization. SRB was sustained in the presence of the applied cathodic polarization during the lab testing period. Crevice environments reduce effectiveness of cathodic protection by decreasing the level of cathodic current in the occluded regions (laminate crevice). Surface corrosion developed under crevice environments with externally applied cathodic polarization and was enhanced with the presence of SRB. SRB can proliferate even on steel anodic surfaces.
- Field tests showed differentiation in both the magnitude and efficacy of CP current associated with reduced availability of surfaces due to marine fouling. The measured SRB bacteria counts in the field specimens indicated that aggressive conditions with high populations of SRB can be maintained even with the CP. Cathodic polarization of the steel array was attained, and the global CP current developed from the bulk zinc anode to the steel array exceeded 10 mA (>3 $\mu A/cm^2$) indicating that the CP could reduce the overall rate of corrosion of the steel array even

with the presence of surface fouling. However, localized corrosion can still develop below fouling encrustations.

- Smaller local CP currents were measured at Site I, where uniform and compact fouling and calcareous deposits formed compared to Site II with loose fouling layers, Localized regions of the steel array with surface fouling may not have sufficient levels of CP. indicating that the barrier provided by the fouling layers and surface deposits do not provide overall corrosion protection but fouling layers can reduce the available surface area to support cathodic reactions.

8.3. Mitigation of MIC in presence of marine fouling condition by coating

- In laboratory testing, MIC due to SRB only occurred with the presence of coating defects that exposed the steel substrate. SRB could develop on polyurea. SRB was also shown to develop on the surface of the antifouling coating. However, SRB-inoculated solutions showed that the biocides in the tested anti-fouling coating strongly reduced SRB growth. However, SRB can proliferate on the surface of steel specimen if the anti-fouling coating is degraded. The topcoat of the antifouling coating, that contained the antibacterial and antifouling components, was shown to degrade in time.
- For laboratory testing, EIS results for coating samples showed impedance behavior where the Nyquist diagrams showed varied responses. Scribed coating samples showed convoluted responses with the presence of multiple time constants that reflected the different surface and interfacial characteristics associated with coating material, steel substrate, surface films (biofilm and oxide). The proposed equivalent circuit analogs were shown to adequately describe different and unique time constants for each impedance loop and provided a useful means to compare admittances for the various time constants even when CPE n terms indicated non-ideal capacitive behavior. A calculation approach was described to decouple the complicated impedance responses to identify the characteristic frequency of each parallel resistive and capacitive terms associated with each time constant. An increase in coating

capacitance for the antifouling coating was related to the self-polishing characteristic of the coating leading to biocide depletion. The results indicated that microbial activity could further create conditions that would promote coating degradation. It was confirmed that the intermediate frequency impedance loop in inoculated samples was associated with SRB activity whether it be bulk biofilm characteristics or the effects on current distribution through coating defects due to the bacteria.

- In fields testing, the water-based copper-free anti-fouling coating showed relatively better antifouling performance and less barnacle growth compared to polyurea coated steel samples and had generally lower surface bacteria populations (SRB, IRB, APB and SFB) over the time of exposure. The polyurea coating did not prevent marine growth from developing in any of the test conditions and significant barnacle attachment was observed by the earliest days of exposure. The observations showed that barnacle larva can settle on the polyurea coating regardless of its mechanical surface properties. Electrochemical results indicated poor barrier properties of the two coatings. Severe corrosion condition was observed for samples with heavy fouling formation, which implicate the adverse effect of immersion and macrofoulers growth on coating durability.
- The antifouling coated test specimens exposed at three natural water field test sites were subjected to different levels of natural fouling tendencies where different fouling organisms proliferate and have varying modalities for surface accretion. Sites I and II exhibited heavier fouling than Site III in part due to the greater salinity in the former. As such, the performance and durability of the antifouling coating can differ. Mitigation of fouling afforded by the antifouling coating was apparent in comparison to non-coated surfaces; however, complete prevention of fouling was not attained during the ~200 days of testing. The reduced efficacy of biocides in the topcoat of the antifouling coating due to the degradation of the antifouling coating by its self-polishing function was generally observed in the testing. Physical

degradation of the topcoat containing the biocides allowed for subsequent development of micro- and macro-fouling. Intermediate maintenance of the coating would be needed for long-term mitigation. Surface populations of SRB were apparently reduced on the antifouling coating in comparison to non-coated steel specimens, but other bacteria still abound.

- In field testing, EIS following a deconvolution calculation approach for antifouling coated coupons was shown to be useful to separate impedance responses associated with coating degradation and development of surface films. In congruity with the visual observations of fouling and coating degradation, EIS showed that the degradation of the coatings at Sites I and II allowed for reduced efficacy of coating biocides, resulting in impedance dispersion associated with the formation of surface films that can be related to the onset of surface fouling. Coating performance at the less aggressive test Site III was shown to be better.

REFERENCES

Abdoli, L., Suo, X., and Li. H.,(2016), Distinctive colonization of Bacillus sp. bacteria and the influence of the bacterial biofilm on electrochemical behaviors of aluminum coatings. Colloids and Surfaces B: Biointerfaces, 145: 688-694.

Abdollahi, H., and Wimpenny. J., (1990), Effects of oxygen on the growth of Desulfovibrio desulfuricans. Microbiology136 (6): 1025-1030.

Al-Darbi MM, Muntasser ZM, Tango M and Islam MR. (2002). Control of microbial corrosion using coatings and natural additives. Energy Sources, 24(11):1009-1018.

ASTM G1-03 (2017), Standard Practice for Preparing, Cleaning, and Evaluating Corrosion Test Specimens. ASTM International, West Conshohocken, Pennsylvania.

Barlo, T.J., and Berry, W.E. (1984). An Assessment of the Current Criteria for Cathodic Protection of Buried Steel Pipelines. Material Performance, 23: 9-16.

Barton, L.L., and Tomei, F.A., (1995), Characteristics and activities of sulfate-reducing bacteria, in L. L. Barton, Sulfate reducing bacteria. Springer, Boston, MA, :1-32.

Beech, A.B., A. Mollica, H.-C. Flemming, V. Scotto, W. Sand. (2000) ,Simple methods for the investigation of the role of biofilms in corrosion. in Brite Euram Thematic Network on MIC of Industrial Materials. Task Group 1, Biofilm Fundamentals.

Beech, Iwona B., and Christine C. Gaylarde. (1999)., Recent advances in the study of biocorrosion: an overview. Revista de microbiologia 30.3: 117-190.

Blackburn, Freeman E. (2004)., Non-Bioassay Techniques for Monitoring MIC. CORROSION 2004. NACE International.

Blackwood, C.S. Lim, S.L.M. Leo, X, Hu, J. Pang. (2017), Macrofouling induced localized corrosion of stainless steel in Singapore seawater. Corrosion Science 129: 152-160.

Blackwood, D. J., Lim, C. S. and Teo. S. L. M. (2010).,Influence of fouling on the efficiency of sacrificial anodes in providing cathodic protection in Southeast Asian tropical seawater. Biofouling 26 (7): 779-785.

Booth, G. H., and A. K. Tiller. (1960), Polarization studies of mild steel in cultures of sulphate-reducing bacteria. Transactions of the Faraday Society 56: 1689-1696.

Borenstein, S.W., (1994). Microbiologically influenced corrosion handbook. (Abington Hall, England: Woodhead Publishing Ltd.): 288.

Brady, R. F., (2006), Fouling-release coatings for warships." Defence Science Journal 55.1 (2005): 75.

Brady, R., (2005), Fouling-release coatings for warships." Defence Science Journal 55 (1): 75.

Brancato, M. S., and R. M. Woollacott. (1982), Effect of microbial films on settlement of bryozoan larvae (Bugula simplex, B. stolonifera and B. turrita). Marine Biology 71 (1): 51-56.

Braun, D.G., (2005)., Manatee Protection Plan, A description of the historic and current presence, abundance and protection of West Indian Manatees and a plan to promote their continued existence in St. Johns County, Florida, chapter 9, September 2009.

Broekaert. M. (2002), Polyurea spray coatings. The technology and latest developments. http://www. huntsman. com/portal/page/portal/polyurethanes.

Bryant, .R.D., and Laishley. E.J., (1990). The role of hydrogenase in anaerobic biocorrosion." Canadian Journal of Microbiology 36 (4): 259-264.

Carlton, J.T., and Ruckelshaus, M.H., (1997), Nonindigenous marine invertebrates and algae. in: D. Simberloff, D.C. Schmitz and T.C. Brown (eds). Strangers in Paradise. Island Press, Washington: 187-201

Castaneda, H., and Benetton, X.D., (2008). SRB-biofilm influence in active corrosion sites formed at the steel-electrolyte interface when exposed to artificial seawater conditions, Corrosion Science 50: 1169–1183.

Chambers, L., Stokes, K.,Walsh, L., and Wood, R. JK., (2006), Modern approaches to marine antifouling coatings. Surface and Coatings Technology 201 (6): 3642-3652

Characklis, W. G.,(2009)., Fouling biofilm development: a process analysis."BIOTECHNOLOGY AND BIOENGINEERING 102 (2) : 310-347.

Chen, Y.M., Rudawski,N.G., Lambers,E., Orazem,M.E., (2017), Application of impedance spectroscopy and surface analysis to obtain oxide film thickness. Journal of The Electrochemical Society, 164 : C563

Chess, P. and Broomfield, J. (2005). Cathodic Protection of Steel in Concrete and Masonry, E and FN Spon, New York, NY.

Clapp, W. P. (1948)., Macro-organisms in sea water and their effect on corrosion. The corrosion handbook. New York: John Wiley & Sons, Inc : 433À41.

Cord-Ruwisch, R., and Friedric,h W.(1986), Corroding iron as a hydrogen source for sulphate reduction in growing cultures of sulphate-reducing bacteria. Applied Microbiology and Biotechnology 25 (2): 169-174.

Costello, J. A. (1969), Corrosion of Metals By Micro-Organisms A Literature Survey." International Biodeterioration Bulletin 5.3 : 101.

Costello, J. A. (1974), Cathodic depolarization by sulfate-reducing bacteria." South African Journal of Science 70 (7): 202-204.

Costerton, J. William, and J. Boivin. (1991). Biofilms and corrosion., Biofouling and Biocorrosion in industrial water systems. Springer Berlin Heidelberg, :195-204.

Costerton, J. W., Cooksey, K., Flemming, H. C., Murthy, P. S., & Venkatesan, R. (Eds.). (2009). Marine and industrial biofouling. Springer Berlin Heidelberg.

Crisp, D.J. (1974), Factors influencing the settlement of marine invertebrate larvae. Chemorecept. Mar. Org. 22:177–265.

De Brito LV, Coutinho R, Cavalcanti EH and Benchimol M. (2007). The influence of macrofouling on the corrosion behaviour of API 5L X65 carbon steel. Biofouling, 23(3):193-201.

De Brito, L.V. Coutinho, R. Cavalcanti, E.H. Benchimol. M. (2007)., The influence of macrofouling on the corrosion behaviour of API 5L X65 carbon steel. Biofouling 23 (3):193-201.

De Levie, R., (1963), On porous electrodes in electrolyte solutions: I. Capacitance effects, Electrochimica Acta. 8 (1963): 751-780.

de Messano, L.V., Reznik, L.Y., Sathler, L. and Coutinho, R , (2014)., Evaluation of biocorrosion on stainless steels using laboratory-reared barnacle Amphibalanus amphitrite. Anti-Corrosion Methods and Materials 61 (6): 402-408.

de Messano,VR., Sathler, L. Reznik,L., Coutinho, R, (2009),The effect of biofouling on localized corrosion of the stainless steels N08904 and UNS S32760." International Biodeterioration & Biodegradation 63 (5): 607-614.

de Rincon, O., and Morris, E., (2003)., Studies on selectivity and establishment of “Pelo de Oso”(Garveia franciscana) on metallic and non-metallic materials submerged in Lake Maracaibo, Venezuela, Anti-corrosion methods and materials. 50 :17-24.

De Romero, M, De Rincon, O., and Ocando, L., (2009). Cathodic protection efficiency in the presence of SRB: State of the art. CORROSION 2009. NACE International.

De Romero, M., Ocando, L., de Rincón, O., Parra, J., Ruiz, R., Bracho, M., Romero, G. and Quintero, A.(2006), Cathodic polarization effect on sessile SRB growth and iron protection. CORROSION 2006.

De Romero, M.F., de Rincón, O.T., Sanz, M., Rincón, B., Ocando, L., Campos, W. and Bracho, M., (2008), Evaluation of Cathodic Protection in presence of Sulfate Reducing Bacteria mixed cultures." CORROSION 2008 .

Dexter, S.C., and La Fontaine, J.P., (1998). Effect of natural marine biofilms on galvanic corrosion. Corrosion, 54, :851-861.

Dexter. SC., (1993), Role of microfouling organisms in marine corrosion, Biofouling, 7:97-127.

Diaz, C., Urquidi-Macdonald, M., Macdonald, D.D., Ramamurthy,A.C., Van Ooji, W.J., and Sabata, A., (1993), Interpretation of Electrochemical Impedance Data for Damaged Automotive Paint Films, in Corrosion control for low-cost reliability, 12th international corrosion congress, Paper No. 455, NACE International, Houston, TX.

Dickinson, W. H., and Z. Lewandowski. (1996), Manganese biofouling and the corrosion behavior of stainless steel. Biofouling 10 (1-3): 79-93.

Dickinson, W. H., Z. Lewandowski, and R. D. Geer. (1996), Evidence for surface changes during ennoblement of type 316L stainless steel: Dissolved oxidant and capacitance measurements. Corrosion 52.12: 910-920.

Dilling, W., and Cypionka.H., (1990) Aerobic respiration in sulfate-reducing bacteria." FEMS Microbiology Letters 71 (1-2): 123-127.

Donham, J. E., (1976), The Role of Bacteria in the Corrosion of Oil Field Equipment." TPC Publication 3.

Duana, J., Wua, S., Zhanga, X., Huangb, G., Duc, M., Houa, B., (2008). Corrosion of carbon steel influenced by anaerobic biofilm in natural seawater. Electrochimica Acta, 54: 22–28.

Eashwar, M. Subramanian G., Chandrasekaran P., Balakrishnan. K. (1992), Mechanism for barnacle-induced crevice corrosion in stainless steel. Corrosion 48 (7): 608-612.

Eashwar, M. Subramanian, G. and Chandrasekaran. P. (1990)., Marine fouling and corrosion studies in the coastal waters of Mandapam, India. Bulletin of Electrochemistry 6 (08): 699-702.

Eashwar, M., Subramanian, G., Chandrasekaran, P., Manickam, S. T., Maruthamuthu, S., & Balakrishnan, K. (1995). The interrelation of cathodic protection and marine macrofouling. Biofouling, 8(4), 303-312.

Edyvean, R. G., Terry, J., L. A., and Picken. G. B., (1985), Marine fouling and its effects on offshore structures in the North Sea. A review. International biodeterioration 21 (4): 277-284.

Egan, S., James, S., Holmström, C. and Kjelleberg, S , (2002)., Correlation between pigmentation and antifouling compounds produced by Pseudoalteromonas tunicata. Environmental Microbiology 4 (8) :433-442.

Enos, D.G., Taylor, S.R., (1996). Influence of sulfate-reducing bacteria on alloy 625 and austenitic stainless steel weldments,Corrosion, 52: 831-842.

Feio, M.J., Rainha, V., Fonseca, I.T., Reis, M.A. and Lino, A.R., (2000), The influence of the Desulfovibrio desulfuricans 14 ATCC 27774 on the corrosion of mild steel. Materials and Corrosion 51 (10): 691-697.

Felder, D.L. and Camp, D.K. (2009), Gulf of Mexico–Origins, Waters, and Biota. Biodiversity. Texas A&M Press, College Station, Texas.

Fessler, R.R., Markworth, A.J. , and Parkins, R.N. , (1983), Cathodic protection levels under disbonded coatings," Corrosion 39 (1):20-25.

Fischer, K.P., (1981), Cathodic protection in saline mud containing sulfate reducing bacteria." Material Performance 20: 41.

Fleming, H.C.,and Ridgway,H., (2009), Biofilm Control: Conventional and Alternative Approaches, In Marine and Industrial Biofouling. Edited by Fleming, H.-C., R.Venkatesan, and K.E. Cooksey, Springer. :103-117.

Flemming, H.C., Murthy, P.S., Venkatesan, R. and Cooksey, K., (2009)., Marine and industrial biofouling. Springer Berlin Heidelberg (Vol. 333).

Fonseca, I.T., Feio, M.J., Lino, A.R., Reis, M.A. and Rainha, V.L., (1998),The influence of the Thiemedi on the corrosion of mild steel by Desulfovibrio desulfuricans bacteria: an electrochemical study. Electrochimica Acta 43 (1): 213-222.

Galicia, M., Goujon, V., Aguirre-Ramírez, M., Castaneda, H., (2017), Interfacial and corrosion characterization of zinc rich-epoxy primers with carbon nanotubes exposed to marine bacteria. In Corrosion 2017, New Orleans, LA, USA, 26–30 March 2017; NACE International: Houston, TX, USA.

Gandy, A. F., and Gandy.E.T., (1980), Microbiology for environmental scientists and engineers. McGraw-Hill, .

Geesey, G.G., (1993), Biofilm formation, in A practical manual on microbiologically influenced corrosion, G. Kobrin, Editor., NACE: Houston, TX, USA.

Geesey, G.G., Costerton, J.W. (1986), The microbial ecology of surface colonization and of consequent corrosion", in Biologically Influenced Corrosion (NACE reference book 8), S.C. Dexter, Editor. . (Houston, TX: NACE).

Grdeń, M., (2017)., Impedance study on the capacitance of silver electrode oxidised in alkaline electrolyte, Journal of Solid State Electrochemistry. 21: 3333-3344.

Gu, T., Jia, R., Unsal, T., and Xu, D., (2019),Toward a better understanding of microbiologically influenced corrosion caused by sulfate reducing bacteria. Journal of materials science & technology, 35: 631-636.

Gu, T., Zhao, K., and Nesic, S., (2009) A new mechanistic model for MIC based on a biocatalytic cathodic sulfate reduction theory. In CORROSION 2009. NACE International, Paper No. 09390.

Gubner, R. and. Beech, I. B , (2009), Statistical assessment of the risk of biocorrosion in tidal waters, CORROSION/99. Paper No. 99184, NACE International, San Antonio, Texas.

Guezennec, J.G. (1994). Cathodic protection and microbially induced corrosion. International biodeterioration & biodegradation, 34(3-4): 275-288.

Hamilton, W. A. (2003), Microbially influenced corrosion as a model system for the study of metal microbe interactions: a unifying electron transfer hypothesis. Biofouling 19 (1): 65-76.

Hao, O.J., Chen, J.M., Huang, L. and Buglass, R.L., (1996), Sulfate-reducing bacteria." Critical reviews in environmental science and technology 26 (2): 155-187.

Hardy, J. A. (1983), Utilisation of cathodic hydrogen by sulphate-reducing bacteria. British Corrosion Journal 18 (4) 190-193.

Hardy, J. A.; Hamilton, W. A. (1981). The oxygen tolerance of sulfate-reducing bacteria isolated from the North Sea waters. Microbiology, 6: 259-262.

Hartt, W.H., Culberson, C.H., & Smith, S.W. (1984). "Calcareous deposits on metal surfaces in seawater—A critical review." Corrosion, 40(11): 609-618.

Hellio, C., Maréchal, J.P., Da Gama, B.A., Pereira, R.C., and Clare, A. S. (2009),Natural marine products with antifouling activities, In C. Hellio & D. Yebra (Eds.), Advances in marine antifouling coatings and technologies , Woodhead Publishing , Cambridge, UK, :572–622.

Hodgkiess, T., and A. Nevilie.(1998), Localized effects of macrofouling species on electrochemical corrosion of high grade alloys. No. CONF-980316-. NACE International, Houston, TX (United States).

Hoog, N.A.; Mayer, M.J.J.; Miedema, H.; Olthuis, W.; Tomaszewska, A.A.; Paulitsch-Fuchs, A.H.; van den Berg, A. (2015), Online monitoring of biofouling using coaxial stub resonator technique. Sens. Bio Sens. Res.3:79–91.

Horvath, J., and Mihaly Novak. (1964), Potential/pH equilibrium diagrams of some Me-S-H2O ternary systems and their interpretation from the point of view of metallic corrosion. Corrosion Science 4.1 (4):159-178.

Houghton, D. R. (1978). Marine fouling and offshore structures. Ocean Management 4.2(4): 347-352.

Hsu, C.H., and Mansfeld,F., (2001), Technical note: Concerning the conversion of the constant phase element parameter Y0 into a capacitance. Corrosion. 57 :747–748.

Hu, An. (2004), Investigation of sulfate-reducing bacteria growth behavior for the mitigation of microbiologically influenced corrosion (MIC). Diss. Ohio University.

Iversen, A., (2002), MIC on Stainless Steels in Wastewater Treatment Plants-Field Tests and a Risk Assessment. CORROSION 2002. NACE International.

Iverson, W. P. (1984), Mechanism of anaerobic corrosion of steel by sulfate reducing bacteria." Materials performance 23 (3): 28-30.

Jack, T.R., Van Boven, G., Wilmott, M. and Worthington, R.G., (1995), Evaluation of coating performance after exposure to biologically active soils. No. CONF-950304-. NACE International, Houston, TX (United States),

Jack, T.R., Wilmott, M.J., Sutherby, R.L., and Worthingham, R.J., (1996), External corrosion of line pipe-A summary of research activities. Materials Performance 35: 3:17-23.

Javaherdashti, R, Nwaoha, C., and Tan, H., (2013). Corrosion and materials in the oil and gas industries. CRC Press.

Javaherdashti, R., (1999), A review of some characteristics of MIC caused by sulphate reducing bacteria: Past, present and future," Anticorrosion Methods and Materials, 46:173-180.

Javaherdashti, R., (2008), Microbiologically Influenced Corrosion. An Engineering Insight." (London, England: Springer-Verlag), :164.

Jayaraman, A., Earthman, J.C., Wood, T.K., (1997), Corrosion inhibition by aerobic biofilms on SAE 1018 steel. Applied Microbiology and Biotechnology, 47: 62–68.

Jia, R., Unsal, T., Xu, D., Lekbach, Y., and Gu, T., (2019), Microbiologically influenced corrosion and current mitigation strategies: A state of the art review. International biodeterioration & biodegradation, 137: 42-58.

Jia., R, Wang. D., Jin, P., Unsal, T., Yang, D., Yang, J., Xu, D., and Gu, T., (2019), Effects of ferrous ion concentration on microbiologically influenced corrosion of carbon steel by sulfate reducing bacterium Desulfovibrio vulgaris, Corrosion Science, 153 :127-137.

Jones, J., B. Little, and F. Mansfeld.(1992), ESEM/EDS, SEM/EDS and EIS studies of coated 4140 steel exposed to marine, mixed microbial communities including SRB. International Power Generation Conference, Atlanta-Georgia..

Kaplan, E.H., (1988), A field guide to southeastern and Caribbean seashores: Cape Hatteras to the Gulf coast, Florida, and the Caribbean, Houghton Mifflin Co. Boston, MA.

Keough MJ and Raimondi PT. (1995). Responses of settling invertebrate larvae to bioorganic films: effects of different types of films. Journal of Experimental Marine Biology and Ecology, 185(2):235-253.

King, R.A. and Miller, J.D.A., (1971). Corrosion by the sulphate-reducing bacteria. Nature, 233(5320),:491-492.

Kloeke, F.V.O., Bryant, R.D., Laishley, E.J., (1995), Localization of cytochromes in the outer membrane of Desulfovibrio vulgaris (Hildenborough) and their role in anaerobic biocorrosion, Anaerobe, 1: 351-358.

Kobrin, G., (2006), Corrosion by microbiological organisms in natural water. Material Performance, 15.

Kuang, D., and. Cheng, Y.F, (2015), Study of cathodic protection shielding under coating disbondment on pipelines," Corrosion Science 99: 249-257.

Kuhr, CAH Von Wolzogen, and Van der Vlugt, L. S., (1934), The graphitization of cast iron as an electrobiochemical process in anaerobic soils." Water (den Haad) 18 : 147-165.

LaQue, (1982), Topics for research in marine corrosion. Canada. Materials Performance 21 (4): 13-18.

Lau, K., and Sagüés, A., (2011), Impedance of reinforcing steel with disbonded dual polymer–zinc coating, Electrochimica Acta. 56 :7815-7824.

Lau, S.C., Mak, K.K., Chen, F. and Qian, P.Y.(2002), Bioactivity of bacterial strains isolated from marine biofilms in Hong Kong waters for the induction of larval settlement in the marine polychaete Hydroides elegans. Marine Ecology Progress Series 226: 301-310.

Lee, J.S., Ray, R., Little, B., (2010), Influence of experimental conditions on the outcome of laboratory investigations using natural coastal seawaters, Corrosion. 66 : 015001-015001.

Lee, W., Lewandowski, Z., Nielsen, P.H. and Hamilton, W.A., (1995), Role of Sulfate-reducing Bacteria in Corrosion of Mild Steel: a Review," Biofouling 8, :165-168.

Lehaitre, M. Delauney, L. and Compère. C. (2008), Biofouling and underwater measurements. Real-time observation systems for ecosystem dynamics and harmful algal blooms: Theory, instrumentation and modelling. Oceanographic Methodology Series. UNESCO, Paris :463-493.

Lejars M, Margaillan A and Bressy C. (2012). Fouling release coatings: a nontoxic alternative to biocidal antifouling coatings. Chemical reviews, 112(8):4347-4390.

Lejars, M., Margaillan, A., and Bressy.C., (2012), Fouling release coatings: a nontoxic alternative to biocidal antifouling coatings. Chemical reviews, 112:4347-4390.

Lin, J., and Madida, B., (2015), Biofilms affecting progression of mild steel corrosion by Gram positive Bacillus sp. Journal of basic microbiology 55 (10): 1168-1178.

Linhardt, P., (2006), MIC of Stainless Steel in Freshwater and the Cathodic Behaviour of Biomineralized Mn-Oxides, Electrochimica Acta, 12.

Littauer, E., and D. M. Jennings. "The prevention of marine fouling by electrical currents." Proc. 2nd Int. Congress on Marine Corrosion and Fouling. 1968.

Little, B. J. and Lee, J.S., (2014), Microbiologically influenced corrosion: An Update," International Materials Reviews, 59: 384-393.

Little, B. J., and Lee. J. (2009) Microbiologically influenced corrosion. Kirk-Othmer Encyclopedia of Chemical Technology.

Little, B., P. Wagner, and D. Duquette. (1988), Technical note: microbiologically induced increase in corrosion current density of stainless steel under cathodic protection. Corrosion 44 (5): 270-274.

Little, B., Wagner, P., and Mansfeld, F., (1992), An overview of microbiologically influenced corrosion. Electrochimica acta. 37:2185-2194.

Little, Brenda J., and Patricia A. Wagner. (1993), The interrelationship between marine biofouling and cathodic protection. No. NRL/PP/7333-92-0002. NAVAL RESEARCH LAB STENNIS SPACE CENTER MS, .

Liu, H., Xu, L., Zeng, J., (2000). Role of corrosion products in biofilms in microbiologically induced corrosion of carbon steel," British Corrosion Journal, 35:131-135.

Liu, H.; Huang, L.; Huang, Z.; Zheng, J. (2007)., Specification of sulfate reducing bacteria biofilms accumulation effects on corrosion initiation. Mater. Corros. 58:44–48.

Maki, J.S., Rittschof, D., Costlow, J.D. and Mitchell, R,. (1988), Inhibition of attachment of larval barnacles, Balanus amphitrite, by bacterial surface films. Marine Biology 97 (2) : 199-206.

Mansfeld, F. (1995), Use of electrochemical impedance spectroscopy for the study of corrosion protection by polymer coatings. J. Appl. Electrochem. 25: 187–202.

Mansfeld, F.(1981), Recording and analysis of AC impedance data for corrosion studies. Corrosion, 37: 301–307.

Mansfeld, F., (2007), The interaction of bacteria and metal surfaces, Electrochimica Acta 52: 7485-7488.

Maruthamuthu, S., Eashwar, M., Manickam, S. T., Ambalavanan, S., Venkatachari, G., & Balakrishnan, K. (1990). Marine fouling on test panels and in-service structural steel in Tuticorin harbour.

McPherson, B.F., Sonntag, W.H., and Sabanskas, M., (1984), Fouling Community of the Loxahatchee River Estuary, Florida, 1980-81, Estuaries. 7:149-157.

Mehta, A.J., and Jones, C.P., (1977),Matanzas Inlet: glossary of inlets report# 5, Florida Sea Grant Program, Report No 21.

Melchers, R. E. (2005), Effect of nutrient-based water pollution on the corrosion of mild steel in marine immersion conditions. Corrosion 61 (3): 237-245.

Melchers, R. E. (2007), The effects of water pollution on the immersion corrosion of mild and low alloy steels, Corrosion Science 49 (8): 3149-3167.

Melchers, R. E. (2014). Long-term immersion corrosion of steels in seawaters with elevated nutrient concentration. Corrosion Science, 81, 110-116.

Melchers, R.E. and Jeffrey, R.J.,(2013). Accelerated low water corrosion of steel piling in harbours. Corrosion engineering, science and technology, 48(7): 496-505.

Millero, F.J. (1986), The thermodynamics and kinetics of the hydrogen sulfide system in natural waters, Marine Chemistry. 18: 121-147.

Mohanty, S.S., Das, T., Mishra, S.P. and Chaudhury, G.R., (2000), Kinetics of $SO4^{-}$ 2 reduction under different growth media by sulfate reducing bacteria. BioMetals 13 (1): 73-76.

Moreno, C., Franco, R., Moura, I., Gall,J., Moura, J., (1993), Voltammetric studies of the catalytic electron-transfer process between the Desulfovibrio gigas hydrogenase and small proteins isolated from the same genus, European Journal of Biochemistry, 217: 981-989.

Munger CG. (1985), Corrosion prevention by protective coatings." United States (US): OSTI.GOV.

Muntasser Z, Al-Darbi M, Tango M and Islam MR. (2002),. Prevention of microbiologically influenced corrosion using coatings. In CORROSION 2002. NACE International.Paper No. 02029.8pp

Muntasser Z, Al-Darbi M, Tango M and Islam MR. (2002). Prevention of microbiologically influenced corrosion using coatings. In CORROSION 2002. NACE International.Paper No. 02029.8pp.

Murthy, S.P., and Venkatesan, R., (2009), Industrial Biofilms and their Control. In Marine andIndustrial Biofouling. Edited by Fleming, H.-C., Venkatsan, R., and K.E. Cooksey, Springer. : 65-100.

Myers, C. R., and Nealson, K.H., (1988)., Bacterial manganese reduction and growth with manganese oxide as the sole electron acceptor. Science 240.4857 : 1319.

NACE-SP0408 (2014). Cathodic Protection of Reinforcing Steel in Buried or Submerged Concret Structures. NACE Standard. ISBN: 1-57590-223-0.

Narayan, R., Bose, S., and Bandyopadhyay, A., (2012) Biomaterials Science: Processing, Properties and Applications II: Ceramic Transactions. Vol. 237. John Wiley & Sons.

Neville, T. Hodgkiess. (1998)., Comparative study of stainless steel and related alloy corrosion in natural sea water.British Corrosion Journal 33 (2): 111-120.

Newman, R. C., B. J. Webster, and R. G. Kelly. (1991), The electrochemistry of SRB corrosion and related inorganic phenomena. ISIJ international 31 (2): 201-209.

Newman, R.C., Wong, W.P., Ezuber, H. and Garner, A. (1989), Pitting of stainless steels by thiosulfate ions. Corrosion 45 (4):282-287.

Nunez, S., Eastman, A.D and Babnick, R.J., (1989), Cathodic protection shielding definition, AGA Corrosion Supervisory Committee. nutrient concentration. Corrosion science 81: 110-116.

O'Dell, J.W., (1993), The determination of chemical oxygen demand by semiautomated colorimetry-method 410.4. Cincinnati, Ohio: Environmental Monitoring Systems Laboratory, Office of Research and Development, US Environmental Protection Agency.

Obuekwe, C.O., Westlake, D.W., Cook, F.D. and Costerton, J.W, (1981), Surface changes in mild steel coupons from the action of corrosion-causing bacteria." Applied and environmental microbiology 41 (3): 766-774.

O'Connor, Nancy J., and Donnia L. Richardson. (1996)., Effects of bacterial films on attachment of barnacle (Balanus improvisus Darwin) larvae: laboratory and field studies. Journal of Experimental Marine Biology and Ecology 206 (1-2): 69-81.

O'Connor, Nancy J., and Donnia L. Richardson. (1998)., Attachment of barnacle (Balanus amphitrite Darwin) larvae: responses to bacterial films and extracellular materials." Journal of Experimental Marine Biology and Ecology 226 (1): 115-129.

Odom, J. M. (1993), Industrial and environmental activities of sulfate-reducing bacteria." The sulfate-reducing bacteria: Contemporary perspectives. Springer New York, :189-210.

Olivares, G.Z, Esquivel, R.G., Gayosso, M.J., Trejo, A.G., Gurrión, C.C., and Villalobos, E.B. (2006), Influence of Sulfate Reducing Bacteria on the Cathodic Protection Potential of XL52 Steel. CORROSION 2006, Paper No. 06075 (Houston, TX: NACE, 2006).

Olivares, G.Z., Mejia, G.M., Caloca, G.G., Esquivel, R.G., Lopez, I.G., Ulloa-Ochoa, C.M. and Dabur, F.R., (2003)., Sulfate Reducing Bacteria Influence on the Cathodic Protection of Pipelines That Transport Hydrocarbons. CORROSION 2003. NACE International, 2003.

Palanichamy, S. ,Subramanian. G. (2014)., Hard foulers induced crevice corrosion of HSLA steel in the coastal waters of the Gulf of Mannar (Bay of Bengal), India. Journal of Marine Science and Application 13 (1): 117-126.

Palraj, S., and G. Venkatachari. (2006)., Corrosion and bio fouling characteristics of mild steel in Mandapam waters. Materials performance 45 (6): 46-50.

Palraj,S, Venkatachari, G.and Subramanian. G. (2002)., Bio-fouling and corrosion characteristics of 60/40 brass in Mandapam waters.A nti-Corrosion Methods and Materials 49(3):194-1988.

Pankhania, I. P., A. N. Moosavi, and W. A. Hamilton. (1986), Utilization of cathodic hydrogen by Desulfovibrio vulgaris (Hildenborough). Microbiology 132 (12): 3357-3365.

Pedersen, A., Hermansson, M., (1991). Inhibition of metal corrosion by bacteria. Biofouling, 3: 1–11.

Permeh, S., B. Li, M. Echeverría, B. Tansel, K. Lau, and M. Duncan.2018. Microbially influenced steel corrosion with crevice conditions in natural water. In Proc., Corrosion 2018. Houston: National Association of Corrosion Engineers International.

Permeh, S., Boan, M. E., Tansel, B., & Lau, K. (2019a). Susceptibility of bridge steel and concrete components to microbiological influenced corrosion (MIC) and microbiological influenced deterioration (MID) in Florida (No. BDV29-977-26).

Permeh, S., C. Reid, M. E. Boan, K. Lau, B. Tansel, M. Duncan, and I. Lasa. 2017. Microbiological influenced corrosion (MIC) in Florida marine environment: A case study. In Proc., Corrosion 2017. Houston: National Association of Corrosion Engineers International.

Permeh, S., M. E. Boan, B. Tansel, K. Lau, and M. Duncan. 2019d. Exploration of the influence of microbe availability on MIC of steel marine fouling environments. In Proc., Corrosion 2019. Houston: National Association of Corrosion Engineers International.

Permeh. S, Lau. K, Duncan. M, (2019b), Characterization of Biofilm Formation and Coating Degradation by Electrochemical Impedance Spectroscopy. Coatings. 9(8): 518. DOI: 10.3390/coatings9080518

Permeh. S, Lau. K, Echeverria. M, Duncan M., (2021b), Influence of Macro- and Micro-Fouling on Corrosion of Steel Bridge Piles Submerged in Natural Waters, ASCE Journal of Materials in Civil Engineering, 33(6). DOI: 10.1061/(ASCE)MT.1943-5533.0003687

Permeh. S, Lau. K, Echeverria. M, Duncan. M, (2021a), Electrochemical characteristics of antifouling coated steel structure submerged in Florida natural waters to mitigate micro- and macrofouling, Construction and Building Materials Journal, V. 274, 122087. DOI: 10.1016/j.conbuildmat.2020.122087.

Permeh. S, Lau. K., Duncan. M, (2019c), Degradation of Coatings for Steel in Environments Susceptible to Corrosion Associated with Fouling. Structure and Infrastructure Engineering. 16(8):1186-1200. DOI: 10.1080/15732479.2019.1694543

Permeh. S, Lau. K., Echeverria. M., Tansel. B., Duncan. M. (2020b), Cathodic polarization behavior of steel with different marine fouling morphologies on submerged bridge elements with cathodic protection, ASCE Journal of Materials in Civil Engineering, 32(7), 04020184. DOI: 10.1061/(ASCE)MT.1943-5533.0003257

Permeh. S, Lau. K., Tansel. B., Duncan. M, (2020a), Surface conditions for microcosm development and proliferation of SRB on steel with cathodic corrosion protection, Construction and Building Materials Journal, 243: 118209. DOI: 10.1016/j.conbuildmat.2020.118209

Pipe, (1981), North Sea fouling organisms and their potential effects on the corrosion of North Sea structures. Marine Corrosion of Offshore Structures: 13-22.

Postgate JR. 1979. The sulphate-reducing bacteria. London: Cambridge University Press (CUP Archive).

Potekhina, J.S., Sherisheva, N.G., Povetkina, L.P., Pospelov, A.P., Rakitina, T.A., Warnecke, F., Gottschal Sahar k, G., (1999). Role of microorganisms in corrosion inhibition of metals in aquatic habitats. Applied Microbiology and Biotechnology, 52: 639–646.

Rajasekar, A., Ting, Y.T., (2011), Role of Inorganic and Organic Medium in the Corrosion Behavior of Bacillus megaterium and Pseudomonas sp. in stainless steel SS 304. Industrial and Engineering Chemistry Research, 50.

Rim-Rukeh, A., and G. Irerhievwie. (2012), Estimation of microbiologically influenced corrosion of X60 steel exposed to a natural freshwater environment." Journal of Emerging Trends in Engineering and Applied Sciences 3.6: 953-958.

Rincon, O. and Morris, E. (2003), Studies on selectivity and establishment of ‘Pelo de Oso’ (Garveia franciscana) on metallic and non-metallic materials submerged in Lake Maracaibo, Venezuela”, Anti-Corrosion Methods and Materials, 50 (1):17-24.

Roberts, D. Rittschof, E. Holm, A.R, Schmidt. (1991), Factors influencing initial larval settlement: temporal, spatial and surface molecular components. Journal of Experimental Marine Biology and Ecology 150 (2): 203-221.

Roy, A.K., Jones, D. A., and Mccright. R. D., (1996), Degradation mode survey galvanic corrosion of candidate metallic materials for high-level radioactive waste disposal containers, Lawrence Livermore National Lab, No. UCRL-ID-125645. b, CA, US.

Salgar-Chaparro, S.J., Lepkova, K., Pojtanabuntoeng, T., Darwin, A. and Machuca, L. L., (2020), Nutrient level determines biofilm characteristics and subsequent impact on microbial corrosion and biocide effectiveness, Applied and environmental microbiology. 86.

Salvago, G., Fumagalli, G., Mollica, A. and Ventura, G., (1987), A statistical evaluation of AISI 316 stainless steel resistance to crevice corrosion in 3.5% NaCl solution and in natural sea water after pre-treatment in HNO3. Corrosion science 27 (9):927-936.

Sanders, P. F. (1988), Monitoring And Control of Sessile Microbes: Cost Effective Ways To Reduce Microbial Corrosion." Microbial Corrosion-1 (1): 191.

Sanders, P. F., and S. Maxwell. (1983), Microfouling, macrofouling and corrosion of metal test specimens in seawater. Microbial Corrosion, : 74-83.

Schippers, A., Rohwerder, T., and Sand. W., (1999), Intermediary sulfur compounds in pyrite oxidation: implications for bioleaching and biodepyritization of coal, Applied microbiology and biotechnology 52 (1): 104-110.

Scott, P. J. B. "Expert consensus on MIC: failure analysis and control, Materials performance 43 (4) :46-50.

Shreir, L.L., (1963), The Microbiology of Corrosion," Corrosion,1,Wiley,J.,New York,pp 252-264.

Skaja, A., (2015), Coatings for Invasive Mussel Control, U.S. Department of the Interior, Bureau of Reclamation, Final Report, Contract No. ST-2015-7095-01.

Soracco, R.J., Pope, D.H., Eggers, J.M. and Effinger, T.N., (1988), Microbiologically influenced corrosion investigations in electric power generating stations. No. CONF-880314--. Houston, TX; National Assoc. of Corrosion Engineers.

Starkey, R.L. (1985), Anaerobic Corrosion--Perspectives About Causes, Biologically Induced Corrosion.: 3-7.

Stoodley, P., Dodds, I., Boyle, J.D. and Lappin-Scott, H.M., (1998), Influence of hydrodynamics and nutrients on biofilm structure. Journal of applied microbiology 85.S1.

Subramanian, and Palanichamy. S, (2013), Influence of fouling assemblage on the corrosion behaviour of mild steel in the coastal waters of the Gulf of Mannar, India. Journal of Marine Science and Application 12(4) :500-509

Swain, G. W., and J. Patrick-Maxwell. (1990), The effect of biofouling on the performance of Al-Zn-Hg sacrificial anodes. Corrosion 46 (3): 256-260.

Telegdi, J., Szabó, T., Al-Taher, F., and Vértes .A., (2010), Coatings against corrosion and microbial adhesion. Materials and Corrosion, 61:1000-1007.

Ter Heijne, D. Liu, Sulonen, M., Sleutels, T., and Fabregat-Santiago, F., (2018), Quantification of bio-anode capacitance in bioelectrochemical systems using Electrochemical Impedance Spectroscopy, Journal of Power Sources. 400: 533-538.

Thierry, D., and Sand, W., (2011)., Microbially influenced corrosion." Corrosion Mechanisms in Theory and Practice. CRC Press, :738-777.

TM0194-2014. Field Monitoring of Bacterial Growth in Oil and Gas Systems; NACE Standard: Houston, TX, USA, 2014.

Tomlinson, M., and Woodward. J.,(2014), Pile design and construction practice. CRC Press, Boca Raton, FL. 2014.

Unabia, C. R. C., and M. G. Hadfield. (1999), Role of bacteria in larval settlement and metamorphosis of the polychaete Hydroides elegans." Marine Biology 133 (1): 55-64.

Venzlaff, H., Enning, D., Srinivasan, J., Mayrhofer, K.J., Hassel, A.W., Widdel, F., Stratmann. M., (2013), Accelerated cathodic reaction in microbial corrosion of iron due to direct electron uptake by sulfate-reducing bacteria, Corros. Sci. 66: 88–96.

Videla, H.A., (1996) Manual of biocorrosion, ed. K. McCombs. , USA: CRC Press, Inc.

Videla, H.A., and Herrera, L.K., (2009), Understanding microbial inhibition of corrosion. A comprehensive overview. International Biodeterioration & Biodegradation, 63: 891–895.

Walters, L.J. Hadfield M. G, and Smith C. M. (1996)., Waterborne chemical compounds in tropical macroalgae: positive and negative cues for larval settlement. Marine Biology 126 (3): 383-393.

Wells S and Sytsma M. (2009). A review of the use of coatings to mitigate biofouling in freshwater. Portland State University, Portland, OR, accessed Feb, 22: 2018.

Wen, K. Zhao, T. Gu and S. Nesic, (2006), Effects of mass transfer and flow conditions on SRB corrosion of mild steel, Paper No. 06666, Corrosion/2006, NACE International, Houston, TX.

Whitehead, K. A., & Verran, J. (2009). The effect of substratum properties on the survival of attached microorganisms on inert surfaces. In Marine and industrial biofouling (pp. 13-33). Springer, Berlin, Heidelberg.

Xu, D., and Gu, T., (2014), Carbon source starvation triggered more aggressive corrosion against carbon steel by the Desulfovibrio vulgaris biofilm. International Biodeterioration & Biodegradation, 91:74-81.

Yebra, Diego Meseguer, Søren Kiil, and Kim Dam-Johansen. (2004), Antifouling technology—past, present and future steps towards efficient and environmentally friendly antifouling coatings." Progress in organic coatings 50 (2): 75-104.

Yebra, DM., Kiil., S., and Dam-Johansen, K., (2004), 0Antifouling technology—past, present and future steps towards efficient and environmentally friendly antifouling coatings.Progress in organic coatings, 50:75-104.

Yuzwa, G. F., and P. Eng. (1991), Corrosion by sulphate reducing bacteria. Alberta Public Works, Supply and Services. Edmonton, Alberta. APPENDICES A. Dependency.

Zardus, J.D., Nedved, B.T., Huang, Y., Tran, C. and Hadfield, M.G., (2008), Microbial biofilms facilitate adhesion in biofouling invertebrates. The Biological Bulletin 214 (1): 91-98.

Zhang, HJ and Dexter, SC. (1995). Effect of biofilms on crevice corrosion of stainless steels in coastal seawater. Corrosion, 51(1):56-66.

Zobell, C.,Allen, E., (1935), The significance of marine bacteria in the fouling of submerged surfaces, Journal of bacteriology. 29: 239.

APPENDIX

Table A1. Resolved impedance parameters from equivalent circuit fitting for laboratory coating samples.

Test	Day	R_S (Ω)	Coating					Biofilm					Oxide					Double Layer				
			R_{po} (Ω)	Y_{0C} (nSs^n)	n_c	f_m (Hz)	C_c (nF)	R_{bf} (Ω)	Y_{0bf} (μSs^n)	n_{bf}	f_m (Hz)	C_{bf} (μF)	R_{ox} (Ω)	Y_{0ox} (μSs^n)	n_{ox}	f_m (Hz)	C_{ox} (μF)	R_p (kΩ)	Y_{0dl} (μSs^n)	n_{dl}	f_m (mHz)	C_{dl} (μF)
AOCN	0	0 0.45	1.2E7 3.1E7	2.9 3.5	0.89 0.91	78 2.1	1.9 2.7	-	-	-	-	-	-	-	-	-	-	-	-	-	-	-
	18	0 9.9	2.1E6 2.9E5	34 56	0.78 0.77	4.9 37	16 16	-	-	-	-	-	-	-	-	-	-	-	-	-	-	-
AOBN	0	17.1 20.6	1.7E7 4.1E7	1.0 0.75	0.95 0.96	13 6.6	0.81 0.66	-	-	-	-	-	-	-	-	-	-	-	-	-	-	-
	18	0 0	2.3E6 2.6E6	64 57	0.73 0.73	2.5 2.4	31 27	-	-	-	-	-	-	-	-	-	-	-	-	-	-	-
AOBD	0	14.4 14.6	1.9E7 8.4E6	1.1 1.4	0.95 0.95	10 19	0.91 1.1	-	-	-	-	-	-	-	-	-	-	-	-	-	-	-
	18	8.2 10.9	9.6E6 6.6E6	17 26	0.82 0.81	1.6 1.6	12 12	-	-	-	-	-	-	-	-	-	-	-	-	-	-	-
AXCN	0	0 4.8	475 620	5.0 2.0	0.86 0.91	5.8E5 5.2E5	0.63 0.54	-	-	-	-	-	-	-	-	-	-	150 280	16 6.6	0.76 0.76	54 79	21 7.9
	18	6.2 12	854 942	33 20	0.79 0.81	1.0E5 1.1E5	1.9 1.6	-	-	-	-	-	-	-	-	-	-	120 95	13 8.4	0.87 0.86	81 231	15 7.9
AXBN	0	5 0.2	432 333	1.3 2.7	0.93 0.88	9.2E5 1.2E6	0.44 0.45	- 78	- 56	- 0.69	- 450	- 4.9	-	-	-	-	-	7.6E5 52	9.2 574	0.68 0.62	0.004 0.76	545 4330
	18	22.6 38	442 35	12.5 43.3	0.85 0.84	2.6E5 1.3E6	1.5 3.8	1100 29	0.52 5880	0.82 0.85	4100 180	0.4 31.4	-	-	-	-	-	570 190	1.6 9060	0.89 0.61	192 0.007	1.6 1.2E6
AXBD	0	8 0	347 366	2.8 3.1	0.90 0.88	7.4E5 1.0E6	0.6 0.5	237 293	4.8 8.6	0.75 0.74	1500 570	0.5 1.0	-	-	-	-	-	342 151	3.2 5.8	0.83 0.88	155 205	3.2 5.6
	18	0 22	463 305	133 16.2	0.70 0.85	1.8E5 3.3E5	2.1 1.7	700 550	2.7 0.7	0.74 0.71	840 1.9E4	0.3 0.03	-	-	-	-	-	702 1.4E4	3.6 11	0.88 0.74	63 0.2	4 61.4
POCN	4	0 0	2.3E10 1.9E10	0.09 0.08	0.97 0.99	0.08 0.12	0.09 0.08	-	-	-	-	-	-	-	-	-	-	-	-	-	-	-
	26	- 0	- 4.9E7	- 0.09	- 0.99	- 38.5	- 0.09	-	-	-	-	-	-	-	-	-	-	-	-	-	-	-
POBN	4	0 0	5.3E11 2.9E12	0.07 0.02	0.97 0.99	0.004 0.004	0.08 0.02	-	-	-	-	-	-	-	-	-	-	-	-	-	-	-
	26	0 0	4.1E06 5.5E06	0.1 0.02	0.95 0.99	600 520	0.07 0.06	-	-	-	-	-	-	-	-	-	-	-	-	-	-	-
POBD	4	0 0	1.8E11 6.1E11	0.09 0.06	0.96 0.98	0.017 0.004	0.1 0.07	-	-	-	-	-	-	-	-	-	-	-	-	-	-	-
	26	0 0	1.8E11 3.7E11	0.1 0.07	0.95 0.97	0.006 0.006	0.1 0.08	-	-	-	-	-	-	-	-	-	-	-	-	-	-	-
PXCN	4	168 350	1134 1246	0.1 0.06	0.98 0.99	1.5E6 1.5E6	0.1 0.09	-	-	-	-	-	1104 657	147 26	0.59 0.83	3.5 22	42 22	116 5.1E5	113 10	0.59 0.83	2.9 0.03	513 17
	26	3	1436	0.2	0.92	1.5E6	0.08	-	-	-	-	-	217	14	0.83	160	4.8	2.8E8	16	0.83	5.0E-6	131

		3	1735	0.2	0.94	1.6E6	0.06						225	14	0.85	140	5.3	5.1E8	10	0.85	0.02	15
PXBN	4	0	649	0.4	0.88	6.0E6	0.05	187	85	0.53	400	2.2	490	53	0.74	23	15	1745	137	0.85	0.29	356
		0	2894	0.2	0.93	1.1E6	0.05	1365	3.9	0.58	1500	0.08	2353	0.8	0.94	130	0.5	932	2.8	0.84	55	3.3
	26	0	708	1.6	0.79	5.5E6	0.04	257	32	0.64	290	2.2	2390	75	0.64	2.5	28	110	0.7	0.57	15	0.1
		-	-	-	-	-	-	-	-	-	-	-	-	-	-	-	-	-	-	-	-	-
PXBD	4	143	558	0.6	0.89	2.8E6	0.1	1545	34	0.65	16	6.8	2271	3.4	0.99	12	6	1E10	7.1	0.99	3.E-6	4.7
		107	914	0.9	0.81	5.2E6	0.03	2602	7.8	0.75	1.3E6	2.1	7619	0.4	0.36	30	0.01	4E10	5.9	0.54	1.E-11	2.7E5
	26	0	693	0.4	0.9	3.5E6	0.07	715	40	0.61	55	4.2	978	112	0.6	7	24	57.2	157	0.87	17	208
		0	829	0.3	0.89	4.2E7	0.04	9.2	4.5	0.54	2.E7	7E-3	1719	15	0.76	20	4.8	9.9E5	204	0.79	0.02	1330

A. Antifouling (at 0 and 18 day), P. Polyurea (at 4 and 26 day)
X. Scribed. O.Non-Scribed
C.Non-inoculated. B Inoculated
N. Naturally Aerated. D De-aerated

Table A2. Resolved impedance parameters from equivalent circuit fitting for field antifouling coated samples.

Site	Depth BMG (m)	R_S (Ω)	Coating					Biofilm					Double Layer				
			R_{po} (Ω)	Y_{0C} (nSs^n)	n_c	f_m (Hz)	C_c (nF)	R_{bf} (Ω)	Y_{0bf} (μSs^n)	n_{bf}	f_m (Hz)	C_{bf} (μF)	R_p (kΩ)	Y_{0dl} (μSs^n)	n_{dl}	f_m (mHz)	C_{dl} (μF)
I	0.9	1.6	1.1	2.2E-3	0.45	1.2E5	1.2E-6	15.7	3.4E-6	0.72	1.3E5	8E-8	906	9.7E-4	0.4	2.5E-1	7.5E-4
	1.2	0.68	8.2	1.7E-4	0.48	1.5E5	1.4E-7	6.9	2.8E-5	0.62	1.6E5	1.6E-7	1040	4.1E-4	0.48	9.8E-1	1.6E-4
	1.5	0.62	10	1.9E-3	0.34	3.0E4	6.5E-7	6.98	1.1E-5	0.73	6.4E4	3.8E-7	698	9.9E-4	0.34	5.0E-1	4.7E-4
	1.55	0.64	5.5	2.1E-3	0.39	1.2E4	2.4E-6	4.2	2.6E-5	0.70	7.5E4	5.2E-7	330	2.8E-3	5.4	1.9E-1	2.6E-3
	1.8	1.2	1.9	1.7E-3	0.42	1.0E5	8.3E-7	4.5	2.6E-5	0.65	2.0E5	1.9E-7	209	2.7E-3	0.48	5.8E-1	1.3E-3
	2.1	0.46	2.7	1.4E-3	0.38	2.7E5	2.2E-7	7.8	3.5E-5	0.68	3.0E4	7.1E-7	356	2.2E-3	0.44	3.1E-1	1.5E-3
	2.4	0.25	1.4	6.2E-3	0.23	6.9E7	1.4E-9	7.6	1.5E-5	0.69	8.7E4	2.7E-7	348	2.6E-3	0.47	2.2E-1	2.1E-3
II	0.6	0.24	377	9.9E-7	0.73	8.7E3	5.2E-8	-	-	-	-	-	530	6.3E-4	0.27	10.2	3.0E-5
	0.77	2.4	15	1.3E-7	0.97	1.4E5	8.3E-8	26.6	7.8E-6	0.71	2.5E4	2.6E-7	593	1.3E-3	0.43	3.0E-1	9.3E-4
	0.91	4.1	7.5	1.1E-7	0.99	2.2E5	1.1E-7	2.01	4.7E-4	0.63	9.7E3	8.4E-6	1.8E2	3.7E-2	0.33	6.7E-4	1.4E0
	1.2	3.68	4.6	3.3E-7	0.96	2.1E5	1.9E-7	3.6	3.1E-5	0.85	7.4E3	6.5E-6	6.7E3	6.7E-3	0.46	4.3E-5	5.8E-1
	1.5	3.02	27	2.4E-7	0.90	1.0E5	6.2E-8	38.1	5.8E-6	0.75	1.3E4	3.5E-7	1.2E3	1.9E-3	0.38	2.0E-2	6.6E-3
	1.77	0.005	8.0	7.9E-6	0.63	6.9E5	3.0E-8	1.2	1.4E-2	0.61	1.4E2	1.1E-3	23.9	8.3E-2	0.52	4.8E-2	1.5E-1
III	0.15	30.6	1.4E4	4.2E-7	0.74	1.8E2	7.1E-8	-	-	-	-	-	2.6E4	2.3E-5	0.43	7.7E1	6.7E-7
	0.3	25.3	1.0E4	8.0E-7	0.69	5.3E-1	9.5E-8	-	-	-	-	-	2.9E4	2.3E-5	0.35	5.3E-1	1.0E-5
	0.6	0	3.4E3	1.9E-6	0.64	5.3E2	1.0E-7	-	-	-	-	-	3.0E5	1.0E-4	0.43	6.4E-5	8.6E-5
	0.9	14.8	2.9E3	7.3E-6	0.55	1.9E2	3.0E-7	-	-	-	-	-	1.8E4	3.9E-4	0.46	2.4E-3	3.8E-3
	0.92	0	3.3E3	3.9E-6	0.59	2.8E2	1.8E-7	-	-	-	-	-	1.9E4	3.7E-4	0.26	8.7E-5	9.5E-2
	1.4	1.1	146	1.4E-6	0.74	1.6E4	7.5E-8	2.1E3	2.6E-5	0.50	5.9E1	1.3E-6	3.8E3	2.2E-4	0.64	2.4E-1	1.9E-4
	1.5	0	5.4E3	4.3E-6	0.58	1.1E2	2.8E-7	-	-	-	-	-	1.9E4	5.0E-4	0.40	5.9E-4	1.4E-2
	1.8	3.6	4.6E3	2.9E-6	0.61	2.1E2	1.8E-7	-	-	-	-	-	2.8E4	5.2E-4	0.39	2.1E-4	2.1E-2

VITA

SAMANBAR PERMEH

Born, Tehran, Iran

2009-2013	B.S., Mining Engineering Amirkabir University of Technology Tehran, Iran
2014-2016	M.S., Environmental Engineering Florida International University Miami, FL, USA
2016 -2021	Doctoral Candidate Florida International University Miami, FL, USA

PUBLICATIONS

Permeh, S., Lau, K., Echeverria, M., Duncan, M., (2021), *Influence of Macro- and Micro-Fouling on Corrosion of Steel Bridge Piles Submerged in Natural Waters*, ASCE Journal of Materials in Civil Engineering, 33 (6) June 2021. DOI: 10.1061/(ASCE)MT.1943-5533.0003687

Permeh, S., Lau, K., Echeverria, M., Duncan, M., (2021), *Electrochemical characteristics of antifouling coated steel structure submerged in Florida natural waters to mitigate micro-and macrofouling*, Construction and Building Materials Journal, 274:122087, March 2021.DOI: 10.1016/j.conbuildmat.2020.122087

Permeh, S., Lau, K., Tansel, B., Duncan, M., (2020), *Surface conditions for microcosm development and proliferation of SRB on steel with cathodic corrosion protection*, Construction and Building Materials Journal, 243:118209, May 2020. DOI: 10.1016/j.conbuildmat.2020.118209

Permeh, S., Lau, K., Echeverria, M., Tansel, B., Duncan, M., (2020), *Cathodic polarization behavior of steel with different marine fouling morphologies on submerged bridge elements with cathodic protection*, ASCE Journal of Materials in Civil Engineering, 32(7) July 2020, 32(7), p. 04020184. DOI: 10.1061/(ASCE)MT.1943-5533.0003257

Permeh, S., Echeverria, M., Lau, K., Duncan, M., (2020), *Effect of Fouling on Cathodic Protection Current on Steel Submerged in Natural Waters*, In Digital Proceedings of the Corrosion 2020, Paper No. 14831, NACE International: Houston, TX, USA.

Permeh, S., Echeverria, M., Lau, K., Duncan, M., (2020), *Diagnostic of Antifouling Coating Durability after Exposure in Natural Waters by Electrochemical Impedance Spectroscopy*, In Proceedings of the Coating +, SSPC2020, Long Beach, CA. February. 2-6.

Permeh, S., Echeverria, M., Lau, K., Tansel, B., Duncan, M., (2019), *Exploration of the Influence of Microbe Availability on MIC of Steel Marine Fouling Environments,* In Proceedings of the Corrosion 2019, Paper No. 13461, Nashville, TN, USA, 24–28 March 2019; NACE International: Houston, TX, USA.

Permeh, S., Lau, K., M. Duncan, (2019), *Degradation of Coatings for Steel in Environments Susceptible to Corrosion Associated with Fouling*, Structure and Infrastructure Engineering. 16 (8):1186-1200, Nov 2019. DOI: 10.1080/15732479.2019.1694543

Permeh, S., Lau, K., M. Duncan, (2019), *Characterization of Biofilm Formation and Coating Degradation by Electrochemical Impedance Spectroscopy*, Coatings.9(8): 518. DOI: 10.3390/coatings9080518

Permeh, S., Echeverria, M., Tansel, B., Lau, K., Duncan, M. (2019), *Update on Mitigation of MIC of Steel in a Marine Environments with Coatings*. In Proceedings of the Coating +, SSPC2019, Orlando, FL. February. 11-14, 2019.

Permeh, S., Li, B., Echeverria, M., Tansel, B., Lau, K., M. Duncan, (2018), *Microbially influenced steel corrosion with crevice conditions in natural water,* In Proceedings of the Corrosion 2018, Paper No. 11529, Phoenix, AZ, USA, 15–19 April 2018; NACE International: Houston, TX, USA.

Permeh, S., Krishna Vigneshwaran, K. K , M., Lau, K., Lasa, I., (2019), *Corrosion of Post-Tensioned Tendons with Deficient Grout. Part 3: Segregated Grout with Elevated Sulfate and Vestigial Chloride Content*, Corrosion 75(7): 848-864. July 2019.

Permeh, S., Krishna Vigneshwaran, K. K . Echeverria, M., Lau, K., Lasa, I., (2018), *Corrosion of Post-Tensioned Tendons with Deficient Grout. Part 2. Segregated Grout with Enhanced Sulfate*, Corrosion 74(4): 457-467. April 2018.

Permeh, S., Reid, C., Echeverria, M., Lau, K., Tansel, B., Duncan, M., Lasa, I., (2017), *Microbiological Influenced Corrosion in Florida Marine Environment: A Case Study*. In Proceedings of the Corrosion 2017, New Orleans, LA, USA, 26–30 March 2017; NACE International: Houston, TX, USA.

Krishna Vigneshwaran, K.K, Permeh. S., Echeverria, M., Lau, K., Lasa, I., (2018), *Corrosion of Post-Tensioned Tendons with Deficient Grout. Part 1. Electrochemical Behavior of Steel in Alkaline Sulfate Solutions,* Corrosion 74(3): 362-371. April 2018 March 2018.